Analytical Approximate Solutions for Various Forms of Aggregation-Breakage Process

THESIS

Submitted in partial fulfillment of the requirements

for the degree of

DOCTOR OF PHILOSOPHY

by

Gourav Arora

(ID No. 2019PHXF0421P)

Under the Supervision of

Prof. Rajesh Kumar

and

Co-Supervision of

Prof. Youcef Mammeri

BITS Pilani

Pilani | Dubai | Goa | Hyderabad | Mumbai

BIRLA INSTITUTE OF TECHNOLOGY AND SCIENCE

PILANI-333031, RAJASTHAN, INDIA

2024

"Success is not final, failure is not fatal: it is the courage to continue that counts."

- Winston Churchill

BIRLA INSTITUTE OF TECHNOLOGY & SCIENCE, PILANI

CERTIFICATE

This is to certify that the thesis entitled, **"Analytical Approximate Solutions for Various Forms of Aggregation-Breakage Process"** submitted by **Mr. Gourav Arora** ID No. **2019PHXF0421P** for the award of Ph.D. degree of the institute embodies original work done by him under our supervision.

Signature of the Supervisor
Name : **PROF. RAJESH KUMAR**
Designation : **Associate Professor**
Department of Mathematics
BITS Pilani, Pilani Campus,
Rajasthan, India
Date: __/__/____

Signature of the Co-Supervisor
Name : **PROF. YOUCEF MAMMERI**
Designation: **Professor**
Department of Mathematics
University Jean Monnet, Saint Etienne, France
Date: __/__/____

Dedicated to
My Beloved Family

Acknowledgements

A journey is undoubtedly smoother when you have companions. During my Ph.D. journey, I've been fortunate to have the company and support of numerous individuals. I am profoundly grateful to all those who have contributed to the successful completion of this doctoral journey, which would not have been possible without their unwavering support, guidance, and encouragement.

Firstly, I would like to extend my heartfelt gratitude to my supervisor, Prof. Rajesh Kumar, for his mentorship, insightful guidance, and invaluable feedback throughout the research process. His expertise and dedication have been instrumental in shaping the direction of this thesis. He has been a guide in academia and a source of motivation during the challenging phases. His belief in my potential has encouraged me to strive for higher standards. The collaborative atmosphere he fostered in our interactions has broadened my perspectives.

I also express my sincere gratitude to my co-supervisor, Prof. Youcef Mammeri, for his guidance and encouragement. I am grateful for the opportunity to learn under his mentorship. I truly appreciate his dedication to my intellectual growth, his willingness to invest time and effort, and his role as a constant pillar of support.

I am also thankful to all the professors of the Department of Mathematics of BITS Pilani, Pilani Campus, for their guidance and valuable suggestions in my research work. I feel fortunate to have my Doctoral Advisory Committee (DAC) members, Prof. Sangita Yadav and Prof. Anirudh Singh Rana, for their insightful discussions and valuable suggestions that have significantly enriched the quality of this work.

I am grateful to Prof. Bhupendra Kumar Sharma (Former Head of the Department) and Prof. Devendra Kumar, Head of the Department of Mathematics, for their unwavering support. I extend my acknowledgment to all the faculty members and research scholars for their valuable assistance and cooperation throughout my research journey. The moments we have shared hold a special corner in my heart and will be cherished for eternity. I convey my heartfelt appreciation for the valuable contribution you have made to my academic

journey.

With great reverence, I express my gratitude to Prof. V. Ramgopal Rao (Vice Chancellor), Prof. Sudhirkumar Barai (Director), Prof. M.B. Srinivas (Dean, AGSRD), and Prof. Shamik Chakraborty (Associate Dean, AGSRD) for providing necessary facilities.

I want to express my gratitude to my parents, Mrs. Shashi Arora and Mr. Prem Parkash Arora, for showering me with boundless love and unwavering encouragement, which have been like a deep well of inspiration. Their invaluable guidance and wisdom have significantly shaped my academic journey. I extend my thanks to my brother, Sunny Arora, for his steadfast belief in me, and without his support, it is impossible to complete this journey.

A heartfelt thanks to my friends Amit, Umesh, Himanshu, Sanjeev, Shipra, Anshu, Ashvini, Yogesh and Ankit for being my unwavering pillars of support throughout this journey. Your encouragement, lively discussions, shared laughter, and countless cherished moments have not only strengthened me but also left an indelible mark on my life, making this journey unforgettable.

A special thanks to my friend Saddam, whose unwavering support and humor made my Ph.D. journey brighter. He has been my go-to person in both challenging and joyous moments. The countless laughs, meaningful conversations, and shared memories have not only lightened the load of my academic pursuits but also made this journey deeply enriching and unforgettable.

Last but not the least, I extend my appreciation to all the participants who generously shared their time and insights to this study. This journey has been a collective effort, and I am humbled by the support I have received. My deepest gratitude goes to every individual who has played a role, no matter how small, in helping me reach this milestone.

Place: BITS Pilani, Pilani Campus

Date: __/__/____ **Gourav Arora**

Abstract

This thesis comprehensively explores partial and integral-partial differential equations, specifically focusing on coagulation, bivariate coagulation, breakage, and growth equations. These models have significant applications in various real-world scenarios, including engineering, pharmaceuticals, food processing, and cloud formations. The primary objective of the thesis is to solve different versions of coagulation models using semi-analytical methods. The initial phase of the research investigates the variational iteration method for growth, aggregation, and coupled aggregation-breakage equations. The optimal variational iteration method is also investigated for pure growth and aggregation equation (for constant kernel). The results are compared with the precise and approximated solutions obtained via the Adomian decomposition method. The superiority of the proposed scheme is highlighted through numerical computations and graphs.

The thesis further addresses the scarcity of semi-analytical methods for the coupled aggregation-breakage and bivariate aggregation models. To this end, the Elzaki-based accelerated homotopy perturbation method (AHPETM) is implemented to solve these models. The theoretical convergence of the scheme is presented for aggregation and bivariate aggregation equations. For numerical validation, the results of the proposed scheme are compared with those of Adomian decomposition method(ADM), homotopy perturbation method (HPM), homotopy analysis method (HAM) and optimized decomposition method (ODM) for aggregation and breakage, demonstrating the efficiency and accuracy of the proposed scheme. The results obtained via AHPETM show more precision with respect to time than the other methods, leading to an extension of the results for coupled aggregation-breakage and bivariate aggregation equations.

The work also delves into the coupled aggregation-growth equation, which holds significant interest due to its wide application in real-life scenarios. The improved optimal homotopy analysis method (IOHAM) is implemented to solve the aggregation and coupled

aggregation-growth equations. The results of IOHAM are compared with the ADM, HPM, HAM, and ODM, with IOHAM surpassing all the mentioned methods for the aggregation equation. Consequently, the results are extended for the coupled aggregation-growth model, and the work includes the convergence analysis of the scheme for aggregation and coupled aggregation growth equations.

Proceeding further, the thesis considers another variant of the aggregation process, namely the condensing coagulation model. Motivated by the limited attempts to solve the model analytically and numerically, the HPM and ADM are employed. The proposed schemes provide closed-form solutions for the product and constant kernels, while the approximated solutions are obtained for physically relevant kernels such as sum and Ruckenstein kernels. The work is further extended to solve the Lifshitz Slyozov model with encounters, and the results align well with the exact solutions.

Lastly, a new implicit form of semi-analytical technique is introduced to solve differential equations that provides accuracy for larger time domains. A detailed analysis is performed to study the convergence of the scheme. The results are compared with standard semi-analytical methods such as ADM, HPM, HAM, and ODM to demonstrate the supremacy of the proposed scheme. The convergence control parameter is incorporated to enhance the scheme's accuracy. Finally, the thesis concludes with a discussion on the possible extensions of the scope for future investigations, paving the way for further research in this field.

Contents

List of Abbreviations

Sr. No.	Abbrevation	Stands for
1	ADM	Adomian decomposition method
2	HPM	Homotopy perturbation method
3	VIM	Variational iteration method
4	OVIM	Optimal variational iteration method
5	ODM	Optimized decomposition method
6	AHPETM	Accelerated homotopy perturbation Elzaki transformation method
7	SCE	Smoluchowski's coagulation equation
8	FE	Fragmentation equation
9	CCFE	Coupled coagulation-fragmentation equation
10	BSCE	Bivariate Smoluchowski's coagulation equation
11	IOHAM	Improved optimal homotopy analysis method
12	CCM	Condensing coagulation model
13	LSE	Lifshitz-Slyozov equation
14	PBE	Population balance equation
15	SAT	Semi-analytical technique

List of Tables

List of Figures

Chapter 1

Introduction

The art of proposing a question must be held of higher value than solving it.

— Georg Cantor

This chapter gives a comprehensive context and motivation for the thesis work. It investigates various coagulation models and performs an extensive literature review. Besides, it defines the main purpose and scope of the current research. A chapter-wise roadmap of the thesis is also presented towards the end of this chapter.

1.1 Overview

Particle processes are widely recognized in various engineering fields, encompassing crystallization, comminution, precipitation, polymerization, aerosol, and emulsion processes. A continuous phase and a dispersed phase of particles with various attributes are involved in these processes. These particles, which could take the form of crystals, grains, drops, or bubbles, possess diverse characteristics such as size, composition, porosity, enthalpy, and others. In numerous contexts, particle size is often considered the sole pertinent property of significance.

Given the potential variability in sizes and properties of particles, a mathematical representation of their distribution or properties is essential for characterization. In cases where particles exhibit uniform shapes, as seen in grinding or crystallization process, a

characteristic shape factor can be established. However, in engineering processes such as fluidized bed agglomeration and pharmaceutical, where particles demonstrate more diverse properties, a multidimensional distribution function becomes necessary for accurate characterization.

Particulate matter may transform their physical properties via several pathways. This thesis delineates its scope to study coagulation, breakage, growth, and synergistic effects. A succinct description of these phenomena is furnished in the following section.

1.1.1 Aggregation

Aggregation (coagulation) is a fundamental process where two or more particles in a suspension come into contact and adhere to each other, forming larger clusters. In the physical realm, aggregation has numerous applications. Within the realm of industrial applications, the principle of aggregation is instrumental in water purification procedures, specifically through the method of flocculation, wherein the conjoined particles are more readily isolated from the aqueous medium. Furthermore, in the pharmaceutical industry, the aggregation of particles can significantly influence the stability and therapeutic effectiveness of medicinal preparations.

During this process, there is a diminution in the aggregate count of particles, yet the mass remains invariant within the system. The scholarly literature provides an array of theoretical frameworks designed to forecast the likelihood of adhesion between two impinging particles. An elaborate elucidation of the chosen model is delineated in the subsequent section. The graphical depiction of the process is presented in Figure 1.1.

Figure 1.1: Aggregation process

1.1.2 Breakage

The phenomenon of breakage (fragmentation) pertains to the division of substances into smaller fragments across diverse circumstances. This process, influenced by factors such as material properties, applied forces, and environmental conditions, plays a significant role in various industries, including food processing for edible portioning, pharmaceuticals for medication efficacy, construction for material management, and recycling for material repurposing. The total number of particles increases in the system during the process while the total mass remains conserved in the system. The visual illustration of the procedure is delineated in Figure 1.2.

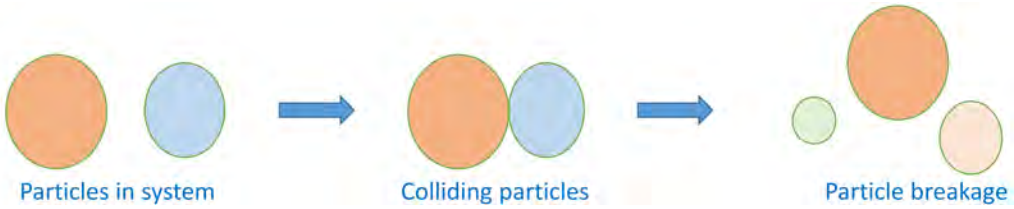

Figure 1.2: Breakage process

1.1.3 Growth

Particle growth transpires when dust or non-particulate matter accumulates on the surface of a particle, leading to an increase in its mass while maintaining the same particle count. During this process, the size of the particle continuously increases. This phenomenon is critical in various fields, such as air filtration, which aids in trapping airborne particles, and in the pharmaceutical industry, which ensures uniformity in drug formulations. Figure 1.3 illustrates the pictorial representation of the process.

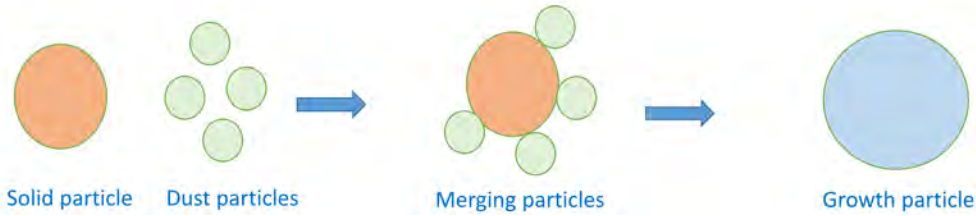

Figure 1.3: Growth process

Following the aforementioned processes, particles undergo a modification of their properties, necessitating the application of mathematical models, particularly population balance equations (PBEs), to analyze the resultant variations in the distribution of particle properties. These models are integral in understanding and managing the complexities of particle dynamics in various scientific and industrial contexts. They characterize the dynamic changes in the distribution of specific properties. In the context of this thesis, which focuses on growth, aggregation and breakage equations, volume is a practical metric for sizing.

1.2 Population balance models

A general one-dimensional PBE for a well mixed system can be written as

$$\begin{aligned}\frac{\partial}{\partial \tau}\mu(\eta,\tau) =& \frac{\mathscr{P}_{in}}{W}\mu_{in}(\eta) - \frac{\mathscr{P}_{out}}{W}\mu_{out}(\eta) - \frac{\partial}{\partial \eta}\left(G(\eta,\tau)\mu(\eta,\tau)\right) + \mathscr{B}_{nuc}(\eta,\tau) \\ &+ \mathscr{B}_{agg}(\eta,\tau) - \mathscr{D}_{agg}(\eta,\tau) + \mathscr{B}_{break}(\eta,\tau) - \mathscr{D}_{break}(\eta,\tau), \qquad (1.2.1)\end{aligned}$$

with appropriate initial and/or boundary conditions. The parameter η denotes the size of the particle, $\mu(\eta,\tau)$ denotes the number density of particle of size η at time τ and the system's volume is denoted by W. On the right-hand side, the initial two expressions signify the influx or efflux within the ongoing procedure. The functions $\mathscr{P}_{in}$ and $\mathscr{P}_{out}$ stand for the inlet and outlet flow rates from the system, respectively. The terms $\mathscr{B}_{nuc}$ and $G(\eta,\tau)$, respectively, denote the rates of nucleation and growth. In a batch process, the absence of inflow and the exclusive consideration of outflow allow for the omission of the first two terms on the right-hand side of the equation. The terms $\mathscr{B}_{agg}$ and $\mathscr{B}_{break}$ represent the formation of particles of size η in aggregation and breakage, respectively, while $\mathscr{D}_{agg}$ and $\mathscr{D}_{break}$ indicate the reduction of particles through these same processes. This streamlined approach simplifies the analysis of particle dynamics within the system. Despite considerations of number density, the dynamics of moments hold significant

attention. The j^{th} moment of the particle size distribution is defined as

$$\mu_j(\tau) = \int_0^\infty \eta^j \mu(\eta, \tau) d\eta. \tag{1.2.2}$$

The zeroth moment $(j = 0)$ represents the aggregate count of particles within the system, while the first moment $(j = 1)$ signifies the total mass encompassed. Beyond these, the second moment of the distribution serves as a metric for evaluating numerical outcomes, specifically reflecting the proportionality to light scattering by particles within the Rayleigh regime.

In the following subsections, we provide the introduction of various models along with the literature survey about the numerical and semi-analytical results.

1.2.1 Smoluchowski's coagulation equation

Consider the non-negative variables i and t to symbolize the particle size and time, respectively, with $v_i(t)$ denoting the number density of particles sized i at time t. The rate at which particles of size i merge with particles of size j is depicted by the coagulation kernel $\kappa_{i,j}$ which is assumed to be non-negative and symmetric. Abiding by the law of mass action, the augmentation in number density of particles of size i can be expressed as

$$\frac{1}{2} \sum_{j=1}^{i-1} \kappa_{i-j,j} v_{i-j}(t) v_j(t). \tag{1.2.3}$$

Similarly, the reduction in the quantity of particles of size i, resulting from collisions with particles of size j, is expressed as

$$\sum_{j=1}^{\infty} \kappa_{i,j} v_i(t) v_j(t). \tag{1.2.4}$$

Hence, the discrete coagulation equation, provided by Smoluchowski in 1917 [1] as an infinite set of non-linear differential equations is governed by

$$\frac{\partial \nu_i(t)}{\partial t} = \frac{1}{2}\sum_{j=1}^{i-1} \kappa_{i-j,j}\nu_{i-j}(t)\nu_j(t) - \sum_{j=1}^{\infty} \kappa_{i,j}\nu_i(t)\nu_j(t),$$

where the first term on right-hand side signifies the birth term and second term denotes the death of the particle of size i. The derivation of the model was based on the Brownian motion of particles. Further, in 1928, Muller proposed the continuous version of the aggregation equation as

$$\frac{\partial \mu(\eta,\tau)}{\partial \tau} = \frac{1}{2}\int_0^{\eta} \kappa(\eta-\omega,\omega)\mu(\eta-\omega,\tau)\mu(\omega,\tau)d\omega - \int_0^{\infty} \kappa(\eta,\omega)\mu(\eta,\tau)\mu(\omega,\tau)d\omega, \tag{1.2.5}$$

where $\mu(\eta,\tau) \geq 0$ is the particle number density function of having particles of size $\eta \in \mathbb{R}^+$ at time $\tau \in [0,\infty)$ in a homogeneous physical system. The expression $\kappa(\eta-\omega,\omega)$, assumed to be non-negative and symmetric, signifies the rate at which particles of sizes $\eta-\omega$ and ω interact, forming a particle with size η. The initial term on the equation's right-hand side indicates the genesis of a particle of size η, termed the birth term. Conversely, the latter term represents the elimination of a particle of size η within the system, known as the death term.

In solid processing, e.g., in foods and pharmaceuticals, product quality is characterized by multiple particle properties, for example, the volume and composition of aggregating particles. To model such phenomenon, more then one dimensional expression is required. Therefore, in the following, the bivariate case is considered, i.e., particles (or individual objects) are characterized by two properties, named η and ζ. The two dimensional aggregation process is governed by

$$\begin{aligned}\frac{\partial \mu(\eta,\zeta,\tau)}{\partial \tau} =& \frac{1}{2}\int_0^{\eta}\int_0^{\zeta} \kappa(\eta-\eta',\zeta-\zeta',\eta',\zeta')\mu(\eta-\eta',\zeta-\zeta',\tau)\mu(\eta',\zeta',\tau)d\eta' d\zeta' \\ &- \int_0^{\infty}\int_0^{\infty} \kappa(\eta,\eta',\zeta,\zeta')\mu(\eta,\zeta,\tau)\mu(\eta',\zeta',\tau)d\eta' d\zeta',\end{aligned} \tag{1.2.6}$$

with the initial condition

$$\mu(\eta,\zeta,0)=\mu_0(\eta,\zeta)\geq 0. \tag{1.2.7}$$

for $\eta,\zeta\in(0,\infty)$ and $\tau\in[0,T]$.

1.2.1.1 Existing numerical and semi-analytical methods

Due to complexity of these models and unavailability of the analytical solutions (except for some simple cases), several numerical [2–7] and semi-analytical [8–12] techniques are applied to solve these problems approximately. Numerical schemes to solve coagulation model (1.2.5) includes finite element method [2], quadrature method of moments [13], finite volume scheme [4], fixed pivot element [5], fast Fourier transformation method [14] and references therein. The drawbacks of the numerical schemes lie on non-physical assumptions such as discretization, linearization, sets of basis functions, and many others. Recently, several authors have developed interest in semi-analytical approaches that offer solutions in series form without making such assumptions. Some of the available strategies are Laplace-variational iteration method (LVIM) [15], Adomian decomposition method (ADM) [16], homotopy perturbation method (HPM) [9], optimal homotopy asymptotic method (OHAM) [17], homotopy analysis method (HAM) [8], Laplace optimized decomposition method [10] and variational iteration method [18]. Interestingly, some of the algorithms provided the closed form series solutions of coagulation equation (1.2.5) considering the aggregation kernels

$$\kappa(\eta,\omega)=1,\eta+\omega,\eta\omega \text{ and } \eta^{\frac{2}{3}}+\omega^{\frac{2}{3}},$$

with exponential initial condition ($\mu(\eta,0)=e^{-\eta},e^{-\eta}/\eta$), see [8, 9, 16] for more detailed computations. It turned out that these closed form solutions are nothing but the actual solution of the models. Hammouch and Mekkaoui in [15] developed the LVIM for solving the coagulation equation (1.2.5) only for two cases of aggregation kernels, constant ($\kappa(\eta,\omega)=1$) and product ($\kappa(\eta,\omega)=\eta\omega$). In [19, 20], ODM is implemented to solve

the coagulation equation using the parameters

$$\kappa(\eta,\omega) = 1, \eta+\omega \text{ and } \eta\omega \text{ with } u(\eta,0) = e^{-\eta}.$$

Recently in [21], HPM is combined with the Pade approximates and results are obtained for various physically relevant kernels such as Shear stress, bilinear, Brownian and Pulvermacher kernels for larger time and spatial domains.

In the literature, it was observed that ADM, HPM, and HAM provide the closed form solutions for the problem (1.2.5), but some drawbacks are observed in these techniques. In [22, 23], it was found that a large number of iterations of the aforementioned methods are required to obtain a more accurate approximation. When dealing with chaotic systems, in [24], authors found that time, time step, and the number of terms must be handled with extreme caution. Further, Odibat [25] has drawn attention to various drawbacks of ADM, including its delayed convergence and inability to handle boundary conditions for solving non-linear PDEs. These shortcoming were avoided by Odibat in [25]. To overcome these issues for model (1.2.5), recently, ODM [19] has been implemented to solve it, but the accuracy was still maintained only for a small period of time.

Further, it is known that the analytical solutions for the bivariate aggregation equation are available only for limited cases, see [26] and references therein. Several numerical methods, such as moving sectional [27], finite difference [28], Monte Carlo [29], sectional quadrature [30], dual quadrature [31], finite volume schemes [32, 33] and references therein, are considered to solve the equation.

1.2.2 Breakage equation

The breakage particulate process is a critical operation in materials engineering, where particle size reduction is pivotal in enhancing product characteristics. This process is employed across various industries to manipulate particles' physical and chemical properties, thereby optimizing product functionality. In the pharmaceutical sector, particle size affects drug dissolution rates and bioavailability, making the breakage process vital for

effective medication delivery. The food industry relies on this process to control product texture and flavor profiles. In mining, it is essential for producing ores, facilitating efficient extraction of valuable minerals. Manufacturing paints, pigments, and other consumer goods also utilize this process to achieve desired color strength and product consistency. Hence, understanding and controlling this process are fundamental for advancing material science and meeting the stringent quality demands of modern industry.

A general form of the breakage equation is given as

$$\frac{\partial u(x,t)}{\partial t} = \int_x^\infty B(x,y)S(y)u(y,t)dy - S(x)u(x,t). \tag{1.2.8}$$

The breakage function, denoted as $B(x,y)$, serves as the probability density function that describes the likelihood of generating a particle of size x from a parent particle of size y. The term $S(x)$ describes the rate at which particles are selected to break. The breakage function satisfies the properties

$$\int_0^x B(x,y)dy = \mathscr{N}(x), \tag{1.2.9}$$

and

$$\int_0^x xB(x,y)dy = x. \tag{1.2.10}$$

The function $\mathscr{N}(x)$ is the number of daughter particle formation obtained from the breakage of particle of size x.

1.2.2.1 Existing numerical and semi-analytical methods

The breakage equation's wide-ranging applications have prompted numerous analytical resolution attempts. Patil and Andrews [34] have analytically resolved the model considering binary breakage and a linear selection function, yet analytical solutions for physically significant kernels remain arduous. Consequently, a spectrum of numerical strategies has been adopted, including the finite volume method [3, 35–37], method of moments [30, 38–40], finite element method [41, 42], stochastic methods [43–45], Haar wavelet [46],

fixed pivot technique [47, 48], and cell average technique [49, 50].

In recent times, there has been a surge in the adoption of semi-analytical methods for resolving the model. In 2019, Singh *et al.* , applied the ADM [16], while Kaur *et al.* utilized the HPM [9] and derived solutions for diverse kernels. Further in work, Kaur *et al.* [8] had also employed the HAM, that yielded identical closed-form solutions as those obtained through ADM and HPM.

Interestingly, combined aggregation-breakage equation is considered which is an intriguing issue for academics. The problem was resolved using a class of numerical or stochastic methods. Lee and Matsoukas [51] employed a stochastic process, namely the constant-N Monte Carlo method, to solve the aggregation with a binary breakage equation. In 2002, Mahoney *et al.* used the finite element method for aggregation, growth, and nucleation equations [52]. Further, number density and moments were computed with the help of the method of moments by Madras *et al.* in [53]. Till date, there is no literature on semi-analytical schemes for coupled aggregation-breakage model.

1.2.3 Growth equation

The phenomenon of particle growth is of paramount importance. For instance, within the realm of nanotechnology, the meticulous regulation of particle growth is imperative for the synthesis of materials endowed with distinct properties tailored for sectors such as information technology, healthcare, energy, and environmental sciences. Concurrently, in the domain of food technology, the principles governing particle growth are strategically utilized to enhance the preservation and prolong the shelf life of food products.

The PBE for the growth process is described as a hyperbolic PDE, given as

$$\frac{\partial \mu(\eta,\tau)}{\partial \tau} + \frac{\partial G(\eta,\tau)\mu(\eta,\tau)}{\partial \tau} = 0, \tag{1.2.11}$$

with $G(\eta,\tau)$ is the growth rate.

1.2.3.1 Existing numerical and semi-analytical methods

The model in question has been addressed through a variety of numerical techniques, including finite difference, finite volume, and finite element methods, as referenced in the works [54, 55]. Additionally, the integrated dynamics of growth combined with aggregation or breakage equation have garnered attention from numerous scholars. Various numerical methods are implemented to solve the combined aggregation growth or breakage growth models such as finite volume [56], method of characteristics [57], and many more [58]. Recently, a combined form of method of characteristics and finite volume scheme is implemented to solve the aggregation growth model, see [59] for detailed literature. However, till now, no semi-analytical technique is used to solve the coupled aggregation growth model.

1.2.4 Condensing coagulation model

This model is the combination of the two models, namely

1. Safronov-Dubovski coagulation equation and

2. inverse coagulation equation.

In 1972, Safronov reformed the Oort and van de Hulst model to another form, known as the Oort-Hulst Safronov (OHS) equation [60]. Further, Dubovski introduced the discrete version of the OHS model in [61]. In 2003 [62], Laurencot *et al.* established a relation between Smoluchowski's coagulation and OHS equations. In the Safronov-Dubovski coagulation model, j-mers divide into j-monomers, provided that $j \leq i$, each j monomer collides instantly with the i-mer. From this collision act, we have j new $i+1$ mers. This description of the coagulation process leads to the balance equation, for $i \geq 1$,

$$\frac{dv_i(t)}{dt} = v_{i-1}(t)\sum_{j=1}^{i-1}\kappa_{i-1,j}jv_j(t) - v_i(t)\sum_{j=1}^{i}\kappa_{i,j}jv_j(t) - \sum_{j=i}^{\infty}\kappa_{i,j}v_i(t)v_j(t),$$

where $v_i(t)$ represents the concentration (number density) of particles of mass i at time t and $\kappa_{i,j}$ for $i \neq j$ is the rate at which particles of masses i and j collide, known as the

coagulation kernel. The term $\kappa_{i,j}$ is non-negative and symmetric for $i, j \geq 1$, *i.e.,* ,

$$\kappa_{i,j} = \kappa_{j,i}.$$

The continuous form of the above model, also called OHS equation, is given by

$$\frac{\partial \mu(\eta,\tau)}{\partial \tau} = -\frac{\partial}{\partial \eta}\left[\int_0^{\eta} \omega\kappa(\eta,\omega)\mu(\eta,\tau)\mu(\omega,\tau)d\omega\right] - \int_{\eta}^{\infty} \kappa(\eta,\omega)\mu(\eta,\tau)\mu(\omega,\tau)d\omega. \tag{1.2.12}$$

In the literature, there also exists an inverse coagulation model in which larger particles are more unstable than the smaller particles [63]. Here, in this case, initially j-mers divide into j-monomers provided that $j > i$ and then each j monomer collides instantly with i-mer. This also leads to have j new $i+1$ mers, and the model looks like

$$\frac{dv_i(t)}{dt} = v_{i-1}(t)\sum_{j=1}^{\infty} \mathscr{L}_{i-1,j} j v_j(t) - v_i(t)\sum_{j=i}^{\infty} \mathscr{L}_{i,j} j v_j(t) - \sum_{j=1}^{i} \mathscr{L}_{i,j} v_i(t) v_j(t), i \geq 1,$$

in discrete setting while the continuous form is given by

$$\frac{\partial \mu(\eta,\tau)}{\partial \tau} = -\frac{\partial}{\partial \eta}\left[\int_{\eta}^{\infty} \omega\mathscr{L}(\eta,\omega)\mu(\eta,\tau)\mu(\omega,\tau)d\omega\right] - \int_0^{\eta} \mathscr{L}(\eta,\omega)\mu(\eta,\tau)\mu(\omega,\tau)d\omega. \tag{1.2.13}$$

Hence, having (1.2.12) and (1.2.13), the continuous version of the condensing coagulation model (CCM) is described as, see [63],

$$\frac{\partial \mu}{\partial \tau} = Q(\mu), \tag{1.2.14}$$

where the collision operator Q is defined as,

$$Q(\mu) = -\frac{\partial}{\partial \eta}\left[\int_0^{\eta} \omega\kappa(\eta,\omega)\mu(\eta,\tau)\mu(\omega,\tau)d\omega\right] - \int_{\eta}^{\infty} \kappa(\eta,\omega)\mu(\eta,\tau)\mu(\omega,\tau)d\omega$$

$$-\frac{\partial}{\partial \eta}\left[\int_{\eta}^{\infty} \omega \mathscr{L}(\eta,\omega)\mu(\eta,\tau)\mu(\omega,\tau)d\omega\right] - \int_{0}^{\eta} \mathscr{L}(\eta,\omega)\mu(\eta,\tau)\mu(\omega,\tau)d\omega. \tag{1.2.15}$$

Similar to the PBE, integral properties of the concentration of particles, *i.e.,* , moments, are also of interest and is defined exactly as before in equation (1.2.2). It is emphasized here that the total mass is conserved, i.e., $\frac{d\mu_1(\tau)}{d\tau} = 0$.

1.2.4.1 Existing numerical and semi-analytical methods

In 2016, Davidson [63] found the analytical solutions of (1.2.14)-(1.2.15) using the method of characteristics for constant and multiplicative kernels under some special initial conditions and considering $\kappa(\eta,\omega) = \mathscr{L}(\eta,\omega)$. Addition to this, he also studied the self-similar solutions for the same by following a characteristic approach as well as discussed equilibrium solution for constant kernel. Further, he investigated the Lifshitz-Slyozov equation(LSE) with encounters. For this, long-time behavior of the solution for three types of initial data is analyzed. Till date, there was no literature available on semi-analytical technique for such models.

1.3 Objectives of the thesis

1. To compute the approximate solutions for the aggregation and coupled aggregation-breakage equations using the variational and optimized variational iteration methods.

2. To study the series solutions of aggregation, breakage, coupled aggregation-breakage and bivariate aggregation equations using accelerated homotopy perturbation Elzaki transformation scheme along with theoretical convergence analysis.

3. To discuss the convergence analysis, theoretical error bound and the implementation of improved optimal homotopy analysis method for aggregation and coupled aggregation-growth models.

4. To obtain the approximated solutions for a variant of coagulation models, namely condensing coagulation equation using homotopy perturbation and Adomian decom-

position methods.

5. To construct a new implicit iterative method for solving ordinary and partial differential equations and comparison with the standard semi analytical methods.

1.4 Organization of the thesis

The dissertation is organized to present approximate solutions for diverse forms of the coagulation and fragmentation equations. It explores various semi-analytical techniques, including HPM, ADM, VIM, IOHAM and AHPETM to find the closed form or finite term series solutions. Additionally, it introduces a novel implicit semi-analytical method for solving nonlinear differential equations. The efficacy and precision of this new approach are demonstrated through comparisons with established methods like ADM, HPM, HAM, and ODM.

Let us briefly summarize the motivation and work done during this dissertation, chapter wise, as below.

Chapter 2 delves into the application of semi-analytical strategies, specifically ADM and VIM, to address the series solutions of aggregation, aggregation-breakage, and pure growth equations. The chapter conducts a comparative analysis of analytical and truncated series solutions in terms of number density and various moments. In the scenario of pure growth, the solutions derived from ADM and VIM are proven to be mathematically equivalent, offering closed-form solutions when the growth rate is constant. The chapter also introduces the optimal variational iteration method (OVIM) and studied for two cases of pure growth and one case of aggregation equation with constant kernels. It is observed that the inaccuracy decreases to some degree but the computations of higher term approximations require large computational time. A number of test cases for each equation is presented to validate the methods' precision and effectiveness by comparing the finite term series solutions.

Moving further, Chapter 3 aims to establish a semi-analytical approach based on HPM to find the closed form or approximated solutions for the population balance equations such

as Smoluchowski's coagulation, fragmentation, coupled coagulation-fragmentation and bivariate coagulation equations. An accelerated form of the HPM is combined with the Elzaki transformation to improve the accuracy and efficiency of the method. It has benefits over the existing semi-analytical techniques such as ADM, ODM, and HAM in the sense that computations of Adomian polynomials and convergence parameters are not required. The novelty of the scheme is shown by comparing the numerical findings with the existing results obtained via ADM, HPM, HAM and ODM for non-linear coagulation equation. This motivates us to extend the scheme for solving the other models mentioned above. The supremacy of the proposed scheme is demonstrated by taking several numerical examples for each problem. The error between exact and series solutions provided in graphs and tables show the accuracy and applicability of the method. In addition to this, convergence of the series solution is also the key attraction of the work.

Chapter 4 describes a semi-analytical technique based on homotopy for solving the aggregation and aggregation-growth equations. Multiple test scenarios are compared to the exact and existing estimated solutions derived using HAM, HPM, ADM, and ODM to demonstrate the precision and effectiveness of the suggested approach, namley IOHAM qualitatively and quantitatively. The aggregation equation yields indistinguishable solutions using ADM, HPM and HAM methodologies. Consequently, there is no discernible enhancement in the truncated series solutions. On the contrary, ODM enhances the solutions to a certain degree. However, the proposed scheme surpasses the accuracy of all previously mentioned methods. Furthermore, integral qualities such as moments are highlighted, and IOHAM enhances the accuracy of moments compared to ODM. In contrast, the HAM still better matches the actual moments. In addition, a comprehensive convergence study of the series solution is investigated.

Proceeding further, Chapter 5 delineates the derivation of analytical approximate solutions for the condensing coagulation and Lifshitz-Slyzov models, employing two semi-analytical methodologies: the homotopy perturbation and Adomian decomposition methods. The work calculates analytical solutions for benchmark kernels, including constant and product kernels. In addition, it formulates approximated solutions for sum and Ruckenstein kernels

that are physically significant as well. The convergence of the solutions obtained via these two methods to the exact solutions is mathematically validated, establishing the methods' credibility. In cases where an analytical solution is known, the chapter contrasts numerical results for number density and the zeroth moment with the exact solutions across various kernels and initial conditions. A graphical illustration of the error margin between the approximated and exact solutions is also provided.

Chapter 6 proposes a novel semi-analytical method to yield solutions over greater temporal extents, as solving differential equations over extended temporal domains is pivotal for many scientific and engineering endeavors. The progression of numerous phenomena in the natural world occurs over prolonged durations, necessitating a comprehensive understanding of their temporal dynamics to facilitate precise prognostications and judicious decision-making. Existing methodologies such as HPM, ADM and HAM are noted for their precision within limited temporal scopes. ODM proposed by Odibat extends this accuracy over a longer term, yet its solutions become untenable over substantial timeframes. Moreover, this work integrates a convergence control parameter to bolster the proposed method's accuracy and operational efficiency. A rigorous theoretical convergence analysis is delineated, substantiating the method's validity. Three examples are numerically examined and discussed to validate the proposed approach empirically.

Finally, in the last chapter, the dissertation reaches its denouement by summarizing its pivotal discoveries and suggesting directions for future academic pursuits.

Chapter 2

Variational iteration and Adomian decomposition methods to solve growth, aggregation and aggregation-breakage equations

This chapter explores semi-analytical techniques, specifically the ADM and the VIM, for solving aggregation, aggregation-breakage, and pure growth equations. A comparison is drawn between analytical and truncated series solutions concerning number density and diverse moments. Furthermore, OVIM is employed to tackle growth and aggregation equations, yielding a reduction in error compared to ADM and VIM, albeit at the expense of increased computational complexity. Various test cases are examined to substantiate the efficacy and precision of the series approximation methods.

Following Section 1.2, PBE which describes aggregation, breakage and growth is mathematically expressed as

$$\frac{\partial u(x,t)}{\partial t}+\frac{\partial [G(x)u(x,t)]}{\partial x} = \frac{1}{2}\int_0^x K(x-y,y)u(x-y,t)u(y,t)dy - \int_0^\infty K(x,y)u(x,t)u(y,t)dy + \int_x^\infty B(x,y)S(y)u(y,t)dy - S(x)u(x,t). \tag{2.0.1}$$

The work of this chapter is published in Journal of Computational Science, 101973(64), 2023

The term $u(x,t)$ is called the number density distribution function with particle size $x \in \mathbb{R}_+ :=]0,\infty[$ at time $t \in \mathbb{R}_+$. The second term on the left-hand side represents the particle's growth process by the growth rate G. The first two terms in the right-hand side of the equation (2.0.1) emerge as a result of aggregation, whereas the other two terms appear due to breakage.

In brief, the goals of this chapter is to solve the aggregation equation using VIM and compare the results with findings of ADM solutions given in [16]. ADM suffers from the extensive work required to derive the Adomian polynomials for non-linear terms whereas VIM has no specific requirement for the non-linear operator and gives the solution in the form of rapidly convergent successive approximations.

Structure of the chapter is as follows: Section 2.1 delves into the basic idea of Adomian decomposition, variational iteration and optimal variational iteration schemes for solving the differential equations. Furthermore, numerical implementations of the methods are studied for solving growth, aggregation and aggregation-breakage models under Section 2.2. In the last section, conclusions drawn from the implementations are discussed.

2.1 Semi-analytical techniques

Let us review briefly the basic ideas behind the VIM, OVIM and ADM to solve the differential equations.

2.1.1 Variational iteration method

J.He proposed the VIM [64, 65], for solving linear and non-linear ordinary and partial differential equations in bounded and unbounded domains. The method is used in various disciplines including physics [66], chemistry[67], biomedical science [68], and engineering science [69]. To understand the algorithm, consider a differential equation in the form

$$T(u) - h(r) = 0, \quad r \in \Omega, \tag{2.1.1}$$

where T is an operator and $h(r)$ is a known analytical function with domain Ω. Above equation can be written as

$$L(u)+N(u)-h(r)=0, \tag{2.1.2}$$

where L and N are linear and non-linear operators, respectively. According to J.He [64], the proposed iterations to solve the differential equation are

$$u_{n+1}(x,t)=u_n(x,t)+\int_0^t \lambda(\zeta)(L(u_n(x,\zeta))+N(\tilde{u}_n(x,\zeta))-h(r))d\zeta \text{ for } n\geq 0, \tag{2.1.3}$$

for $\lambda(\zeta)$ being the Lagrange multiplier, which can be identified via the variational theory. The second term on the right-hand side is called the correction [70]. Here, u_n is the nth approximation and $\tilde{u}_n$ is the restricted variation, i.e. $\delta\tilde{u}_n=0$, where $\delta\tilde{u}_n$ represents the first variation of $\tilde{u}_n$, one may refer to [71] for more details. The initial condition $u(x,0)$ is usually considered as initial guess or zeroth approximation $u_0(x,t)$. As a result, the solution is given by

$$u=\lim_{n\to\infty} u_n. \tag{2.1.4}$$

2.1.2 Optimal variational iteration method

This section is devoted to defining an enhanced version of the VIM [72], where the iterations to solve equation (2.1.1) are given as follows:

$$u_{n+1}(x,t)=u_n(x,t)+h\int_0^t \lambda(\zeta)(L(u_n(x,\zeta))+N(\tilde{u}_n(x,\zeta))-h(r))d\zeta. \tag{2.1.5}$$

Here h is a convergence control parameter which possibly speeds up the VIM's convergence [72–76]. This optimal parameter h is computed by minimizing the $Res(h)$, defined by

$$Res(h)=\sqrt{\int_\Omega (T(u_k)-h(r))d\Omega}.$$

Due to the difficulty in calculating the iterations, residue can also be calculated numerically using the squared residual formula,

$$Res(h) = \sqrt{\frac{1}{M}\sum_{m=1}^{M}(T(u_k(r_m)) - h(r_m))^2},$$

where $r_m \in \Omega$ are arbitrary sample points and M is the number of partitions. Readers are referred to [8, 77] and further citations for detailed explanation.

2.1.3 Adomain decomposition method

The technique was developed in 1988 by George Adomian [78] for solving ordinary and partial linear/non-linear differential equations including differential-algebraic equations, stochastic systems, functional equations, integro-differential equations, and eigenvalue problems, see [16, 79–81] and further references cited therein.
Consider the following differential equation to explain the ADM, see [78],

$$Ly + Ry + Ny = g(x), \tag{2.1.6}$$

where N is a non-linear and L is a linear operator with highest order derivative. It is assumed that L is invertible and R is a linear differential operator of order less than L. Thus, the above equation can be written as

$$y = \phi + L^{-1}g(x) - L^{-1}Ry - L^{-1}Ny, \tag{2.1.7}$$

for ϕ being the function representing the term arising from the given initial conditions. For non-linear equations, non-linear operator $N(y) = F(y)$ is usually represented by an infinite series of the so-called Adomian polynomials

$$F(y) = \sum_{k=0}^{\infty} A_k(y), \tag{2.1.8}$$

where A_k are generated for all kinds of non-linearity of $F(y)$ [82]. According to the ADM, the solution y is defined by the series

$$y = \sum_{n=0}^{\infty} y_n, \tag{2.1.9}$$

where the components $y_0, y_1, y_2, \cdots$ are usually determined recursively by

$$\begin{aligned} y_0 &= \phi + L^{-1}g(x), \\ y_{k+1} &= -L^{-1}(Ry_k) - L^{-1}A_k, \quad k \geq 0. \end{aligned} \tag{2.1.10}$$

By substituting A_k in (2.1.10) leads to the determination of the components of y. Then, using all these components in (2.1.9), we can find the solution y.

2.2 Numerical implementation

This part focuses on the numerical implementations of the series solution schemes mentioned in the previous Section for solving growth, aggregation and aggregation-breakage equations. The approximated series solutions are compared with the available exact solutions for number density and the moments. In addition, errors are computed and represented in tabular form to check the accuracy and reliability of the methods.

2.2.1 Pure growth equation

To solve the pure growth equation, two scenarios are explored. The first case is constant growth, while the second one is linear growth with an exponential initial condition in both the situations. By taking $K(x,y) = 0$ and $S(x) = 0$ in the equation (2.0.1), the growth equation is obtained as

$$\frac{\partial u(x,t)}{\partial t} + \frac{\partial [G(x)u(x,t)]}{\partial x} = 0. \tag{2.2.1}$$

2.2.1.1 Variational iteration method

Using VIM, considering $L = \frac{\partial}{\partial t}$ and the remaining terms as $N(u)$, the iterations for solving the growth equation are

$$u_{n+1}(x,t) = u_n(x,t) + \int_0^t \lambda(\zeta)\left(\frac{\partial u_n(x,\zeta)}{\partial \zeta} + \frac{\partial}{\partial x}[G(x)u_n(x,\zeta)]\right)d\zeta. \tag{2.2.2}$$

Thus, by following [65]

$$\begin{aligned}\delta u_{n+1} &= \delta u_n + \int_0^t \lambda(\zeta)\left(\delta u_n' + \frac{\partial}{\partial x}[G(x)\delta\tilde{u}_n(x,\zeta)]\right)d\zeta \\ &= (1+\lambda(t))\delta u_n - \int_0^t \lambda'(\zeta)\delta u_n d\zeta.\end{aligned} \tag{2.2.3}$$

Hence, the stationary conditions are

$$\lambda'(\zeta) = 0 \text{ and } 1+\lambda(t) = 0,$$

which yields $\lambda(\zeta) = -1$.

2.2.1.2 Adomian decomposition method

Consider $L = \frac{\partial}{\partial t}$, where L^{-1} is given by

$$L^{-1} = \int_0^t [.]dt.$$

Operating L^{-1} on both sides of equation (2.2.1) leads to

$$u(x,t) = u_0(x) - L^{-1}\left[\frac{\partial[G(x)u(x,t)]}{\partial x}\right]. \tag{2.2.4}$$

Following ADM, introduce the solution $u(x,t)$ of (2.2.1) as

$$u(x,t) = \sum_{j=0}^{\infty} c_j(x,t). \tag{2.2.5}$$

Substituting (2.2.5) in the equation (2.2.4) gives the iterations as follows

$$c_0(x,t) = u_0(x), \quad c_{n+1}(x,t) = -L^{-1}\left[\frac{\partial[G(x)c_n(x,t)]}{\partial x}\right],$$

which lead to a complete determination of the solution components $c_j(x,t)$. For the numerical simulations, the n-term truncated series solution can be obtained as

$$u_n(x,t) := \sum_{j=0}^{n} c_j(x,t).$$

Test case 1 (TC-1): Constant growth

Iterations to compute the solution by proposed VIM are, by following the recursive scheme (2.2.2), by setting $G(x) = 1$ and with the initial condition $u(x,0) = e^{-x}$,

$$u_{n+1}(x,t) = u_n(x,t) - \int_0^t \left(\frac{\partial u_n(x,t)}{\partial t} + \frac{\partial u_n(x,t)}{\partial x}\right) dt. \tag{2.2.6}$$

Having this, we obtain the successive terms of the approximated solution as

$$\begin{aligned} u_1(x,t) =& u_0(x,t) - \int_0^t \left(\frac{\partial}{\partial t}u_0(x,t) + \frac{\partial}{\partial x}u_0(x,t)\right) dt \\ =& e^{-x} - \int_0^t \left(\frac{\partial}{\partial t}(e^{-x}) + \frac{\partial}{\partial x}(e^{-x})\right) dt = (1+t)e^{-x}, \end{aligned}$$

and in a similar manner,

$$u_2(x,t) = \left(\frac{1}{2!}t^2 + t + 1\right)e^{-x}, \quad u_3(x,t) = \left(\frac{t^3}{3!} + \frac{t^2}{2!} + t + 1\right)e^{-x},$$

and proceeding further the expression for $u_n(x,t)$ is

$$u_n(x,t) = \left(\frac{t^n}{n!} + \cdots + \frac{t^3}{3!} + \frac{t^2}{2!} + t + 1\right)e^{-x}.$$

According to equation (2.1.4), the solution is given by

$$u(x,t) = \lim_{n\to\infty} u_n(x,t) = e^{t-x},$$

which is the exact solution of the problem.

Now, considering the same data for $G(x)$ and $u_0(x)$, ADM leads to the following iterations

$$c_0(x) = e^{-x}, \quad c_1(x,t) = te^{-x}, \quad c_2(x,t) = \frac{1}{2!}t^2e^{-x}, \quad c_3(x,t) = \frac{1}{3!}t^3e^{-x}, \cdots, c_n(x,t) = \frac{1}{n!}t^ne^{-x}.$$

So, here again, the exact solution is defined by

$$u(x,t) = \sum_{j=0}^{\infty} c_j(x,t) = \sum_{j=0}^{\infty} \frac{1}{j!}t^ne^{-x} = e^{t-x}.$$

It can be observed that the truncated solutions using ADM and VIM are identical in this case. Thus, the numerical results are plotted for VIM and OVIM only. In addition, truncation errors employing proposed strategies are provided in Table 1 for various values of n. Such truncation error is computed using the formula given as, see [16] for ADM error,

$$\text{Absolute Error} = \sum_{i=1}^{n} |u_n^i - u_i| h_i, \tag{2.2.7}$$

where $u_n^i = u_n(x_i,t)$ and $u_i = u(x_i,t)$. From Table 2.1 where the absolute error is presented,

n	2	4	6	8	10
VIM	74.266	42.0473	15.1825	3.6177	0.599277
OVIM	68.3984	35.1237	11.8776	2.17243	0.299946

Table 2.1: Truncation error when $t = 4.5$ and $x \in [0,5]$ taking $h_i = 0.01$ for TC-1

it is evident that error decreases with increasing number of approximations and OVIM performs better than VIM. The number density and the first moment at $t = 4.5$ are depicted

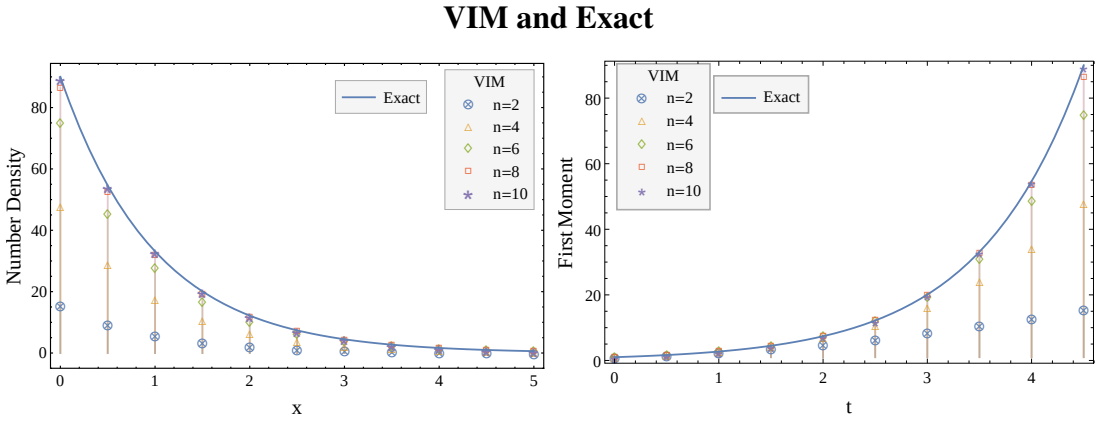

(a) Number density (b) First moment

Figure 2.1: Number density and first moment for TC-1

in Figure 2.1. It is shown that as number of terms in the series solution increases, the estimated results are in excellent agreement to the analytical solutions of number density and first moment. Further, Figure 3 presents the absolute error using ten-term truncated solution obtained using VIM and OVIM. It is clear that the involvement of the convergence parameter improves the accuracy of the truncated solution. Moreover, one can observe from Figure 2.2 that as time increases, the error increases, which can be reduced by considering more components of the truncated solution as demonstrated in Table 2.1 as well.

Test case 2: Linear growth

In this case, taking $G(x) = x$ in the growth equation and $u(x,0) = u_0(x,t) = e^{-x}$, the recursive scheme (2.2.2) provides the iterations for VIM as follows

$$u_1(x,t) = e^{-x} - \int_0^t \left(\frac{\partial}{\partial t}(e^{-x}) + \frac{\partial}{\partial x}(xe^{-x}) \right) dt = e^{-x}(tx - t + 1),$$

$$u_2(x,t) = e^{-x}\left(\frac{t^2}{2}\left(x^2 - 3x + 1\right) + t(x-1) + 1 \right),$$

$$u_3(x,t) = e^{-x}\left(t^3\left(\frac{x^3}{6} - x^2 + \frac{7x}{6} - \frac{1}{6} \right) + t^2\left(\frac{x^2}{2} - \frac{3x}{2} + \frac{1}{2} \right) + t(x-1) + 1 \right).$$

Similarly, one can compute the higher order terms using MATHEMATICA. Similar to the

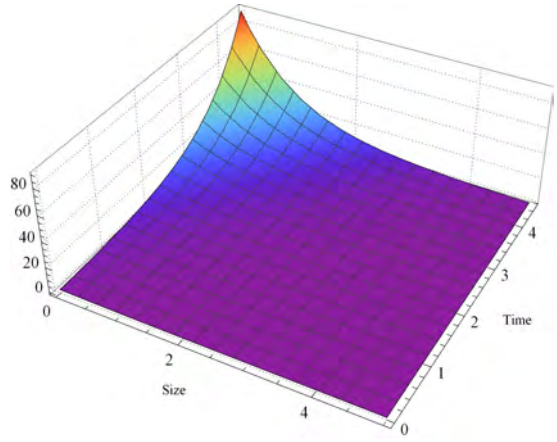

(a) Exact solution

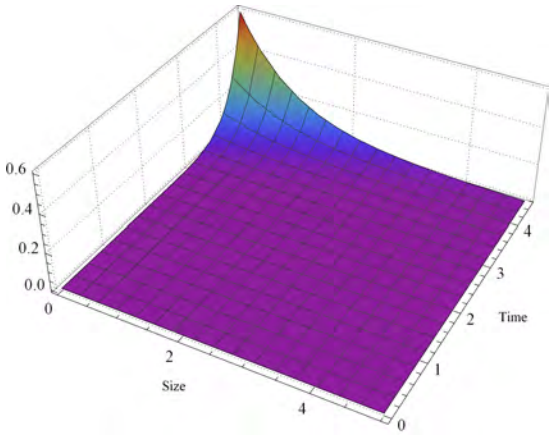

(b) VIM absolute error

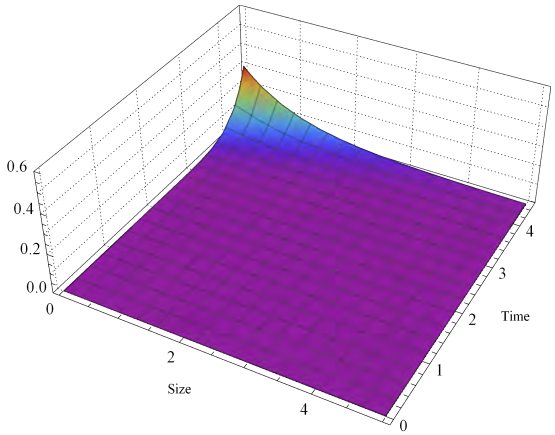

(c) OVIM absolute error

Figure 2.2: Exact solution and absolute error for TC-1

previous test case, the first few successive iterations for ADM are obtained as

$$c_0(x,t) = e^{-x}, \quad c_1(x,t) = t\left(-e^{-x}\right)(1-x),\ c_2(x,t) = -\frac{1}{2}t^2e^{-x}\left(-x^2+3x-1\right),$$

$$c_3(x,t) = -\frac{1}{3}t^3e^{-x}\left(-\frac{x^3}{2}+3x^2-\frac{7x}{2}+\frac{1}{2}\right),\ c_4(x,t) = -\frac{1}{4}t^4e^{-x}\left(-\frac{x^4}{6}+\frac{5x^3}{3}-\frac{25x^2}{6}+\frac{5x}{2}-\frac{1}{6}\right).$$

Therefore, the n term truncated solution is given by

$$u_n(x,t) = \sum_{j=0}^{n} c_j(x,t),$$

where the exact solution for the model is $u(x,t) = e^{-e^{-t}x-t}$. Again it is noticed that the truncated solutions using ADM and VIM are same, so the numerical simulations are visualized for VIM and OVIM only. The truncation error is summarized in Table 2.2 below and the decreasing trend of error is marked with increasing n. As expected, OVIM again provides less error as compared to VIM for all n.

n	2	4	6	8	10
VIM	0.7156	0.6396	0.5134	0.4243	0.3486
OVIM	0.4355	0.2311	0.04584	0.1348	0.0057

Table 2.2: Truncation error when $t = 1.5$ and $x \in [0,10]$ taking $h_i = 0.01$ for TC-2.

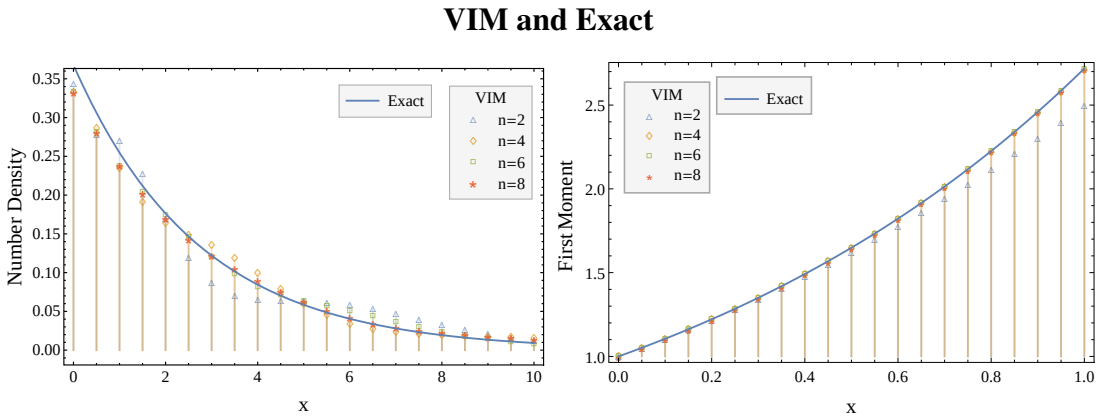

(a) Number density (b) First moment

Figure 2.3: Number density and first moment for TC-2

Further to see this, in Figure 2.3, a comparison between the truncated and exact solutions for the number density and first moment is made at $t = 1.2$ by taking various values of n. It is clear from the figure that as the number of terms increases, truncated solutions both for the number density and the total mass move closer to the analytical ones. It is worth to point out that the zeroth moment in the above two cases is constant for both exact and approximated solutions. The accuracy of the methods can also be seen from Figure 2.4 which gives the plot of the absolute errors obtained using OVIM and VIM. It indicates that the error is negligible for $n = 8$ for both the schemes with OVIM showing advantages

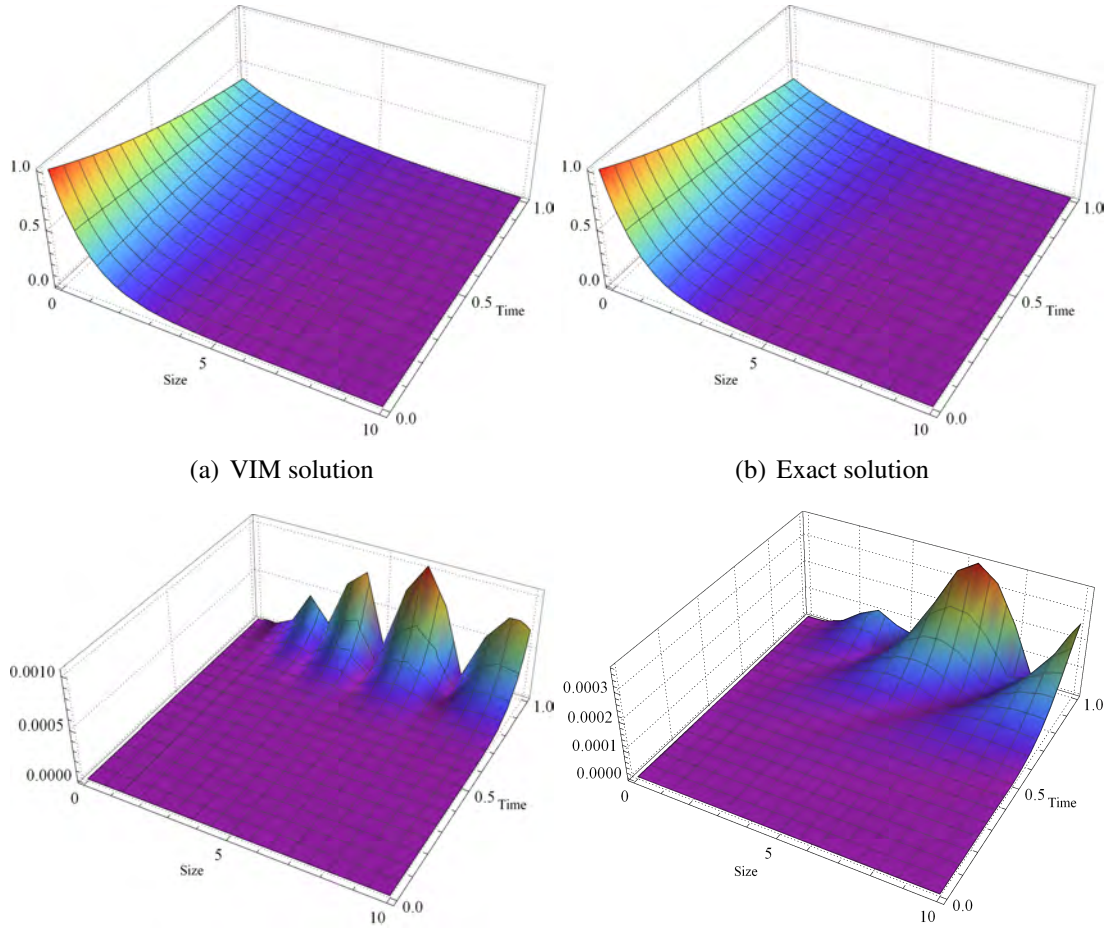

(a) VIM solution

(b) Exact solution

(c) VIM absolute error

(d) OVIM absolute error

Figure 2.4: Truncated solution, exact solution and absolute error for TC-2

over VIM.

2.2.2 Aggregation equation

This section is devoted to solving the aggregation equation using VIM and the obtained numerical results will be compared to the ADM solutions provided in [16]. Three test cases are considered consisting of constant, sum and product kernels with exponential initial condition to show the advantages of VIM over ADM. Following the idea of Section 2.1.1, VIM iterations to solve the aggregation equation (2.0.1), with $G = 0$ and $S = 0$ lead

to

$$u_{n+1}(x,t) = u_n(x,t) - \int_0^t \left(\frac{\partial u_n(x,t)}{\partial t} - \frac{1}{2}\int_0^x K(x-y,y)u_n(x-y,t)u_n(y,t)dy + \int_0^\infty K(x,y)u_n(x,t)u_n(y,t)dy \right) dt. \quad (2.2.8)$$

Let us simplify these iterations for the following problems.

Test case 3: Constant kernel

Consider $K(x,y) = 1$ with the initial condition $u_0(x) = e^{-x}$, then the recursive relation (2.2.8) reduces to

$$u_{n+1}(x,t) = u_n(x,t) - \int_0^t \left(\frac{\partial u_n(x,t)}{\partial t} - \frac{1}{2}\int_0^x u_n(x-y,t)u_n(y,t)dy + \int_0^\infty u_n(x,t)u_n(y,t)dy \right) dt. \quad (2.2.9)$$

Hence, the first few successive iterations are computed as

$$u_1(x,t) = e^{-x} - \int_0^t \left(\frac{\partial}{\partial t}(e^{-x}) - \frac{1}{2}\int_0^x e^{-(x-y)}e^{-y}dy + \int_0^\infty e^{-x}e^{-y}dy \right) dt = e^{-x}\left(t\left(\frac{x}{2}-1\right)+1 \right),$$

$$u_2(x,t) = e^{-x}\left(t^3\left(\frac{x^3}{144} - \frac{x^2}{12} + \frac{x}{4} - \frac{1}{6}\right) + t^2\left(\frac{x^2}{8} - \frac{3x}{4} + \frac{3}{4}\right) + t\left(\frac{x}{2}-1\right)+1 \right).$$

and so on. The exact solution to this problem is provided in [83] as

$$u(x,t) = \frac{4e^{-\frac{2x}{t+2}}}{(t+2)^2}.$$

Using the error formula (2.2.7), in Table 2.3, the errors between the exact and semi-analytical solutions using ADM, VIM and OVIM are evaluated for various values of n. It is clear from this table that VIM and OVIM not only provide better estimation than ADM but errors are significantly reduced and close to zero for $n = 6$ and higher. To see this further, five term truncated solution as well as the zeroth moment from ADM, VIM

and OVIM are plotted along with the exact number density and moment in Figure 2.5 and one can observe that OVIM and VIM are in excellent agreement with the analytical ones as compared to ADM. Figure 2.6 displays $3D$ plots of approximated and exact solutions along with the errors for the number density. The novelty of VIM is visible from the error graphs 2.6(d) and 2.6(e) which guarantee that ADM's error is relatively higher than VIM and OVIM as time progresses.

n	3	4	5	6
ADM	0.141249	0.0902173	0.0570828	0.0358428
VIM	0.0274487	0.0055058	0.0055058	0.000914124
OVIM	0.0274487	0.0041382	5.41422×10^{-5}	4.96436×10^{-6}

Table 2.3: Truncation error when $t = 1.2$ and $x \in [0, 10]$ taking $h_i = 0.01$ for TC-3.

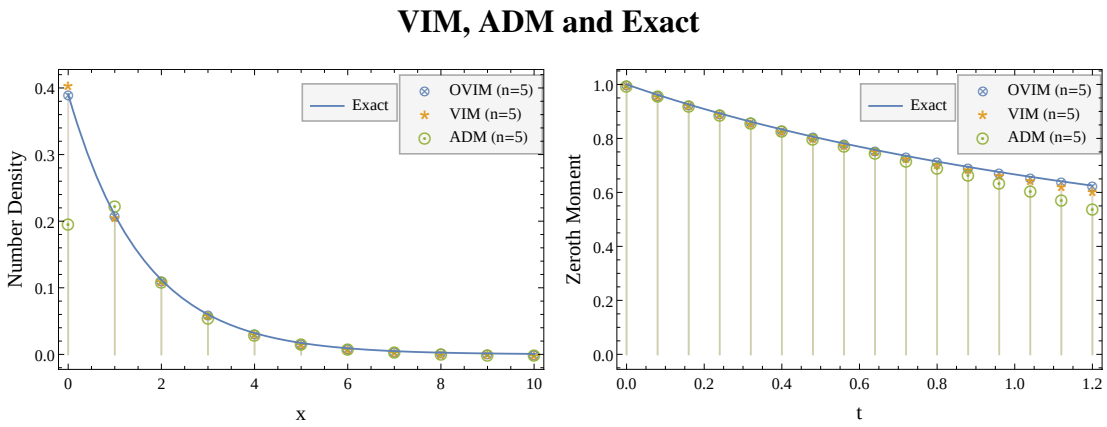

(a) Number density (b) Zeroth moment

Figure 2.5: Number density and zeroth moment for TC-3

Remark 2.2.1. *The inclusion of the convergence control parameter enhances the VIM's accuracy and efficiency to some degree but raises its computing cost heavily. Therefore, computing the OVIM iterations are based on the model's complexity. For instance, it was difficult to calculate the higher-order components of the series solution for non-linear aggregation (except for constant kernel) and combined aggregation-breakage equations. It is worth to mention that* $17.87 \approx 18$ *minutes was required to compute a 4-term estimated solution in OVIM, whereas VIM only needed 18 seconds for aggregation equation*

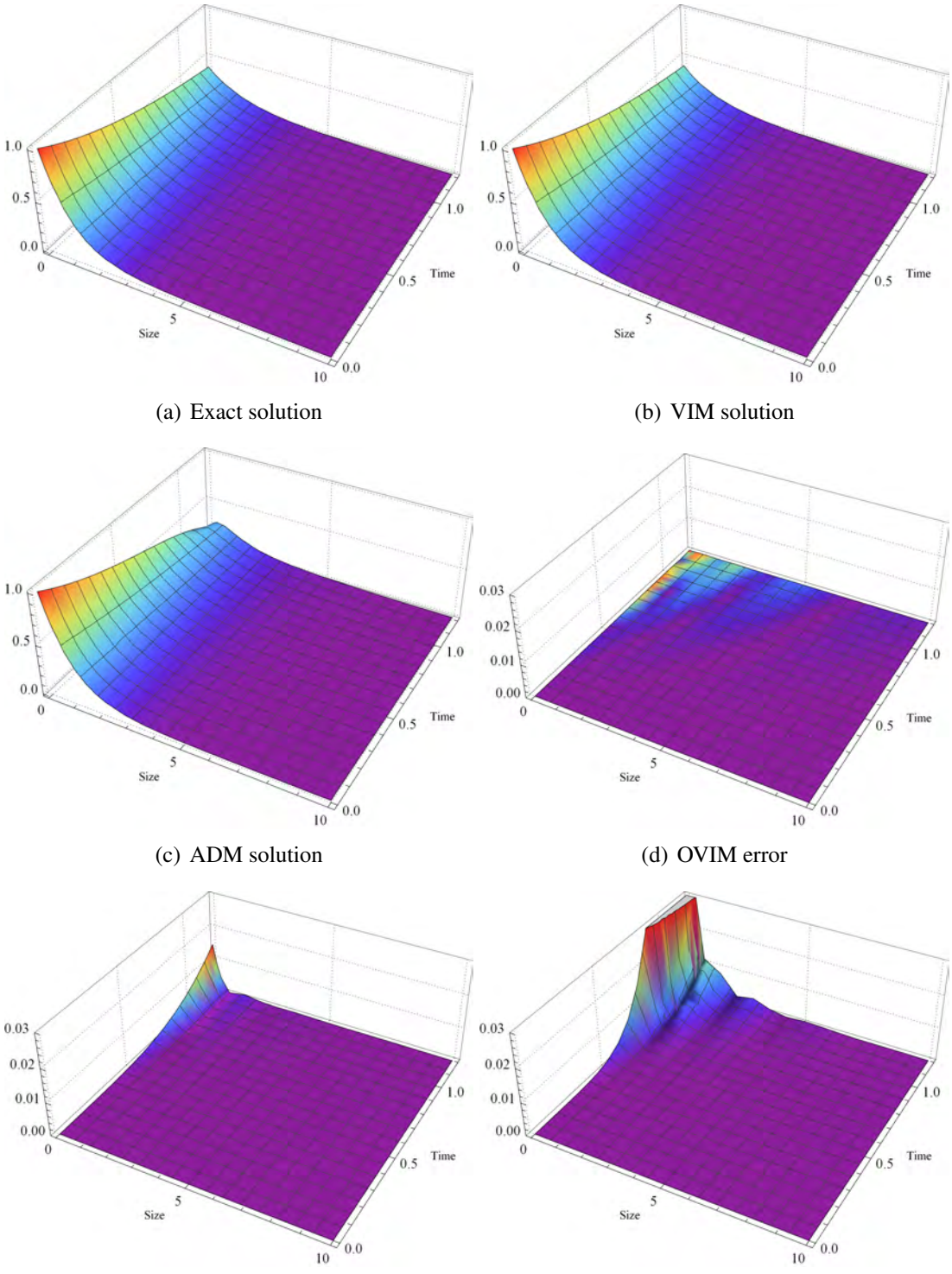

(a) Exact solution

(b) VIM solution

(c) ADM solution

(d) OVIM error

(e) VIM error

(f) ADM error

Figure 2.6: Number density and absolute error for TC-3

with constant kernel. Consequently, the computations for OVIM are omitted for further discussion.

Test case 4: Sum kernel

Considering $K(x,y) = x+y$ with initial data $u_0(x) = e^{-x}$ lead to the following form of recursive relation

$$u_{n+1}(x,t) = u_n(x,t) - \int_0^t \left(\frac{\partial u_n(x,t)}{\partial t} - \frac{1}{2}\int_0^x (x+y)u_n(x-y,t)u_n(y,t)dy + \int_0^\infty (x+y)u_n(x,t)u_n(y,t)dy \right) dt. \tag{2.2.10}$$

Thus, the first few terms of the series solutions due to VIM are

$$\begin{aligned} u_1(x,t) =& e^{-x}\left(t\left(\frac{x^2}{2} - x - 1\right) + 1\right), \\ u_2(x,t) =& e^{-x}\left(t^3\left(\frac{x^6}{720} - \frac{x^5}{72} - \frac{x^4}{36} + \frac{x^3}{3} - \frac{x^2}{6} - \frac{x}{3}\right) + t^2\left(\frac{x^4}{12} - \frac{x^3}{2} - \frac{x^2}{4} + \frac{3x}{2} + \frac{1}{2}\right)\right. \\ & \left. + t\left(\frac{x^2}{2} - x - 1\right) + 1\right), \end{aligned}$$

and so on. Continuing in the similar manner, one can compute the higher term approximated solutions with the help of MATHEMATICA. The exact solution for the problem is given in [16], as

$$u(x,t) = \frac{e^{\left(e^{-t}-2\right)x-t} I_1\left(2\sqrt{1-e^{-t}}x\right)}{\sqrt{1-e^{-t}}x},$$

where I_1 is the modified Bessel function of the first kind. The number density of the VIM and ADM solutions for $n = 4$ at $t = 0.7$ are compared with the analytical result in Figure 2.7. VIM performs better with a four term approximated solution. ADM, on the other hand, needs a sixteen-term truncated solution to achieve the same level of accuracy. Interestingly, for both approaches, four-term truncated solutions yield similar results and match exactly with the precise total number of particles in Figure 2.7(b). Figure 2.8 also illustrates that ADM has deviations when the VIM is nearly equal to the analytical solution of particle concentration for $n = 4$. Finally, from Figures 2.8(d) and 2.89(e), it is clear that

the VIM error is very small compared to the error due to ADM truncated solutions and thus, it clearly justifies the accuracy of studying VIM. **Test case 5: Product kernel**

VIM, ADM and Exact

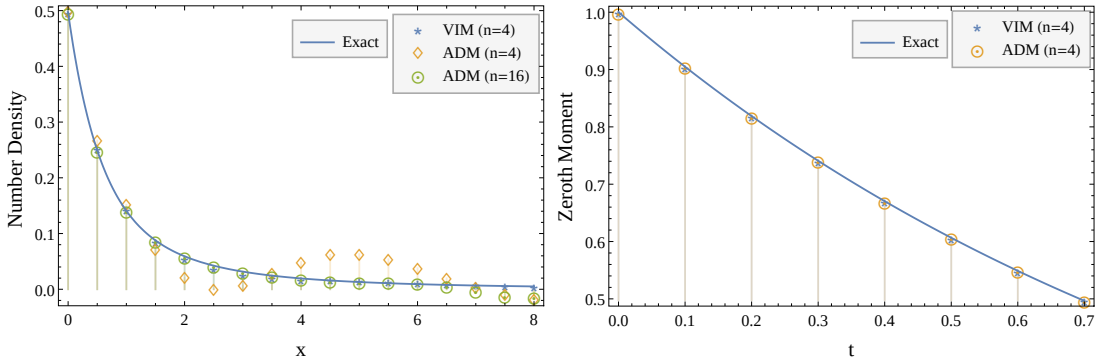

(a) Number density (b) Zeroth moment

Figure 2.7: Number density and zeroth moment for TC-4

Let us take $K(x,y) = xy$ and the initial condition $u_0(x) = e^{-x}$, the recursive relation (2.2.8) becomes

$$u_{n+1}(x,t) = u_n(x,t) - \int_0^t \left(\frac{\partial u_n(x,t)}{\partial t} - \frac{1}{2}\int_0^x xyu_n(x-y,t)u_n(y,t)dy + \int_0^\infty xyu_n(x,t)u_n(y,t)dy \right) dt. \tag{2.2.11}$$

Using the above defined relation, truncated solutions are obtained as

$$u_1(x,t) = e^{-x}\left(\frac{tx^3}{12} - tx + 1\right),$$
$$u_2(x,t) = e^{-x}\left(t^3\left(\frac{x^9}{544320} - \frac{x^7}{3780} + \frac{x^5}{180}\right) + t^2\left(\frac{x^6}{720} - \frac{x^4}{12} + \frac{x^2}{2}\right) + t\left(\frac{x^3}{12} - x\right) + 1\right),$$

and so on. The exact solution for this problem is provided in [16] as

$$u(x,t) = e^{(-(1+t)x)} \sum_{k=0}^{\infty} \frac{t^k x^{3k}}{(k+1)!\Gamma(2k+1)}.$$

Again, truncation errors are determined for $n = 2,3,4,5$ using both VIM and ADM by

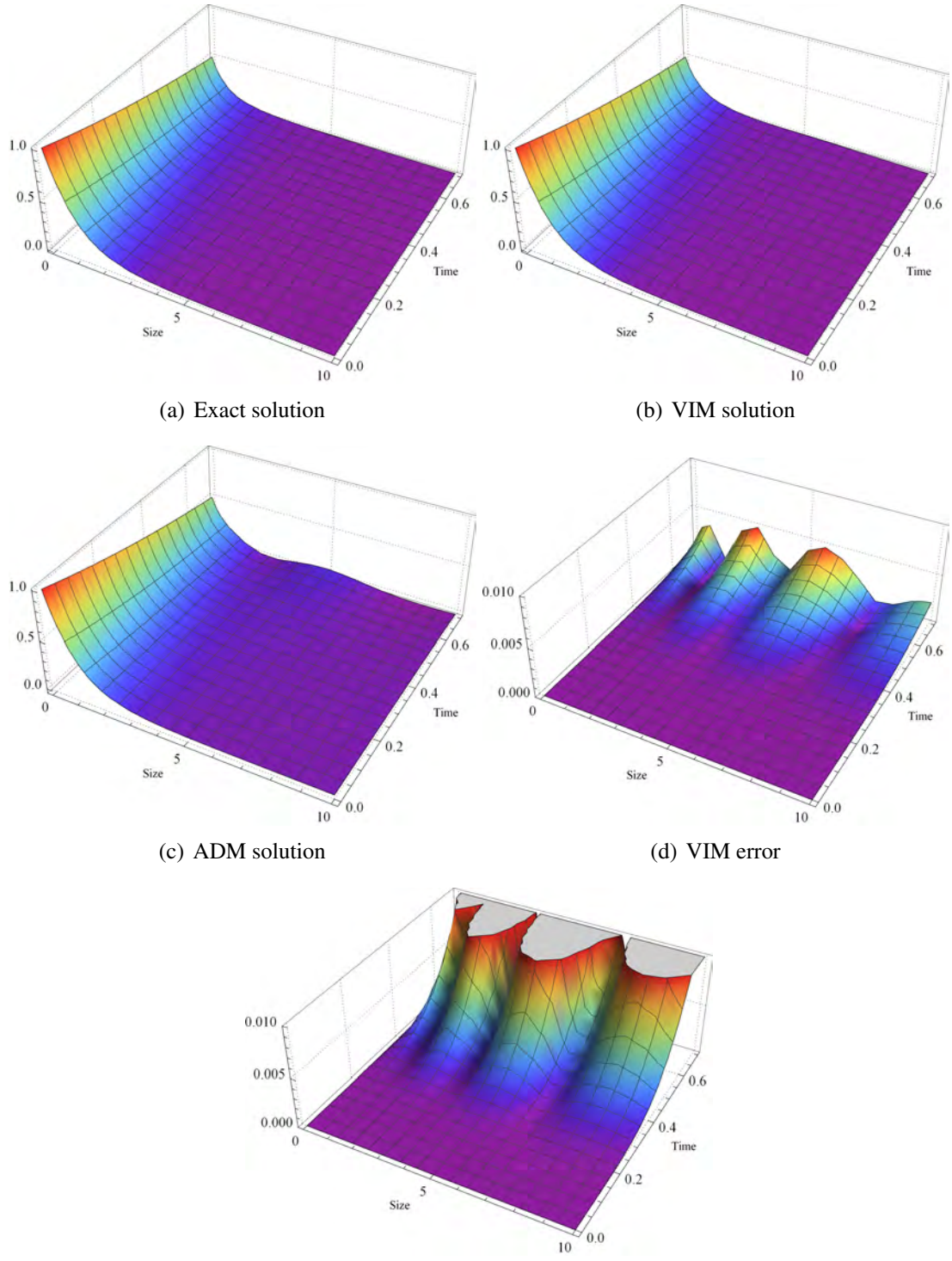

(a) Exact solution

(b) VIM solution

(c) ADM solution

(d) VIM error

(e) ADM error

Figure 2.8: Number density and absolute error for TC-4

n	2	3	4	5
ADM	0.178261	0.213002	0.200261	0.257254
VIM	0.146182	0.111638	0.0957513	0.0662966

Table 2.4: Truncation error when $t = 0.7$ and $x \in [0, 10]$ taking $h_i = 0.01$ for TC-5.

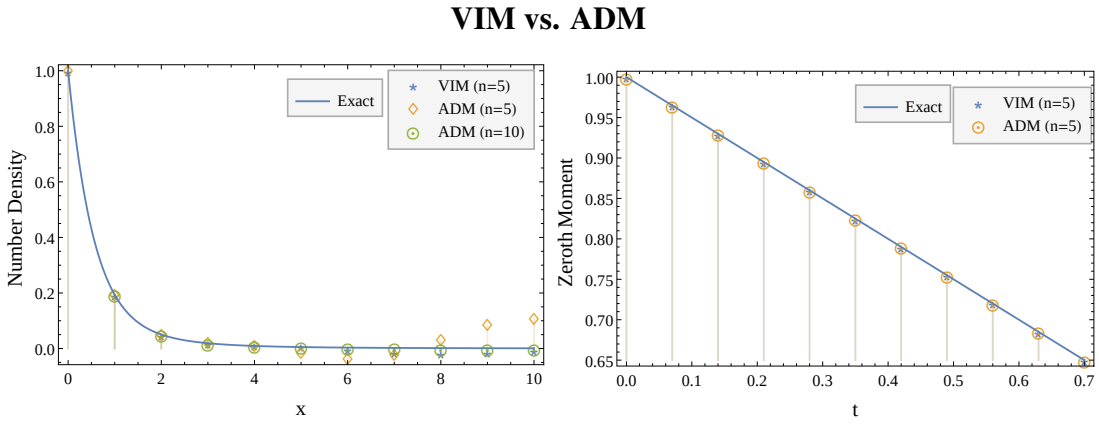

(a) Number density (b) Zeroth moment

Figure 2.9: Number density and the zeroth moment for TC-5

comparing the results with the exact solution in Table 2.4. It indicates that the error due to ADM is not only higher but having oscillatory nature while VIM consistently provides decreasing trend of errors with increasing n. Truncated solutions for number density and the zeroth moment at $t = 0.8$ are shown in Figure 2.9 along with the exact ones. As observed in the prior case, similar results are being pursued here. The exact number density and the VIM-based number density plots are identical taking $n = 5$ iterations. However, ADM reveals fluctuations in number density for $n = 5$ that can be improved by using a ten-term approximation. In addition to this, both these methods predict the zeroth moment accurately for $n = 5$, see Figure 2.9(b). The superiority of VIM over ADM is also justified from Figure 2.10 which represents $3D$ plots for the number density using $n = 5$ and the errors between the exact and approximate series solutions.

2.2.3 Aggregation-breakage equation

This subsection gives numerical implementation and comparison between VIM and ADM solutions for the aggregation-breakage equation. With the initial conditions e^{-x} and $4xe^{-2x}$,

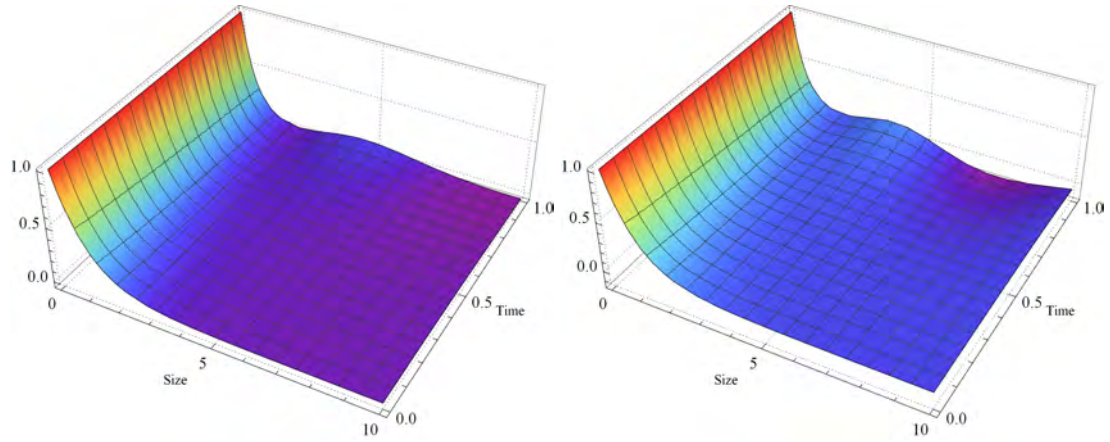

(a) Exact solution

(b) VIM solution

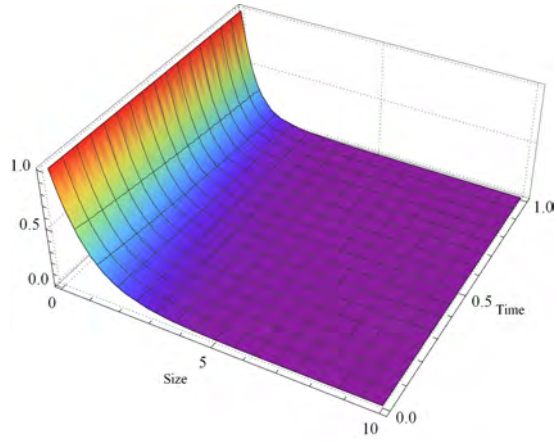

(c) ADM solution

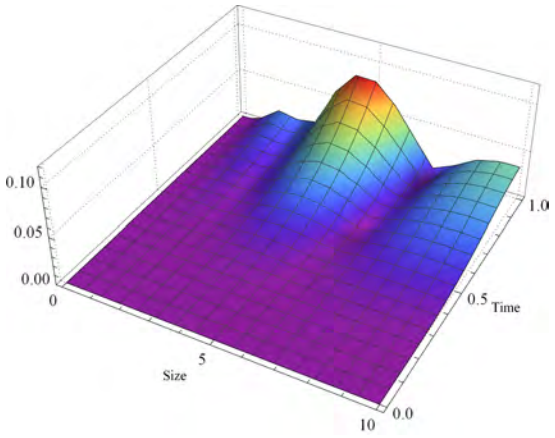

(d) VIM error

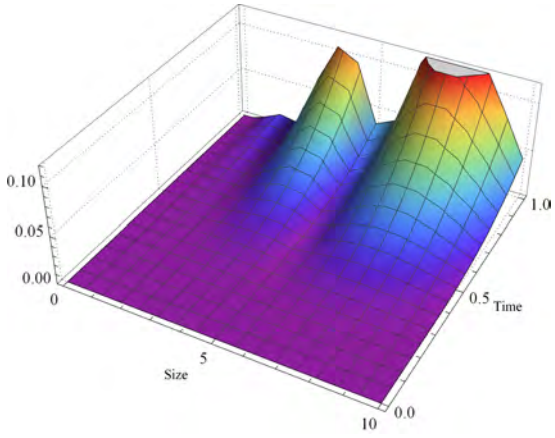

(e) ADM error

Figure 2.10: Number density and absolute error for TC-5

two test cases are investigated to solve the equation (2.0.1) in series form consisting of constant aggregation kernel $K(x,y)=1$, binary breakage kernel $B(x,y)=2/y$, selection rate $S(x)=x$ and growth rate $G=0$. Before proceeding to discussion of the numerical counterpart, let us write VIM and ADM iterations for the coupled model.

2.2.3.1 Variational iteration method

Using the VIM as defined in Section 2.1, considering $L=\frac{\partial}{\partial t}$ and the remaining terms as $N(u)$, iterations to solve the equation (2.0.1) with $G=0$ are governed by

$$\begin{aligned} u_{n+1}(x,t) =& u_n(x,t) - \int_0^t \left[\frac{\partial u_n(x,t)}{\partial t} - \frac{1}{2}\int_0^x K(x-y,y)u_n(x-y,t)u_n(y,t)dy \right. \\ &\left. + \int_0^\infty K(x,y)u_n(x,t)u_n(y,t)dy - \int_x^\infty B(x,y)S(y)u_n(y,t)dy + S(x)u_n(x,t) \right] dt. \end{aligned} \tag{2.2.12}$$

2.2.3.2 Adomian decomposition method

Following Section 2.2, operating L^{-1} on equation (2.0.1) having $G=0$ and by denoting the functions $f_1(u)=u(x-y,t)u(y,t)$ and $f_2(u)=u(x,t)u(y,t)$ lead to

$$\begin{aligned} u(x,t) = u_0(x) - \int_0^t \left[\frac{1}{2}\int_0^x K(x-y,y)f_1(u)dy - \int_0^\infty K(x,y)f_2(u)dy \right. \\ \left. + \int_x^\infty B(x,y)S(y)u(y,t)dy - S(x)u(x,t) \right] dt. \end{aligned}$$

According to [78], ADM introduces the solution $u(x,t)$ and the non-linear polynomials $f_i(u)$, $i=1,2$ as

$$u(x,t)=\sum_{j=0}^{\infty} c_j(x,t), \quad f_1(u)=\sum_{j=0}^{\infty} A_j, \quad f_2(u)=\sum_{j=0}^{\infty} B_j$$

where A_j and B_j are Adomian polynomials, given for $n\geq 1$ as

$$A_{n-1}=\sum_{j=0}^{n-1} c_j(x-y,t)c_{n-j-1}(y,t),$$

and

$$B_{n-1} = \sum_{j=0}^{n-1} c_j(x,t)c_{n-j-1}(y,t).$$

Thus, the scheme would be as follows

$$\begin{aligned} c_0(x,t) =& c_0, \\ c_n(x,t) =& -L^{-1}\left(\frac{1}{2}\int_0^x K(x-y,y)A_{n-1}dy - \int_0^\infty K(x,y)B_{n-1}dy + \int_x^\infty B(x,y)S(y)c_n(y,t)dy \right. \\ & \left. - S(x)c_n(x,t)\right), \quad n = 1,2,3,\cdots. \end{aligned} \tag{2.2.13}$$

Let us simplify the formulations (2.2.12) and (2.2.13) for the particular cases of kernels.

Test case 6: As mentioned, taking $K(x,y) = 1$, $B(x,y) = \frac{2}{y}$, $S(x) = x$, $G(x) = 0$ with initial condition $u(x,0) = e^{-x}$, the VIM iterations are obtained using (2.2.12) as

$$u_1(x,t) = e^{-x}\left(t\left(1-\frac{x}{2}\right)+1\right),$$

$$u_2(x,t) = e^{-x}\left(t^3\left(\frac{x^3}{144}-\frac{x^2}{12}+\frac{x}{4}-\frac{1}{6}\right)+t^2\left(\frac{x^2}{8}-\frac{x}{4}-\frac{1}{4}\right)+t\left(1-\frac{x}{2}\right)+1\right).$$

Proceeding in a similar pattern, higher order terms can be calculated using MATHEMATICA. Next, following (2.2.13), the first few iterations of the ADM solutions are

$$c_1(x,t) = -\frac{1}{2}te^{-x}(x-2), \quad c_2(x,t) = t^2e^{-x}\left(\frac{x^2}{8}-\frac{x}{4}-\frac{1}{4}\right),$$

$$c_3(x,t) = t^3e^{-x}\left(-\frac{x^3}{48}+\frac{x}{3}-\frac{1}{6}\right), \quad c_4(x,t) = t^4e^{-x}\left(\frac{x^4}{384}+\frac{x^3}{96}-\frac{5x^2}{48}-\frac{x}{24}+\frac{7}{48}\right).$$

Using MATHEMATICA, one can find further iterations and then the nth term approximate series solution is described as

$$u_n(x,t) = \sum_{j=0}^{n} c_j(x,t).$$

Since, the analytical solutions for the number density and the zeroth moment are not

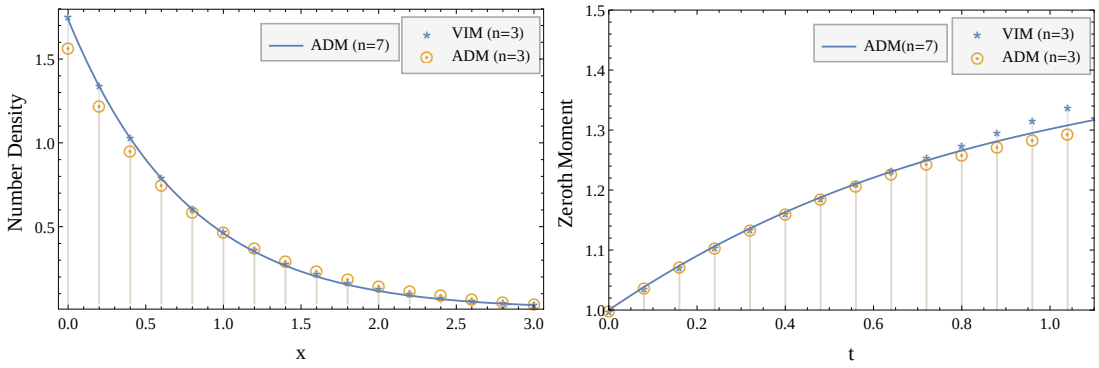

(a) Number density (b) Zeroth moment

Figure 2.11: Number density and zeroth moment for TC-6

available in this case, the solution components are plotted for both the methods using $n = 3$ and 7 for ADM and $n = 3$ for VIM. At $t = 1.1$, it can be seen from Figure 2.11 that the seven term ADM solution and the zeroth moment coincide with the three term truncated number density and the zeroth moment obtained using VIM. Same observations for number density are made from $3D$ plots presented in Figures 2.12(a)-(c). Moreover, considering three term VIM solution as a standard solution, Figures 2.12(d) and 2.12(e) depict that the error between three term VIM solution with seven term ADM solution is almost negligible as compared to the error with three term ADM solution.

Test case 7: Consider the same aggregation, breakage and growth kinetics parameters as taken in the previous Test case 6 but with different initial condition $u(x,0) = 4xe^{-2x}$. The first two iterations for VIM are computed as

$$u_1(x,t) = e^{-2x}\left(t\left(\frac{4x^3}{3} - 4x^2 + 2\right) + 4x\right),$$

$$u_2(x,t) = e^{-2x}\left(t^3\left(\frac{2x^7}{945} - \frac{4x^6}{135} + \frac{4x^5}{45} + \frac{2x^4}{9} - \frac{10x^3}{9} + \frac{2x^2}{3} + \frac{2x}{3} - \frac{1}{3}\right)\right.$$

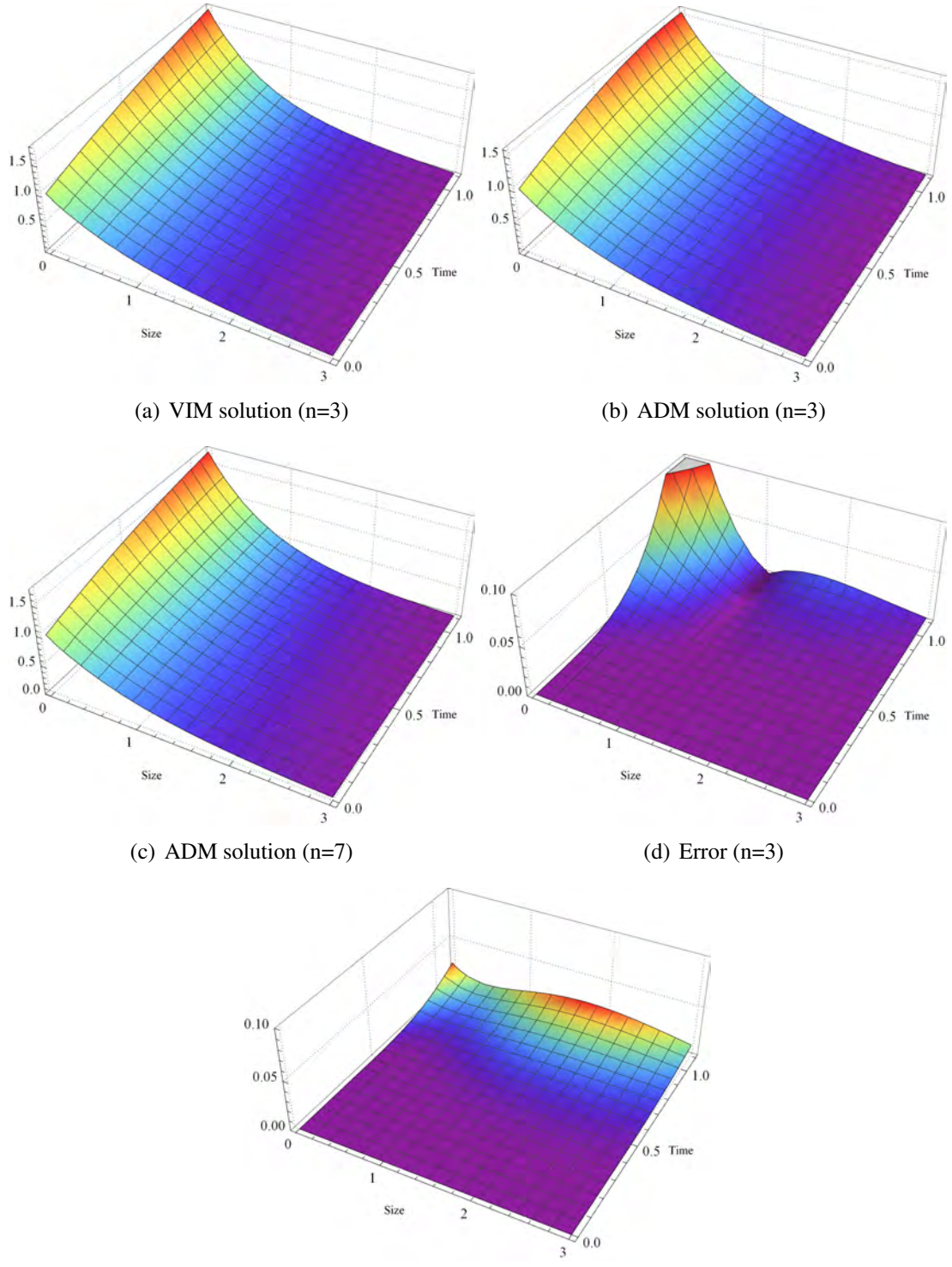

(a) VIM solution (n=3)

(b) ADM solution (n=3)

(c) ADM solution (n=7)

(d) Error (n=3)

(e) Error (n=7)

Figure 2.12: Number density and error for TC-6

$$+t^2\left(\frac{2x^5}{15}-\frac{4x^4}{3}+2x^3+3x^2-3x-\frac{1}{2}\right)+t\left(\frac{4x^3}{3}-4x^2+2\right)+4x\Big).$$

Due to complexity of the expression, we have not provided the higher terms here. For ADM, the first few terms of the series solution are

$$c_1(x,t)=te^{-2x}\left(\frac{4x^3}{3}-4x^2+2\right),\quad c_2(x,t)=t^2e^{-2x}\left(\frac{2x^5}{15}-\frac{4x^4}{3}+2x^3+3x^2-3x-\frac{1}{2}\right),$$

$$c_3(x,t)=t^3e^{-2x}\left(\frac{2x^7}{315}-\frac{2x^6}{15}+\frac{2x^5}{3}-\frac{31x^3}{9}+\frac{4x^2}{3}+\frac{13x}{6}-\frac{1}{3}\right),$$

$$c_4(x,t)=t^4e^{-2x}\left(\frac{x^9}{5670}-\frac{2x^8}{315}+\frac{x^7}{15}-\frac{x^6}{6}-\frac{5x^5}{9}+\frac{65x^4}{36}+\frac{17x^3}{18}-\frac{11x^2}{4}-\frac{x}{6}+\frac{7}{24}\right).$$

The comparison of three term VIM and ADM truncated solutions with seven term ADM

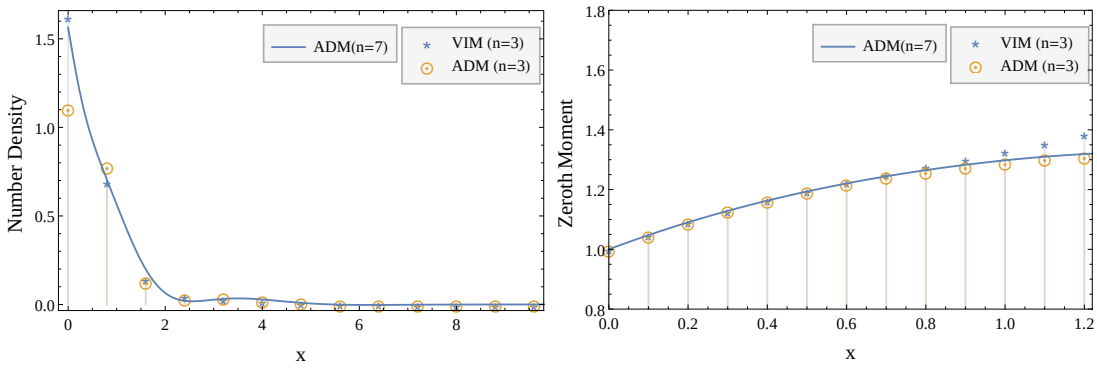

(a) Number density (b) Zeroth moment

Figure 2.13: Number density and zeroth moment for TC-7

approximate solution is shown in Figure 2.13. It is noticed that the ADM seven term truncated solution is nearly identical to the three term VIM solution, which is again ensured from 3*D* Figure 2.14. The errors between ADM seven term solution with three term solutions of VIM and ADM are presented in Figures 2.14(d) and 2.14(e), demonstrating

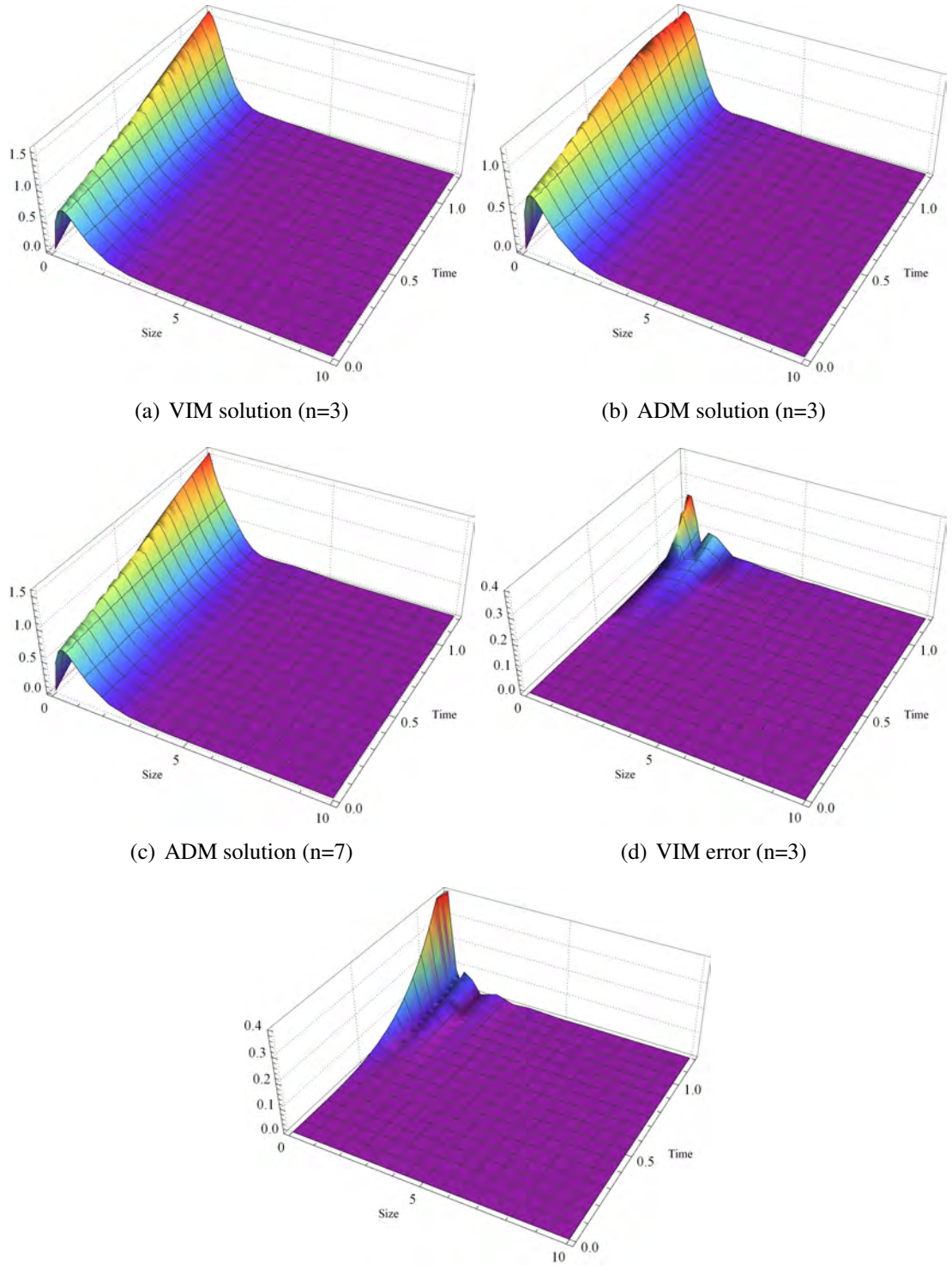

(a) VIM solution (n=3)

(b) ADM solution (n=3)

(c) ADM solution (n=7)

(d) VIM error (n=3)

(e) ADM error (n=3)

Figure 2.14: Number density and error for TC-7

that VIM outperforms ADM.

2.3 Conclusions

In comparison to the ADM, this chapter established that the VIM provided better estimates for solving the non-linear aggregation or coupled aggregation-breakage models for the number density and the zeroth moment. For the pure growth process, both formulations were exactly the same for the particle density and finite term series solutions were shown in excellent agreement with the analytical ones. Both ADM and VIM gave closed form solutions for the growth equation having constant growth rate. Further, to accelerate the accuracy of the solution, OVIM was implemented to solve the growth model and aggregation equation with constant kernel. However, the computational cost restricted us from applying the technique for other considered problems. The accuracy of VIM over ADM [16] for the aggregation model was shown by comparing the series approximated solutions and moment with the analytical solutions. Three different test cases were implemented to justify the better efficiency and accuracy of VIM over ADM. In addition, finite term solutions were computed for solving the coupled aggregation-breakage terms, and numerical simulations were compared between ADM and VIM results in the absence of analytical solutions. Despite the advantages of the VIM over ADM, we would like to enlighten the readers with some limitations of the method. It was observed that the terms obtained using VIM were quite complicated, and it was hard to find the closed-form solution. Additionally, it also required large computational cost for finding the higher order components of the series solution.

Chapter 3

Elzaki transform based accelerated homotopy perturbation method for multi-dimensional coagulation and coupled coagulation-fragmentation equations

This chapter aims to establish a semi-analytical approach based on the HPM to find the closed form or approximated solutions for the population balance equations such as Smoluchowski's coagulation, fragmentation, coupled coagulation-fragmentation, and bivariate coagulation equations. An accelerated form of the HPM is combined with the Elzaki transformation to improve the accuracy and efficiency of the method. The supremacy of the proposed scheme, called AHPETM, is demonstrated by taking several numerical examples for each problem. In addition, convergence of the series solution is also the key attraction of the work.

The considerable part of this chapter is published in Journal of Applied Analysis and Computation, 14(5),1-32, 2024

Let us recall the mathematical formulation of pure fragmentation equation 1.2.8,

$$\frac{\partial u(x,t)}{\partial t} = \int_x^\infty B(x,y)S(y)u(y,t)dy - S(x)u(x,t), \tag{3.0.1}$$

and the non-linear Smoluchowski's coagulation equation (1.2.5),

$$\frac{\partial u(x,t)}{\partial t} = \frac{1}{2}\int_0^x K(x-y,y)u(x-y,t)u(y,t)dy - \int_0^\infty K(x,y)u(x,t)u(y,t)dy, \tag{3.0.2}$$

with the initial condition $u(x,0) = f(x)$.

Further, the bivariate equation for the coagulation process is given by

$$\begin{aligned}\frac{\partial u(x,y,t)}{\partial t} =& \frac{1}{2}\int_0^x \int_0^y K(x-x',y-y',x',y')u(x-x',y-y',t)u(x',y',t)dx'dy' \\ &- \int_0^\infty \int_0^\infty K(x,x',y,y')u(x,y,t)u(x',y',t)dx'dy',\end{aligned} \tag{3.0.3}$$

with the initial condition $u(x,y,0) = u_0(x,y) \geq 0$.

The chapter is organized as follows: Section 3.1 discusses a brief outline of the Elzaki transformation. In Section 3.2, the general methodology of HPM and AHPETM are presented. In Section 3.3, AHPETM is developed for aforementioned population balance equations. Further, Section 3.4 gives a detailed convergence analysis of the proposed iterative scheme. In Section 3.5, the developed formulations are adopted to demonstrate solutions for several kernels and the supremacy of the scheme over HPM, ADM, HAM, and ODM solutions are shown by means of numerical simulations.

3.1 Elzaki transformation and its properties

Tarig Elzaki developed the Elzaki transformation in 2011 [84, 85], which is the modification of the general Laplace and Sumudu transformations to solve the differential equation in the time domain. In [84, 85], authors show the efficiency and accuracy of the Elzaki transformation on a large class of differential and integral equations. To understand the

definition of the transformation, consider a set

$$A = \left\{ f(t) : \exists M, k_1, k_2 > 0, |f(t)| < M e^{\frac{|t|}{k_j}}, \text{ if } t \in (-1)^j \times [0, \infty) \right\}$$

then the Elzaki transformation is defined as

$$E[f(t)] = T[v] = v \int_0^\infty f(t) e^{-\frac{t}{v}} dt, \quad t > 0,$$

and the inverse of Elzaki transformation [86] is defined as

$$E^{-1}[T[v]] = \frac{1}{2\pi i} \int_0^\infty e^{tv} T\left[\frac{1}{v}\right] v dv.$$

Some of the Elzaki transformation for standard functions are listed in Table 3.1.

Table 3.1: Properties of Elzaki transformation

$f(t)$	$E[f(t)]$
1	v^2
t^n	$n! v^{n+2}$
e^{at}	$\frac{v^2}{1-av}$
$E[f(t)+g(t)]$	$E[f(t)]+E[g(t)]$
$E[f^n(t)]$	$\frac{T[v]}{v^n} - \sum_{k=0}^{n-1} v^{2-n+k} f^k(0), \quad n \geq 1$

3.2 Methodology

In this section, we review the basics of HPM and AHPETM for solving general differential equations. Then the schemes are applied to solve multi-dimensional coagulation and coupled coagulation-fragmentation equations.

3.2.1 Review of HPM

Let us consider the general differential equation

$$D(c) - h(x) = 0, \quad x \in \Omega \tag{3.2.1}$$

with the boundary conditions

$$B\left(c, \frac{\partial c}{\partial n}\right) = 0, r \in \partial\Omega, \tag{3.2.2}$$

where D and B are the differential and boundary operators, respectively. One can usually decompose the differential operator into linear (L) and non-linear (N) operators, implying that equation (3.2.1) becomes

$$L(c) + N(c) - h(x) = 0. \tag{3.2.3}$$

Now, according to HPM, a homotopy $H : \Omega \times [0,1] \to \mathbb{R}$ is constructed that satisfies

$$H[v(x,p)] = (1-p)[L[v(r,p)] - L[(c_0)]] + p[D[v(r,p)] - h(x)] = 0, \tag{3.2.4}$$

where c_0 is the initial guess for the equation (3.2.1) and p is the embedding parameter that increases monotonically from 0 to 1. According to the HPM, we can write the solution of the equation (3.2.1) in the form of series as

$$v = \sum_{k=0}^{\infty} p^k v_k = v_0 + pv_1 + p^2 v_2 + \cdots. \tag{3.2.5}$$

Substituting equation (3.2.5) in (3.2.4) and letting $p \to 1$, the solution is obtained as follows

$$c = \lim_{p \to 1} v = \sum_{k=0}^{\infty} v_k. \tag{3.2.6}$$

3.2.2 Accelerated homotopy perturbation Elzaki transformation method

Consider a non-linear differential equation

$$\frac{\partial^n c}{\partial t^n} + L[c(x,t)] + N[c(x,t)] = b(x) \tag{3.2.7}$$

with the initial conditions $c^i(x,0) = g_i(x), \quad i = 0,1,2,\cdots,n-1$, where $c^i(x,t)$ denotes the i^{th} order derivative of $c(x,t)$ with respect to t. Taking Elzaki transformation and using its properties on equation (3.2.7) finally provide, by following [87],

$$E[c(x,t)] = \sum_{k=0}^{n-1} v^{k+2} c^k(x,0) + v^n E[b(x) - L[c(x,t)] - N[c(x,t)]]. \tag{3.2.8}$$

Now, applying the homotopy perturbation method to the equation (3.2.8), we get

$$(1-p)(E[c(x,t)] - E[c(x,0)]) + p\Bigg(E[c(x,t)] - \sum_{k=0}^{n-1} v^{k+2} c^k(x,0) - v^n E[b(x) - L[c(x,t)] - N[c(x,t)]]\Bigg) = 0. \tag{3.2.9}$$

Let the unknown function $c(x,t)$ and non-linear operator $N[c(x,t)]$ can be written in series form as

$$c(x,t) = \sum_{n=0}^{\infty} v_n p^n \tag{3.2.10}$$

and

$$N[c(x,t)] = \sum_{n=0}^{\infty} H_n p^n \tag{3.2.11}$$

where H_n represents the accelerated He's polynomial with

$$H_n(x,t) = N(\sum_{i=0}^{n} v_i) - \sum_{i=0}^{n-1} H_i, \text{ for } n \geq 1 \text{ and } H_0 = N(v_0). \tag{3.2.12}$$

Substituting the values of $c(x,t)$ and $N[c(x,t)]$ from the equations (3.2.10) and (3.2.11) into equation (3.2.9) give

$$E[\sum_{n=0}^{\infty} v_n p^n] = \sum_{k=0}^{n-1} v^{k+2} c^k(x,0) + p\left\{ v^n E\left[g(x) - L[\sum_{n=0}^{\infty} v_n p^k] + \sum_{n=0}^{\infty} H_n p^n \right] \right\}.$$

Applying inverse Elzaki transformation and comparing the coefficients of powers of p, the components of series solution, i.e., $v_i's$ are given in Table 3.2 and hence the solution of the

Table 3.2: Components of series solution

v_0	$c(x,0)$
v_1	$\sum_{k=1}^{n-1} \frac{t^k}{k!} c^k(x,0) + E^{-1}\{v^n E[b(x) - L[v_0] + H_0]\}$
v_2	$-E^{-1}\{v^n E[L[v_1] + H_1]\}$
$\vdots$	$\vdots$
v_n	$-E^{-1}\{v^n E[L[v_{n-1}] + H_{n-1}]\}$

equation (3.2.7) is obtained by taking $p \to 1$ in the equation (3.2.10).

3.3 AHPETM for coagulation fragmentation equations

In the below section, AHPETM is extended to solve Smoluchowski's coagulation, pure fragmentation, coupled coagulation-fragmentation and bivariate coagulation equations.

3.3.1 Smoluchowski's coagulation equation

Consider the non-linear aggregation equation (3.0.2) with initial condition $u(x,0) = u_0(x)$. Applying Elzaki transformation, an integral form is obtained as

$$E[u(x,t)] = v^2 u(x,0) + vE\left[\frac{1}{2}\int_0^x K(x-y,y)u(x-y,t)u(y,t)dy - \int_0^{\infty} K(x,y)u(x,t)u(y,t)dy\right]. \tag{3.3.1}$$

In order to apply the scheme, compare equation (3.3.1) with the transformed equation (3.2.8), which provides $L[u] = 0, \quad b(x) = 0$ and

$$N[u] = -\frac{1}{2}\int_0^x K(x-y,y)u(x-y,t)u(y,t)dy + \int_0^\infty K(x,y)u(x,t)u(y,t)dy. \tag{3.3.2}$$

Now, applying the HPM on equation (3.3.1) as defined in equation (3.2.9), we get

$$\begin{aligned}&(1-p)(E[u(x,t)] - E[u(x,0)]) + p\Bigg(E[u(x,t)] - v^2u(x,0) - \\ &vE\left[\frac{1}{2}\int_0^x K(x-y,y)u(x-y,t)u(y,t)dy - \int_0^\infty K(x,y)u(x,t)u(y,t)dy\right]\Bigg) = 0.\end{aligned} \tag{3.3.3}$$

According to the methodology defined in Section 3.2.2, $u(x,t) = \sum_{n=0}^{\infty} v_n p^n$ and the non-linear operator $N[u] = \sum_{n=0}^{\infty} H_n p^n$, where H_n for SCE is given by

$$\begin{aligned}H_n =& \frac{1}{2}\int_0^x K(x-y,y)\sum_{i=0}^{n} v_i(x-y,t)\sum_{i=0}^{n} v_i(y,t)dy \\ &- \int_0^\infty K(x,y)\sum_{i=0}^{n} v_i(x,t)\sum_{i=0}^{n} v_i(y,t)dy - \sum_{i=0}^{n-1} H_i, \quad n \geq 1,\end{aligned} \tag{3.3.4}$$

with $H_0 = N[v_0]$. Using the above defined decomposition in equation (3.3.3) and comparing the powers of p, the n^{th} component of the series solution is

$$\begin{aligned}v_{n+1}(x,t) = E^{-1}\Bigg\{&vE\Bigg(\frac{1}{2}\int_0^x K(x-y,y)\sum_{i=0}^{n} v_i(x-y,t)\sum_{i=0}^{n} v_i(y,t)dy \\ &- \int_0^\infty K(x,y)\sum_{i=0}^{n} v_i(x,t)\sum_{i=0}^{n} v_i(y,t)dy\Bigg) - \sum_{i=0}^{n} H_i\Bigg\}, \quad n > 0,\end{aligned} \tag{3.3.5}$$

where $v_0(x,t) = u(x,0)$ and hence, the n term truncated series solution is calculated by

$$\Psi_n^{SCE}(x,t) := \sum_{j=0}^{n} v_j(x,t). \tag{3.3.6}$$

3.3.2 Fragmentation equation

Considering the pure fragmentation equation (3.0.1) and applying Elzaki transformation, the following integral operator form is achieved

$$E[u(x,t)] = v^2 u(x,0) + E\left(\int_x^\infty B(x,y)S(y)u(y,t)dy - S(x)u(x,t)\right). \tag{3.3.7}$$

Next, equation (3.3.7) is compared with the equation (3.2.8) for the implementation of AHPETM. It is observed that for the case of pure breakage equation $N[u(x,t)] = b(x) = 0$ and

$$L[u(x,t)] = -\int_x^\infty B(x,y)S(y)u(y,t)dy + S(x)u(x,t).$$

By following the steps discussed in the previous Section 3.2.2, a homotopy is generated as follows

$$(1-p)\{E[u(x,t)] - E[u(x,0)]\} + p\Bigg(E[u(x,t)] - v^2 u(x,0) - vE\left[\int_x^\infty B(x,y)S(y)u(y,t)dy - S(x)u(x,t)\right]\Bigg). \tag{3.3.8}$$

According to the proposed method, AHPETM introduces the solution of unknown function $u(x,t)$ in the form of infinite series as $u(x,t) = \sum_{j=0}^{\infty} v_j(x,t)$. Substituting this into equation (3.3.8) and comparing the coefficients of the powers of p, provide the iterations for the solution as follows

$$v_{n+1}(x,t) = E^{-1}\left\{vE\left[\int_x^\infty B(x,y)S(y)v_n(x,t)dy - S(x)v_n(x,t)\right]\right\}, \quad n \geq 0 \tag{3.3.9}$$

where $v_0(x,t) = u(x,0)$ and the n term truncated solution will be provided as

$$\Psi_n^{FE}(x,t) := \sum_{j=0}^{n} v_j(x,t). \tag{3.3.10}$$

3.3.3 Coupled coagulation-fragmentation equation

The CCFE is governed by

$$\frac{\partial u(x,t)}{\partial t} = \frac{1}{2}\int_0^x K(x-y,y)u(x-y,t)u(y,t)dy - \int_0^\infty K(x,y)u(x,t)u(y,t)dy + \int_x^\infty B(x,y)S(y)u(y,t)dy - S(x)u(x,t). \quad (3.3.11)$$

Applying Elzaki transformation on both sides leads to

$$E[u(x,t)] = v^2u(x,0) + vE\left[\frac{1}{2}\int_0^x K(x-y,y)u(x-y,t)u(y,t)dy - \int_0^\infty K(x,y)u(x,t)u(y,t)dy + \int_x^\infty B(x,y)S(y)u(y,t)dy - S(x)u(x,t)\right]. \quad (3.3.12)$$

For the implementation of AHPETM, expression (3.3.12) is compared with (3.2.8) and the following observations are made

$$b(x) = 0, \quad L[u] = -\int_x^\infty B(x,y)S(y)u(y,t)dy + S(x)u(x,t),$$

and

$$N[u] = -\frac{1}{2}\int_0^x K(x-y,y)u(x-y,t)u(y,t) + \int_0^\infty K(x,y)u(x,t)u(y,t).$$

Following the procedure defined in Section 3.2.2, the iterations to solve the equation (3.3.11) are as follows

$$v_{n+1}(x,t) = E^{-1}\left\{vE\left(\frac{1}{2}\int_0^x K(x-y,y)\sum_{i=0}^n v_i(x-y,t)\sum_{i=0}^n v_i(y,t)dy - \int_0^\infty K(x,y)\sum_{i=0}^n v_i(x,t)\sum_{i=0}^n v_i(y,t)dy - \sum_{i=0}^n H_i + \int_x^\infty B(x,y)S(y)v_n(x,t)dy - S(x)v_n(x,t)\right)\right\}, \text{ for } n > 0 \quad (3.3.13)$$

where $v_0(x,t) = u(x,0)$. Let us denote the n term approximated series solution for CCFE as

$$\Psi_n^{CCFE}(x,t) := \sum_{j=0}^{n} v_j(x,t). \tag{3.3.14}$$

3.3.4 Bivariate Smoluchowski's coagulation equation

Consider 2D aggregation equation (3.0.3) with initial condition $u(x,y,0) = u_0(x,y)$ and applying Elzaki transformation, leads to form as

$$\begin{aligned} E[u(x,y,t)] =& v^2 u(x,y,0) + vE\left[\frac{1}{2}\int_0^x\int_0^y K(x-x',y-y',x',y')u(x-x',y-y',t)\right. \\ & \left. u(x',y',t)dy'dx' - \int_0^\infty\int_0^\infty K(x,x',y,y')u(x,y,t)u(x',y',t)dy'dx'\right]. \end{aligned} \tag{3.3.15}$$

In order to apply the AHPETM, equation (3.3.15) is compared with the transformed equation (3.2.8), implying that $L[u] = 0, \quad b(x) = 0$ and

$$\begin{aligned} N[u] =& -\frac{1}{2}\int_0^x\int_0^y K(x-x',y-y',x',y')u(x-x',y-y',t)u(x',y',t)dy'dx' \\ & + \int_0^\infty\int_0^\infty K(x,x',y,y')u(x,y,t)u(x',y',t)dy'dx'. \end{aligned} \tag{3.3.16}$$

Thanks to equation (3.2.9), applying the HPM on equation (3.3.15) enables us to have

$$\begin{aligned} & (1-p)(E[u(x,t)] - E[u(x,0)]) + p\Bigg(E[u(x,y,t)] - v^2u(x,y,0) - vE \\ & \left[\frac{1}{2}\int_0^x\int_0^y K(x-x',y-y',x',y')u(x-x',y-y',t)u(x',y',t)dy'dx'\right. \\ & \left. - \int_0^\infty\int_0^\infty K(x,x',y,y')u(x,y,t)u(x',y',t)dy'dx'\right]\Bigg) = 0. \end{aligned} \tag{3.3.17}$$

Again, following the idea of Section 3.2.2, $u(x,y,t)=\sum_{n=0}^{\infty} v_n p^n$ and non-linear operator $N[u]=\sum_{n=0}^{\infty} H_n p^n$ where H_n is being given by

$$\begin{aligned} H_n =& \frac{1}{2}\int_0^x K(x-x',y-y',x',y') \sum_{i=0}^{n} v_i(x-x',y-y',t) \sum_{i=0}^{n} v_i(x',y',t)dy'dx' \\ & - \int_0^{\infty} K(x,x',y,y') \sum_{i=0}^{n} v_i(x,y,t) \sum_{i=0}^{n} v_i(x',y',t)dy'dx' - \sum_{i=0}^{n-1} H_i \text{ with } H_0 = N[v_0]. \end{aligned} \tag{3.3.18}$$

Using the above defined decomposition in equation (3.3.17) and comparing the powers of p, we get the n^{th} component of the series solution as follows

$$\begin{aligned} v_{n+1}(x,y,t) =& E^{-1}\left\{ vE\left(\frac{1}{2}\int_0^x \int_0^y K(x-x',y-y',x',y') \sum_{i=0}^{n} v_i(x-x',y-y',t) \right.\right. \\ & \sum_{i=0}^{n} v_i(x',y',t)dy'dx' - \int_0^{\infty}\int_0^{\infty} K(x,x',y,y') \sum_{i=0}^{n} v_i(x,y,t) \\ & \left.\left. \sum_{i=0}^{n} v_i(x',y',t)dy'dx' \right) \right\}, \text{ for } n>0, \end{aligned} \tag{3.3.19}$$

where $v_0(x,y,t)=u(x,y,0)$. Let us denote the n term truncated solution by

$$\Psi_n^{BSCE}(x,y,t) := \sum_{j=0}^{n} v_j(x,y,t). \tag{3.3.20}$$

3.4 Convergence analysis

3.4.1 Smoluchowski's coagulation equation

Consider the Banach space $\mathbb{X}=\mathbb{C}([0,T]:\mathbb{L}^1[0,\infty),\|.\|)$ over the norm defined as

$$\|u\| = \sup_{s\in[0,t_0]} \int_0^{\infty} |u(x,s)|dx < \infty.$$

Let us use equation (3.3.1) in the operator form as

$$u(x,t) = \tilde{\mathcal{N}}[u]$$

where

$$\tilde{\mathcal{N}}[u] = u(x,0) + E^{-1}\{vE[N[u]]\} \tag{3.4.1}$$

and $N[u]$ is given by

$$N[u] = \frac{1}{2}\int_0^x K(x-y,y)u(x-y,t)u(y,t)dy - \int_0^\infty K(x,y)u(x,t)u(y,t)dy.$$

Theorem 1. *Let us consider the coagulation equation* (3.0.2) *with kernel* $K(x,y) = 1$ *for all* $x,y \in (0,\infty)$. *If* v_i^s *are the components of the series solution computed using* (3.3.5) *and* Ψ_n^{SCE} *being the n term truncated solution provided in equation* (3.3.6)*, then* Ψ_n^{SCE} *converges to the exact solution u with the error bound*

$$\|u - \Psi_n^{SCE}\| \leq \frac{\Delta^n}{1-\Delta}\|v_1\|$$

where $\Delta = t_0^2 e^{2t_0 L}(\|u_0\| + 2t_0L^2 + 2t_0L) < 1$ *and* $L = \|u_0\|(T+1)$.

Proof. Two separate phases complete the theorem's proof. The contractive nature of the non-linear operator $\tilde{\mathcal{N}}$ is initially demonstrated. Then convergence of the truncated solution towards the exact one is established.

Step 1: As presented in [16], equation (3.4.1) can be written in the equivalent form as

$$\frac{\partial}{\partial t}[u(x,t)\exp[H[x,t,u]]] = \frac{1}{2}\exp[H[x,t,u]]\int_0^x K(x-y,y)u(x-y,t)u(y,t)dy$$

where $H[x,t,u] = \int_0^t \int_0^\infty K(x,y)u(y,s)dyds$. Thus the equivalent operator $\tilde{N}$ is given by

$$\tilde{N}[u] = u(x,0)\exp[-H(x,t,u)] + \frac{1}{2}\int_0^t \exp[H(x,s,u) - H(x,t,u)]$$

$$\int_0^{\infty} K(x,y)u(x-y,s)u(y,s)dyds.$$

Since $\tilde{N}$ is contractive (Singh *et al.* established in [16]) and equivalent to $N[u]$, the non-linear operator $N[u]$ is also contractive, i.e.,

$$\|Nu - Nu^*\| \leq \delta\|u - u^*\|, \tag{3.4.2}$$

where $\delta := t_0 e^{2t_0 L}(\|u_0\| + 2t_0L^2 + 2t_0L) < 1$ (for suitably chosen t_0) and $L = \|u_0\|(T+1)$. Now, using the definition and basic properties of Elzaki and Laplace transformations as well as employing (3.4.2), we get

$$\begin{aligned}
\|\tilde{\mathcal{N}}u - \tilde{\mathcal{N}}u^*\| &= \|E^{-1}\{vE(N(u))\} - E^{-1}\{vE(N(u^*))\}\| \\
&= \left\| \frac{1}{2\pi}\int_0^{\infty}\left(\frac{1}{v^2}\int_0^{\infty}(Nu - Nu^*)e^{-tv}dt\right)e^{tv}vdv \right\| \\
&\leq \frac{1}{2\pi}\int_0^{\infty}\left(\frac{1}{v}\int_0^{\infty}\delta\|u-u^*\|e^{-tv}dt\right)e^{tv}dv \\
&= \frac{1}{2\pi}\int_0^{\infty}\frac{1}{v}\mathscr{L}(\delta\|u-u^*\|)e^{tv}dv \\
&= \mathscr{L}^{-1}\left\{\frac{1}{v^2}\mathscr{L}(\delta\|u-u^*\|)\right\} \leq \delta t_0\|u-u^*\| \text{ for a suitable } t_0.
\end{aligned}$$

Step 2: Now, in this phase, an n term truncated solution is computed using the iterations defined in (3.3.5) and then error is estimated. Given that,

$$\begin{aligned}
\Psi_n^{SCE} =& \sum_{i=0}^{n} v_i(x,t) \\
=& u(x,0) + E^{-1}\{vE(N(u_0))\} + E^{-1}\{vE(N(u_0+u_1) - H_0)\} + \cdots \\
&+ E^{-1}\{vE(N(\sum_{j=0}^{n-1}u_j) - \sum_{j=0}^{n-2}H_i)\} \\
=& u(x,0) + E^{-1}\{vE(N[v_0] + N[v_0+v_1] + \cdots + N[v_0+v_1+\cdots+v_{n-1}] - \\
&(H_0 + (H_0+H_1) + \cdots + (H_0+H_1+\cdots+H_{n-2})))\} \\
=& u(x,0) + E^{-1}\{vE(N(\Psi_{n-1}^{SCE}))\} = \tilde{\mathcal{N}}[\Psi_{n-1}^{SCE}].
\end{aligned}$$

Using the contractive mapping of $\tilde{\mathcal{N}}$ leads to

$$\|\Psi_{n+1}^{SCE} - \Psi_n^{SCE}\| \leq \Delta \|\Psi_n^{SCE} - \Psi_{n-1}^{SCE}\|,$$

and thus, we have

$$\|\Psi_{n+1}^{SCE} - \Psi_n^{SCE}\| \leq \Delta^n \|\Psi_1^{SCE} - \Psi_0^{SCE}\|.$$

Using the triangle inequality for all $n, m \in \mathbb{N}$ with $n > m$, we have

$$\begin{aligned}
\|\Psi_n^{SCE} - \Psi_m^{SCE}\| &\leq \|\Psi_n^{SCE} - \Psi_{n-1}^{SCE}\| + \|\Psi_{n-1}^{SCE} - \Psi_{n-2}^{SCE}\| + \cdots + \|\Psi_{m+1}^{SCE} - \Psi_m^{SCE}\| \\
&\leq (\Delta^{n-1} + \Delta^{n-2} + \cdots + \Delta^m) \|\Psi_1^{SCE} - \Psi_0^{SCE}\| \\
&= \frac{\Delta^m (1 - \Delta^{n-m})}{1 - \Delta} \|u_1\| \leq \frac{\Delta^m}{1 - \Delta} \|u_1\|,
\end{aligned}$$

which converges to zero as $m \to \infty$, implies that there exists a Ψ such that $\lim_{n \to \infty} \Psi_n^{SCE} = \Psi$. Therefore,

$$u(x,t) = \sum_{i=0}^{\infty} v_i = \lim_{n \to \infty} \Psi_n^{SCE} = \Psi,$$

which is the exact solution of the coagulation equation (3.0.2). The theoretical error is obtained by fixing m and letting $n \to \infty$ in the above formulation. □

3.4.2 Pure breakage equation

Let $\mathbb{X} = \mathbb{C}([0,T] : \mathbb{L}^1[0,\infty), \|.\|])$ be a Banach space with the norm

$$\|u\| = \sup_{t \in [0,t_0]} \int_0^{\infty} e^{\lambda x} |u(x,t)| dx, \text{ where } \lambda > 0. \tag{3.4.3}$$

Now, equation (3.0.1) can be rewritten in the operator form as

$$u = \tilde{\mathscr{L}}[u] = u(x,0) + E^{-1} v E(L[u])$$

with $L[u]$ being the right-hand side of equation (3.0.1).

Theorem 2. *Let Ψ_n^{FE} be the n term truncated series solution of the fragmentation problem defined in equation (3.0.1). Then Ψ_n^{FE} converges to the exact solution and provides the error estimates*

$$\|u-\Psi_n^{FE}\| \leq \frac{\vartheta^n}{1-\vartheta}\|v_1\|, \tag{3.4.4}$$

where v_1 is provided in equation (3.3.9), if the following conditions hold

B1. $B(x,y)=c\dfrac{x^{r-1}}{y^r}$ *where* $r=1,2,3,\cdots$ *and c is a +ve constant satisfying* $\int_0^y xB(x,y)dx=y$,

B2. $S(x)\leq x^k$, *where* $k=1,2,3,\cdots$,

B3. λ *is chosen such that* $e^{\lambda y}-1<1$,

B4. $\vartheta:=\dfrac{k!(t_0)^2}{\lambda^{k+1}}<1$ *for suitable* t_0.

Proof. Let us begin with the proof that the operator $\tilde{\mathscr{L}}$ is contractive. In order to do so, we use the fact that the operator $L[u]$ is a contractive operator under the assumptions mentioned in B1-B3, i.e., $\|L[u]-L[u^*]\|\leq\rho\|u-u^*\|$ where $\rho=\dfrac{k!t_0}{\lambda^{k+1}}<1$ by following ([16] Theorem 2.1). Now, thanks to Elzaki and Laplace transformations, one can write

$$\begin{aligned}
\|\mathscr{L}[u]-\mathscr{L}[u^*]\| &= \|E^{-1}\{vE(L[u])\}-E^{-1}\{vE(L[u^*])\}\| \\
&= \left\|\frac{1}{2\pi}\int_0^\infty\left(\frac{1}{v^2}\int_0^\infty(Lu-Lu^*)e^{-tv}dt\right)e^{tv}vdv\right\| \\
&\leq \frac{1}{2\pi}\int_0^\infty\left(\frac{1}{v}\int_0^\infty\rho\|u-u^*\|e^{-tv}dt\right)e^{tv}dv \\
&= \frac{1}{2\pi}\int_0^\infty\frac{1}{v}\mathscr{L}(\rho\|u-u^*\|)e^{tv}dv \\
&= \mathscr{L}^{-1}\left\{\frac{1}{v}\mathscr{L}(\rho\|u-u^*\|)\right\}\leq\vartheta\|u-u^*\| \text{ where } \vartheta=\rho t_0.
\end{aligned}$$

We proceed further to obtain the estimate (3.4.4). By using the iteration formula (3.3.9), the n-term truncated solution is computed as

$$\begin{aligned}\Psi_n^{FE} =& E^{-1}\{vE[v_0]\} + E^{-1}\{vE[v_1]\} + \cdots + E^{-1}\{vE[v_{n-1}]\} \\ =& E^{-1}\{vE[v_0 + v_1 + \cdots + v_{n-1}]\} = E^{-1}\{vE[\Psi_{n-1}^{FE}]\}.\end{aligned}$$

Therefore, we have

$$\|\Psi_{n+1}^{FE} - \Psi_n^{FE}\| \leq \vartheta \|\Psi_n^{FE} - \Psi_{n-1}^{FE}\| \leq \vartheta^n \|\Psi_1^{FE} - \Psi_0^{FE}\|.$$

The above can be used to establish the following, for all $n, m \in \mathbb{N}$ with $n > m$,

$$\begin{aligned}\|\Psi_n^{FE} - \Psi_m^{FE}\| &\leq \|\Psi_n^{FE} - \Psi_{n-1}^{FE}\| + \|\Psi_{n-1}^{FE} - \Psi_{n-2}^{FE}\| + \cdots + \|\Psi_{m+1}^{FE} - \Psi_m^{FE}\| \\ &\leq (\vartheta^{n-1} + \vartheta^{n-2} + \cdots + \vartheta^m)\|\Psi_1^{FE} - \Psi_0^{FE}\| \\ &= \frac{\vartheta^m(1-\vartheta^{n-m})}{1-\vartheta}\|v_1\| \leq \frac{\vartheta^m}{1-\vartheta}\|v_1\|.\end{aligned}$$

Thanks for Hypothesis B4, the above tends to zero as $m \to \infty$ which means that there exists a Ψ such that $\lim_{n\to\infty} \Psi_n^{FE} = \Psi$. Thus, we obtain the exact solution of the breakage equation (3.0.1) as

$$u(x,t) = \sum_{i=0}^{\infty} v_i = \lim_{n\to\infty} \Psi_n^{FE} = \Psi.$$

□

3.4.3 Bivariate Smoluchowski's coagulation equation

Consider a Banach space $X = \mathbb{C}([0,T] : L^1[0,\infty) \times L^1[0,\infty), \|.\|)$ with the enduced norm

$$\|u\| = \sup_{s\in[0,t_0]} \int_0^{\infty}\int_0^{\infty} |u(x,y,s)|dxdy < \infty.$$

To demonstrate the convergence analysis, let us write the operator form of the equation (3.3.15) as

$$u = \tilde{Q}[u], \tag{3.4.5}$$

where $\tilde{Q}$ is given by

$$\tilde{Q}[u] = u_0(x,y) + E^{-1}[vE[Q[u]]] \tag{3.4.6}$$

and

$$\begin{aligned} Q[u] = &-\frac{1}{2}\int_0^x \int_0^y K(x-x',y-y',x',y')u(x-x',y-y',t)u(x',y',t)dy'dx' \\ &+ \int_0^\infty \int_0^\infty K(x,x',y,y')u(x,y,t)u(x',y',t)dy'dx'. \end{aligned}$$

The iterative scheme's convergence concept is splitted into two components, firstly, we establish that the operator $\tilde{Q}$ is contractive (Theorem 3) and then proceed further to discuss the worst case upper bound for error (Theorem 4) below. To show the operator $\tilde{Q}$ is contractive, initially we prove that Q is contractive. To do so, an equivalent form of the equation (3.0.3) is taken as

$$\begin{aligned} \frac{\partial}{\partial t}[u(x,y,t)\exp[R(x,y,t,u)]] = \frac{1}{2}\exp[R(x,y,t,u)] \int_0^x \int_0^y K(x-x',x',y-y',y') \\ u(x-x',y-y',t)u(x',y',t)dy'dx', \end{aligned} \tag{3.4.7}$$

where $R(x,y,t,u) = \int_0^t \int_0^\infty \int_0^\infty K(x,x',y,y')u(x',y',t)dx'dy'dt$. Thus the equivalent operator $\mathscr{N}$ is given by

$$\begin{aligned} \mathscr{N}[u] = u(x,y,0)\exp[-R(x,y,t,u)] + \frac{1}{2}\int_0^t \exp[R(x,y,s,u) - R(x,y,t,u)] \\ \int_0^x \int_0^y K(x-x',x',y-y',y')u(x-x'y-y',s)u(x',y',s)dy'dx'ds. \end{aligned} \tag{3.4.8}$$

Since, $\mathscr{N}$ and Q are equivalent, it is sufficient to show that $\mathscr{N}$ is contractive.

Theorem 3. *The operator $\tilde{Q}$, defined in equation (3.4.6) is contractive for all $u, u^* \in \mathbb{X}$ if the following conditions*

- $K(x,x',y,y') = 1 \quad \forall x,x',y,y' \in (0,\infty)$ *and*
- $\Delta = t_0^2 e^{2t_0 L}(\|u\| + 2t_0L^2 + 2t_0L) < 1$ *where* $L = \|u_0\|(T+1)$ *hold.*

Proof. Consider $u, u^* \in \mathbb{X}$, then

$$\begin{aligned}\mathscr{N}[u] - \mathscr{N}[u^*] =& u(x,y,0)\exp[-R(x,y,t,u)] - u^*(x,y,0)\exp[-R(x,y,t,u^*)] \\ &+ \frac{1}{2}\int_0^t \exp[R(x,y,s,u) - R(x,y,t,u)] \int_0^x \int_0^y u(x-x',y-y',s) \\ &u(x',y',s)dy'dx'ds - \frac{1}{2}\int_0^t \exp[R(x,y,s,u^*) - R(x,y,t,u^*)] \\ &\int_0^x \int_0^y u^*(x-x'y-y',s)u^*(x',y',s)dy'dx'ds.\end{aligned}$$

Let us define an another operator

$$H[x,y,s,t] = \exp\{R[x,y,s,u] - R[x,y,t,u]\} - \exp\{R[x,y,s,u^*] - R[x,y,t,u^*]\}.$$

It can be easily proven that

$$|H[x,y,s,t]| \leq (t-s)\exp\{(t-s)B\}\|u-u^*\| \leq B_1\|u-u^*\|,$$

where $B_1 = te^{tB}$ and $B = \max\{\|u\|, \|u^*\|\}$. Further,

$$\begin{aligned}\mathscr{N}[u] - \mathscr{N}[u^*] =& u_0(x,y)H(x,y,0,t) + \frac{1}{2}\int_0^t H(x,y,s,t)\int_0^x \int_0^y u(x-x',y-y',s) \\ &u(x',y',s)dy'dx'ds + \frac{1}{2}\int_0^t \exp[R(x,y,s,u^*) - R(x,y,t,u^*)] \\ &\Bigg[\int_0^x \int_0^y u^*(x-x'y-y',s)\{u(x',y',s) - u^*(x',y',s)\}dy'dx' \\ &+ \int_0^x \int_0^y u(x',y',s)\{u(x-x',y-y',s) - u^*(x-x',y-y',s)\}dx'dy'\Bigg]ds. \quad (3.4.9)\end{aligned}$$

To show the non-linear operator $\mathscr{N}$ is contractive, a set D is defined such as $D = \{u \in \mathbb{X} : \|u\| \leq 2L\}$. Taking norm on both sides of (3.4.9) provides

$$\begin{aligned}
\|\mathscr{N}[u] - \mathscr{N}[u^*]\| &\leq B_1\|u-u^*\|\|u_0\| + B_1\|u-u^*\| \int_0^t \left[\frac{1}{2}\|u\|^2\right] ds \\
&\quad + \int_0^t B_1 \left[\frac{1}{2}(\|u\| + \|u^*\|)\|u-u^*\|\right] ds \\
&\leq B_1 \left[\|u_0\| + \frac{1}{2}t\|u\|^2 + \frac{1}{2}t(\|u\| + \|u^*\|)\right] \|u-u^*\| \\
&\leq t_0 e^{2t_0 L} \left[\|u_0\| + 2t_0L^2 + \frac{1}{2}t_0(2L+2L)\right] \|u-u^*\| \\
&= \delta\|u-u^*\|,
\end{aligned}$$

for a suitable choice of t_0. So, the operator $\mathscr{N}$ is contractive if $\delta = t_0 e^{2t_0 L}\left[\|u_0\| + 2t_0L^2 + 2t_0L\right] < 1$, hence Q is contractive. Now we are in position to demonstrate that $\tilde{\mathscr{Q}}$ is contractive. Consider,

$$\begin{aligned}
\|\tilde{Q}u - \tilde{Q}u^*\| &= \|E^{-1}(vE[Qu]) - E^{-1}(vE[Qu^*])\| \\
&= \|\frac{1}{2\pi}\int_0^\infty \left(\frac{1}{v^2}\int_0^\infty (Qv - Qv^*)e^{-vt}dt\right) e^{vt} v dv\| \\
&\leq \frac{1}{2\pi}\int_0^\infty \left(\frac{1}{v}\int_0^\infty \|Qu - Qu^*\|e^{-vt}dt\right) e^{vt}dp \\
&\leq \frac{1}{2\pi}\int_0^\infty \left(\frac{1}{v}\int_0^\infty \delta\|u-u^*\|e^{-vt}dt\right) e^{vt}dv \\
&= \frac{1}{2\pi}\int_0^\infty \frac{1}{v}\mathscr{L}(\delta\|u-u^*\|)e^{vt}dv \\
&= \mathscr{L}^{-1}\left\{\frac{1}{v}\mathscr{L}(\delta\|u-u^*\|)\right\} = \delta t_0\|u-u^*\| = \Delta\|u-u^*\|.
\end{aligned}$$

Hence, the above accomplishes the contractive nature of $\tilde{Q}$. □

Theorem 4. *Assuming that the criteria of Theorem 3 holds and v_i's are the elements of the series solution calculated by equation (3.3.19). Then the series solution converges to the*

exact solution with the error bound

$$\|u - \Psi_n^{BCSE}\| = \frac{\Delta^n}{1-\Delta}\|v_1\|,$$

whenever $\Delta < 1$ *and* $\|v_1\| < \infty$.

Proof. The proof is similar to the Theorem 1, hence it is omitted here. □

Remark 3.4.1. *It is worth mentioning that the iterations and hence the finite term series solutions, computed using the HAM [8], HPM [9], ADM [16] and ODM [19] are identical to the iterations obtained using the AHPETM for the breakage equation which is linear. As a result, we have omitted the numerical implementations for pure breakage equation. So, the main focus of all the approaches is on approximating the non-linearity, which has no bearing on the linearity in the equations.*

3.5 Numerical results and discussion

This section verifies numerically the effectiveness of the suggested approach for coagulation, combined fragmentation-coagulation, and bivariate aggregation equations. Three physical test cases are considered and results for the number density and moments are compared with the precise solution as well as established and recently developed methods (ADM, HPM, HAM, ODM) for SCE. Due to the improved and significant results noticed in SCE, the numerical implementation is made for solving the coupled CFE and BSCE. Two test cases of CFE and one example of BSCE are taken into account to justify the effectiveness of our scheme.

3.5.1 Smoluchowski's coagulation equation

Example 3.5.1. *Consider the case of constant aggregation kernel* $K(x,y) = 1$ *with the exponential initial data* $u(x,0) = e^{-x}$ *and for this the exact solution*

$$u(x,t) = \frac{4}{(2+t)^2} e^{-\frac{2x}{2+t}},$$

is discussed in [16].

Employing the equations (3.3.5) and (3.3.6), first three components of the series solutions are given as follows

$$v_0(x,t) = e^{-x}, \quad v_1(x,t) = \frac{1}{2}te^{-x}(x-2),$$

$$v_2(x,t) = t^3\left(\frac{x^3}{144} - \frac{x^2}{12} + \frac{x}{4} - \frac{1}{6}\right)e^{-x} + t^2\left(\frac{x^2}{8} - \frac{3x}{4} + \frac{3}{4}\right)e^{-x},$$

$$\begin{aligned} v_3(x,t) =& \frac{1}{40642560}t^3e^{-x}\Big(t^4x^7 + 14t^3(7-4t)x^6 + 588(t-2)t^2(2t-3)x^5 \\ & - 2940t(t(t(4t-21)+36)-24)x^4 + 11760(5(t-4)t((t-3)t+6)+48)x^3 \\ & - 35280(t(t(t(4t-35)+120)-240)+192)x^2 + 70560\Big(t\Big(t(t(2t-21)+90) \\ & - 240\Big) + 288\Big)x - 10080(t(t(t(4t-49)+252)-840)+1344)\Big). \end{aligned}$$

It is essential to mention here that the components v_i are quite complicated and due to the complexity of the terms, it is hard to find a closed-form solution. Therefore, a three-term truncated solution is considered. However, thanks to MATHEMATICA, one can compute the higher order terms using equation (3.3.5). To see the accuracy of proposed method, the approximated three-term and exact solutions are plotted in Figures 3.1(a) and 3.1(b). One can scrutinize that the AHPETM solution shows a remarkable agreement with the exact one. Table 3.3 depicts the numerical errors of AHPETM at different time levels for $n = 3,4,5$ and 6 using the formula

$$\text{Error} = \Delta_m = \sum_{i=1}^{m} |u_n(x_i,t) - u(x_i,t)|h_i, \tag{3.5.1}$$

where m defines the number of subintervals, h_i the length of the interval and $u(x,t)$ is the exact solution provided in [16]. As one can notice, the inaccuracy grows as time increases

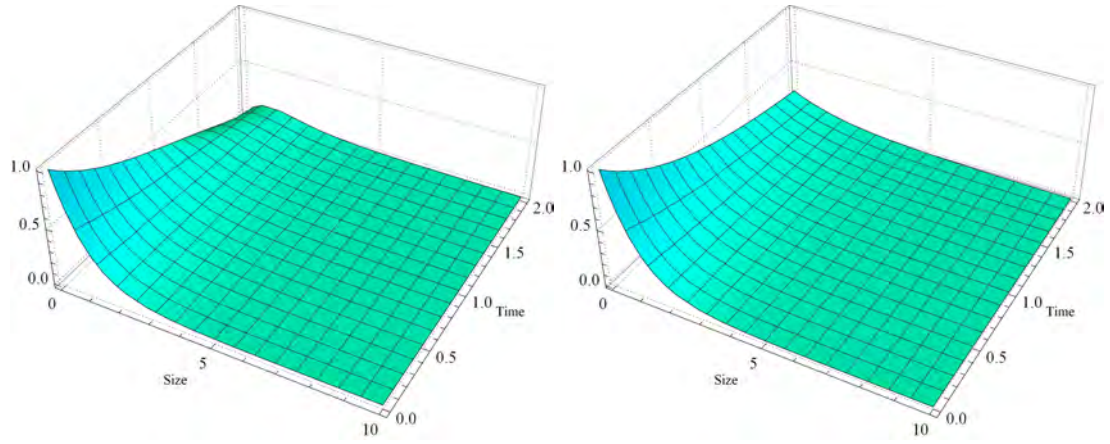

(a) AHPETM ($n = 3$) (b) Exact solution

Figure 3.1: Number density for AHPETM and exact solutions for Example 3.5.1

Table 3.3: Numerical errors at $t = 0.5, 1, 1.5$ and 2 for $n = 3, 4, 5, 6$ for Example 3.5.1

n	$t = 0.5$	$t = 1$	$t = 1.5$	$t = 2$
3	0.0014	0.0153	0.0543	0.1239
4	1.366×10^{-4}	2.656×10^{-3}	1.294×10^{-2}	3.632×10^{-2}
5	1.072×10^{-5}	3.7972×10^{-4}	2.5718×10^{-3}	9.0682×10^{-3}
6	7.154×10^{-7}	4.6146×10^{-5}	4.3241×10^{-4}	1.8931×10^{-3}

for a fixed number of terms and error decreases when more terms in the approximated solutions are taken into account. Further, to see the beauty of our algorithm, errors between exact and AHPETM solutions are compared with the errors between exact and other well-established approximated solutions obtained via HPM/ADM/HAM and ODM in Figure 3.2. It is important to point out here that the HAM [8]/ADM [16]/HPM [9] provide the same iterations and hence the identical finite term series solution for the considered model. It is noticed that HPM is very badly approximated in comparison to ODM while AHPETM further improves the error of ODM very significantly. Figure 3.2(a) represents the concentration of particles at time $t = 2$ and the solutions obtained using HPM and ODM blow up where the AHPETM solution matches well with the exact

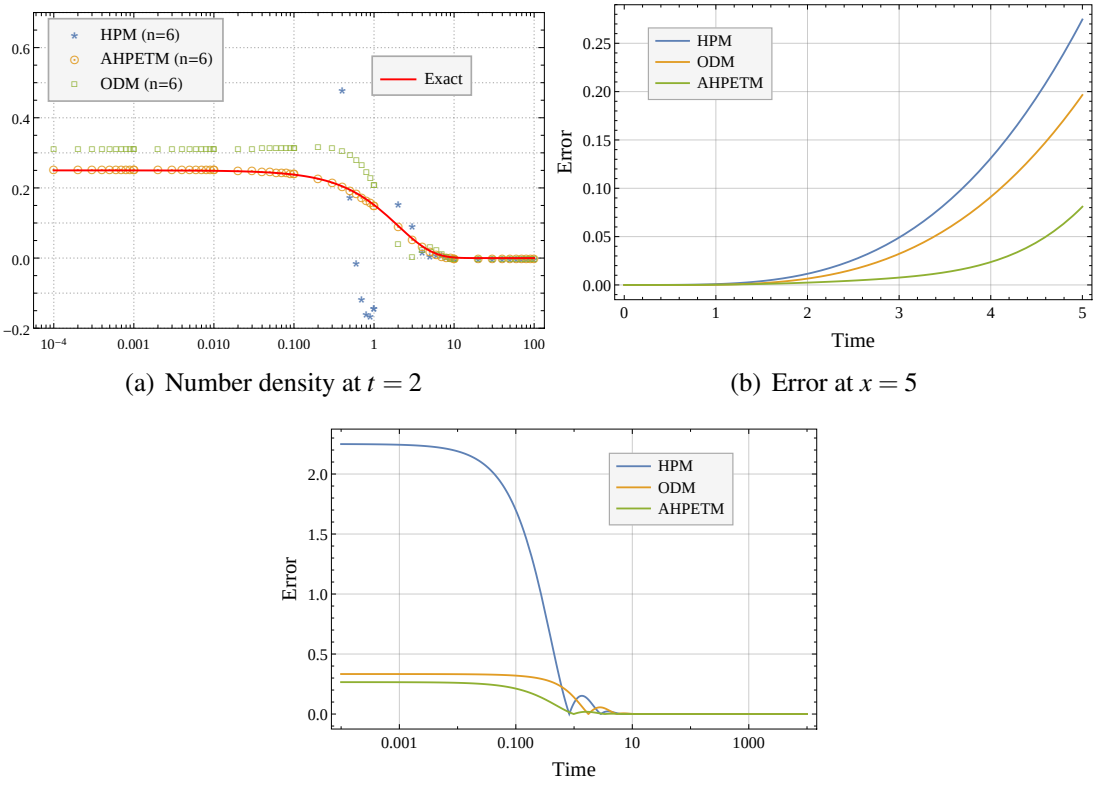

(a) Number density at $t = 2$

(b) Error at $x = 5$

(c) Error at $t = 2$

Figure 3.2: Number density and error for Example 3.5.1

solution. Results for error from Figure 3.2(b) indicate that all the schemes are quite efficient for a short time where as for a significant time, the errors due to HPM and ODM are relatively very high compared to AHPETM. Further, Figure 3.2(c) depicts the error plots of approximated solutions with precise solution for a fixed time $t = 2$ and it is observed that the AHPETM performs well over HPM and ODM for large space domain. In addition to this, integral properties associated with number density are plotted in Figure 3.3. The zeroth (total number of particles), first (total mass) and second (energy dispersed by the system) moments are displayed and comparison are made with the precise moments. In Figure 3.3(a), AHPETM offers superior approximations in the zeroth moment while HPM under predicts the result and deviates almost exponentially from the exact one. ODM shows much better approximation than HAM but still suffers fluctuations. In Figure 3.3(b), the first moments of AHPETM and HPM exhibit close correspondence with the precise

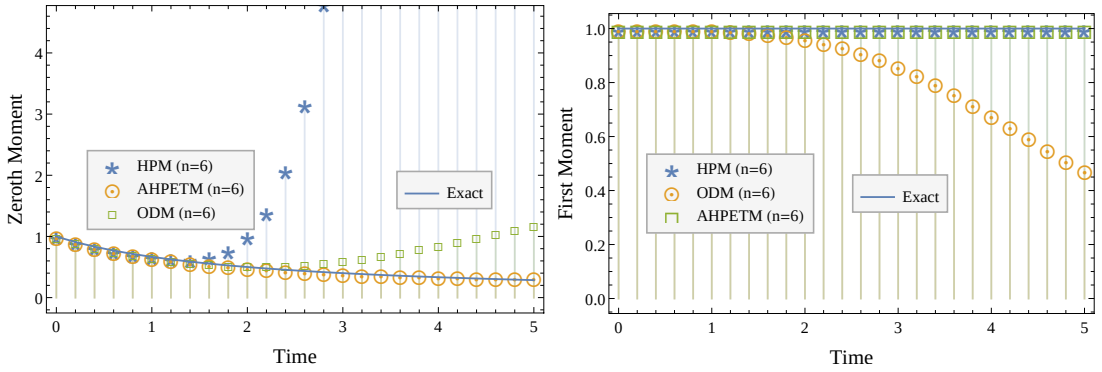

(a) Zeroth moments

(b) First moments

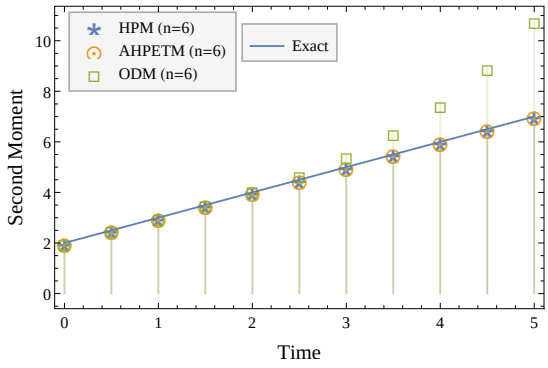

(c) Second moments

Figure 3.3: Zeroth, first and second moments for Example 3.5.1

moments, whereas ODM demonstrates a decline in precision. Notably, AHPETM and HPM yield solutions that conserve mass effectively, contrasting with ODM's inability to replicate the model's dynamics accurately. As shown in Figure 3.3(c), AHPETM continues to be the best option as the second moment produced by AHPETM and HPM coincides with the exact ones but ODM does not offer a decent estimate.

Example 3.5.2. *Let us take aggregation kernel $K(x,y) = x+y$ with the exponential initial condition $u(x,0) = e^{-x}$. The exact number density is provided in [88] as*

$$u(x,t) = \frac{e^{\left(e^{-t}-2\right)x-t} I_1\left(2\sqrt{1-e^{-t}}x\right)}{\sqrt{1-e^{-t}}x},$$

where I_1 is the Bessel function of the first kind.

Using the equations (3.3.5) and (3.3.6), first few components of the series solution are

determined as

$$v_0(x,t) = e^{-x}, \quad v_1(x,t) = \frac{1}{2}te^{-x}\left(x^2 - 2x - 2\right),$$

$$v_2(x,t) = \frac{1}{720}t^2e^{-x}\Big(tx(x^5 - 10x^4 - 20x^3 + 240x^2 - 120x - 240) + 60x^4 - 360x^3 - 180x^2 + 1080x + 360\Big).$$

Continuing in a similar fashion, it is easy to compute the higher order components to find better-approximated results. A four-term truncated solution is considered here and the results are compared with the HPM and ODM solutions using the same number of terms. As observed in the previous case, AHPETM is again found to be more accurate

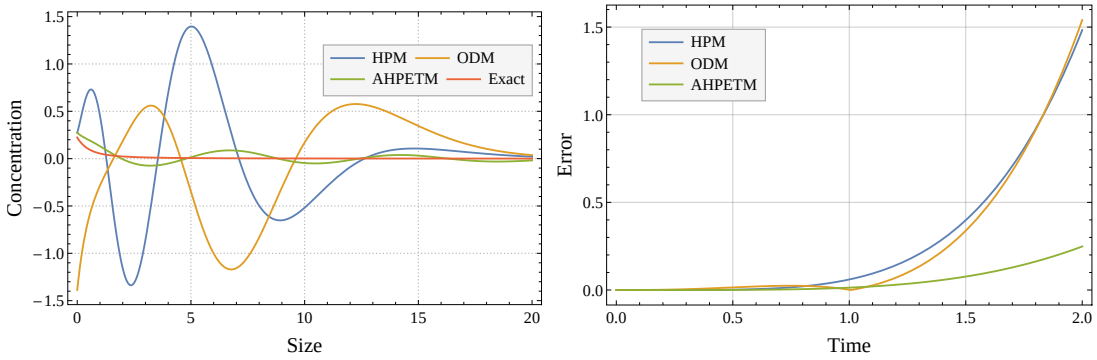

(a) Number density at $t = 2$

(b) Error at $x = 5$

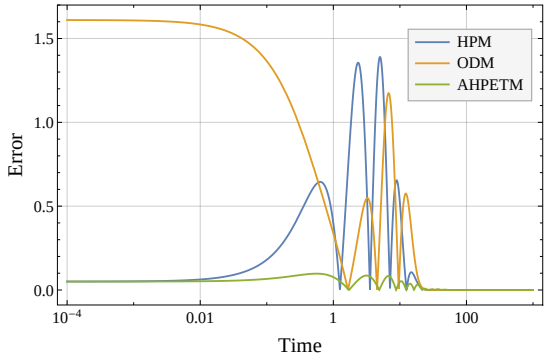

(c) Error at $t = 1.5$

Figure 3.4: Number density and error for Example 3.5.2

than HPM and ODM, see Figure 3.4. This is clear from Figure 3.4(a) which displays

Table 3.4: Absolute error for $x = 5$ at different time levels for Example 3.5.2

t	AHPETM error	ODM error	HPM error
0.2	2.71288×10^{-5}	1.0352×10^{-3}	1.4248×10^{-4}
0.4	5.3035×10^{-4}	9.2238×10^{-3}	3.8424×10^{-3}
0.6	2.3932×10^{-3}	3.1524×10^{-2}	2.4873×10^{-2}
0.8	5.8862×10^{-3}	7.223×10^{-2}	9.060×10^{-2}
1.0	0.0102	0.1327	0.2422
1.2	0.0137	0.2117	0.5345
1.4	0.0131	0.3057	1.0357
1.6	0.038	0.4085	1.8271

the number density at $t = 2$ for all the schemes. Further, Figure 3.4(b) and Table 3.4 demonstrate that for a fixed x and at different values of time t, AHPETM provide the best results over both HPM and ODM. In fact, the errors due to HPM and ODM grow almost exponentially as the time increases, while AHPETM performs consistently. Finally, Figure 3.4(c) depicts that the error due to AHPETM is not only significantly smaller than the existing approximated solutions of HPM and ODM but also close to zero for large spatial domain. Moving further, approximated and exact moments are compared for AHPETM in Figure 3.5. Surprisingly, ODM under predicts the zeroth moment and over predicts the first and second moments, respectively, while HPM and AHPETM gave almost identical findings and provided an excellent approximations to the exact zeroth, first and second moments. One important point to note here is that the AHPETM four term series solution can approximate the moments accurately up to time $t = 1.5$, while the ODM with 7 terms can only achieve the same level of accuracy up to time $t = 0.4$. This shows the superiority of the proposed scheme.

Example 3.5.3. *Consider the case of product aggregation kernel $K(x,y) = xy$ with the exponential initial condition $u(x,0) = e^{-x}$ and the precise solution is provided in [89] as*

$$u(x,t) = \sum_{k=0}^{\infty} \frac{t^k x^{3k} \exp(-(t+1)x)}{(k+1)!\Gamma(2k+2)}.$$

Using the recursive scheme defined in equation (3.3.5), a five term truncated solution is

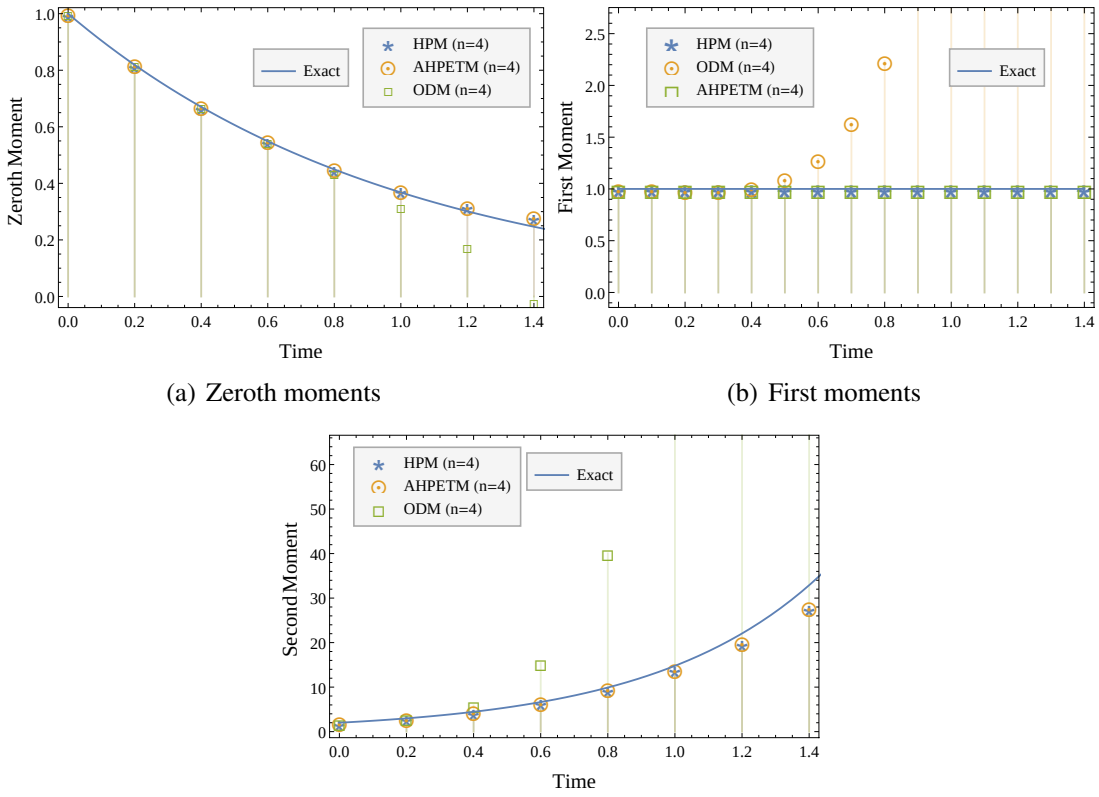

(a) Zeroth moments

(b) First moments

(c) Second moments

Figure 3.5: Zeroth, first and second moments for Example 3.5.2

considered. Due to complexity of the terms, only few given here as

$$v_0(x,t) = e^{-x}, \quad v_1(x,t) = \frac{1}{12} t e^{-x} x \left(x^2 - 12\right),$$

$$v_2(x,t) = \frac{1}{544320} \left(t^2 e^{-x} x^2 \left(tx^7 - 144tx^5 + 3024tx^3 + 756x^4 - 45360x^2 + 272160 \right) \right).$$

Figure 3.6 contrasts the error between the exact and truncated solutions obtained via HAM/HPM/ADM, ODM, and AHPETM. The figure demonstrates that the AHPETM outperforms both HPM and ODM results. Figure 3.7 further indicates the scheme's superiority as the unexpected behavior of the HPM and ODM solutions are noticed, where as the AHPETM offers better estimates of the exact solution. Figure 3.8 continues by contrasting the analytical moments with the approximated moments. In situations where

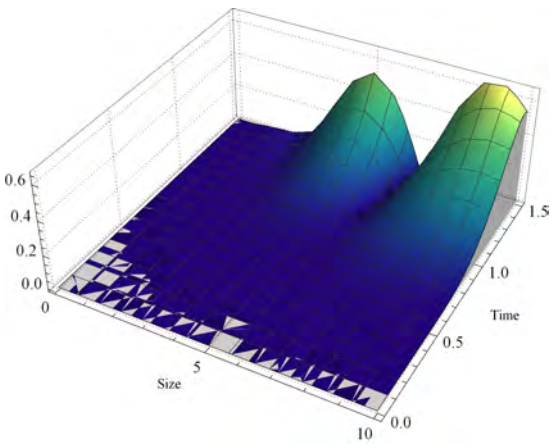

(a) AHPETM error $(n = 5)$

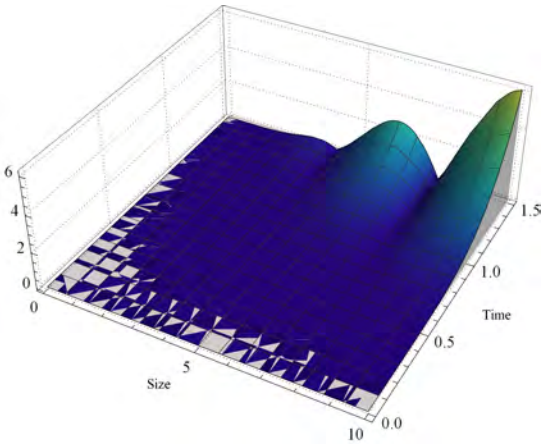

(b) HPM error $(n = 5)$

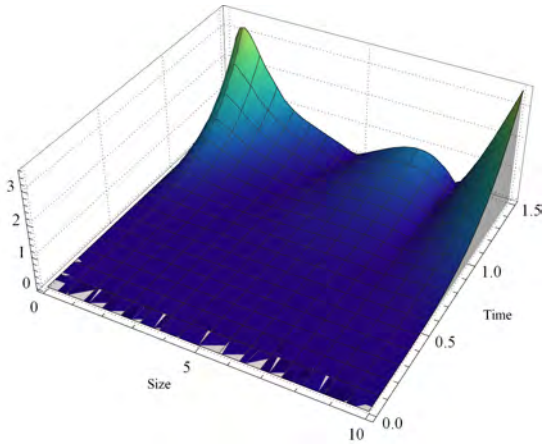

(c) ODM error $(n = 5)$

Figure 3.6: AHPETM, HPM/ADM/HAM & ODM errors for Example 3.5.3

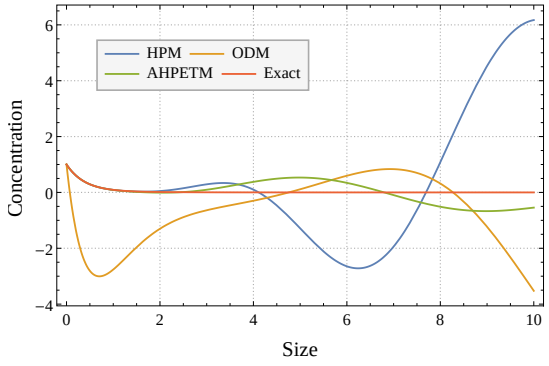

(a) Number density at $t = 2$

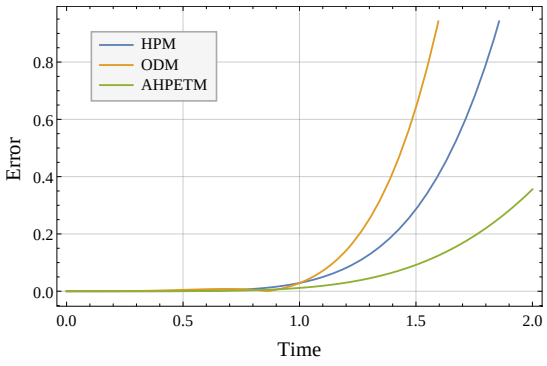

(b) Error at $x = 5$

Figure 3.7: Number density and error for Example 3.5.3

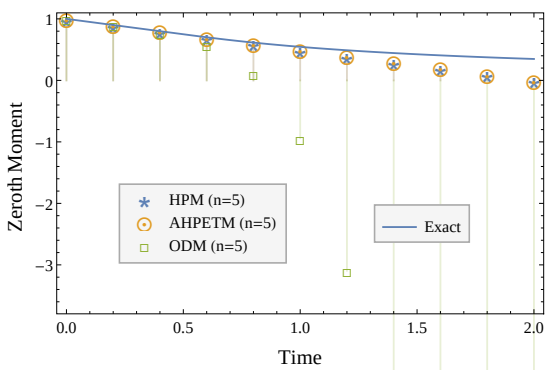

(a) Zeroth moments

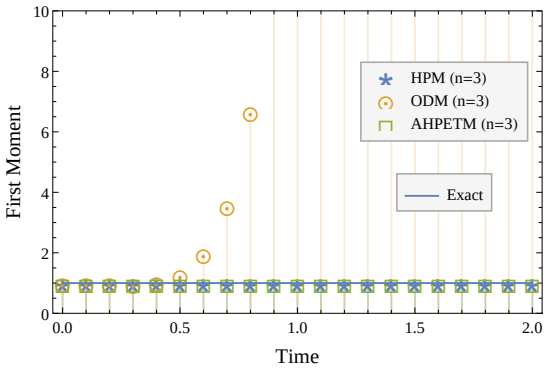

(b) Zeroth moments

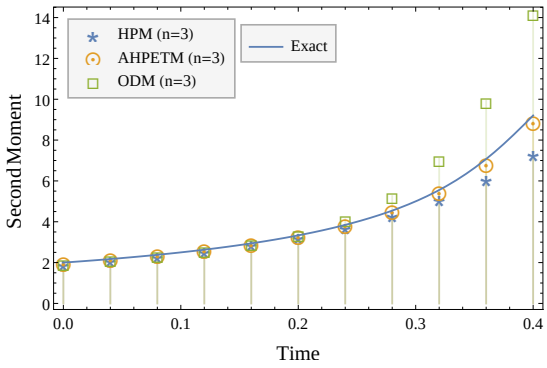

(c) Second moments

Figure 3.8: Zeroth, first and second moments for Example 3.5.3

the HPM and AHPETM moments are almost identical and closer to the exact moments, as seen in the prior occurrences, ODM moments explode.

Remark 3.5.1. *It has been noted that both AHPETM and HPM offer a more precise approximation for the moments, whereas ODM does not achieve the same level of accuracy. Conversely, ODM offers a more accurate approximation than HPM for the number density, and AHPETM enhances the results for number density even further. Consequently, AHPETM demonstrates greater efficiency compared to both HPM and ODM.*

From the above illustrations, it can be seen that in all contexts, AHPETM performs better than ADM, HPM, HAM, and ODM. Therefore, due to the novelty of the proposed scheme, we use AHPETM to solve the more complex models such as coupled aggregation-breakage and bivariate aggregation equations.

3.5.2 Coupled aggregation-breakage equation

Example 3.5.4. *Considering the case of constant aggregation rate* $(K(x,y)=1)$*, binary breakage* $(B(x,y)=2/y)$ *with the selection rate* $S(x)=\frac{x}{2}$ *and for the initial condition* $u(x,0)=4xe^{-2x}$*, the exact solution for the problem* (3.3.11) *is provided in [90].*

Using the iterations defined in equation (3.3.13), components $v_i's$ of the solutions are computed as follows

$$v_0(x,t)=4xe^{-2x},\quad v_1(x,t)=\frac{1}{3}te^{-2x}\left(4x^3-6x^2-6x+3\right),$$

$$v_2(x,t)=\frac{1}{3780}\left(t^2e^{-2x}\left(8tx^7-56tx^6-84tx^5+840tx^4-420tx^3-1260tx^2+630tx+504x^5-2520x^4-1890x^3+9450x^2+945x-1890\right)\right).$$

A four-term truncated solution is computed with the aid of "MATHEMATICA". At a

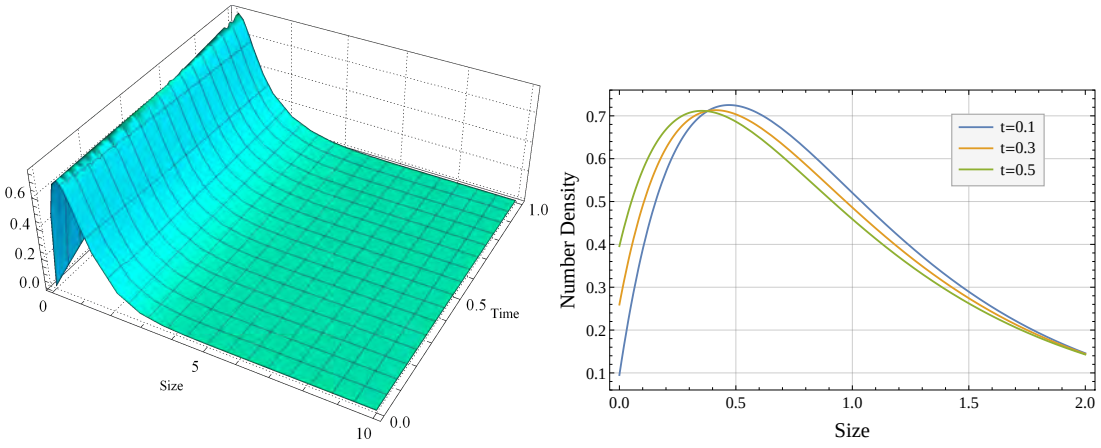

(a) Number density $(n=4)$ (b) Time distribution

Figure 3.9: Number density for Example 3.5.4

specific period t, the number density of particles of size x is shown in Figure 3.9(a). It is observed from Figures 3.9(a) and (b) that smaller particles tend to increase as time goes on, while larger particles start to fragments into smaller ones. The error between the exact and

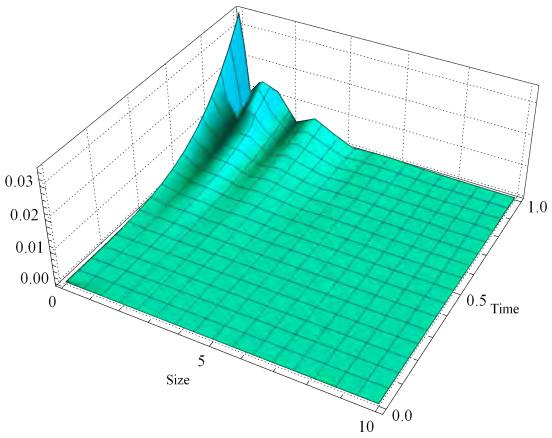

(a) Truncated error

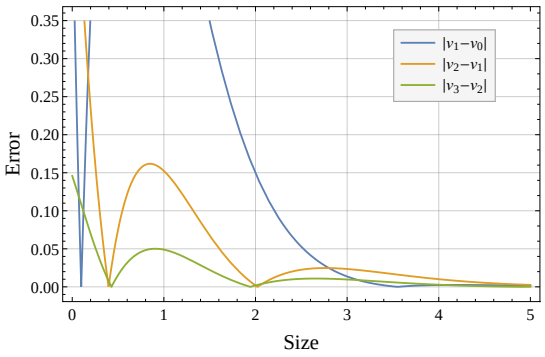

(b) Error at $t = 0.5$

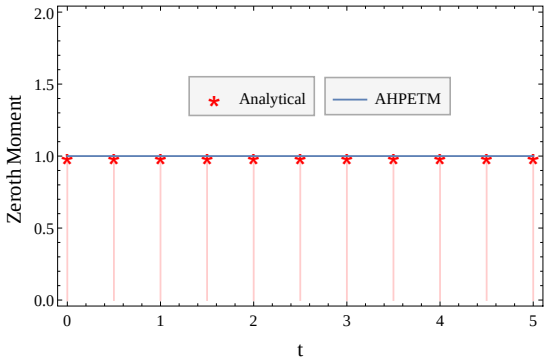

(c) Zeroth moment

Figure 3.10: Error and moment for Example 3.5.4

truncated solutions is presented in Figure 3.10(a) and is found to be nearly insignificant. Further, Figure 3.10(b) gives the absolute difference between the subsequent components of the series solution and it is clear that the difference between the second and third terms nearly vanishes, which serves as the inspiration for the decision to truncate the solution for three terms. As shown in Figure 3.10(c), the truncated solution exhibits steady state behavior for the number of particles as the zeroth moment is constant. This behavior was also analyzed analytically in [90], and thus demonstrating the method's novelty.

Example 3.5.5. *Consider another example of the coupled aggregation-breakage equation* (3.3.11) *with the same parameters as taken in Example 3.5.4 but with selection rate* $S(x) = 2x$ *and initial condition* $u(x,0) = 32xe^{-4x}$. *Similar to the previous case, here as well, steady state behavior of zeroth moment was studied in [90].*

Thanks to the formula (3.3.13), three terms of the truncated solution are computed as

$$v_0(x,t) = 32xe^{-4x}, \quad v_1(x,t) = \frac{8}{3}te^{-4x}\left(32x^3 - 24x^2 - 12x + 3\right),$$

and

$$v_2(x,t) = \frac{8}{945}t^2e^{-4x}\Big(1024tx^7 - 3584tx^6 - 2688tx^5 + 13440tx^4 - 3360tx^3 - 5040tx^2 + 1260tx + 8064x^5 - 20160x^4 - 7560x^3 + 18900x^2 + 945x - 945\Big).$$

Due to the complexity involved in the terms, a four-term truncated solution is considered.

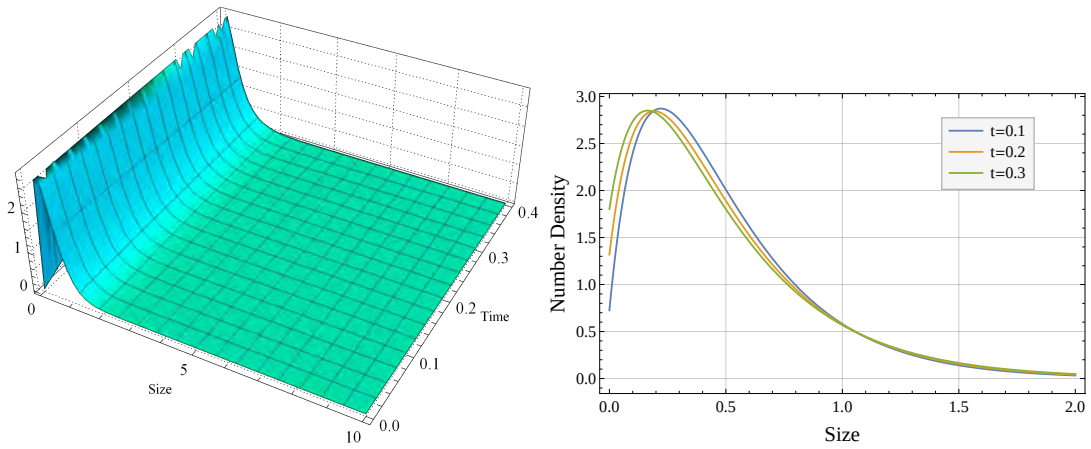

(a) Number density $(n = 4)$ (b) Time distribution

Figure 3.11: Number density for Example 3.5.5

The number density of particle in the system is presented in Figure 3.11(a). Further, Figure 3.11(b) presents the concentration of particles at different time levels, and an increment in smaller particles is encountered, where as larger particles start breaking as time increases. In Figure 3.12(a), the difference between the consecutive terms is presented, and the error between the third and fourth terms seems to be vanishing, which leads us to truncate the solution for three terms. The error between exact and approximated solutions is provided in Figure 3.12(b). As expected, in Figure 3.12(c), AHPETM shows the steady-state nature of zeroth moment and is exactly matching with the precise total number of particles.

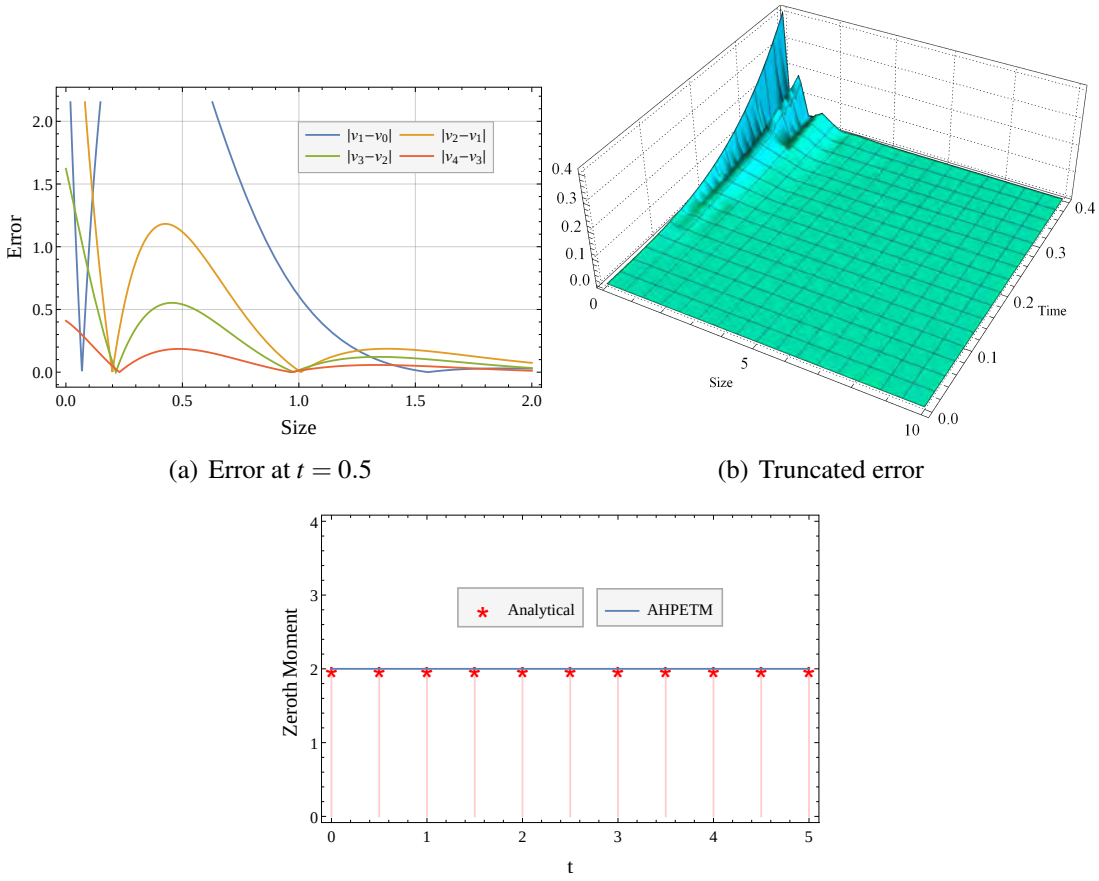

(a) Error at $t = 0.5$

(b) Truncated error

(c) Zeroth moment

Figure 3.12: Error and moment for Example 3.5.5

3.5.3 Bivariate aggregation equation

Example 3.5.6. *Let us take two-dimensional aggregation equation* (3.0.3) *with the constant aggregation kernel* $K(x,x',y,y') = 1$ *and the initial condition* $u(x,y,0) = \frac{16N_0xy}{m_1^2m_2^2}\exp\{-\frac{2x}{m_1} - \frac{2y}{m_2}\}$ *for which the parameters and the exact solution are given in Table 3.5. For more details, readers may refer to [91].*

The first three elements of the series solution are provided below using the iterations specified in equation (3.3.19)

$$v_0(x,y,t) = u_0(x,y,0), \quad v_1(x,y,t) = 5.42535\times 10^{11} txye^{-50x-50y}\left(x^2y^2 - 0.1152\times 10^{-4}\right),$$

Table 3.5: Parameters and exact solution for Example 3.5.6

N_0, p_1, p_2	1
m_1, m_2	0.04
$u(x,t)$	$\frac{(4N_0)}{(m_1m_2)(t+2)^2}\left((p_1+1)^{p_1+1}(p_1+1)^{p_2+1}\right)\exp\left(-\frac{(p_1+1)x}{m_1}-\frac{(p_2+1)y}{m_2}\right)$ $\sum_{k=0}^{\infty}\frac{\left(\frac{t}{t+2}\right)^k\left(((p_1+1)^{p_1+1})^k((p_2+1)^{p_2+1})^k\left(\frac{x}{m_1}\right)^{(k+1)(p_1+1)-1}\left(\frac{y}{m_2}\right)^{(k+1)(p_2+1)-1}\right)}{\Gamma((p_1+1)(k+1))\Gamma((p_2+1)(k+1))}$

and

$$\begin{aligned}v_2(x,y,t) =& 3.10441\times10^{-10}xye^{-50x-50y}\Big(8.06248\times10^{27}t^3x^6y^6-9.10222\times10^{24}t^3x^4y^4\\&+8.73813\times10^{20}t^3x^2y^2-3.35544\times10^{15}t^3+1.36533\times10^{25}t^2x^4y^4\\&-2.62144\times10^{21}t^2x^2y^2+1.50995\times10^{16}t^2+6t\Big).\end{aligned}$$

Continuing in a similar pattern, a four-term truncated solution is computed and compared with the exact solution. Figure 3.13(a) gives the number density at time $t = 0.4$ and it is marked that larger particles almost disappear, and microscopic particles dominate the system. A minimal error is seen between the exact and truncated solutions, according to the error curve shown in Figure 3.13(b). In addition to this, Figures 3.13(c)- 3.13(e) present the contour plots of the errors by taking two, three, and four terms truncated series solutions. One can observe that as the number of terms increases, the error reduces significantly. Finally, Figure 3.13(f) shows that the approximated moments, namely $\mu_{0,0}, \mu_{1,0}, \mu_{2,0}$, provide a great agreement with the corresponding exact moments.

3.6 Conclusions

This study employed AHPETM to solve the fragmentation, multi-dimensional coagulation, and linked aggregation-fragmentation equations. Due to the complexity in the models, convergence analysis were discussed for fragmentation and multi-dimensional aggregation

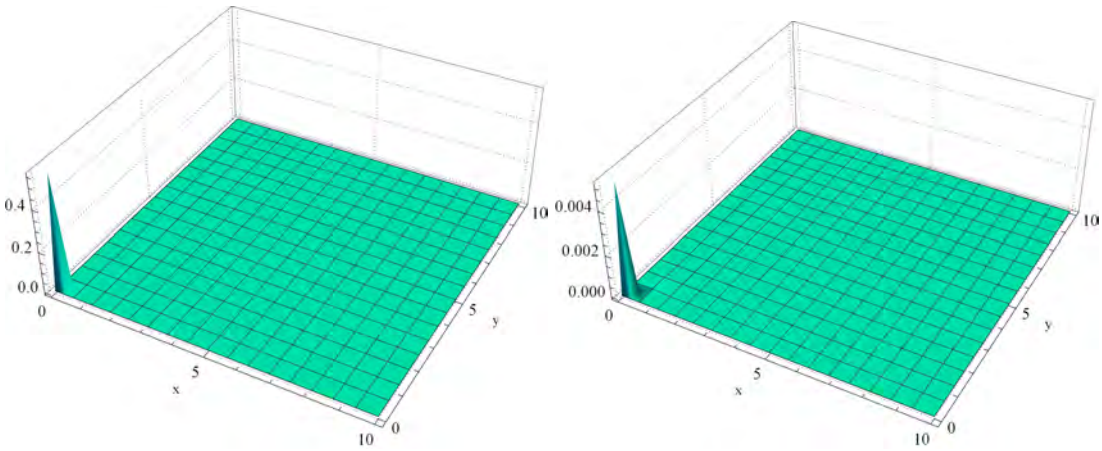

(a) Number density $(n = 4)$ (b) Truncated error

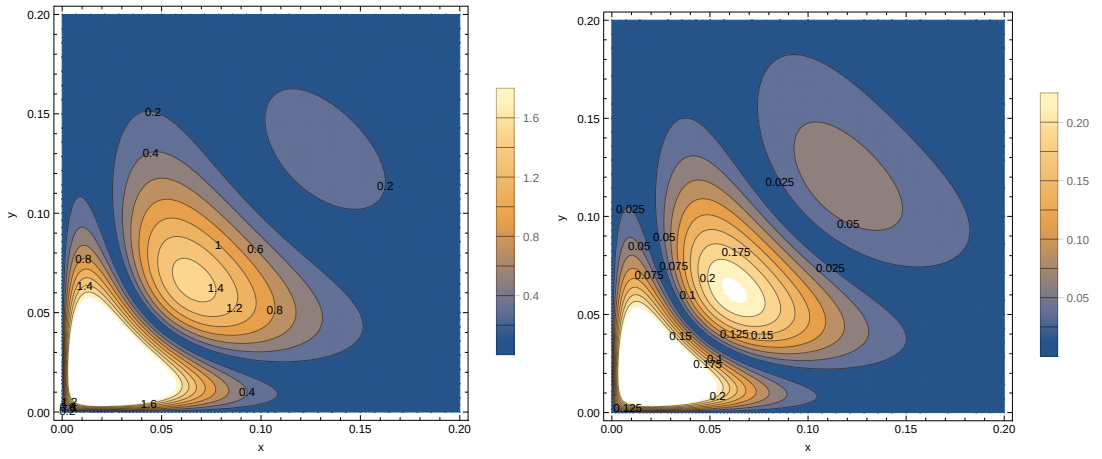

(c) $|\Phi_2(x,y,t) - u(x,y,t)|$ (d) $|\Phi_3(x,y,t) - u(x,y,t)|$

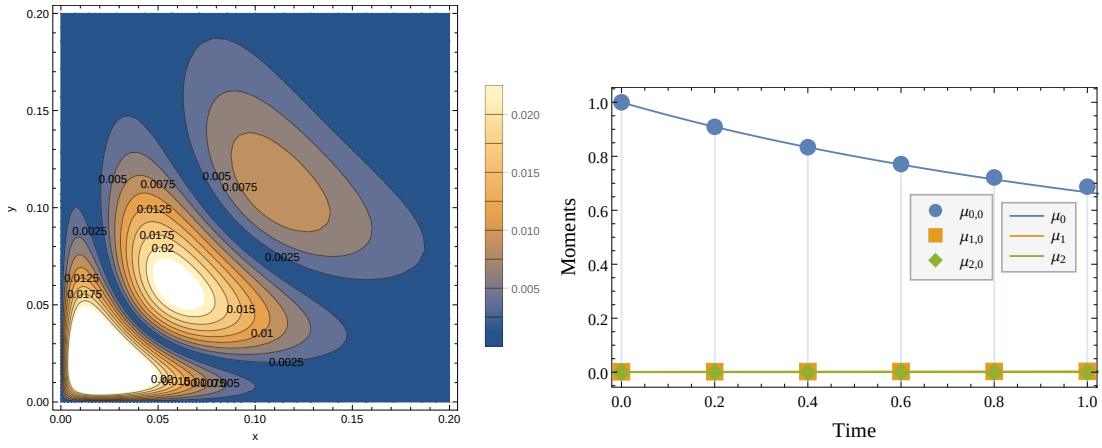

(e) $|\Phi_4(x,y,t) - u(x,y,t)|$ (f) Moments

Figure 3.13: Number density, error and moments for Example 3.5.6

equations considering the constant kernels. With the help of MATHEMATICA, this article also contained the detailed numerical investigations for each of the predefined models. It was observed that, for pure fragmentation equation which is linear, all the schemes offered the same results. However, for non-linear aggregation equation, AHPETM significantly outperformed the results of ADM, HAM, HPM and ODM even after a lengthy period of time. This justified the method's reliability and applicability. AHPETM was also designed to solve non-linear 2-D aggregation and combined aggregation-fragmentation equations due to the accuracy and efficiency observed in the pure aggregation equation and remarkable results were obtained in each case. In future, it would be interesting to implement AHPETM for tackling static beam and other engineering nonlinear problems [92–94]. One can include a convergence control parameter and Pade approximation to enhance the approach that may offer a more refined and effective scheme.

Chapter 4

New approximate solutions for Smoluchowski's aggregation and coupled aggregation-growth equations

This chapter describes an improved version of homotopy analysis method for solving the aggregation and aggregation-growth equations. Several physical examples are considered to examine the precision and efficiency of the approach by comparing the results with exact and existing estimated solutions derived using HAM, HPM, ADM and ODM. Furthermore, moments are also highlighted. Interestingly, IOHAM enhances the accuracy of moments compared to ODM, while HAM still better matches the actual moments. In addition, a comprehensive convergence study of the series solution is investigated.

Consider a system enduring a particulate process, where $\mu(x,t)$ is the number density of particles of size x at time t. Consequently, the aggregation-growth equation is [95]:

$$\frac{\partial \mu(x,t)}{\partial t} = \frac{\partial}{\partial x}\left(G(x)\mu(x,t)\right) + \frac{1}{2}\int_0^x \beta(x-y,y)\mu(x-y,t)\mu(y,t)dy - \int_0^\infty \beta(x,y)\mu(x,t)\mu(y,t)dy, \tag{4.0.1}$$

with the initial condition

$$\mu(x,0) = \mu_0(x). \tag{4.0.2}$$

The left part of equation (4.0.1) depicts the evolution of x-sized particles. In the first term on the right-hand side, the function $G(x)$ represents the growth rate of the particle of size x. The second and third terms define the aggregation process as discussed in preceding chapters.

The article is structured as follows: In the subsequent section, a brief of the HAM and IOHAM are discussed. In Section 4.2, the recursive scheme corresponding to the general aggregation-growth equation is developed using IOHAM. Section 4.3 presents the convergence analysis of the series solution to the exact solution. Section 4.4 is devoted to a detailed discussion of several numerical examples. Finally, we present some concluding remarks in Section 4.5.

4.1 Methodology

4.1.1 HAM

The fundamental concept behind the homotopy analysis method is to approximate the series solution for non-linear differential equations [96]. This section briefly summarizes HAM for solving the initial value problem for the first-order differential equation. Consider,

$$\mathscr{D}[u'(t), u(t)] = 0, \quad u(0) = u_0, \text{ for } t > 0, \tag{4.1.1}$$

where $\mathscr{D}$ is a non-linear differential operator, $u(t)$ is a unknown function. According to the scheme [96], one can construct the homotopy as follows

$$(1-q)\mathscr{L}[\Phi(t;q) - u_0(t)] = qhH\mathscr{D}[\Phi'(t;q), \Phi(t;q)], \tag{4.1.2}$$

where $q \in [0,1]$ is an embedding parameter, h is convergence control parameter, $u_0(t)$ is an initial guess, $H(t) \neq 0$ is an auxiliary function and $\mathscr{L}$ is a linear operator. It is clear from (4.1.2) that as q varies from 0 to 1, $\Phi(t;q)$ varies from initial guess $u_0(t) = \Phi(t;0)$ to the exact solution $u(t) = \Phi(t;1)$. Following the idea of HAM, $\Phi(t;q)$ can be expressed as a power series in q of the form,

$$\Phi(t;q) := \sum_{j=0}^{\infty} q^j \phi_j. \tag{4.1.3}$$

If the series (4.1.3) converges at $q = 1$, the homotopy series solution is obtained as follows

$$u(t) = \Phi(t;1) = \sum_{j=0}^{\infty} \phi_j. \tag{4.1.4}$$

To obtain the components ϕ_j, substituting (4.1.3) in equation (4.1.2) and equating the coefficients of powers of q, give the zeroth order deformation equation

$$\mathscr{L}[\phi_0(t) - u_0(t)] = 0, \tag{4.1.5}$$

and the high order deformation equations

$$\mathscr{L}[\phi_j] = \mathscr{L}[\phi_{j-1}] + hHP_{j-1}, \quad j \geq 1, \tag{4.1.6}$$

where $P_j's$, are given by

$$P_j(t) = \frac{1}{j!}\frac{\partial^j}{\partial q^j}\mathscr{D}\left(\sum_{i=0}^{\infty} q^i \phi_i'(t), \sum_{i=0}^{\infty} q^i \phi_i(t)\right). \tag{4.1.7}$$

4.1.2 Improved optimal homotopy analysis method

Liao in [96], explains that HAM provides the flexibility to provide solutions to non-linear problems through the use of different base functions that can be constructed based on the initial guess and the auxiliary linear operator. This section describes an enhanced

version of the HAM for regulating the convergence rate and region. In order to improve the accuracy of the solution, linear operator $\mathscr{L}$ is chosen of the form

$$\mathscr{L}[u] = \frac{\partial u}{\partial t} + qk(u_0)hHu, \tag{4.1.8}$$

where

$$k(u_0) = \frac{\frac{\partial \mathscr{D}}{\partial u}(u_0', u_0)}{\frac{\partial \mathscr{D}}{\partial u'}(u_0', u_0)}.$$

Therefore, the new modified homotopy is defined as follows

$$(1-q)\left[\frac{\partial}{\partial t} + qk(u_0)hH\right][\Phi(t;q) - u_0] = qhH\mathscr{D}(\Phi'(t;q), \Phi(t;q)). \tag{4.1.9}$$

To felicitate the calculations, initial condition u_0 is considered as the zeroth-order approximation or the initial guess. Now, considering that the unknown function Φ can be written into the form of infinite series as mentioned in equation (4.1.3) and following the same procedure as HAM, iterations to solve the non-linear problems are discussed in Table 4.1 below: Hence the n-term truncated series solution is given by $\Psi_n(t) := \sum_{j=0}^{n} \phi_j(t)$. The

Table 4.1: Table of the coefficients for IOHAM

$\phi_0(t)$	$u_0(x)$
$\phi_1(t)$	$\int_0^t hHP_0(\tau)d\tau$
$\phi_2(t)$	$\int_0^t \left(\frac{\partial}{\partial t}\phi_1 + hH(P_1(\tau) - k(u_0)\phi_1(\tau))\right)d\tau$
$\phi_{k+1}(t)$	$\int_0^t \left(\frac{\partial}{\partial t}\phi_k + hH(\frac{\partial}{\partial t}\phi_k(\tau) + P_k(\tau) - k(u_0)(\phi_k(\tau) - \phi_{k-1}(\tau)))\right)d\tau, \quad k \geq 2.$

optimal parameter h is computed by minimizing the residual $Res(h)$, defined by

$$Res(h) = \sqrt{\int_\Omega (\mathscr{D}[\Psi'(t), \Psi(t)])d\Omega}.$$

Due to the difficulty in calculating the iterations, residue can also be calculated numerically using the squared residual formula,

$$Res(h) = \sqrt{\frac{1}{M}\sum_{m=1}^{M}(\mathscr{D}[\Psi'(t_m), \Psi(t_m)])^2},$$

where $t_m \in \Omega$ are arbitrary sample points. Readers are referred to [8, 77] and further citations for detailed explanation.

4.2 Development of IOHAM for aggregation-growth Equation

In this section, IOHAM is extended to solve the aggregation-growth equation (4.0.1). According to the IOHAM defined in Section 4.1.2, the optimal linear operator $\mathscr{L}$ is defined as

$$\mathscr{L}[\mu] = \frac{\partial \mu}{\partial t} + qk(\mu_0)hH\mu,$$

where

$$k(\mu_0) = -\frac{1}{2}\int_0^x \beta(x-y,y)\mu_0(y,t)dy + \int_0^\infty \beta(x,y)\mu_0(y,t)dy - \frac{\partial}{\partial x}[G(x)], \tag{4.2.1}$$

with initial approximation or zeroth approximation is considered as $\phi_0 = \mu(x,0)$, then a homotopy is constructed as follows

$$\begin{aligned}(1-q)\left[\frac{\partial}{\partial t} + qk(\mu_0)hH\right][\phi(t;q) - \mu_0] = qhH\Bigg(&\frac{\partial \phi(x,t)}{\partial t} + \int_0^\infty \beta(x,y)\phi(x,t)\phi(y,t)dy \\ &- \frac{\partial}{\partial t}[G(x)\phi(x,t)] - \frac{1}{2}\int_0^x \beta(x-y,y)\phi(x-y,t)\phi(y,t)dy\Bigg).\end{aligned} \tag{4.2.2}$$

Considering $H=1$, substituting equation (4.1.3) in (4.2.2) and then comparing the powers of q, zeroth and higher order deformation equations are obtained via

$$\begin{cases} \phi_0(x,t) = & \mu(x,0) \\ \phi_1(x,t) = & \displaystyle\int_0^t \left(\frac{\partial \phi_0}{\partial t} + h\left(\frac{\partial \phi_0}{\partial t} - \frac{\partial}{\partial t}[G(x)\phi_0(x,t)] - \frac{1}{2}\int_0^x \beta(x-y,y)A_0 dy + \int_0^\infty \beta(x,y)B_0 dy \right) \right) dt \\ \phi_2(x,t) = & \displaystyle\int_0^t \left(\frac{\partial \phi_1}{\partial t} + h\left(\frac{\partial \phi_1}{\partial t} - \frac{\partial}{\partial t}[G(x)\phi_1(x,t)] - \frac{1}{2}\int_0^x \beta(x-y,y)A_1 dy \right.\right. \\ & \left.\left. + \displaystyle\int_0^\infty \beta(x,y)B_1 dy - k(\mu_0)\phi_1 \right) \right) dt \\ \phi_n(x,t) = & \displaystyle\int_0^t \left(\frac{\partial \phi_{n-1}}{\partial t} + h\left(\frac{\partial \phi_{n-1}}{\partial t} - \frac{\partial}{\partial t}[G(x)\phi_{n-1}(x,t)] - \frac{1}{2}\int_0^x \beta(x-y,y)A_{n-1} dy \right.\right. \\ & \left.\left. + \displaystyle\int_0^\infty \beta(x,y)B_{n-1} dy - k(\mu_0)(\phi_{n-1}-\phi_{n-2}) \right) \right) dt, \quad n \geq 3, \end{cases} \tag{4.2.3}$$

where

$$A_n = \frac{1}{n!}\frac{d^n}{d\lambda^n}\left(f_1\left(\sum_{k=0}^{\infty} \phi_k \lambda^k \right) \right)_{\lambda=0}, \quad B_n = \frac{1}{n!}\frac{d^n}{d\lambda^n}\left(f_2\left(\sum_{k=0}^{\infty} \phi_k \lambda^k \right) \right)_{\lambda=0}$$

for $f_1(\mu) = \mu(x-y,t)\mu(y,t)$ and $f_2(\mu) = \mu(x,t)\mu(y,t)$. Hence, the nth-order deformation equation is governed by

$$\mathscr{L}\left[\phi_n - \chi_n \phi_{n-1}\right] = hH(\mathscr{R}_n + k(\mu_0)\left[\chi_n \phi_{n-1} - \chi_{n-1}\phi_{n-2}\right]) \tag{4.2.4}$$

where

$$\begin{aligned} \mathscr{R}_n = & \frac{\partial \mu_{n-1}(x,t)}{\partial t} - \frac{\partial (G(x)\mu_{n-1}(x,t))}{\partial x} - \frac{1}{2}\int_0^x \beta(x-y,y) \sum_{j=0}^{n-1} \mu_j(t,y-x)\mu_{n-1-j}(x,t)dy \\ & + \sum_{j=0}^{n-1} \int_0^\infty \beta(x,y)\mu_j(x,t)\mu_{n-1-j}(x,t)dy \end{aligned} \tag{4.2.5}$$

and the characteristic function χ_n is given by

$$\chi_n = \begin{cases} 0 & \text{if } n < 1, \\ 1 & \text{if } n \geq 1. \end{cases} \tag{4.2.6}$$

Remark 4.2.1. *It is worth mentioning that IOHAM is an enhancement to the recently developed ODM [25]. It involves the convergence control parameter h, which increases the convergence rate of the truncated solution to the exact solution. A particular case of* $h = -1$ *reduces IOHAM to the ODM.*

4.3 Convergence analysis

In this section, the convergence criterion of the iterative scheme, provided in equation (4.2.3), for solving the aggregation-growth equation is discussed. Further, the convergence of truncated series solution and error bounds of the approximated solution are presented for the pure aggregation equation.

Theorem 4.3.1. *If the iterative components* ϕ_n *are constructed using the higher-order deformation equation* (4.2.4) *with* $\mathscr{R}_n$ *given by equation* (4.2.5)*, then the series solution* $\sum_{n=0}^{\infty} \phi_n$ *is the exact solution to the problem* (4.0.1) *as long as it converges.*

Proof. Let us assume that the series $(\phi_n)_{n=0}^{\infty}$ converges to $\mu(x,t)$. Then one can write

$$\mu(x,t) = \sum_{n=0}^{\infty} \phi_n(x,t) \text{ which implies that } \lim_{n\to\infty} \phi_n(x,t) = 0. \tag{4.3.1}$$

Considering this, it is easy to see that

$$\sum_{n=0}^{j} [\phi_n(x,t) - \chi_n \phi_{n-1}(x,t)] = \phi_1 + (\phi_2 - \phi_1) + \cdots + (\phi_j - \phi_{j-1}) = \phi_j(x,t),$$

and hence, we get

$$\sum_{n=0}^{\infty} [\phi_n(x,t) - \chi_n \phi_{n-1}(x,t)] = \lim_{n\to\infty} \phi_n(x,t) = 0.$$

Using the linear property of the operator $\mathscr{L}$ leads to

$$\sum_{n=0}^{\infty} \mathscr{L}\left[\phi_n - \chi_n \phi_{n-1}\right] = \mathscr{L} \sum_{n=0}^{\infty} \left[\phi_n - \chi_n \phi_{n-1}\right] = 0.$$

Thus, recalling the mth-order deformation equation

$$\sum_{n=0}^{\infty} \mathscr{L}\left[\phi_n - \chi_n \phi_{n-1}\right] = hH \sum_{n=1}^{\infty} \left(\mathscr{R}_n + k(\mu_0)\left(\chi_n \phi_{n-1} - \chi_{n-1}\phi_{n-2}\right)\right) = 0,$$

entails that

$$\sum_{n=1}^{\infty} \mathscr{R}_n[\phi_{n-1}] = 0, \tag{4.3.2}$$

as $h, H \neq 0$. Therefore,

$$\sum_{n=1}^{\infty} \mathscr{R}_n = \sum_{n=1}^{\infty} \left[\frac{\partial \mu_{n-1}(x,t)}{\partial t} - \frac{\partial (G(x)\mu_{n-1}(x,t))}{\partial x} - \frac{1}{2}\int_0^x \beta(x-y,y) \right.$$
$$\left. \sum_{j=0}^{n-1} \mu_j(x-y,t)\mu_{n-1-j}(y,t)dy + \sum_{j=0}^{n-1} \int_0^{\infty} \beta(x,y)\mu_j(x,t)\mu_{n-1-j}(y,t)dy \right].$$

Changing the order of sum simplifies to

$$\sum_{n=1}^{\infty} \mathscr{R}_n = \sum_{n=1}^{\infty} \frac{\partial \mu_{n-1}(x,t)}{\partial t} - \sum_{n=1}^{\infty} \frac{\partial (G(x)\mu_{n-1}(x,t))}{\partial x} - \frac{1}{2}\int_0^x \beta(x-y,y)$$
$$\sum_{j=0}^{\infty} \sum_{n=j+1}^{\infty} \mu_j(x-y,t)\mu_{n-1-j}(x,t)dy + \sum_{j=0}^{\infty} \sum_{n=j+1}^{\infty} \int_0^{\infty} \beta(x,y)\mu_j(x,t)\mu_{n-1-j}(y,t)dy.$$

Letting $k = n-1-j$, the above reduces to

$$\sum_{n=1}^{\infty} \mathscr{R}_n = \sum_{n=1}^{\infty} \frac{\partial \mu_{n-1}(x,t)}{\partial t} - \sum_{n=1}^{\infty} \frac{\partial (G(x)\mu_{n-1}(x,t))}{\partial x} - \frac{1}{2}\int_0^x \beta(x-y,y) \sum_{j=0}^{\infty} \mu_j(x-y,t)$$
$$\sum_{k=0}^{\infty} \mu_k(y,t)dy + \int_0^{\infty} \beta(x,y) \sum_{j=0}^{\infty} \mu_j(x,t) \sum_{k=0}^{\infty} \mu_k(y,t)dy.$$

Recalling equations (4.3.1) and (4.3.2), we have

$$\frac{\partial \mu(x,t)}{\partial t} = \frac{\partial (G(x)\mu(x,t))}{\partial x} + \frac{1}{2}\int_0^x \beta(x-y,y)\mu(y-x,t)\mu(y,t)dy - \int_0^\infty \beta(x,y)\mu(x,t)\mu(y,t)dy, \tag{4.3.3}$$

implying that $\mu(x,t)$ is the exact solution of the aggregation-growth equation (4.0.1). □

We will now discuss the convergence of the recursive formula (4.2.3). Here, it is hard to handle the coupled aggregation-growth model and so for the sake of convenience $G(x) = 0$ is considered, i.e., the case of pure aggregation is handled. Let us rewrite the equation (4.0.1) into the following form

$$\mu(x,t) = \mu(x,0) + \int_0^t \left(\frac{1}{2}\int_0^x \beta(x-y,y)\mu(x-y,s)\mu(y,s)dy - \int_0^\infty \beta(x,y)\mu(x,s)\mu(y,s)dy \right) ds. \tag{4.3.4}$$

Further, for a fixed $T > 0$, consider a strip

$$\mathscr{W} := \{(x,t) : 0 \le t \le T, 0 < x < \infty\}$$

and define $\varphi(T)$ be the space of all continuous functions $\mu(x,t)$ with the norm

$$\|\mu\|_{\varphi(T)} := \sup_{0\le t\le T} \int_0^\infty |\mu(x,s)|dx < L. \tag{4.3.5}$$

Let us write equation (4.3.4) into the operator form as

$$\mu = \mathscr{N}[\mu], \tag{4.3.6}$$

where $\mathscr{N}$ is given by

$$\mathscr{N}[\mu] = \mu(x,0) + \int_0^t \left(\frac{1}{2}\int_0^x \beta(x-y,y)\mu(x-y,s)\mu(y,s)dy - \int_0^\infty \beta(x,y)\mu(x,s)\mu(y,s)dy \right) ds.$$

To show the contractiveness of the non-linear operator $\mathscr{N}$, an equivalent form of the equation (4.3.4) is defined as

$$\frac{\partial}{\partial t}[\mu(x,t)\exp[\mathscr{K}(t,x,\mu)]] = \frac{1}{2}\exp[\mathscr{K}(s,x,\mu)]\int_0^x \beta(x-y,y)\mu(x-y,t)\mu(y,t)dy$$

where $\mathscr{K}(t,x,\mu) := \int_0^t\int_0^\infty \beta(x,y)\mu(y,s)dyds$. Thus, we have $\mu = \tilde{\mathscr{N}}\mu$, where

$$\tilde{\mathscr{N}} = \mu(x,0)\exp[-\mathscr{K}(t,x,\mu)] + \frac{1}{2}\int_0^t \exp[\mathscr{K}(s,x,\mu)-\mathscr{K}(t,x,\mu)] \int_0^x \beta(x-y,y)\mu(x-y,s)\mu(y,s)dyds. \tag{4.3.7}$$

Since $\mathscr{N}$ and $\tilde{\mathscr{N}}$ are equivalent, it is enough to show that $\tilde{\mathscr{N}}$ is contractive.

Theorem 4.3.2. *The non-linear operator $\tilde{\mathscr{N}}$ introduced in (4.3.7) is contractive, i.e., $\|\tilde{\mathscr{N}}[\mu]-\tilde{\mathscr{N}}[\mu^*]\| \le \|\mu-\mu^*\|$ for all $\mu,\mu^* \in \varphi(T)$ holds if*

- $\beta(x,y) = 1$ *for all* $x,y \in (0,\infty)$,
- $\delta := \tau e^{\tau L}(\|\mu_0\| + \frac{1}{2}\tau L^2 + \tau L) < 1$, *where* $\tau = \min\{\tau_0,\tau_1\}$.

Proof. We begin this by showing $\|\tilde{\mathscr{N}}[\mu]\| < L$ for small $\tau > 0$. Consider,

$$\begin{aligned}
\|\tilde{\mathscr{N}}[\mu]\| &\le \|\mu_0\exp[-\mathscr{K}[t,x,\mu]]\| + \frac{1}{2}\left\|\int_0^t (\exp[\mathscr{K}(s,x,\mu)-\mathscr{K}(t,x,\mu)])\int_0^x \mu(x-y,s)\mu(y,s)dyds\right\| \\
&\le \|\mu_0\| + \frac{1}{2}\left\|\int_0^t \exp\left[-\int_s^t\int_0^\infty \mu(y,t)dyds\right]\int_0^x \mu(x-y,s)\mu(y,s)dyds\right\| \\
&\le \|\mu_0\| + \frac{1}{2}\int_0^\infty\int_0^t\int_0^x \mu(x-y,s)\mu(y,s)dydsdx.
\end{aligned}$$

Further, by changing the order of integration and using the equation (4.3.5), imply that

$$\begin{aligned}
\|\tilde{\mathscr{N}}[\mu]\| &\le \|\mu_0\| + \frac{1}{2}\int_0^t\int_0^\infty\int_0^\infty \mu(z,s)\mu(y,s)dzdyds \\
&\le \|\mu_0\| + \frac{1}{2}L^2 t.
\end{aligned}$$

Hence, $\|\tilde{\mathscr{N}}[\mu]\| < L$ holds true if $\|\mu_0\| + \frac{1}{2}L^2\tau_0 \le L$ for a suitable $t = \tau_0$. This inequality

holds if $\tau_0 \leq \frac{1}{2\|\mu_0\|}$ and

$$\frac{1-\sqrt{1-2\tau_0\|\mu_0\|}}{\tau_0} \leq L \leq \frac{1+\sqrt{1-2\tau_0\|\mu_0\|}}{\tau_0}.$$

Now, we concentrate on demonstrating that the mapping $\tilde{\mathscr{N}}$ is contractive. For this, consider

$$\begin{aligned}\tilde{\mathscr{N}}[\mu]-\tilde{\mathscr{N}}[\mu^*] =&\mu_0(x)\mathscr{H}(0,x,t)+\frac{1}{2}\int_0^t\int_0^x \mathscr{H}(s,x,t)\mu(x,x-y)\mu(y,s)dyds\\ &+\frac{1}{2}\int_0^t \exp[\mathscr{K}(s,x,\mu)-\mathscr{K}[t,x,\mu^*]]\Bigg[\int_0^x \mu^*(x-y,s)\{\mu(y,s)-\mu^*(y,s)\}\\ &+\int_0^x \mu(y,s)\{\mu(x-y,s)-\mu^*(x-y,s)\}dyds\Bigg],\end{aligned}$$

where $\mathscr{H}(s,x,t)=\exp[\mathscr{K}(s,x,\mu)-\mathscr{K}(t,x,\mu)]-\exp[\mathscr{K}(s,x,\mu^*)-\mathscr{K}(t,x,\mu^*)]$ and it can be easily shown that

$$|\mathscr{H}(s,x,t)| \leq \gamma\|\mu-\mu^*\|,$$

where $\gamma = te^{t\mathscr{B}}$ for $\mathscr{B}=\max\{\|\mu\|,\|\mu^*\|\}$. Hence, we have

$$\begin{aligned}\|\tilde{\mathscr{N}}[\mu]-\tilde{\mathscr{N}}[\mu^*]\| \leq&\gamma\|\mu_0\|\|\mu-\mu^*\|+\gamma\|\mu-\mu^*\|\int_0^t\frac{1}{2}\|\mu\|^2ds+\int_0^t\gamma\left[\frac{1}{2}(\|\mu\|+\|\mu^*\|)\|\mu-\mu^*\|\right]ds\\ \leq&\gamma\left[\|\mu_0\|+\frac{1}{2}t\|\mu\|^2+\frac{1}{2}t(\|\mu\|+\|\mu^*\|)\right]\|\mu-\mu^*\|\\ =&\delta\|\mu-\mu^*\|,\end{aligned}$$

which for $\delta=\gamma(\|\mu_0\|+\frac{1}{2}\tau_1L^2+\tau_1L)<1$ for suitable τ_1 indicates that the operator $\tilde{\mathscr{N}}$ is contractive. □

Theorem 4.3.3. *Let $\phi_1,\phi_2,\ldots,\phi_n$ are the components of the series solution and $\Psi_n=\sum_{i=0}^n\phi_i$ be n term truncated series solution. Then the approximated series solution con-*

verges to the exact one with the error bound

$$\|\mu(x,t)-\Psi_m(x,t)\| \leq \frac{\Delta^m}{1-\Delta}\|\mu_1\|,$$

assuming that all the conditions of Theorem 4.3.2 hold. In addition, the following conditions are also imposed:

A1. $k(\mu_0) \in L^\infty$, *i.e.,* $|k(\mu_0)| \leq k$ *for some* $k \in \mathbb{R}^+$,

A2. ϕ_n *is a Cauchy sequence, i.e., for any* $n > m$, $\|\phi_n - \phi_m\| < \varepsilon$ *where* $\varepsilon < \frac{1}{n^p}$ *such that* $p > 1$.

Proof. Using (4.2.3), $(n+1)$-term approximated series solution is defined as

$$\Psi_{n+1} = \int_0^t \left((1+h)\frac{\partial \Psi_n}{\partial t} - \frac{1}{2}h\int_0^x (\sum_{i=0}^n A_i)dy + h\int_0^\infty (\sum_{i=0}^n B_i)dy - hk(\mu_0)\phi_n\right)dt. \quad (4.3.8)$$

Following [97], one can obtain the inequalities $\sum_{i=0}^n A_i \leq f_1(\Psi_n)$ and $\sum_{i=0}^n B_i \leq f_2(\Psi_n)$. Using these, the above equation reduces to,

$$\Psi_{n+1} \leq \int_0^t \left((1+h)\frac{\partial \Psi_n}{\partial t} - h\mathcal{N}[\Psi_n] - hk(\mu_0)\phi_n\right)dt.$$

Therefore, using the conditions of Theorem 4.3.2 and A1, we have

$$\begin{aligned}\|\Psi_{n+1}-\Psi_{m+1}\| \leq& \|(\Psi_n-\Psi_m)(1+h)\| + |h|\|\mathcal{N}[\Psi_n]-\mathcal{N}[\Psi_m]\| + k(\mu_0)h\|\phi_n-\phi_m\| \\ \leq& |1+h|\|\Psi_n-\Psi_m\| + \delta|h|\|\Psi_n-\Psi_m\| + \varepsilon kh\tau \\ \leq& \Delta\|\Psi_n-\Psi_m\| + \varepsilon kh\tau,\end{aligned}$$

where $\Delta := |1+h| + \delta|h|$. Hence, the following results is observed

$$\begin{aligned}\|\Psi_{m+1}-\Psi_m\| \leq& \Delta\|\Psi_m-\Psi_{m-1}\| + \varepsilon kh\tau \leq \Delta^2\|\Psi_{m-1}-\Psi_{m-2}\| + \varepsilon kh\tau(1+\Delta) \\ \leq& \Delta^m\|\Psi_1-\Psi_0\| + \varepsilon kh\tau(1+\Delta+\Delta^2+\cdots+\Delta^{m-1})\end{aligned}$$

$$= \Delta^m \|\Psi_1 - \Psi_0\| + \varepsilon k h \tau \left(\frac{1-\Delta^m}{1-\Delta} \right).$$

Using the properties of norm for all $n, m \in \mathbb{N}$ with $n > m$, it is certain that

$$\begin{aligned}
\|\Psi_n - \Psi_m\| \leq & \|\Psi_{m+1} - \Psi_m\| + \|\Psi_{m+2} - \Psi_{m+1}\| + \cdots + \|\Psi_n - \Psi_{n-1}\| \\
\leq & (\Delta^m + \Delta^{m+1} + \cdots + \Delta^{n-1}) \|\Psi_1 - \Psi_0\| + \\
& \varepsilon k h \tau \left[\frac{1-\Delta^m}{1-\Delta} + \frac{1-\Delta^{m+1}}{1-\Delta} + \cdots + \frac{1-\Delta^{n-1}}{1-\Delta} \right] \\
\leq & \frac{\Delta^m}{1-\Delta} \|\phi_1\| + \frac{\varepsilon k h \tau}{1-\Delta} (n-m),
\end{aligned}$$

which converges to zero as $m \to \infty$ under the assumption A2. This implies that there exists a Ψ such that $\lim_{n\to\infty} \Psi_n = \Psi$. Thus, we have $\Psi = \sum_{n=0}^{\infty} \phi_n = \mu(x,t)$, which is the exact solution of the aggregation equation. Further, by fixing m and letting $n \to \infty$, error bound is obtained as

$$\|\mu(x,t) - \Psi_m(x,t)\| \leq \frac{\Delta^m}{1-\Delta} \|\mu_1\|.$$

This concludes the proof of the theorem. □

Remark 4.3.4. *Consider the convergence control parameter h with $\Delta < 1$, so that*

$$\Delta = |1+h| + \delta|h| < 1 \implies \delta < \frac{1-|1+h|}{|h|}, \quad h \neq 0.$$

From the RHS of the above equation, we get

$$\frac{1-|1+h|}{|h|} = \begin{cases} -1 - \frac{2}{h} & h < -1, \\ 1 & -1 \leq h < 0. \\ -1 & h > 0 \end{cases}$$

Therefore, one can choose the parameter $h \in [-1, 0)$.

4.4 Numerical implementation

This section consists of three test cases of the pure aggregation ($G(x) = 0$) equation and one test case of the coupled aggregation-growth equation with different physical kernels. For choosing these problems, physical motivation is provided in Section 1. Due to the non-linearity in the equation, it is hard to find the closed-form solution. Therefore, semi-analytical results are obtained by truncating the series solutions. The accuracy of the truncated results are analyzed by comparing approximated number density and moments with the exact ones. Further, the estimated order of convergence (EOC) is computed and plotted using the formula

$$\text{EOC} = \ln\left(\frac{||\mu(x,t) - N_{2i}||}{||\mu(x,t) - N_{4i}||}\right) / \ln(2),$$

where N_i are the numerical results observed using i degrees of freedom. It is worth to mention that the observations about EOC are identical for all the cases, and hence simulations are plotted for constant kernel only. Throughout the computations, we consider $H = 1$.

4.4.1 Aggregation equation

Example 4.4.1. *Consider $\beta(x,y) = 1$ and $G(x) = 0$ in equation (4.0.1) with initial condition $\mu(x,0) = e^{-x}$ for which the exact solution of the problem is given in [89] as*

$$\mu(x,t) = \frac{4e^{-\frac{2x}{t+2}}}{(t+2)^2}.$$

Using the equation (4.2.1), one gets

$$k(\mu_0) = \frac{1}{2}(\sinh(x) - \cosh(x) + 1) - 1,$$

and employing equation (4.2.3), components of the series solutions are obtained as

$$\phi_1(x,t) = ht\left(e^{-x} - \frac{e^{-x}x}{2}\right),$$

$$\phi_2(x,t) = \frac{1}{8}hte^{-x}\left(h\left(te^{-x}(x-2) + t(x-4)(x-1) - 4x + 8\right) - 4x + 8\right),$$

$$\begin{aligned}\phi_3(x,t) = \frac{1}{96}hte^{-3x}\Big(e^{2x}\Big(&h^2\left(t^2\left(-2x^3 + 20x^2 - 50x + 29\right) + 24t\left(x^2 - 5x + 4\right) - 48(x-2)\right)\\ &+ 12h\left(t\left(2x^2 - 11x + 10\right) - 8(x-2)\right) - 48(x-2)\Big) - 2h^2t^2(x-2)\\ &- 2hte^{x}\left(h\left(t\left(x^2 - 8x + 8\right) - 12(x-2)\right) - 6(x-2)\right)\Big).\end{aligned}$$

Due to the increasing complexity of the components of the series terms, a three-term solution is being considered. Moreover, it is noticed that three terms approximations is good enough for predicting the exact solution. To achieve the greater precision, one can use MATHEMATICA software to calculate the higher-order terms. Figure (4.1) depicts a comparison between the exact and truncated series solutions obtained using IOHAM and ODM. It can be observed that for a short period, both ODM and IOHAM show a good agreement with the exact solution. In contrast, ODM does not match well with the precise number density as time increases, while IOHAM continues to provide a more accurate approximation. In Figures (4.2)(a) and (4.2)(b), errors are displayed to demonstrate the novelty of the proposed schemes. Figure (4.2)(a) displays that errors obtained from all the defined methods are almost negligible up to time $t = 2$ for a fixed x. However, as time progresses, HAM and ODM errors explode, whereas IOHAM error is still insignificant. Figure (4.2)(b) demonstrates the absolute difference between two consecutive terms for time $t = 1$. The difference between the second and third terms is negligible, which leads us to conclude that the contribution of the higher-order terms is negligible and thus, motivates us to shorten the solution to three terms. The accuracy of the three-term truncated solutions can also be observed in Figure (4.2)(c), which depicts a comparison of the number density at time $t = 1$. It can be visualized that the HAM under estimates and ODM over predicts the particle concentration, whereas IOHAM has a remarkable agreement with the actual

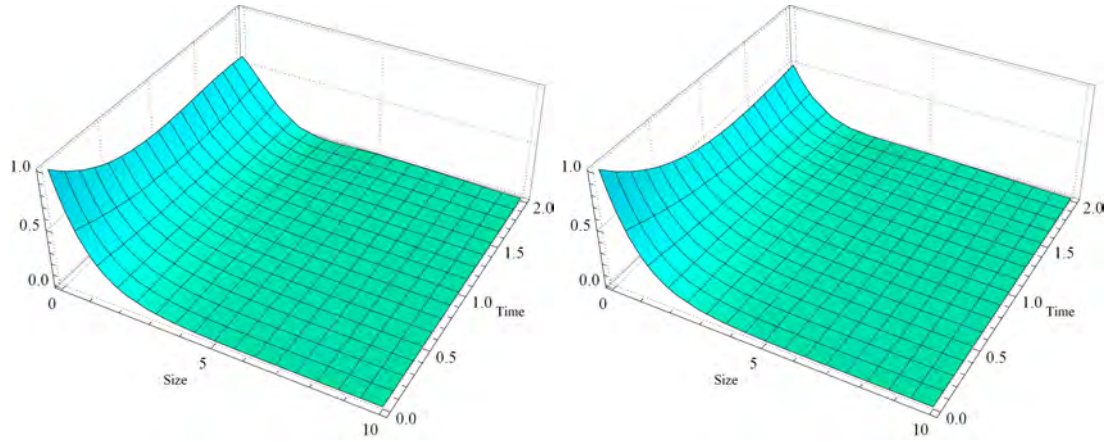

(a) ODM ($n = 3$)

(b) IOHAM ($n = 3$)

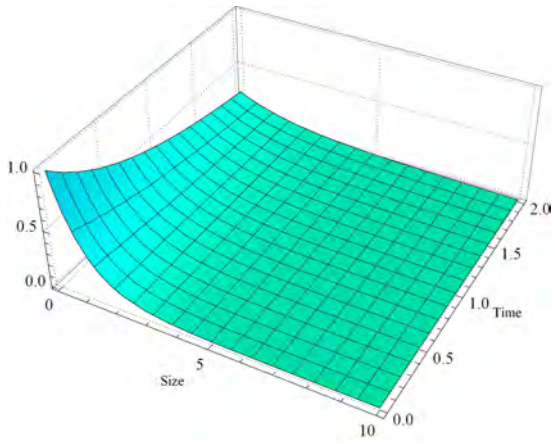

(c) Exact

Figure 4.1: ODM, IOHAM and exact solutions for Example 4.4.1

values. In addition, the 3D absolute errors between exact and truncated solutions using HAM, ODM, and IOHAM are plotted in Figure (4.3). Figures (4.3)(a) and (4.3)(b) indicate that HAM and ODM maintain their accuracy for a brief time. However, the error grows as time passes, whereas in Figure (4.3)(c), IOHAM accuracy persists for a considerable period of time.

Proceeding further, Figure (4.4) compares the zeroth, first, and second moments of the truncated solution to those of the exact solution. The first figure demonstrates that the total number of particles obtained from all truncated solutions correspond well with the precise solution for a specific time. As time passes, HAM and ODM moments deviate from the

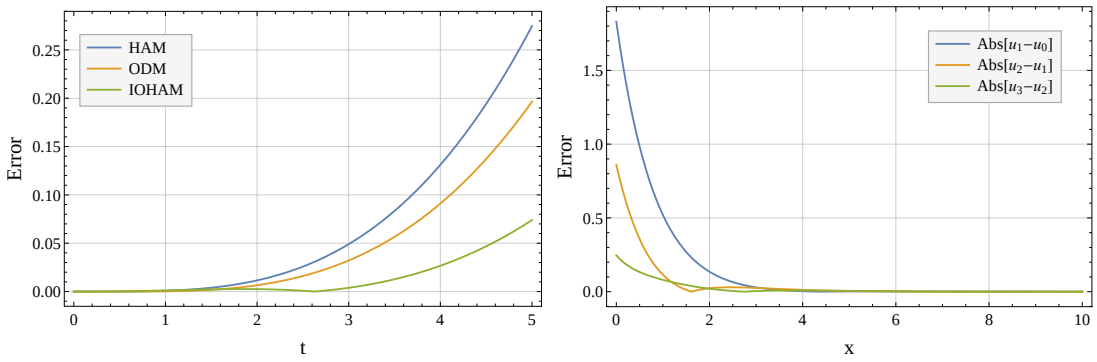

(a) Error at $x = 5$ (b) Error at $t = 1$

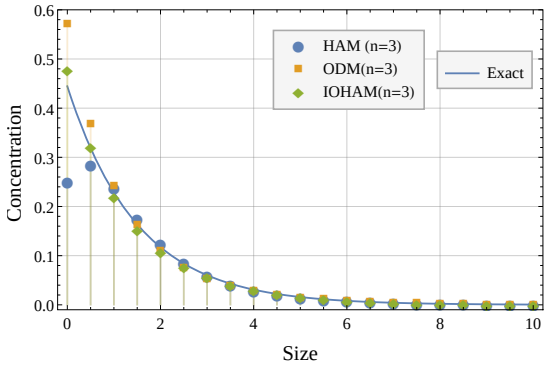

(c) Concentration

Figure 4.2: Concentration and error for 4.4.1

exact one rapidly. In contrast, IOHAM provides a stable and more accurate estimation of a time of greater significance. It is worth mentioning here that the total mass is conserved in all the truncated solutions, as shown in Figure (4.4)(b). Finally, Figure (4.4)(c) shows that the second moment generated by the truncated solution utilizing all methods correspond well to the exact second moment. Further, to add some more novelty of the IOHAM, it can be observed from the error distribution plot in Figure 4.5(a) that as the number of terms increases, the error reduces. In Figure 4.5(b), EOC is provided for HAM, ODM, and IOHAM and it is noticed that the order of convergence is one for all the schemes. However, graph indicates that IOHAM converges towards one faster than ODM and HAM.

Example 4.4.2. *The IOHAM series solution for the aggregation parameter* $\beta(x,y) = (x+y)$ *with exponential initial condition* $\mu_0(x) = e^{-x}$ *is computed and compared with the*

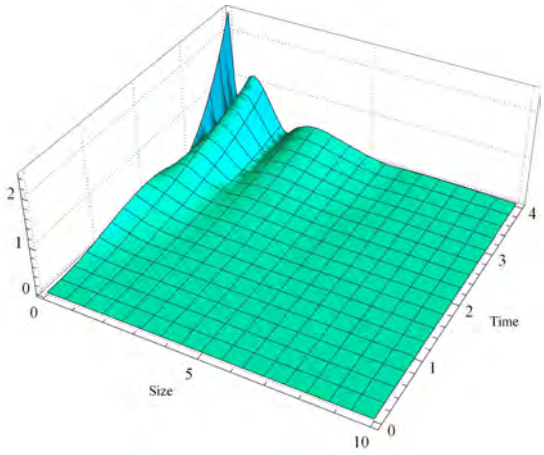

(a) ODM error

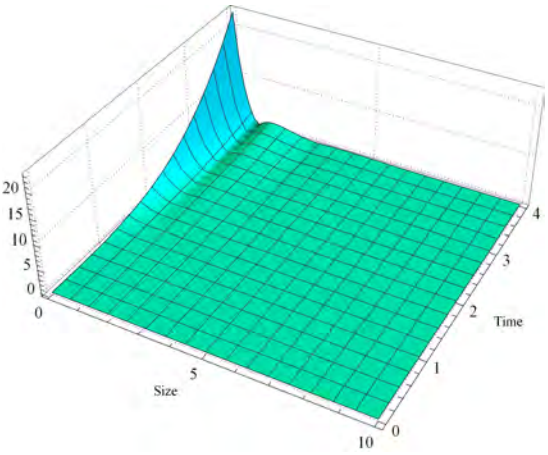

(b) HPM error

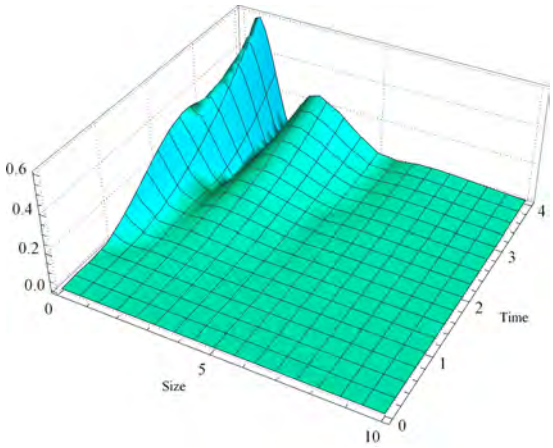

(c) IOHAM error

Figure 4.3: Error for Example 4.4.1

exact solution given in [88] as

$$\mu(x,t) = \frac{e^{\left(e^{-t}-2\right)x-t} I_1\left(2\sqrt{1-e^{-t}}x\right)}{\sqrt{1-e^{-t}}x},$$

where I_1 is the Bessel function of the first kind.

Employing equations (4.2.1) and (4.2.3), $k(\mu_0)$ and the first few components of the series solutions are obtained as follows

$$k(\mu_0) = -x + \frac{1}{2}x(\sinh(x) - \cosh(x) + 1) - 1, \quad \phi_0(x,t) = e^{-x},$$

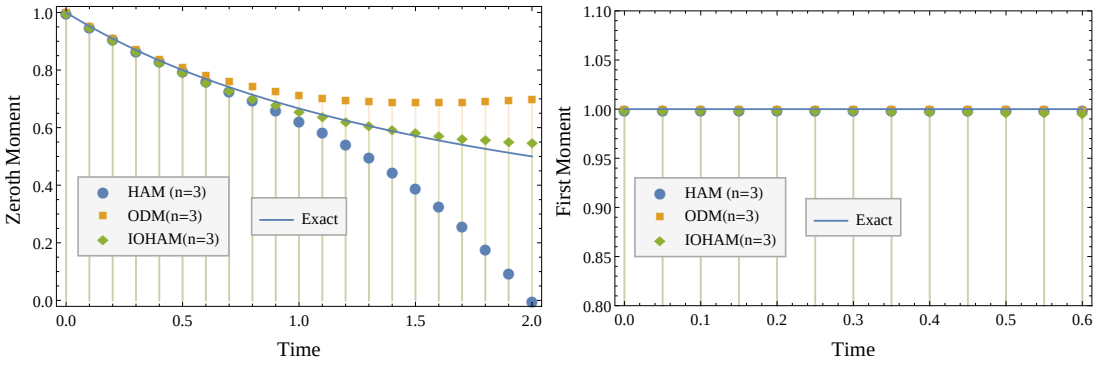

(a) Zeroth moment (b) First moment

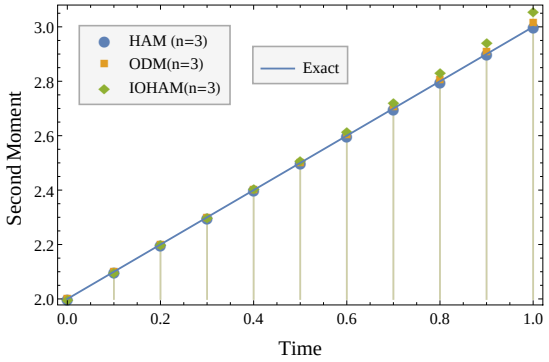

(c) Second moment

Figure 4.4: Moments for Example 4.4.1

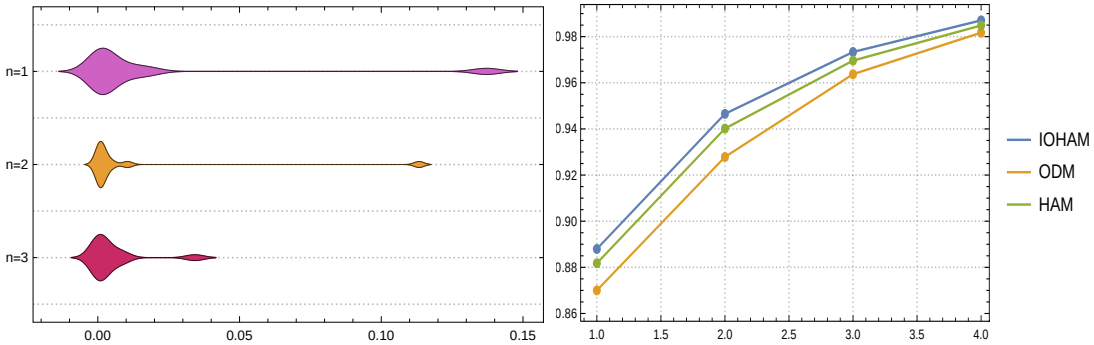

(a) Error distribution (b) Order of convergnce

Figure 4.5: Error distribution and order of convergence for Example 4.4.1

$$\phi_1(x,t) = ht\left(e^{-x}(x+1) - \frac{1}{2}e^{-x}x^2\right).$$

Figure (4.6)(a) depicts the concentration of particles at time $t = 3$, for a three-term truncated solution. It is shown that ODM and HAM fails to estimate the number density

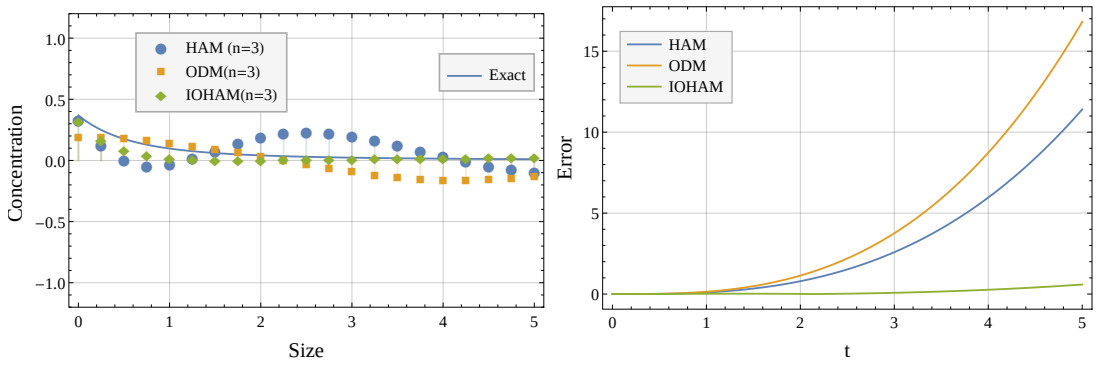

(a) 2D Concentration

(b) Error at $x = 5$

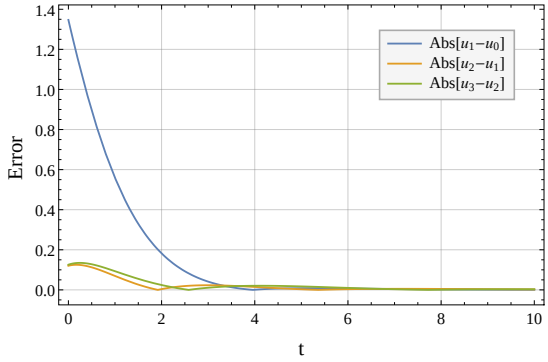

(c) Error at $t = 1$

Figure 4.6: Concentration and error for Example 4.4.2

accurately and exhibit variations, whereas, IOHAM displays a remarkable agreement with the actual solution. In Figure (4.6)(b), the error is plotted over a longer period of time for $x = 5$, and it is important to note that the error obtained using HAM and ODM increases virtually exponentially, whereas the error produced using IOHAM remains tolerable. In addition, Figure (4.6)(c) provides the rationale for truncating the solutions to three terms, since it is obvious that the absolute difference between two successive terms is decreasing and the absolute difference between the second and third terms is nearly negligible. Figure (4.7) depicts contour plots of the errors between finite term series solutions and precise ones and it is observed that HAM exhibits an unacceptable amount of error for smaller size particles but a low amount of error for larger size particles. The same observation is also made for ODM from Figure (4.7)(b), but the error decreases significantly as compared to HAM. However, this error is still difficult to tolerate. Figure

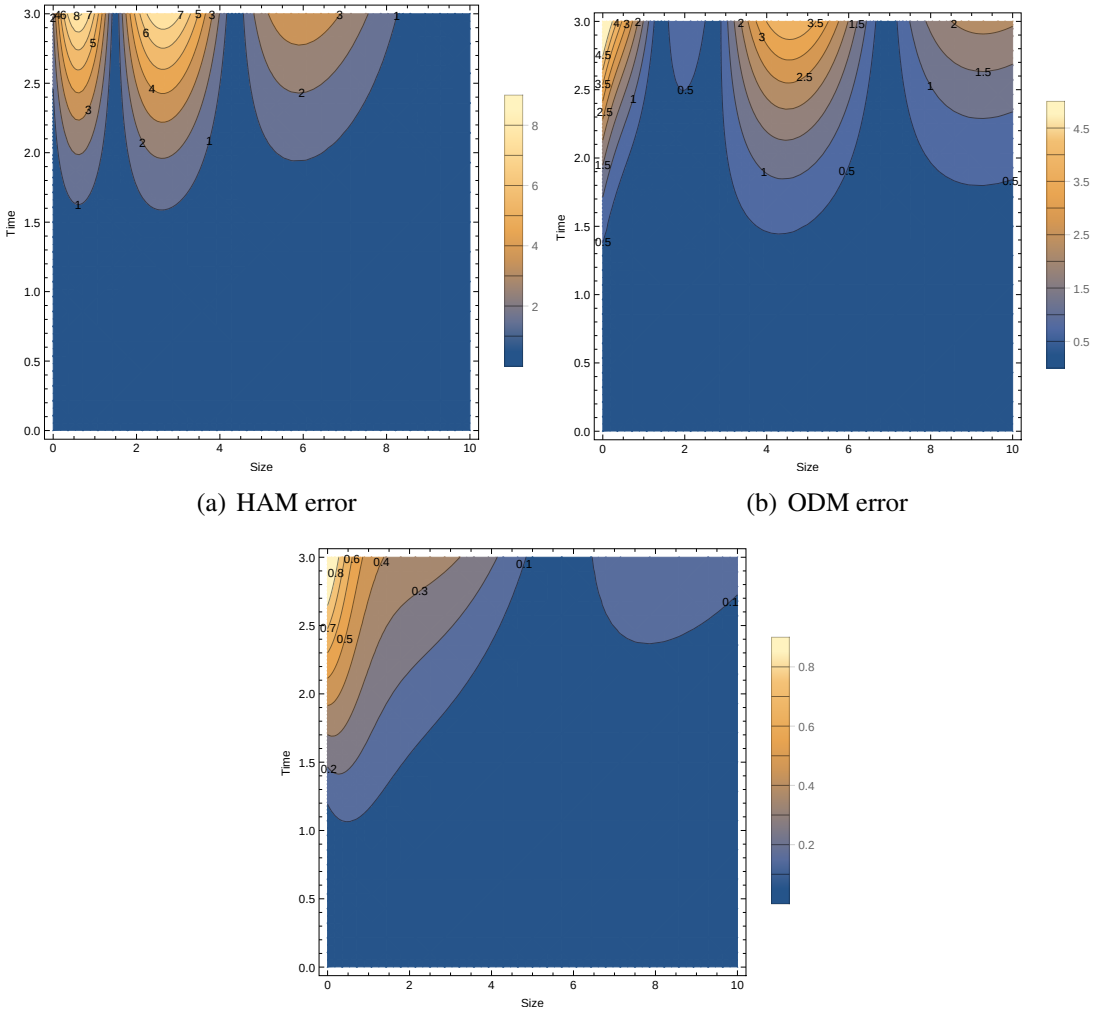

(a) HAM error

(b) ODM error

(c) IOHAM error

Figure 4.7: Error for Example 4.4.2

(4.7)(c) demonstrates that IOHAM yields a negligible error in comparison to the other two approaches, which justify the superiority of the suggested method. Additionally, Figure (4.8) compares the approximated and actual zeroth, first and second moments. It indicates that, over a length of time, all of the stated approaches produce an excellent estimate of the exact moments. However, as time progresses, ODM deviates from the exact solution, but IOHAM continues to provide a better approximation. Notably, where HAM fails to anticipate the number density properly, it delivers a remarkable matching with precise moments. Similar to the preceding example, it is observed that as the number of terms

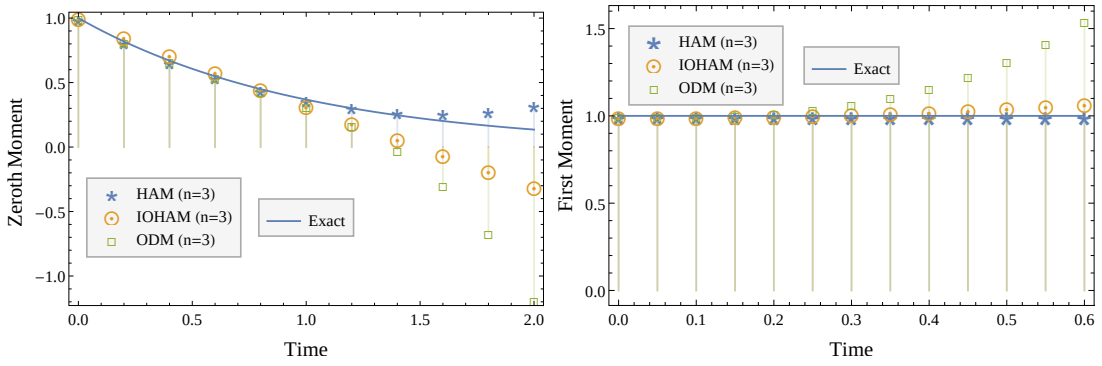

(a) Zeroth moment (b) First moment

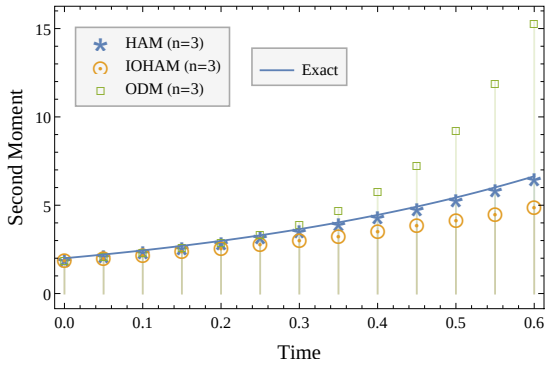

(c) Second moment

Figure 4.8: Moments for Example 4.4.2

increases, the error decreases, and the order of convergence for each technique is 1.

Example 4.4.3. *The IOHAM series solution for the aggregation parameter* $\beta(x,y) = xy$ *with exponential initial condition* $\mu_0(x) = e^{-x}$ *is computed and compared with the exact solution given in [89] as*

$$\mu(x,t) = \sum_{k=0}^{\infty} \frac{t^k x^{3k} \exp(-(t+1)x)}{(k+1)!\Gamma(2k+2)}.$$

Using the formula defined in equation (4.2.1) and recursive relation (4.2.3), one gets

$$\phi_0(x,t) = e^{-x}, \quad \phi_1(x,t) = ht\left(e^{-x}x - \frac{1}{12}e^{-x}x^3\right),$$

$$\phi_2(x,t) = \frac{1}{720} h t e^{-2x} x \Big(e^x \left(h \left(t \left(x \left(x \left(x^3 - 45x + 30 \right) + 180 \right) - 360 \right) - 60x^2 + 720 \right) - 60x^2 + 720 \right) - 15ht(x+2)\left(x^2 - 12\right) \Big).$$

In this instance, the same pattern of particle concentration is observed as in earlier

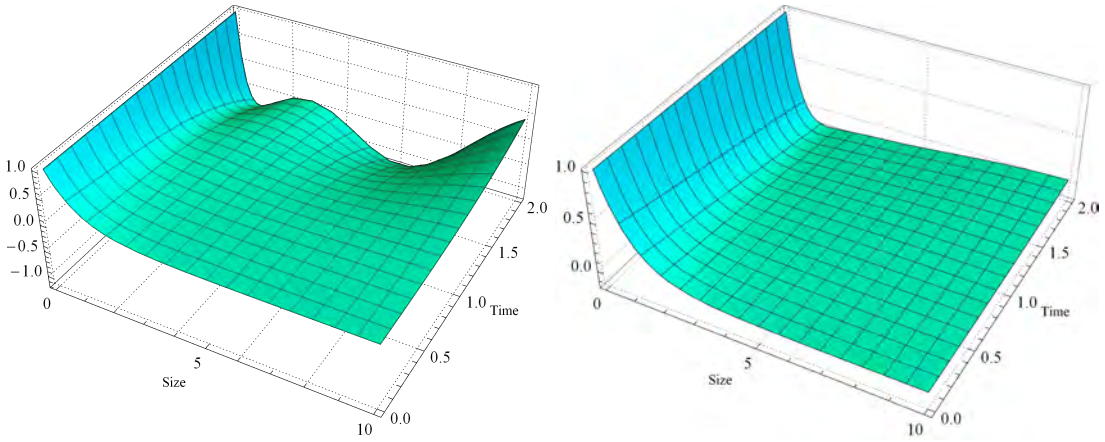

(a) ODM ($n = 3$)

(b) IOHAM ($n = 3$)

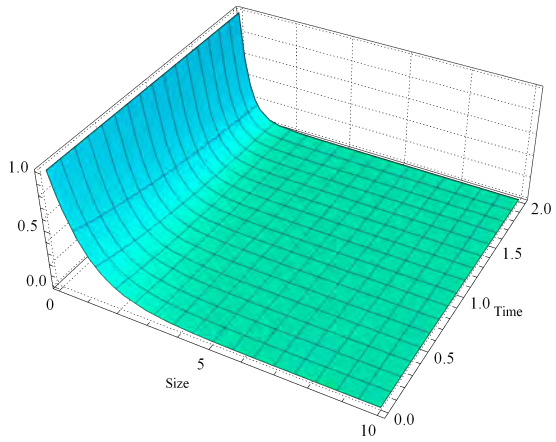

(c) Exact ($n = 3$)

Figure 4.9: ODM, IOHAM and exact solutions for Example 4.4.3

instances. One can see from Figure (4.9) that IOHAM gives a great agreement with the exact solution whereas ODM fails to maintain the precision. Figure (4.10)(a) compares the amount of particles in the system when HAM, ODM, and IOHAM are utilized. It is visualized that HAM over estimates the concentration, while ODM under estimates

it. However, IOHAM contributes significantly to the precise solution. Figure (4.10)(b) depicts error for a fixed x, and it can be noticed that for HPM and ODM, error develops at a relatively rapid pace with time, whereas IOHAM maintains accuracy for large instances. Further, Figure (4.11) presents the error obtained employing HAM, ODM, and IOHAM.

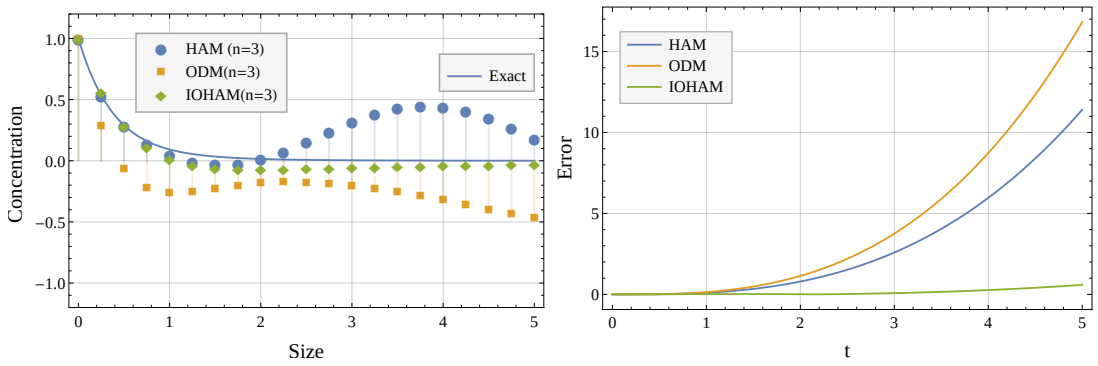

(a) 2D Concentration (b) Error at $x = 5$

Figure 4.10: Concentration and error for Example 4.4.3

As evident in the previous cases, IOHAM still maintains its supremacy and provides a better approximation to the exact solution as compared to other methods.

4.4.2 Aggregation-growth

Example 4.4.4. *Let us now consider the generalized aggregation-growth equation* (4.0.1) *with linear growth rate* $G(x) = x$*, coagulation kernel* $\beta(x,y) = 1$ *and the initial condition* $\mu(x,0) = e^{-x}$*. Exact solution for the problem is given by*

$$\mu(x,t) = \frac{e^{-\frac{e^{-t}x}{\frac{t}{2}+1}-t}}{\left(\frac{t}{2}+1\right)^2}.$$

To get the IOHAM solution iterations, using the equations (4.2.1) and (4.1.2) yield

$$k(\mu_0) = \frac{1}{2}(\sinh(x) - \cosh(x) + 1) - 2, \quad \phi_0(x,t) = e^{-x},$$

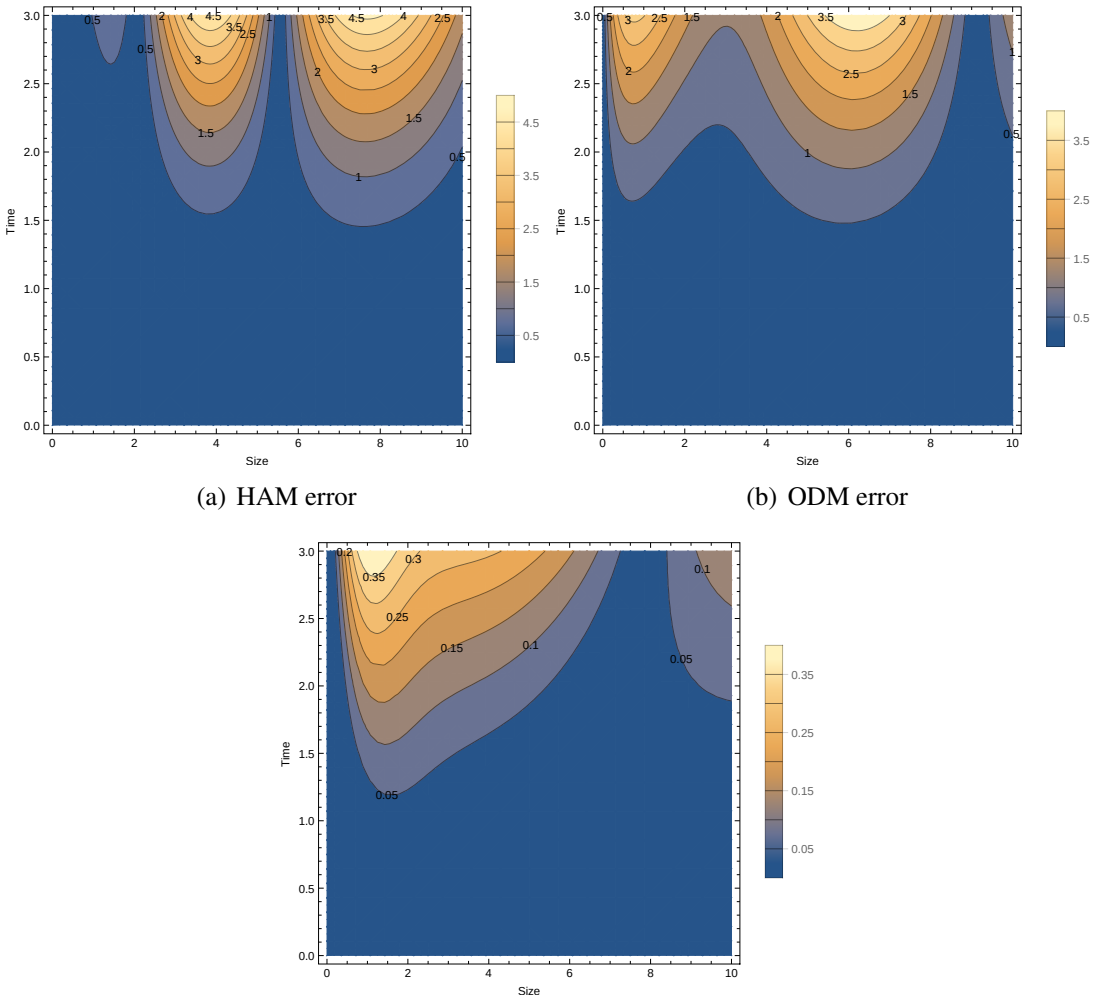

(a) HAM error

(b) ODM error

(c) IOHAM error

Figure 4.11: Error for Example 4.4.3

$$\phi_1(x,t) = ht\left(2e^{-x} - \frac{3e^{-x}x}{2}\right),$$

$$\phi_2(x,t) = \frac{1}{8}hte^{-x}\left(h\left(te^{-x}(3x-4)+t(x(9x-25)+6)-12x+16\right)-12x+16\right),$$

$$\phi_3(x,t) = \frac{1}{96}hte^{-3x}\Big(2h^2t^2(4-3x) - 2hte^{x}(h(t(7x(3x-8)+12)-36x+48)-18x+24)$$
$$+ e^{2x}(h(ht(t(39-2x(9x(3x-16)+143))+24(x(9x-25)+6))+48h(4-3x)$$
$$+ 12tx(18x-59)+96(3t-3x+4))+48(4-3x))\Big).$$

Examining a solution for a truncated series with four terms, it becomes evident from

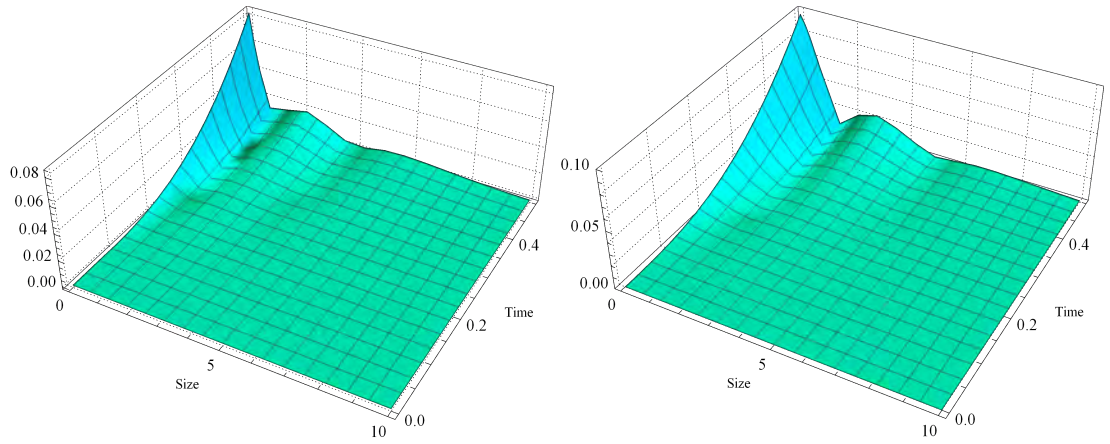

(a) IOHAM error (b) ODM error

Figure 4.12: Errors for Example 4.4.4

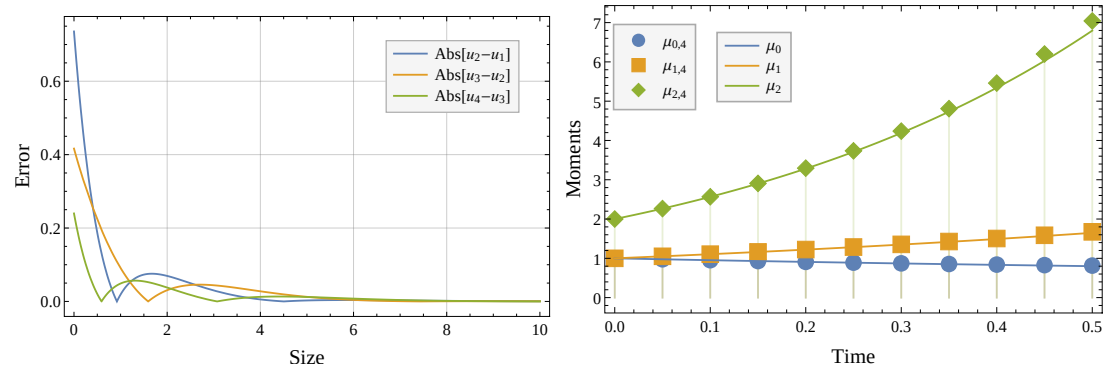

(a) $|u_i - u_{i-1}|$ for $i = 2,3,4$ (b) Moments

Figure 4.13: Absolute difference of consecutive terms and moments for Example 4.4.4

Figure 4.12 that the IOHAM solution corresponds to the exact answer and provides a more precise approximation than ODM. In addition, Figure 4.13(a) demonstrates that for a fixed period of time, the difference between consecutive terms diminishes, indicating that after a certain period of time, the contribution of higher terms disappears, which leads us to truncate the solution for a four-term approximation. In Figure 4.13(b), the convergence of precise and truncated series solutions moments reveal considerable concordance where $\mu_{i,n}$ represents the i^{th} moment with utilizing n-term truncated series solution.

4.5 Conclusions

The chapter developed a new approximated solution for the aggregation and coupled aggregation-growth equations. In this work, a recently developed semi-analytical technique, IOHAM, was employed. Additionally, the convergence analysis of the truncated series solution for this method was examined for the aggregation equation. The numerical results were compared with the existing solutions obtained using HAM, HPM, ADM, and ODM. It was observed that all HAM, HPM, and ADM provided the same results. The ODM improves the solution to some extent, but our proposed scheme improved all the solutions obtained via predefined semi-analytical methods. Moreover, for the first time, an analytical approximate method was implemented for solving the coupled aggregation-growth equation.

Chapter 5

Homotopy perturbation and Adomian decomposition methods for condensing coagulation and Lifshitz-Slyzov models

This chapter implements HPM and ADM to the condensing coagulation and Lifshitz-Slyzov equations. Closed form solutions are derived for constant and product kernels. Additionally, approximated solutions are obtained for additive and Ruckenstein kernels. Mathematical demonstration confirms that the series solutions produced by these approaches align with the exact solution set, thereby validating the method's reliability.

Let us recall the condensing coagulation model describe in Section 1.2.4 as,

$$\frac{\partial c}{\partial t} = Q(c), \tag{5.0.1}$$

where the collision operator Q is defined as,

$$\begin{aligned} Q(c) = &-\frac{\partial}{\partial x}\left[\int_0^x yK(x,y)c(x,t)c(y,t)dy\right] - \int_x^\infty K(x,y)c(x,t)c(y,t)dy \\ &-\frac{\partial}{\partial x}\left[\int_x^\infty yL(x,y)c(x,t)c(y,t)dy\right] - \int_0^x L(x,y)c(x,t)c(y,t)dy, \end{aligned} \tag{5.0.2}$$

This work is published in GEM-International Journal of Geomathematics, 14(4), 2023

where $c(x,t)$ represents the concentration (number density) of particles of mass x at time t and $K(x,y)$ and $L(x,y)$ are the rate at which particles of masses x and y collide, known as the coagulation kernels. The coagulation kernels are non-negative and symmetric, *i.e.,*

$$K(x,y) = K(y,x) \text{ and } L(x,y) = L(y,x). \tag{5.0.3}$$

Such models are not easy to solve analytically and therefore, in this work, we demonstrate two semi-analytical approaches, namely HPM and ADM to find the approximate solutions for CCM and LSE in series form. These techniques are used to solve linear/non-linear ordinary and partial differential equations and also integro-partial differential equations, see [98–104] and further citations for more details.

The organization of this chapter is as follows. In Section 5.1, the basic idea behind the homotopy perturbation and Adomian decomposition methods are presented. Proceeding further, the approximate solutions are compared between two different schemes and/or with the available exact solutions in Section 5.2 considering various kernels. We also plan to discuss these schemes to solve the LSE in Section 5.3 and compare the results with analytical solutions. At the end, some conclusions are reported.

5.1 Semi-analytical methods

In this section, HPM and ADM are explained for solving CCM.

5.1.1 Homotopy perturbation method

This method was proposed by J. He in 1999 [99, 100] for ordinary/partial differential equations, in which the solution is considered as a sum of infinite series, which converges to the exact solution. To understand this, let us consider,

$$A(c) - h(r) = 0, r \in \Omega \subset \mathbb{R}^n, \tag{5.1.1}$$

with boundary condition

$$B\left(c, \frac{\partial c}{\partial n}\right) = 0, r \in \partial\Omega, \tag{5.1.2}$$

where A is a general differential operator and B is a boundary operator. Usually, the operator A can be decomposed into linear and non-linear parts and so equation (5.1.1) can be rewritten as

$$L(c) + N(c) - h(r) = 0, \tag{5.1.3}$$

for L and N being linear and non-linear operators, respectively. Thanks to HPM, construct a homotopy $v(r,p) : \Omega \times [0,1] \to \mathbb{R}$ that satisfies,

$$H[v(r,p)] = (1-p)[L(v(r,p)) - L(c_0)] + p[A(v(r,p)) - h(r)] = 0, \tag{5.1.4}$$

where c_0 is an initial condition associated with problem (5.1.1) and $p \in [0,1]$ is an embedding parameter. According to the HPM, let us assume

$$v = \sum_{k=0}^{\infty} p^k v_k. \tag{5.1.5}$$

Substituting (5.1.5) in (5.1.4) and then letting $p = 1$, we obtain the solution as,

$$c(x,t) = \lim_{p \to 1} v = \sum_{k=0}^{\infty} v_k. \tag{5.1.6}$$

Now, we proceed further to solve the CCM equation (5.0.1)-(5.0.2) with initial condition taken as

$$c(x,0) = c_0(x). \tag{5.1.7}$$

For simplicity and to compare the approximate solutions with available exact solutions, let us assume that $K(x,y) = L(x,y)$ which reduces the equation (5.0.1) to

$$\frac{\partial c}{\partial t} = Q(c) = -\frac{\partial}{\partial x}\left[\int_0^\infty yK(x,y)c(x,t)c(y,t)dy\right] - \int_0^\infty K(x,y)c(x,t)c(y,t)dy. \quad (5.1.8)$$

Construct the homotopy of the equation (5.1.8) as follows,

$$H(v,p) = (1-p)\left[\frac{\partial v}{\partial t} - \frac{\partial c_0}{\partial t}\right] + p\left[\frac{\partial v}{\partial t} + \frac{\partial}{\partial x}\left(\int_0^\infty yK(x,y)v(x,t)v(y,t)dy\right) + \int_0^\infty K(x,y)v(x,t)v(y,t)dy\right] = 0. \quad (5.1.9)$$

Using the expression (5.1.5) in (5.1.9), collecting the terms in powers of p and then setting their coefficients to zero, we get

$$\begin{aligned}
p^0 &: \frac{\partial v_0}{\partial t} = \frac{\partial c_0}{\partial t},\\
p^1 &: \frac{\partial v_1}{\partial t} = -\frac{\partial}{\partial x}\left(\int_0^\infty yK(x,y)v_0(x,t)v_0(y,t)dy\right) - \int_0^\infty yK(x,y)v_0(x,t)v_0(y,t)dy - \frac{\partial c_0}{\partial t},\\
&\qquad v_1(x,0) = 0,\\
p^2 &: \frac{\partial v_2}{\partial t} = -\frac{\partial}{\partial x}\left(\int_0^\infty yK(x,y)\left(v_0(x,t)v_1(y,t) + v_1(x,t)v_0(y,t)\right)dy\right)\\
&\qquad - \int_0^\infty yK(x,y)\left(v_0(x,t)v_1(y,t) + v_1(x,t)v_0(y,t)\right)dy, \quad v_2(x,0) = 0,\\
p^3 &: \frac{\partial v_3}{\partial t} = -\frac{\partial}{\partial x}\left(\int_0^\infty yK(x,y)\left(v_0(x,t)v_2(y,t) + v_1(x,t)v_1(y,t) + v_2(x,t)v_0(y,t)\right)dy\right)\\
&\qquad - \int_0^\infty yK(x,y)\left(v_0(x,t)v_2(y,t) + v_1(x,t)v_1(y,t) + v_2(x,t)v_0(y,t)\right)dy, \quad v_3(x,0) = 0,\\
&\qquad \vdots\\
p^k &: \frac{\partial v_k(x,t)}{\partial t} = -\frac{\partial}{\partial x}\left[\sum_{l=0}^{k-1}\int_0^\infty yK(x,y)v_l(x,t)v_{k-l-1}(y,t)dy\right] -\\
&\qquad \left[\sum_{l=0}^{k-1}\int_0^\infty K(x,y)v_l(x,t)v_{k-l-1}(y,t)dy\right], v_k(x,0) = 0.
\end{aligned}$$

Let us consider $v_0 = c_0 = f(x)$, consequently $\dfrac{\partial c_0}{\partial t} = 0$. Therefore, we have

$$
\begin{aligned}
v_1 &= \int_0^t \left(-\frac{\partial}{\partial x} \left(\int_0^\infty yK(x,y)v_0(x,t)v_0(y,t)dy \right) - \int_0^\infty yK(x,y)v_0(x,t)v_0(y,t)dy \right) dt, \\
v_2 &= \int_0^t \left(-\frac{\partial}{\partial x} \left(\int_0^\infty yK(x,y) \left(v_0(x,t)v_1(y,t) + v_1(x,t)v_0(y,t) \right) dy \right) \right. \\
&\quad \left. - \int_0^\infty yK(x,y) \left(v_0(x,t)v_1(y,t) + v_1(x,t)v_0(y,t) \right) dy \right) dt, \\
&\vdots \\
v_k &= \int_0^t \left(-\frac{\partial}{\partial x} \left[\sum_{l=0}^{k-1} \int_0^\infty yK(x,y)v_l(x,t)v_{k-l-1}(y,t)dy \right] \right. \\
&\qquad \left. - \left[\sum_{l=0}^{k-1} \int_0^\infty K(x,y)v_l(x,t)v_{k-l-1}(y,t)dy \right] \right) dt. \qquad (5.1.10)
\end{aligned}
$$

Setting $p = 1$ results in an approximation to the solution of the problem (5.1.8) and one gets

$$
c(x,t) = \lim_{p \to 1} v = v_0 + v_1 + v_2 + v_3 + \dots. \qquad (5.1.11)
$$

We will formulate the right-hand side of (5.1.10) for different kernels later on.

5.1.2 Adomian decomposition method

This method was introduced by George Adomian in 1988 [78]. To apply the scheme for solving the equation (5.1.8) with initial condition given as in equation (5.1.7), let us rewrite the equation (5.1.8) as follows

$$
\boldsymbol{L}c(x,t) = -\frac{\partial}{\partial x} \left[\int_0^\infty yK(x,y)f(c)dy \right] - \int_0^\infty K(x,y)f(c)dy. \qquad (5.1.12)
$$

Here $\boldsymbol{L} = \frac{\partial}{\partial t}$ is a linear differential operator and the inverse operator $\boldsymbol{L}^{-1}$ is defined as

$$
\boldsymbol{L}^{-1} = \int_0^t [.]dt, \qquad (5.1.13)
$$

and

$$f(c) = c(x,t)c(y,t). \tag{5.1.14}$$

Operating $\boldsymbol{L}^{-1}$ on both the sides of (5.1.12) with initial condition $c(x,0) = c_0(x)$ gives

$$c(x,t) = c_0(x) - \boldsymbol{L}^{-1}\left[\frac{\partial}{\partial x}\int_0^\infty yK(x,y)f(c)dy + \int_0^\infty K(x,y)f(c)dy\right]. \tag{5.1.15}$$

Following [78], it is known that ADM provides the solution $c(x,t)$ and the non-linear function $f(c)$ by the infinite series,

$$c(x,t) = \sum_{n=0}^{\infty} v_n(x,t), \quad f(c) = \sum_{n=0}^{\infty} A_n(x,t), \tag{5.1.16}$$

where $A_n's$ are called Adomian polynomials. Thanks to [82], these polynomials are given as,

$$A_0 = v_0(x,t)v_0(y,t), \quad A_1 = v_0(x,t)v_1(y,t) + v_1(x,t)v_0(y,t),$$

and in general A_{n-1} is

$$A_{n-1} = \sum_{j=0}^{n-1} v_j(x,t)v_{n-j-1}(y,t), \quad \text{for} \quad n \geq 1.$$

So, the iteration using ADM would be as follows

$$\begin{aligned} v_0 &= c_0(x) \\ v_n &= -\boldsymbol{L}^{-1}\left(\frac{\partial}{\partial x}\int_0^\infty yK(x,y)A_{n-1}dy + \int_0^\infty K(x,y)A_{n-1}dy\right), n = 1,2,3,\cdots. \end{aligned} \tag{5.1.17}$$

Using the value of A_n in (5.1.17) leads to

$$v_n = -\boldsymbol{L}^{-1}\left(\frac{\partial}{\partial x}\int_0^\infty yK(x,y)\sum_{j=0}^{n-1} v_j(x,t)v_{n-j-1}(y,t)dy + \int_0^\infty K(x,y)\sum_{j=0}^{n-1} v_j(x,t)v_{n-j-1}(y,t)dy\right). \tag{5.1.18}$$

Note that (5.1.18) is exactly the same as equation (5.1.10), concluding that the series solutions for CCM are same by using both ADM and HPM.

5.2 Numerical results

In this section, approximate solutions for the number density and the total number of particles obtained by ADM or HPM are compared with the exact solutions when constant and product kernels are taken with some given initial conditions. There are exceptional cases where the analytical solution for number density or moments are not available and it is not always possible to find such a solution to many problems. So, we choose a midway and try to investigate the problem's semi-analytic solutions. In all the cases, truncated series solution is provided for different values of n and the error plot is discussed.

5.2.1 Multiplicative kernel

Consider (5.1.8) with kernel $K(x,y) = xy$ and the initial condition $c_0(x) = e^{-x}$. Now, for approximate solution by ADM, using these values in the equation (5.1.10) yields

$$v_0(x,t) = e^{-x}, \quad v_1(x,t) = e^{-x}t(x-2), \quad v_2(x,t) = \frac{1}{2}e^{-x}t^2(2+(-4+x)x),$$

$$v_3(x,t) = \frac{1}{6}e^{-x}t^3(6+(-6+x)x)x, \quad v_4(x,t) = \frac{1}{24}e^{-x}t^4(12+(-8+x)x)x^2$$

and proceeding further, one gets the general form as $v_k(x,t) = \frac{1}{k!}e^{-x}t^k(k(k-1)+(-2k+x)x)x^{k-2}$. Hence, following (5.1.6) leads to

$$c(x,t) = \sum_{k=0}^{\infty} v_k(x,t) = \sum_{k=0}^{\infty} \frac{1}{k!}e^{-x}t^k(k(k-1)+(-2k+x)x)x^{k-2} = e^{x(t-1)}(t-1)^2. \tag{5.2.1}$$

It is the exact solution of the CCM, as given in Davidson's thesis [63]. To see the efficiency of proposed algorithm finite n-term truncated series solution can be obtained via

$$c_n(x,t) = \sum_{j=0}^{n} v_j(x,t),$$

and numerical simulations are compared with the exact solutions. Further, to check the accuracy of the scheme, we compute the truncation error using the formula

$$\text{Error} = \Delta_m = \sum_{i=1}^{m} |c_n(x,t) - c(x,t)| h_i, \tag{5.2.2}$$

where m defines the number of subintervals, h_i the length of the interval and $c(x,t)$ is the exact solution. Table 5.1 shows the truncation error for different values of n. Using

n	2	4	6	8	10
Δ_n	0.00417	0.000038	37.0722×10^{-5}	40.8357×10^{-7}	40.8645×10^{-9}

Table 5.1: Truncation error when $t = 0.7$ & $x \in [0,10]$ for $n = 2,4,6,8,10$ taking $h_i = 0.01$.

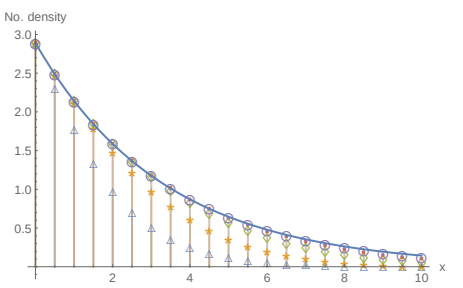

(a) Exact vs. series solutions at $t = 0.7$

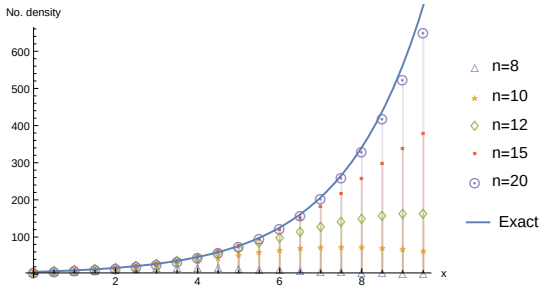

(b) Exact vs. series solutions at $t = 1$

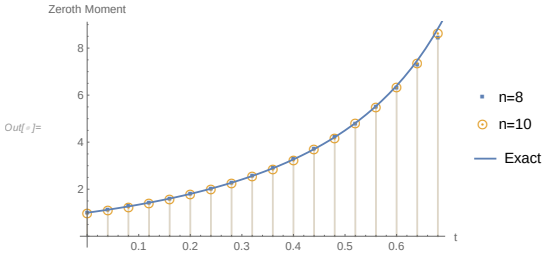

(c) Zeroth moment

Figure 5.1: Number density and zeroth moment

the error formula defined in equation (5.2.2), we observe that the error decreases by increasing the number of terms. Figure 5.1(a) provides the comparison between exact and approximated number density for $n = 2,4,6,8$ and 10 while the exact zeroth moment is compared with 8 and 10 terms approximated solutions in Figure 5.1(b). It is noticed that

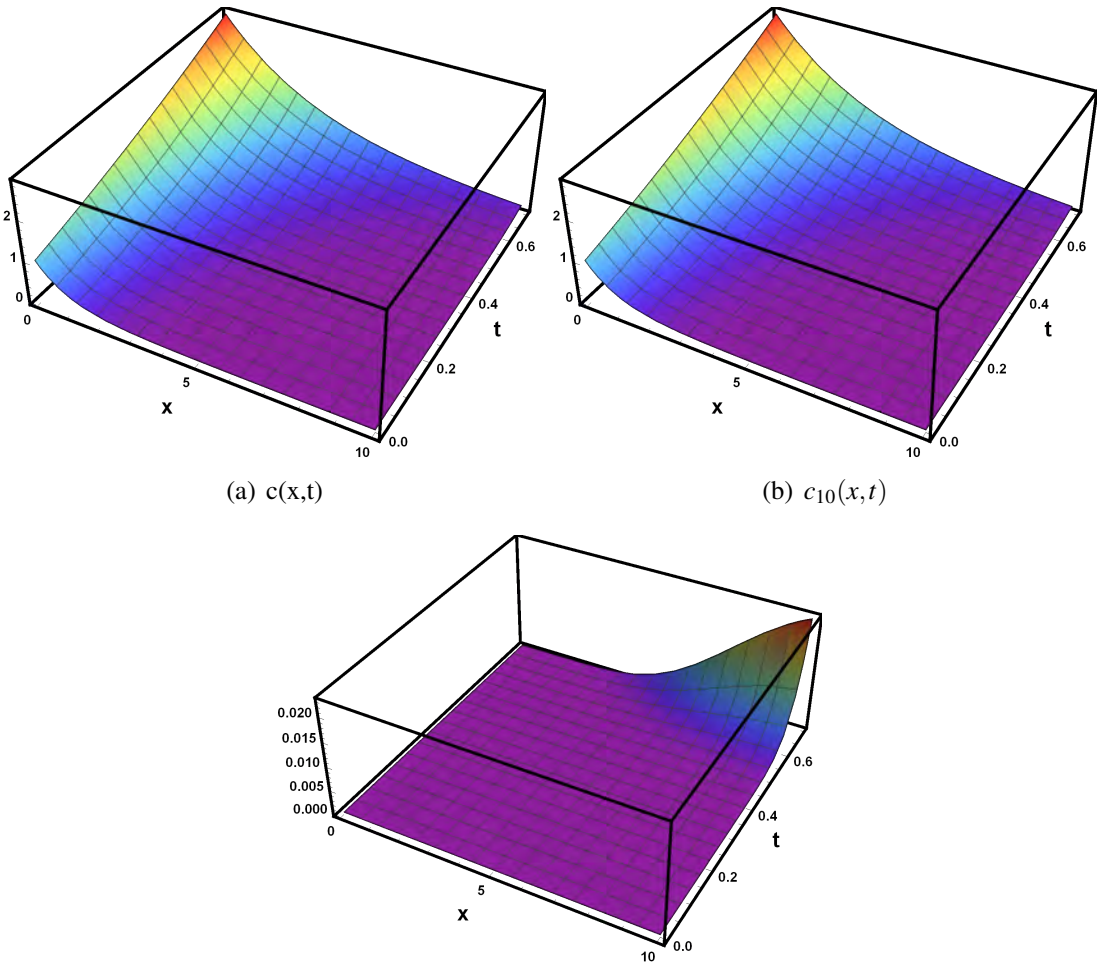

(a) c(x,t)

(b) $c_{10}(x,t)$

(c) $|c(x,t)-c_{10}(x,t)|$

Figure 5.2: Number density and error

the series solution converges towards the exact solution for large n and in fact $c_{10}(x,t)$ coincides with the exact concentration and allows excellent agreement with the zeroth moment at $t = 0.7$. In addition, Figure 5.2 has a similar pattern of behavior that is a three-dimensional plot of the exact and truncated solutions reveals that the results are almost identical, and the error is minimal.

5.2.2 Constant kernel

In this case, the exact solutions for the number density are available for two different initial conditions $c_0(x) = xe^{-x}$ and $c_0(x) = x^2e^{-x}$, see [63]. In the first case, thanks to HPM and

ADM, we are able to sum the series and the result is exactly matching with the available analytical solutions. While for the second case, few term approximations are considered and approximate solutions are compared with the exact solutions.

5.2.2.1 Case 1: Consider $K(x,y) = \alpha$ and $c_0(x) = xe^{-x}$

Using these values in equation (5.1.10), we get

$$v_0(x,t) = xe^{-x}, \quad v_1(x,t) = \alpha t e^{-x}(x-2), \quad v_2(x,t) = \alpha^2 t^2 e^{-x}(x-2),$$

$$v_3(x,t) = \alpha^3 t^3 e^{-x}(x-2), \quad v_4(x,t) = \alpha^4 t^4 e^{-x}(x-2), \ldots, v_n(x,t) = \alpha^n t^n e^{-x}(x-2), n \neq 0.$$

Hence, equation (5.1.6) leads to

$$c(x,t) = \sum_{n=0}^{\infty} v_n(x,t) = \sum_{n=1}^{\infty} \alpha^n t^n e^{-x}(x-2) + xe^{-x} = -\frac{\alpha t e^{-x}(x-2)}{\alpha t - 1} + xe^{-x}, \quad \alpha t < 1 \tag{5.2.3}$$

which is the exact solution for the problem. Let us consider the aggregation kernel $\alpha = 1$ for numerical investigations, which leads us to the restriction on time that is $t < 1$ as $\alpha t < 1$. One may take a small value of alpha to study the behavior of particles for ample time. Figure 5.3 represents the comparison of the exact and truncated solutions for

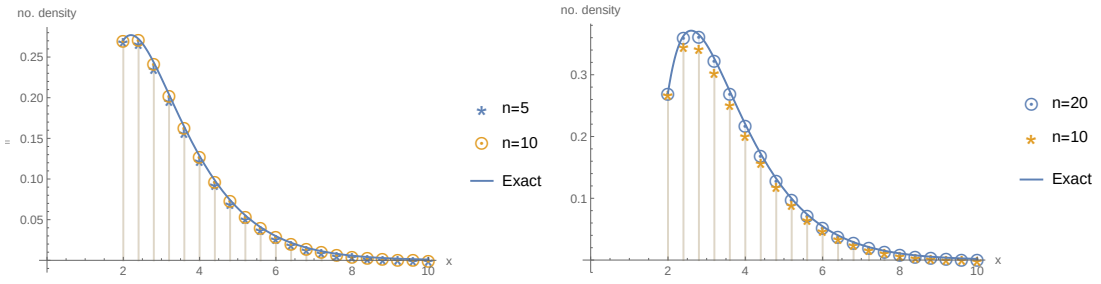

(a) $c_n(x,t)$ vs. $c(x,t)$ for $n = 5, 10$ at $t = 0.6$ (b) $c_n(x,t)$ vs. $c(x,t)$ for $n = 10, 20$ at $t = 0.8$

Figure 5.3: Exact and series solutions for number density by taking (a) $n = 5, 10$ at $t = 0.6$ and (b) $n = 10, 20$ at $t = 0.8$ for $\alpha = 1$

several values of n. Similar to the previous test case, again it is reported from this figure that as the number of series terms increases, more accuracy with respect to time can be

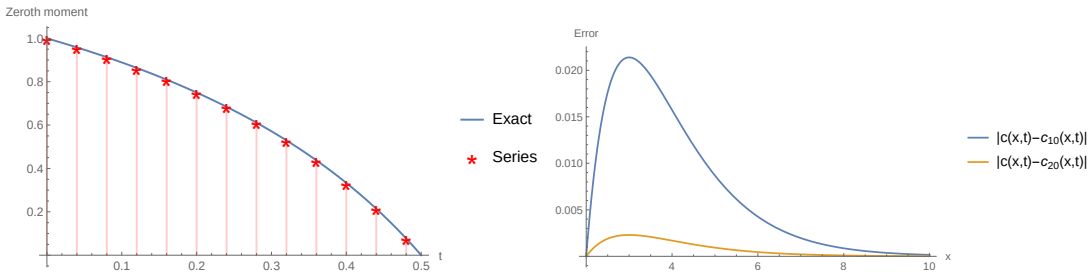

(a) Zeroth moment (b) Error

Figure 5.4: (a) Exact and 10-term zeroth moment and (b) errors between exact and approximated number density for $n = 10, 20$ considering $\alpha = 1$

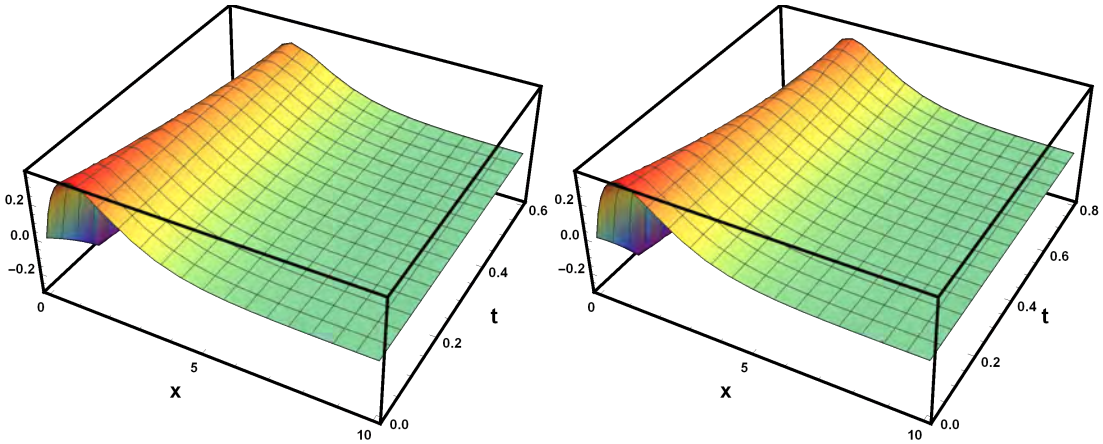

(a) $c_6(x,t)$ at $t = 0.6$ (b) $c_6(x,t)$ at $t = 0.8$

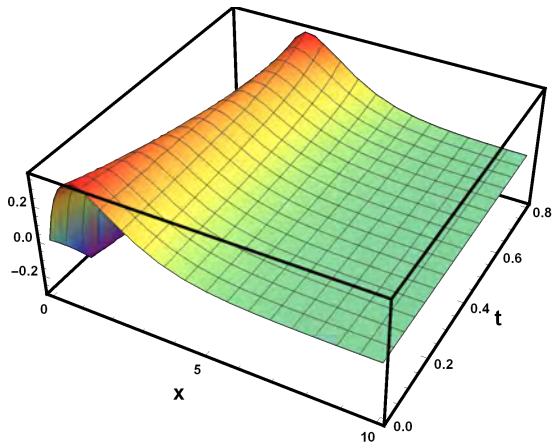

(c) $c_8(x,t)$ at $t = 0.8$

Figure 5.5: Number density

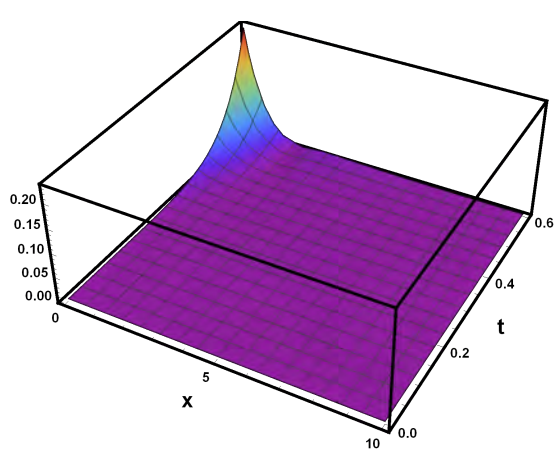

(a) $|c(x,t)-c_6(x,t)|$ at $t=0.6$

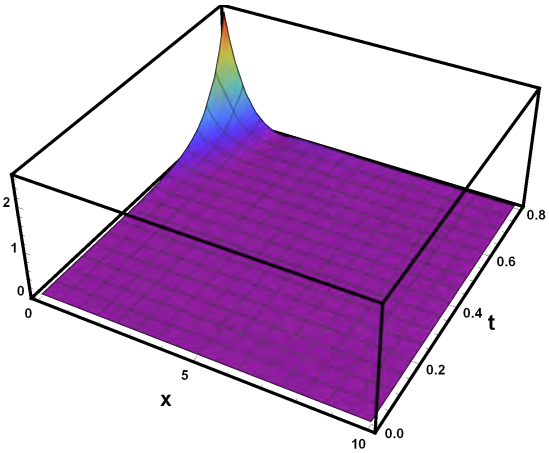

(b) $|c(x,t)-c_6(x,t)|$ at $t=0.8$

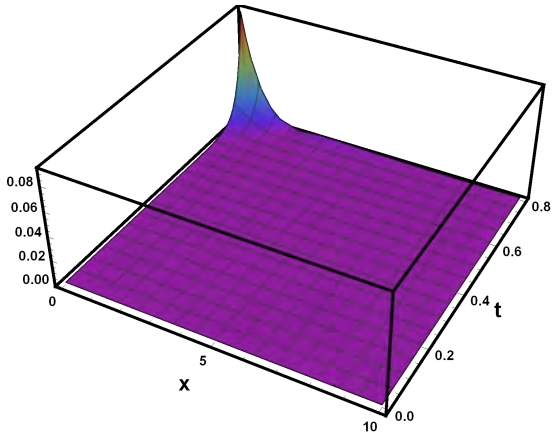

(c) $|c(x,t)-c_8(x,t)|$ at $t=0.8$

Figure 5.6: Error

achieved. It can also be observed that for $t=0.6$, $c_{10}(x,t)$ coincides with the exact solution in Figure 5.3(a), while the same holds true for $c_{20}(x,t)$ when $t=0.8$ in Figure 5.3(b). This concludes that, for large computational time, one has to take more number of terms to achieve better accuracy. A similar observation has also been noticed in [16] for solving coagulation-fragmentation models. Further, in Figure 5.4(a), total number of particles computed via HPM is visualized for $n=10$ and the result is found to be in good match with the exact moment. Also, the error plots between the exact and 10-term, 20-term series solutions are given in Figure 5.4(b). One can easily see that the error decreases for large n and is very insignificant for $n=20$. The same observation we have noticed for Figure

(5.5), and Figure (5.6) represents truncated number density and error between exact and truncated solution at time $t = 0.6$ and $t = 0.8$.

To study the model's behavior for a considerable time, one more case is taken into account, i.e., $\alpha = \frac{1}{10}$. Figure 5.7 shows that the approximate solution enjoys a remarkable agreement with the exact solution, and the error is almost negligible at time $t = 8$.

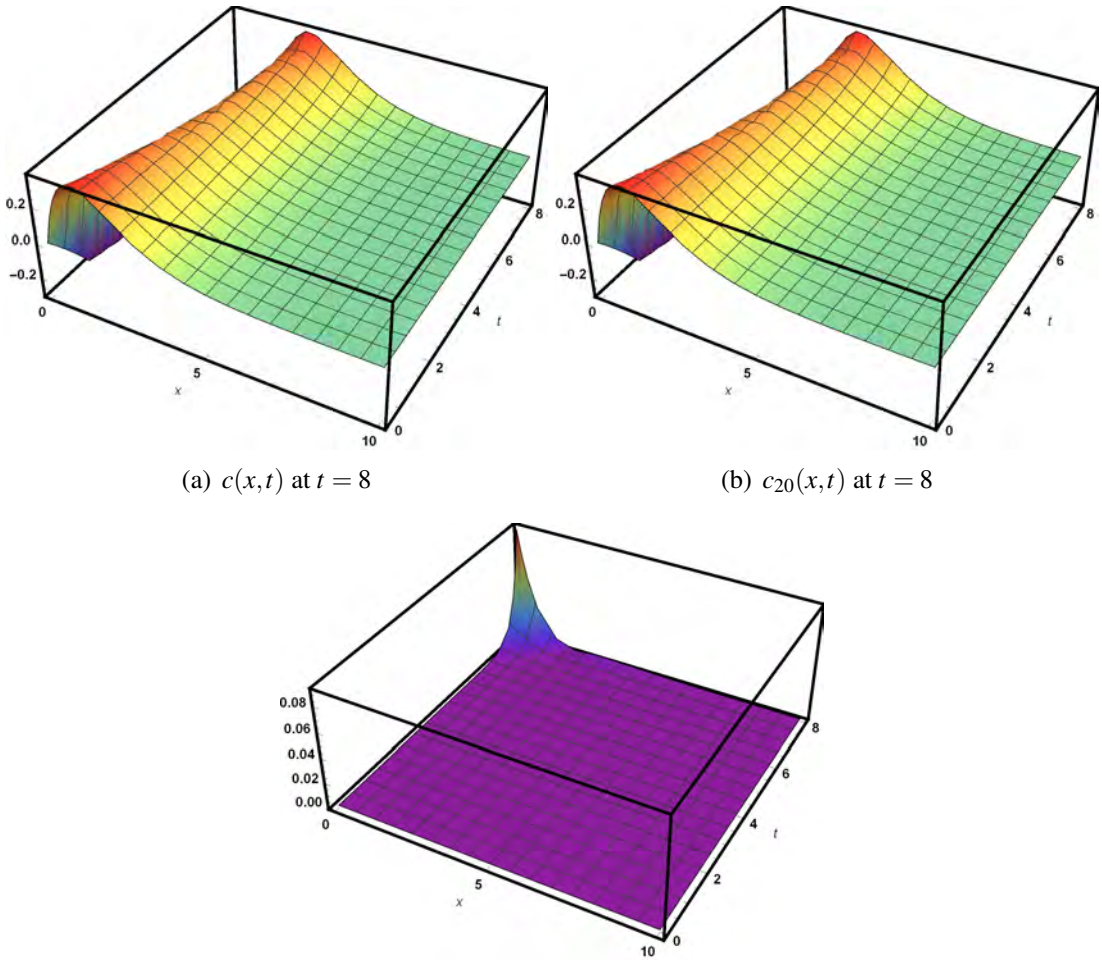

(a) $c(x,t)$ at $t = 8$

(b) $c_{20}(x,t)$ at $t = 8$

(c) $|c(x,t) - c_{20}(x,t)|$ at $t = 8$

Figure 5.7: Number density and error

5.2.2.2 Case 2: Assume $K(x,y) = \alpha$ and $c_0(x) = x^2 e^{-x}$

Taking these values of K and $c_0(x)$, equation (5.1.10) provide

$$v_0(x,t) = x^2 e^{-x}, \quad v_1(x,t) = 4\alpha t e^{-x}(x-3)x,$$

$$v_2(x,t) = 2\alpha^2 t^2 e^{-x}(x(5x-24)+18), \quad v_3(x,t) = 8\alpha^3 t^3 e^{-x}(x-6)(2x-3),$$

$$v_4(x,t) = 4\alpha^4 t^4 e^{-x}((x-48)x+90) \quad \text{and} \quad v_5(x,t) = 16\alpha^5 t^5 e^{-x}(x+3)(5x-12).$$

Having the above, considering a 5 term approximation yields

$$c(x,t) \approx \sum_{k=0}^{5} v_k(x,t), \tag{5.2.4}$$

where the exact solution is given in Davidson's thesis [63] as,

$$c(x,t) = \frac{e^{6\alpha t - x}(x-6\alpha t)^2}{2\alpha t + 1}, \quad x - 6\alpha t > 0. \tag{5.2.5}$$

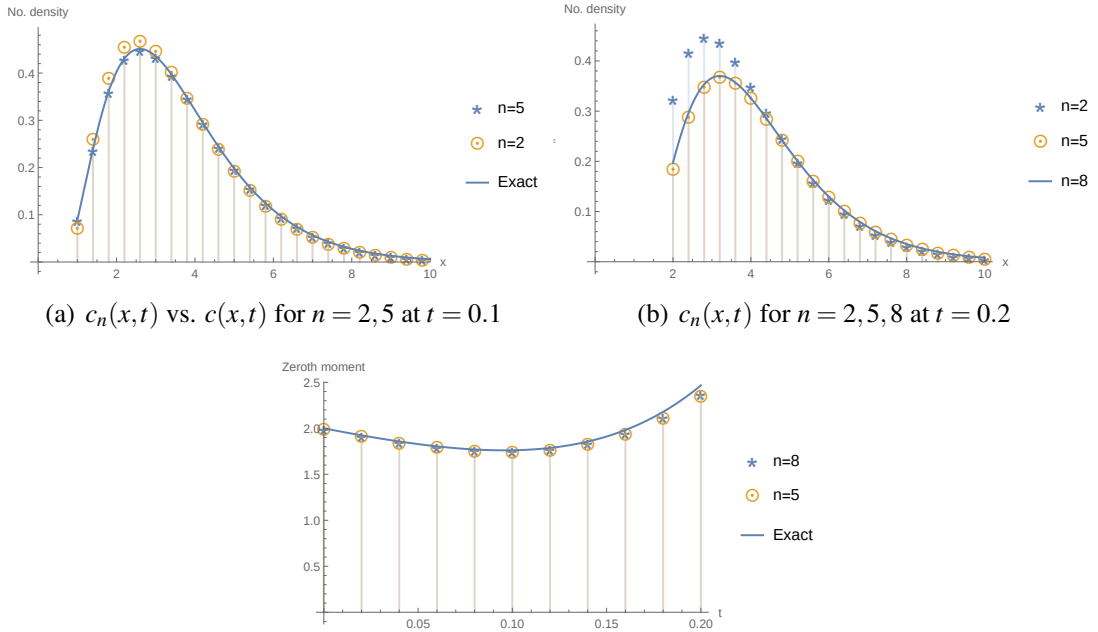

(a) $c_n(x,t)$ vs. $c(x,t)$ for $n = 2,5$ at $t = 0.1$

(b) $c_n(x,t)$ for $n = 2,5,8$ at $t = 0.2$

(c) Zeroth moment

Figure 5.8: (a) Exact and series solutions for $n = 2,5$ at $t = 0.1$ and (b) series solutions for $n = 2,5,8$ at $t = 0.2$ and (c) comparison of exact and numerical zeroth moments at $t = 0.2$

We analyze the curve for the truncated solutions along with the exact ones for two values of n in Figure 5.8(a). This figure indicates that for $n = 5$, the numerical simulation curve

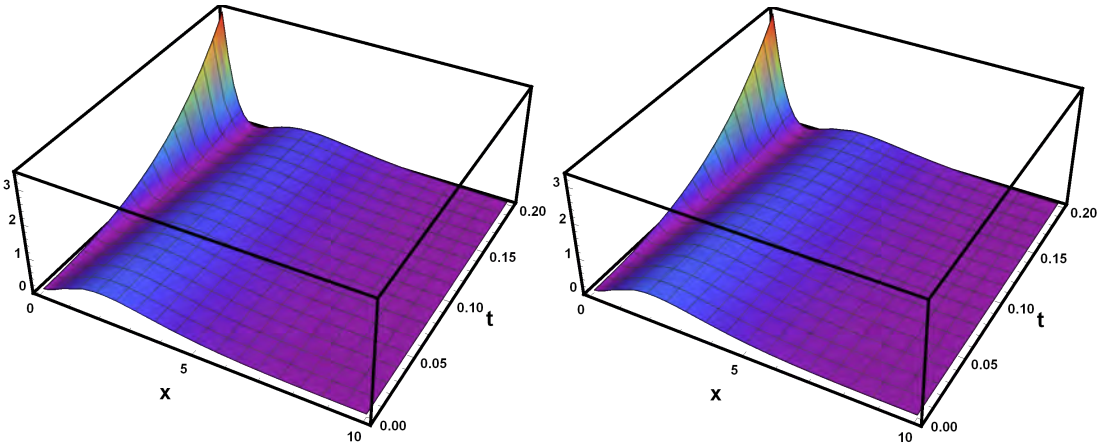

(a) Exact solution (b) $c_8(x,t)$

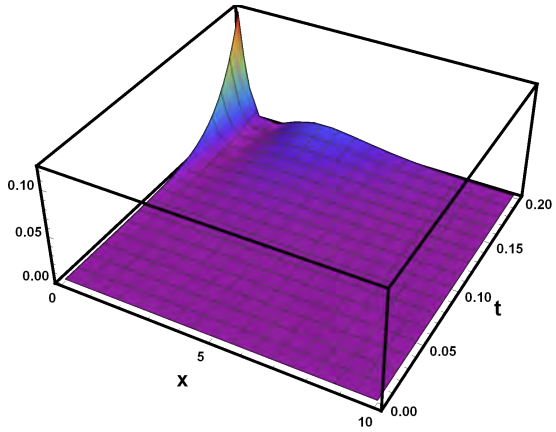

(c) $|c(x,t) - c_8(x,t)|$

Figure 5.9: Number density and error

coincides with the exact solution at $t = 0.1$. Figure 5.8(b) shows the truncated solutions for $n = 2, 5, 8$ at time $t = 0.2$ and it is concluded that results for $n = 5$ and $n = 8$ are almost identical which leads us to truncate the series at $n = 5$. Figure 5.9 also exhibits a similar pattern, and the error resulting from the 8-term truncated solution is virtually insignificant. Further, in Figure 5.8(c), zeroth moment is shown to be in good accuracy with the 8-term series solution.

The above illustrations show the reliability of our proposed methods. Thus, motivate us to extend the results for the physical relevant kernels, for instance sum and Ruckenstein kernels, where the analytical solutions are not available.

5.2.3 Sum kernel

In this case, given the initial condition $c_0(x) = xe^{-x}$ and the kernel $K(x,y) = \frac{1}{10}(x+y)$, an approximate solution for the number density is determined for various values of n. When the solution is truncated at $n = 10, 12, 15$ and 18, an error plot is displayed by considering c_{18} as a standard solution. equation (5.1.10) gives

$$v_0(x,t) = xe^{-x}, \quad v_1(x,t) = \frac{1}{10}te^{-x}\left(x^2-6\right), \quad v_2(x,t) = \frac{1}{200}t^2e^{-x}(x(x(x+2)-6)-24),$$
$$v_3(x,t) = \frac{1}{6000}t^3e^{-x}(x(x(x(x+6)+16)-60)-240).$$

Hence, assuming a 18-term approximation, i.e., $c(x,t) \approx \sum_{k=0}^{18} v_k(x,t)$ yields

$$c(x,t) \approx \frac{1}{6000}t^3e^{-x}(x(x(x(x+6)+16)-60)-240) + \frac{1}{200}t^2e^{-x}(x(x(x+2)-6)-24)$$
$$+ \frac{1}{10}te^{-x}\left(x^2-6\right) + e^{-x}x + \cdots.$$

The analytic approximate number density obtained via HPM is plotted for $n = 10, 12, 15$ and 18 in Figure 5.10 and it is clearly visible that results for $n = 15$ and 18 are similar to each other. One can also verify this by computing the error between $|c_{18}(x,t) - c_k(x,t)|$ for $k = 10, 12, 15$ see Figure (5.11) for the justification of such behavior.

5.2.4 Ruckenstein kernel

This kernel has been suggested as a model for the deterioration of supported metal catalysts [105] and used to represent the process of particle migration and coalescence on a heated substrate. Consider equation (5.1.8) for Ruckenstein kernel $(K(x,y) = x^{2/3} + y^{2/3})$ and exponential initial condition $(u(x,0) = x^2e^{-x})$, iteration for HPM will be as follows

$$v_0(x,t) = x^2e^{-x}, \quad v_1(x,t) = e^{-x}\left(4t(x-4)x^{5/3} + \frac{2}{11}t(4x-11)x\Gamma\left(\frac{14}{3}\right)\right),$$
$$v_2(x,t) = \frac{8}{81}t^2e^{-x}\left(1134x^{4/3} - 729x^{7/3} + 81x^{10/3} + 6(x(57x-346)+385)x^{2/3}\Gamma\left(\frac{8}{3}\right)\right.$$

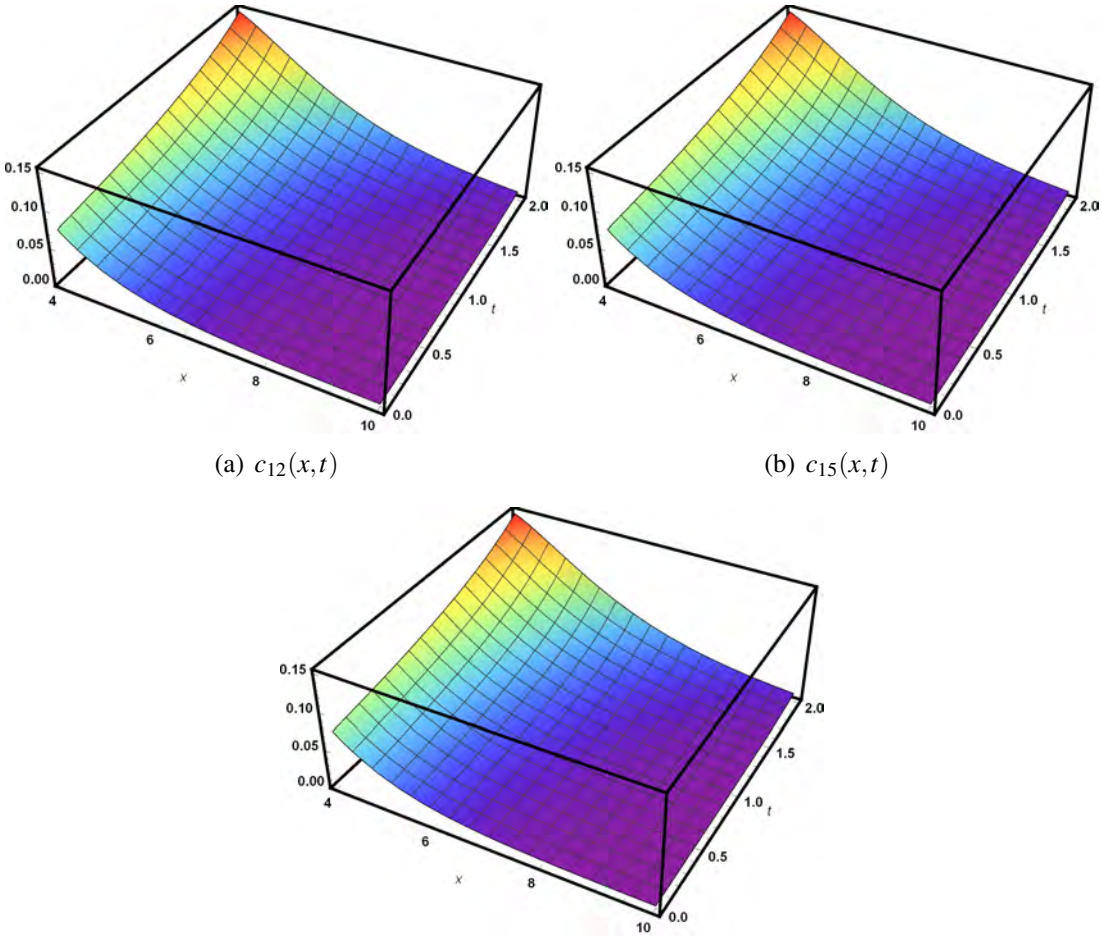

(a) $c_{12}(x,t)$ (b) $c_{15}(x,t)$

(c) $c_{18}(x,t)$

Figure 5.10: Number density $c_n(x,t)$ for $n = 10, 12, 15$ and 18

$$+21(4x-5)x\Gamma\left(\frac{7}{3}\right)+(x(347x-1584)+968)\Gamma\left(\frac{8}{3}\right)^2\Big).$$

It is worth mentioning that the terms of the solutions are quite complicated and take an ample amount of computational time in this scenario. Due to that reason, a three-term truncated solution is considered. Figure 5.12(a)-(c) presents the number density distribution for $n = 2, 3$ and 4 terms. One can observe the unpredictable behavior of number density distribution. The reason behind this may lie in the unavailability of the higher order terms and exact solutions. However, the first moment's prediction is quite well as it shows the mass conservation of the number of particles. The same type of

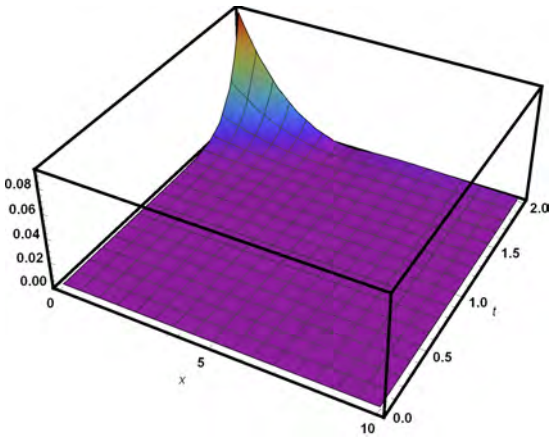

(a) $|c_{18}(x,t) - c_{10}(x,t)|$

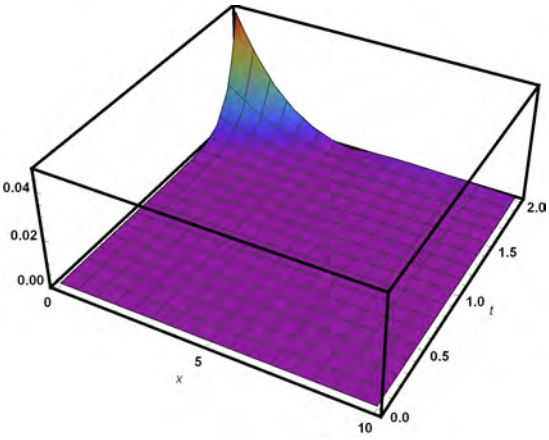

(b) $|c_{18}(x,t) - c_{12}(x,t)|$

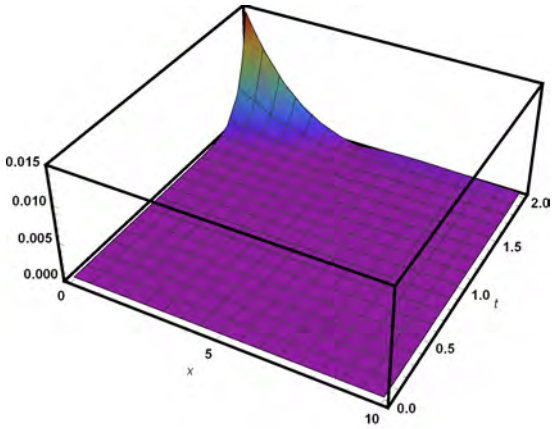

(c) $|c_{18}(x,t) - c_{15}(x,t)|$

Figure 5.11: Error $|c_{18}(x,t) - c_k(x,t)|$ for $k = 10, 12, 15$

behavior of the truncated solution was seen by G. Kaur *et al.* in [8] and concluded that closed form or higher order terms were necessary to accurately forecast the behavior of the number distribution and integral properties.

5.3 Lifshitz-Slyozov equation with encounters

The standard Lifschitz-Slyozov system, as introduced in [106] and [107], describes the evolution of a solution of polymers. Davidson analyze the long-time behavior of the solutions for LSE with the encounter having three types of initial data in [63]. The model is similar to the CCM with addition of some advection term. So, the mathematical equation

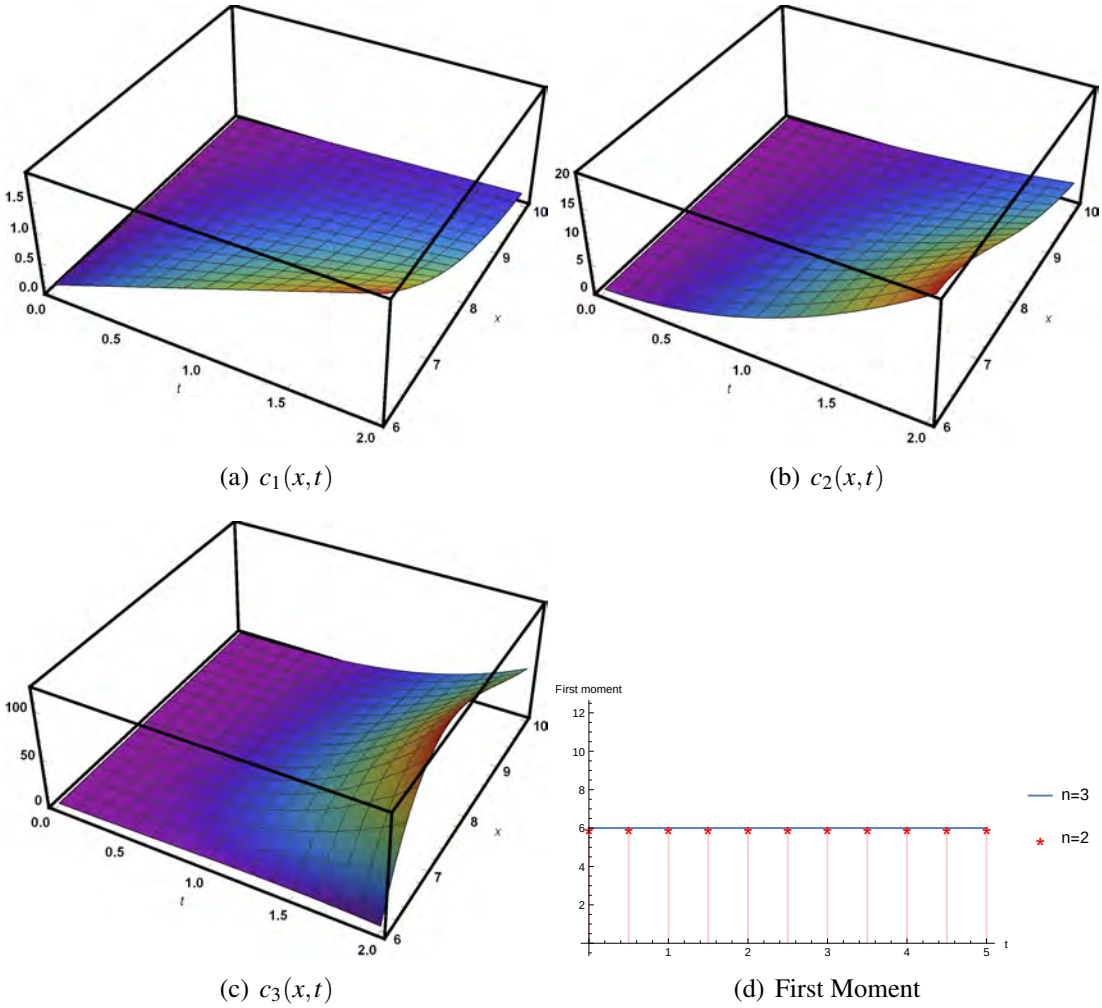

(a) $c_1(x,t)$ (b) $c_2(x,t)$

(c) $c_3(x,t)$ (d) First Moment

Figure 5.12: Number density $c_n(x,t)$ for $n = 2,3,4$ and first moment.

is described as

$$\frac{\partial c}{\partial t} = -\frac{\partial}{\partial x}[f(x,t)c(x,t)] + Q(c), \tag{5.3.1}$$

where

$$f(x,t) = x[u(t) - x^{-1}] \tag{5.3.2}$$

and

$$Q(c) = -\frac{\partial}{\partial x}\left[\int_0^x yK(x,y)c(x,t)c(y,t)dy\right] - \int_x^\infty K(x,y)c(x,t)c(y,t)dy$$
$$-\frac{\partial}{\partial x}\left[\int_x^\infty yL(x,y)c(x,t)c(y,t)dy\right] - \int_0^x L(x,y)c(x,t)c(y,t)dy. \tag{5.3.3}$$

Here, $f(x,t)$ is the average rate at which the particle cluster expands by acquiring new particles. For the further analysis, the same condition on kernels taken as before is considered, i.e, $K(x,y) = L(x,y) = L \geq 0$. Note that, for such model as well, mass remains a conserved quantity which is given by the expression

$$\int_0^\infty xc(x,t)dx := M_1(t) = M_1(0), \tag{5.3.4}$$

for $M_1(0)$ being the initial mass. In order to implement HPM or ADM on equation (5.3.1), let us rewrite this in some equivalent form. Multiplying equation (5.3.1) by x, integrating with respect to x over 0 to ∞ and using equation (5.3.4) give

$$\int_0^\infty x\frac{\partial}{\partial x}[f(x,t)c(x,t)]dx = \int_0^\infty xQ(c)dx. \tag{5.3.5}$$

One can easily compute that $\int_0^\infty xQ(c)dx = 0$. Therefore, applying integration by parts provide

$$0 = \int_0^\infty f(x,t)c(x,t)dx.$$

Substitute the value of $f(x,t)$ from (5.3.2) to get

$$u(t) = \frac{\int_0^\infty c(x,t)dx}{\int_0^\infty xc(x,t)dx} := \frac{M_0(t)}{M_1(0)}. \tag{5.3.6}$$

By having (5.3.2), $K(x,y) = L(x,y) = L$ and relation (5.3.4), equation (5.3.1) can be simplified as

$$\begin{aligned}\frac{\partial c(x,t)}{\partial t} &= -\frac{\partial}{\partial x}\{[xu(t)-1]c(x,t)\} - LM_1(0)\frac{\partial c(x,t)}{\partial x} - LM_0(t)c(x,t)\\ &= \left(1 - LM_1(0) - \frac{M_0(t)}{M_1(0)}x\right)\frac{\partial c(x,t)}{\partial x} - \left(LM_0(t) + \frac{M_0(t)}{M_1(0)}\right)c(x,t). \end{aligned} \tag{5.3.7}$$

By multiplying the above equation by x^r and integrating with respect to x from 0 to ∞ yields the moments equation as

$$\frac{dM_r(t)}{dt} = rLM_1M_{r-1} - LM_0M_r. \tag{5.3.8}$$

Solving for the zeroth moment $M_0(t)$, it is easy to see that $r = 0$ enable us to have

$$M_0(t) = \frac{M_0(0)}{LM_0(0)t+1}.$$

If the initial condition $c_0(x) = e^{-x}$, one can find that $M_0(0) = M_1(0) = 1$. Therefore, using all these desired values in equation (5.3.1), we get

$$\frac{\partial c(x,t)}{\partial t} = -\frac{\partial}{\partial x}\left(\left[\frac{x}{1+Lt} - 1\right]c(x,t)\right) + Q(c). \tag{5.3.9}$$

Now, we apply HPM and ADM to find the series solution of the above defined model.

5.3.1 Series Solution by HPM

Using the procedure defined in Section 2, we construct a homotopy as,

$$H(v,p) = (1-p)\left[\frac{\partial v}{\partial t} - \frac{\partial c_0}{\partial t}\right] + p\left[\frac{\partial c(x,t)}{\partial t} + \frac{\partial}{\partial x}\left(\left[\frac{x}{1+Lt} - 1\right]c(x,t)\right) - Q(c)\right] = 0. \tag{5.3.10}$$

Substituting the series solution $v(x,t) = \sum_{k=0}^{\infty} v_k(x,t)p^k$, in the equation (5.3.10) and collecting the coefficients of powers of p leads to

$$\begin{aligned} p^0: \;\; v_0(x,t) =& c_0(x), \\ p^k: \;\; \frac{\partial v_k}{\partial t} =& -\frac{\partial}{\partial x}\left(\left[\frac{x}{1+Lt}-1\right]c_{k-1}\right) - \frac{\partial}{\partial x}\left[\sum_{l=0}^{k-1}\int_0^{\infty} yLc_l(x,t)c_{k-l-1}(y,t)dy\right] \\ & -\left[\sum_{l=0}^{k-1}\int_0^{\infty} Lc_l(x,t)c_{k-l-1}(y,t)dy\right], \; k=1,2,\ldots. \end{aligned}$$

This can further be rewritten as,

$$\begin{aligned} v_k(x,t) =& -\int_0^t \frac{\partial}{\partial x}\left(\left[\frac{x}{1+Lt}-1\right]c_{k-1}\right) - \frac{\partial}{\partial x}\left[\sum_{l=0}^{k-1}\int_0^{\infty} yLc_l(x,t)c_{k-l-1}(y,t)dy\right] \\ & -\left[\sum_{l=0}^{k-1}\int_0^{\infty} Lc_l(x,t)c_{k-l-1}(y,t)dy\right]dt. \end{aligned} \tag{5.3.11}$$

5.3.2 Series solution by ADM

Consider the equation (5.3.9) with taking $L = \frac{\partial}{\partial t}$ as a linear differential operator and the inverse operator $\boldsymbol{L}^{-1}$ is defined as $\boldsymbol{L}^{-1} = \int_0^t [.]dt$. Then the equation (5.3.9) becomes

$$\boldsymbol{L}c(x,t) = -\frac{\partial}{\partial x}\left(\left[\frac{x}{1+Lt}-1\right]c(x,t)\right) + Q(c). \tag{5.3.12}$$

Applying the same procedure for ADM as defined in Section 3, one gets

$$\begin{aligned} v_0 =& c_0(x), \\ v_k =& \boldsymbol{L}^{-1}\left(-\frac{\partial}{\partial x}\left(\left[\frac{x}{1+Lt}-1\right]c_{k-1}\right) - \frac{\partial}{\partial x}\left[\sum_{l=0}^{k-1}\int_0^{\infty} yLc_l(x,t)c_{k-l-1}(y,t)dy\right]\right. \\ & \left.-\left[\sum_{l=0}^{k-1}\int_0^{\infty} Lc_l(x,t)c_{k-l-1}(y,t)dy\right]\right), k=1,2,\ldots, \end{aligned} \tag{5.3.13}$$

which is again the same as equation (5.3.11), concluding that the results from HPM and ADM are identical.

5.3.3 Numerical results

The LSE for number density and zeroth moment with initial condition $c(x,0) = e^{-x}$ is discussed here. For this initial condition and the constant kernel $K(x,y) = L$, the analytical solution is provided in [63] as

$$c(x,t) = (Lt+1)^{-\frac{1}{L}-1} e^{(L-1)t - x(Lt+1)^{-1/L}}.$$

Thus, the truncated series solutions for the concentration and total number of particles are compared with the exact solutions for various values of n and error plots are given to illustrate the convergence of numerical solutions towards the exact one.

By using the given data, equation (5.3.11) enables us to have the following first four terms of the series solution as

$$\begin{aligned}
v_0(x,t) =& e^{-x}, \quad v_1(x,t) = e^{-x}\left(\frac{(x-1)\log(Lt+1)}{L} - t\right), \\
v_2(x,t) =& \frac{e^{-x}(\log(Lt+1)(-2Lt(x-2)+((x-3)x+1)\log(Lt+1)+2)+Lt(Lt-2))}{2L^2}, \\
v_3(x,t) =& \frac{1}{6L^3}e^{-x}\Big(L^3t^3 - 6L^2t^2 + 6Lt + \log(Lt+1)\{-3L^2t^2x + 9L^2t^2 + 6Ltx - 6Lt - 6\} + \\
& \log^2(Lt+1)\{3Ltx^2 - 15Ltx - 6x + 12Lt + 9\} + \log^3(Lt+1)\{-x^3 + 6x^2 - 7x + 1\}\Big).
\end{aligned}$$

Figure 5.13(a) shows the numerical simulations for $n = 2,4$ and a comparison with the exact solution. One can clearly see that a convergence of approximated solution towards the exact solution can be established. Fortunately, for $n = 4$, results from HPM overlaps with the exact number density. Also, Figure 5.13(b) indicates that as the number of terms approximation increases, the error between the exact and ADM solutions reduces and becomes insignificant for $t = 0.5$. The same data is depicted in Figure (5.14), which demonstrates that the 4-term truncated solution has a considerable agreement with the analytical solution, and the error is relatively small. Finally, Figure 5.13(c) compares the

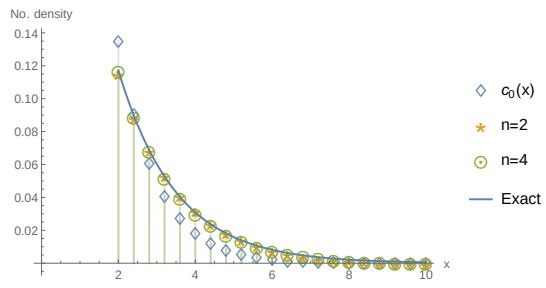

(a) Exact vs. series solutions at $t = 0.5$

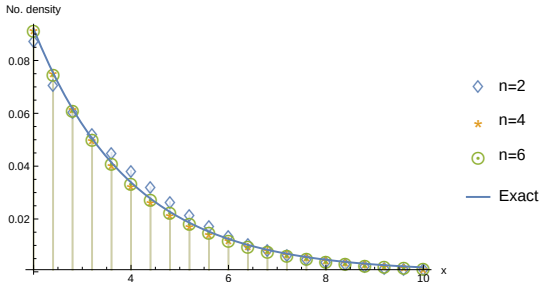

(b) Exact vs. series solutions at $t = 1$

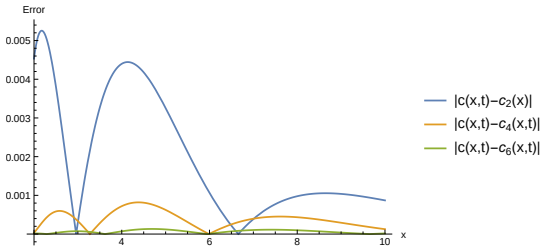

(c) Error at $t = 1$

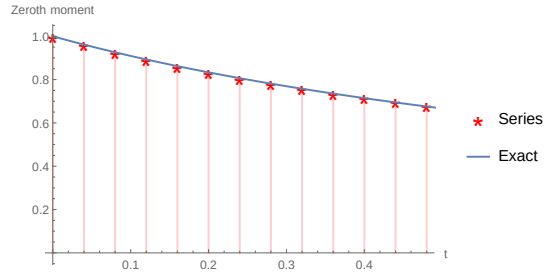

(d) Zeroth moment

Figure 5.13: For $n = 2, 4$ and $t = 0.5$ (a) exact and series solutions for number density (b) errors between exact and truncated number densities (c) exact and 4 terms zeroth moment

zeroth moment of the exact and the truncated solutions which concludes that the zeroth moment using HPM is exactly matching with the analytical solution for $n = 4$.

5.4 Conclusions

This chapter dealt with the approximated and/or exact solutions for the CCM and LSE achieved by applying ADM and HPM. Both strategies provided a recursive relation for obtaining the exact answers in terms of sum of an infinite series, as well as approximate solutions. It was observed that the solutions via HPM were the same as via ADM. For the product and constant kernels, series solutions for number density and zeroth moment for CCM were compared with the available analytical solutions. Moreover, errors between truncated series solutions were reported for sum kernel to justify the convergence of the scheme in the absence of exact solutions. Similar results were also obtained and noticed the convergence of ADM or HPM towards the solutions of LS equation. Since, the total mass is constant for both the models, we observed the same using series solutions and

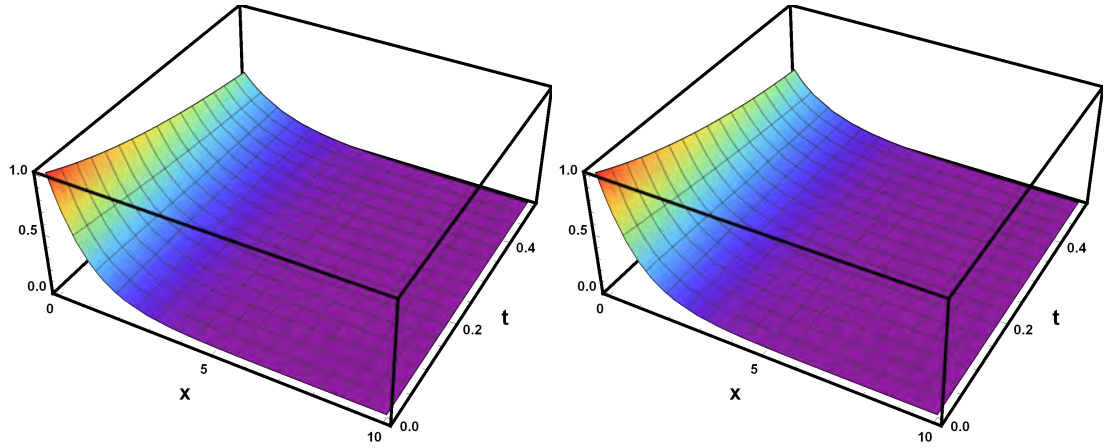

(a) Exact

(b) $c_4(x,t)$

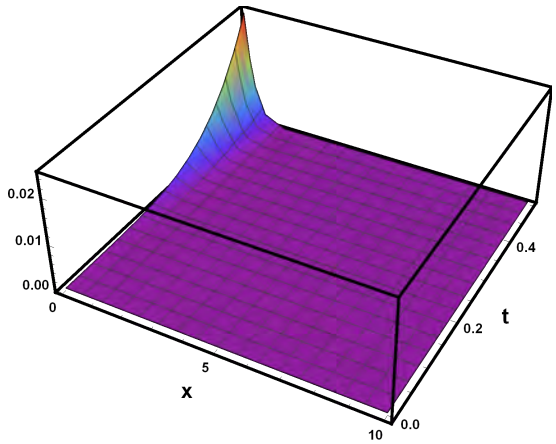

(c) Error$|c(x,t)-c_4(x,t)|$

Figure 5.14: Exact solution, truncated solution and error

therefore, omitted the plots.

Chapter 6

An implicit semi-analytical technique: development, analysis and applications

It is observed in the preceding chapters that HPM, ADM, HAM, ODM and IOHAM maintain precision within limited temporal scopes. Hence, in order to solve the problems over expended period of time, this chapter proposes a novel implicit semi-analytical method that provides solutions over greater temporal extents. The idea is implemented here for the nonlinear differential equations and implementation for the aggregation-breakage model is an open avenue.

Differential equations are crucial in representing the dynamics of systems across various fields of science and engineering [108–110]. These equations govern the temporal behavior of systems, depicting the changes in variables affected by internal mechanisms and external influences. Many realistic problems entail complex systems or boundary conditions that make analytical solutions infeasible or unattainable, especially over extensive time domains. Nevertheless, solving the equations over large time domains is imperative to comprehend and forecast the behavior of dynamic systems encountered in various scientific and engineering domains. From modeling climate change dynamics to simulating complex biological processes or analyzing financial systems' stability [111, 112], differential equations serve as the foundation for capturing the evolution of variables over time.

Various numerical methods are employed to approximate the solutions of such problems. However, these schemes come with computational challenges, such as discretization and truncation of the domain, which can introduce errors in the solution. These errors can accumulate and propagate over time, affecting the accuracy of the solution. Numerical techniques such as finite element [113–115] and finite difference [116, 117] are highly contextualized techniques based on domain discretization. Hence, devising a more feasible and precise method to solve the differential equation over a longer time domain is an unresolved and essential topic.

To overcome the drawbacks of the numerical techniques, various semi-analytical approaches such as ADM [118], HAM [119], HPM [120, 121], ODM [25] and iterative finite difference methods [122, 123] have been implemented to solve nonlinear differential, delayed-differential and integro-differential equations [18, 92, 93, 124–126]. Moreover, SAT are methods that can solve linear or non-linear differential equations without discretization, linearization, or special transformation and can provide approximate solutions in the form of infinite series or polynomials.

6.0.1 Literature review

The ADM, introduced by George Adomian, is a technique for solving ordinary and partial differential equations [127]. In 1986, it was also applied to stochastic models [128]. Many researchers use this method to find the exact solutions of various differential equations, including integral and integro-differential ones [11, 129, 130]. However, the algorithm has some drawbacks as well. The accuracy of the method and the convergence of series solution are limited to a small region and to achieve a precise solution for a larger domain, one must calculate more series terms. Recently, Odibat discusses some additional limitations of the ADM [25], such as its inability to satisfy the boundary conditions for some non-linear systems. To address these issues, Odibat proposes the ODM, a technique for solving both linear and nonlinear differential equations [25] by approximating the nonlinear term with a Taylor series expansion. The author asserts that the ODM has higher accuracy and quicker convergence than the ADM.

HPM [99] has received significant attention in addressing nonlinear problems due to series solution obtained [100, 102, 131] with easily computable terms. However, the perturbation methods rely on small/large parameters, also called perturbation quantities. Therefore, these methods are only suitable for weakly non-linear problems and for small domains. The HAM [96, 119] is one of the most dependable and efficient SAT for solving non-linear DEs. Unlike HPM or any other traditional non-perturbation technique, HAM does not depend on the selection of base function or other small/large physical parameters. It offers a simpler way to guarantee the fast convergence of series solution. The main benefit of the HAM is its ability to control the convergence speed and region [96]. As a result, the HAM can handle even highly non-linear problems.

Several SAT have been proposed in recent years to improve the precision and effectiveness of the solutions for longer time domains. Odibat [25] argues that ODM outperforms the conventional SAT such as HAM, HPM, and ADM in accuracy. Hence, it would be worthwhile to devise a new semi-analytical method that can produce more precise results than ODM.

6.0.2 Novelty and contribution

The work presents an implicit SAT for resolving ordinary and partial differential equations, accompanied by the introduction of a convergence control parameter to enhance accuracy. A theoretical analysis of the proposed method's convergence is conducted, followed by presenting results for significant physical problems like Ricarti [132] and Burgers' equations [125]. Numerical simulations demonstrate the superior performance of the proposed method compared to HAM, HPM, and ADM.

The subsequent sections are structured as follows: Section 6.1 examines different semi-analytical methodologies, offering a succinct overview of HAM, HPM, ADM, and ODM. Section 6.2 introduces an implicit iterative method for differential equations, and the convergence control parameter is also incorporated. Additionally, Section 6.3 conducts an extensive investigation into the convergence characteristics of the proposed methodology. In Section 6.4, the scheme's numerical implementation is delineated for both ordinary and

partial differential equations. Lastly, the concluding section underscores critical remarks and prospects for future research.

6.1 Semi-analytical methods: A comprehensive survey

This section introduces the core ideas of prominent SAT for addressing nonlinear differential equations. Let us consider the nonlinear differential equation of the form:

$$\mathscr{N}[\mu(x,t),\mu'(x,t)]=0, \tag{6.1.1}$$

based on the initial condition $\mu(x,0)=\mu_0(x)$. In the above expression, $\mathscr{N}$ signifies the nonlinear differential operator, $\mu(x,t)$ is an unknown analytic function, and $\mu'(x,t)=\frac{\partial \mu}{\partial t}$.

6.1.1 Homotopy analysis method

Considering the equation (6.1.1) and following HAM, a homotopy is constructed as follows

$$(1-q)\mathscr{L}[\theta(x,t;q)-\mu_0(x)]-qhH\mathscr{N}[\theta(x,t;q),\theta'(x,t;q)]=0, \tag{6.1.2}$$

here $q\in[0,1]$ is an embedding parameter, $H,h\neq 0$ are auxiliary function and auxiliary parameter respectively and $\mathscr{L}$ being a linear operator. It is evident that as the parameter q progresses from 0 to 1, the function $\theta(x,t;q)$ evolves from the initial approximation $\mu_0(x)=\theta(x,t;0)$ to the exact solution $\mu(x,t)=\theta(x,t;1)$ of the given problem (6.1.1). The fundamental concept of HAM posits that the solution to the nonlinear problem can be expressed as a power series expansion in terms of the parameter q, as

$$\theta(x,t;q)=\sum_{k=0}^{\infty}q^k v_k(x,t). \tag{6.1.3}$$

As postulated, the series solution outlined in equation (6.1.3) is required to fulfill the stipulations of equation (6.1.1). In order to ascertain the components of the series solution, one must insert equation (6.1.3) into equation (6.1.2) and equate the coefficients corresponding

to the identical powers of q, thereby yielding the requisite deformation equations as,

$$\begin{aligned}
\mathscr{L}[v_1] =& Hh\mathscr{A}_0(v_0),\\
\mathscr{L}[v_2] =& \mathscr{L}[v_1] + Hh\mathscr{A}_1(v_0,v_1),\\
\mathscr{L}[v_3] =& \mathscr{L}[v_2] + Hh\mathscr{A}_2(v_0,v_1,v_2),\\
&\vdots\\
\mathscr{L}[v_n] =& \mathscr{L}[v_{n-1}] + Hh\mathscr{A}_3(v_0,v_1,v_2,\cdots,v_{n-1}),
\end{aligned}$$

where,

$$\mathscr{N}(\sum_{i=0}^{j} q^i v_i'(x,t), \sum_{i=0}^{j} q^i v_i(x,t)) = \mathscr{A}_0(v_0) + q\mathscr{A}_1(v_0,v_1) + q^2\mathscr{A}_2(v_0,v_1,v_2) + \cdots + q^j\mathscr{A}_j(v_0,v_1,\cdots,v_j).$$

In conclusion, the precise solution to the problem is formally articulated as follows

$$\lim_{q\to 1}\theta(x,t;q) = \mu(x,t) = v_0 + v_1 + v_2\cdots$$

.

6.1.2 Adomian decomposition method

Considering the equation (6.1.1) and decomposing in the form

$$\mathscr{L}[\mu(x,t)] + \mathscr{R}[\mu(x,t)] + N[\mu(x,t)] = g(x,t),$$

$\mathscr{L}$ represents the linear operator of the utmost order, assuming it is invertible. The term $\mathscr{R}$ denotes the residual portion of the linear operator, while N signifies the nonlinear differential operator. On further simplification, one can write

$$\mu(x,t) = \omega(x,t) + \mathscr{L}^{-1}g(x,t) - \mathscr{L}^{-1}\mathscr{R}[\mu(x,t)] - \mathscr{L}^{-1}N[\mu(x,t)], \tag{6.1.4}$$

where $\omega(x,t)$ appears due to the initial condition. In ADM, the unknown function $\mu(x,t)$ breakdown in the sum of infinite series, *i.e.,*

$$\mu(x,t) = \sum_{j=0}^{\infty} w_j(x,t) \tag{6.1.5}$$

and the nonlinear term $N[\mu(x,t)]$ is represented by

$$N[\mu(x,t)] = \sum_{j=0}^{\infty} A_j(x,t), \tag{6.1.6}$$

where Adomian polynomials $A_j's$ are provided by

$$A_j(x,t) = \frac{1}{j!}\frac{d^j}{d\lambda^j}\left[\mathscr{N}\left(\sum_{i=0}^{j}\lambda^j c_j(x,t)\right)\right]_{\lambda=0}. \tag{6.1.7}$$

Substituting the equation (6.1.5), (6.1.6) and (6.1.7) in equation (6.1.4) lead to the evaluation of the components of the series solutions as

$$\begin{aligned} w_0(x,t) =& \omega(x,t) + \mathscr{L}^{-1}g(x,t), \\ w_{j+1}(x,t) =& -\mathscr{L}^{-1}(\mathscr{R}w_j(x,t)) - \mathscr{L}^{-1}A_j(x,t), \quad j \geq 0. \end{aligned} \tag{6.1.8}$$

6.1.3 Optimized decomposition method

To understand the methodology, we first look at the ODE and then broaden the explanation for the PDE. Consider the ODE

$$\mathscr{L}[\mu(t)] = \mathscr{N}[\mu(t)] + g(t). \tag{6.1.9}$$

The initial phase of ODM comprises the introduction of an optimized linear operator based on the Taylor series approximations. This is based on the idea that the nonlinear operator $\mathscr{F}[\mathscr{L}[\mu],\mu] = \mathscr{L}(\mu) - \mathscr{N}(\mu)$ may be linearized using a first-order Taylor series expansion around $t = 0$. As a result, the linear operator used to approximate $\mathscr{F}[\mathscr{L}[\mu],\mu]$

at the position (μ_0^*, μ_0) as follows:

$$\mathscr{F}[\mathscr{L}[\mu], \mu] \approx \frac{\partial \mathscr{F}}{\partial \mathscr{L}[\mu]}(\mu_0^*, \mu_0)\,\mathscr{L}[\mu] + \frac{\partial \mathscr{F}}{\partial \mu}(\mu_0^*, \mu_0)\,\mu, \tag{6.1.10}$$

here $\mu_0 = \mu(0)$, and $\mu_0^* = \mathscr{L}[\mu](0)$. Utilizing this approximation, equation (6.1.9) is reformulated as:

$$\mathscr{R}[\mu(t)] = \mathscr{N}[\mu(t)] + \mathscr{K}\,\mu(t) + g(t), \tag{6.1.11}$$

where

$$\mathscr{R}[\mu] = \mathscr{L}[\mu] + \mathscr{K}\,\mu, \tag{6.1.12}$$

and

$$\mathscr{K} = \frac{\frac{\partial \mathscr{F}}{\partial \mu}(\mu_0^*, \mu_0)}{\frac{\partial \mathscr{F}}{\partial \mathscr{L}[\mu]}(\mu_0^*, \mu_0)}. \tag{6.1.13}$$

The efficacy of ODM relies on the precise specification of constant $\mathscr{K}$ and the coefficient of μ within the devised linear operator $\mathscr{R}$. Given the non-trivial invertibility of the linear differential operator $\mathscr{R}$, an iterative approach for the proposed method necessitates decomposing the solution $\mu(t)$ of Eq.(6.1.9) into a series form, expressed as $\mu(t) = \sum_{k=0}^{\infty} \mu_k(t)$. Herein, the constituent functions $(\mu_k(t))_{k=0}^{k=\infty}$ are determined using the iterations

$$\begin{cases} \mu_0(t) = f(t) \\ \mu_1(t) = \mathscr{L}^{-1}\left[A_0(t)\right] \\ \mu_2(t) = \mathscr{L}^{-1}\left[A_1(t) + \mathscr{K}\,\mu_1(t)\right] \\ \mu_{k+1}(t) = \mathscr{L}^{-1}\left[A_k(t) + \mathscr{K}\left(\mu_k(t) - \mu_{k-1}(t)\right)\right], \quad k \geq 2, \end{cases} \tag{6.1.14}$$

where $f(t) = \mathscr{L}^{-1}g(t) + \mu(0)$.

Further, the scope of ODM expands to address PDE as detailed in [25]. To grasp the fundamental concept underlying this extension, contemplate the equation (6.1.1) to the subsequent PDE structure

$$\frac{\partial}{\partial t}\mu(x,t) = \gamma\frac{\partial^2}{\partial x^2}\mu(x,t) + \mathscr{N}[\mu(x,t)], \quad t > 0, \tag{6.1.15}$$

where $\gamma \in \mathbb{R}$ and the equation satisfies the following conditions

$$\begin{cases} \mu(x,0) = f(x), \\ \mu(x,t) \to 0, \text{ as } |x| \to \infty, \quad t > 0. \end{cases} \tag{6.1.16}$$

In accordance with the methodology outlined in [25], it is presupposed that a first-order Taylor series expansion is capable of linearizing the nonlinear function $\mathscr{F}(\mu_t, \mu_{xx}, \mu) = \frac{\partial}{\partial t}\mu - \gamma\frac{\partial^2}{\partial x^2}\mu - \mathscr{N}[\mu]$ at $t = 0$. The linear approximation of $\mathscr{F}$ is represented as follows:

$$\mathscr{F}(\mu_t, \mu_{xx}, \mu) \approx \frac{\partial}{\partial t}\mu - \gamma\frac{\partial^2}{\partial x^2}\mu - \mathscr{K}(x)\mu, \tag{6.1.17}$$

where

$$\mathscr{K}(x) = \left.\frac{\partial \mathscr{N}}{\partial \mu}\right|_{t=0}. \tag{6.1.18}$$

The aforementioned approximation results in the linear representation of the nonlinear PDE (6.1.15) as

$$\mathscr{R}[\mu(x,t)] = \mathscr{N}[\mu(x,t)] - \mathscr{K}(x)\mu(x,t), \quad t > 0, \tag{6.1.19}$$

where $\mathscr{R}[\mu] = \frac{\partial}{\partial t}\mu - \gamma\mu_{xx} - \mathscr{K}(x)\mu$. Instead of resorting to the inverse of the linear operator $\mathscr{R}$, which is not readily invertible, the proposed solution to the problem is taken as $\mu(x,t) = \sum_{k=0}^{\infty}\mu_k(x,t)$ with the coefficients $\mu_k(x,t), k \geq 0$ are determined by the

following equations

$$\begin{cases} \mu_0(t,x) & = f(x) \\ \mu_1(t,x) & = \mathscr{L}^{-1}\left\{A_0(x,t) + \gamma\frac{\partial^2}{\partial x^2}\mu_0(x,t)\right\} \\ \mu_2(x,t) & = \mathscr{L}^{-1}\left\{\left(A_1(x,t) + \gamma\frac{\partial^2}{\partial x^2}\mu_1(x,t)\right) - \left(\gamma\frac{\partial^2}{\partial x^2} + \mathscr{K}(x)\right)\mu_1(x,t)\right\} \\ \mu_k(x,t) & = \mathscr{L}^{-1}\left\{\left(A_{k-1}(x,t) + \gamma\frac{\partial^2}{\partial x^2}\mu_k(x,t)\right) - \left(\gamma\frac{\partial^2}{\partial x^2} + \mathscr{K}(x)\right)(\mu_{k-1}(x,t) - \mu_{k-2}(x,t))\right\},\ k \geq 3, \end{cases} \tag{6.1.20}$$

for $A_k's$ being the Adomian polynomials.

6.2 Implicit semi-analytical technique

In this section, we introduce a novel SAT for solving differential equations, which we call the implicit iterative method (IIM). Unlike other semi-analytical methods, such as homotopy perturbation, homotopy analysis, Adomian decomposition, and optimized decomposition methods, the IIM is implicit in nature and offers superior accuracy. The IIM relies on the concept of Taylor series expansion of a non-linear operator. To illustrate the same, let us consider the following differential equation

$$\mathscr{A}[\mu(x,\tau)] + g(x) = 0, \tag{6.2.1}$$

here $\mathscr{A}$ is a non-linear differential operator and $g(x)$ is a known analytical function. To proceed further, let us decompose the operator as

$$\mathscr{L}[\mu(x,\tau)] + \mathscr{N}[\mu(x,\tau)] + g(x) = 0, \tag{6.2.2}$$

here $\mathscr{L}$ is linear operator and $\mathscr{N}$ is a non-linear operator. The zeroth order approximated solution is obtained by the solution of the linear differential equation

$$\mathscr{L}[\mu_0(x,t)] + g(x) = 0 \text{ with initial condition } \mu_0(x,0) = \mu(x,0). \tag{6.2.3}$$

Now, to find the next approximated solution $\mu_1(x,t)$ that satisfies

$$\mathscr{L}[\mu_1(x,t)] + \mathscr{N}[\mu_1(x,t)] + g(x) \approx 0,$$

we expand the nonlinear part with respect to known previous approximated solution $\mu_0(x,t)$. Hence, the iterative scheme to obtain the first-order iterative solution can be obtained by solving the differential equation

$$\mathscr{L}[\mu_1(x,\tau)] + \mu_1(x,\tau)\mathscr{C}(x) = -\mathscr{N}[\mu_0(x,\tau)] + \mu_0(x,\tau)\mathscr{C}(x) - g(x). \tag{6.2.4}$$

where $\mathscr{C}(x) = \frac{\partial \mathscr{N}}{\partial \mu}\Big|_{t=0}$. Continuing in a similar fashion, the higher-order iterative solution can be obtained by solving the linear differential equation

$$\mathscr{L}[\mu_{n+1}(x,\tau)] + \mu_{n+1}(x,\tau)\mathscr{C}(x) = -\mathscr{N}[\mu_n(x,\tau)] + \mu_n(x,\tau)\mathscr{C}(x) - g(x) \text{ for } n \geq 1. \tag{6.2.5}$$

It is worth mentioning that each iteration of the scheme is the solution of the equation (6.2.1). The increase in the number of iterations leads to the convergence of the approximated solution towards the precise one. In light of this, an analytical solution can be derived as

$$\mu(x,\tau) = \lim_{n\to\infty} \mu_n(x,\tau). \tag{6.2.6}$$

Remark 6.2.1. *For the purpose of facilitating convergence analysis, let us rewrite the iterative scheme in another form, define the operator $\mathscr{A}[\mu_n]$ as*

$$\mathscr{N}[\mu_n] + g(x) - \mathscr{C}(x) := \mathscr{A}[\mu_n],$$

implies that

$$\mu_{n+1} = -\mathscr{L}^{-1}\{\mathscr{A}[\mu_n] + \mathscr{C}(x)\mu_{n+1}\}. \tag{6.2.7}$$

Considering $v_0(x,t) = \mu_0(x,t)$ *and by defining* $v_i(x,t) = \mu_i(x,t) - \mu_{i-1}(x,t)$ *for* $i \geq 1$*, it is easy to see that*

$$\mu(x,\tau) = \lim_{n\to\infty} \mu_n(x,\tau) = \sum_{j=0}^{\infty} v_i(x,\tau).$$

6.2.1 Convergence control parameter

To improve the accuracy of the scheme, one can involve the convergence control parameter h in the iterative scheme [18]. The iterative scheme for the approximate solution is obtained as

$$\mathscr{L}[\mu_{n+1}(x,\tau)] + \mu_{n+1}(x,\tau)\mathscr{C}(x) = h(-\mathscr{N}[\mu_n(x,\tau)] + \mu_n(x,\tau)\mathscr{C}(x) - g(x)) \text{ for } n \geq 1. \tag{6.2.8}$$

As a result, the auxiliary parameter h affects the convergence region and rate of the solution series and allows for a significant improvement by choosing a suitable value for h. This provides a simple way to manipulate and regulate the convergence region and rate of the solution series derived by the IIM. Various techniques to calculate the convergence control parameter are available in the literature, such as the discrete gradient method, CADNA, CESTAC, h-curve, and discrete residual method [132, 133]. This article employs the discrete residual methods [132] to determine the optimal value of the convergence control parameter.

6.3 Convergence analysis

Definition 6.3.1. *[134] The number of significant digits between two real numbers* α_1 *and* α_2 *is expressed by* $\mathscr{C}_{\alpha_1,\alpha_2}$ *and is estimated as*

$$\begin{cases} \mathscr{C}_{\alpha_1,\alpha_2} = \log\left|\dfrac{\alpha_1+\alpha_2}{2(\alpha_1-\alpha_2)}\right| = \log\left|\dfrac{\alpha_1}{\alpha_1-\alpha_2} - \dfrac{1}{2}\right|, \quad \alpha_1 \neq \alpha_2 \\ \mathscr{C}_{\alpha_1,\alpha_1} = \infty. \end{cases}$$

Theorem 6.3.2. *Consider $\mu_n^h(x,t)$ be the n^{th} order approximated solution of the equation* (**??**) *which is obtained via convergence control parameter h independent of n, then*

$$\mathscr{C}_{\mu_n^h,\mu_{n+1}^h} = \mathscr{C}_{\mu_n^h,\mu} + \mathscr{O}\left(\frac{1}{n+1}\right),$$

if $\{\mu_n^h\}$ is a Cauchy sequence i.e., *for any $n > m$, $\|\mu_n^h - \mu_m^h\| < \varepsilon$ where $\varepsilon = \frac{1}{n!}$.*

Proof. To prove the theorem, use the Definition 6.3.1 as follows

$$\mathscr{C}_{\mu_n^h,\mu_{n+1}^h} - \mathscr{C}_{\mu_n^h,\mu} = \log\left|\frac{\mu_n^h + \mu_{n+1}^h}{2(\mu_n^h - \mu_{n+1}^h)}\right| - \log\left|\frac{\mu_n^h + \mu}{2(\mu_n^h - \mu)}\right|.$$

Rearranging the log terms and using (**??**), we get

$$\mathscr{C}_{\mu_n^h,\mu_{n+1}^h} - \mathscr{C}_{\mu_n^h,\mu} = \log\left|\frac{\mu_n^h + \mu_{n+1}^h}{\mu_n^h + \mu}\right| + \log\left|\frac{\mu_n^h - \mu}{v_{n+1}^h}\right|.$$

As n increases, μ_n^h moves closer toward the exact solution. Therefore, one can neglect the first term, and now to deal with the second term, let us consider

$$\begin{aligned}
\log\left|\frac{\mu_n^h - \mu}{v_{n+1}^h}\right| &= \log\left|\frac{\sum_{i=0}^{n} v_i^h - \sum_{i=0}^{\infty} v_i^h}{v_{n+1}^h}\right| \\
&= \log\left|\frac{\sum_{i=n+1}^{\infty} v_i^h}{v_{n+1}^h}\right| \\
&= \log\left|1 + \frac{v_{n+2}^h + v_{n+3}^h + v_{n+4}^h + \cdots}{v_{n+1}^h}\right|.
\end{aligned}$$

Now,

$$\frac{v_{n+2}^h + v_{n+3}^h + v_{n+4}^h + \cdots}{v_{n+1}^h} = \frac{v_{n+2}^h}{v_{n+1}^h} + \frac{v_{n+3}^h}{v_{n+1}^h} = \frac{v_{n+4}^h}{v_{n+1}^h} + \cdots = \frac{\mu_{n+2}^h - \mu_{n+1}^h}{\mu_{n+1}^h - \mu_n^h} + \frac{\mu_{n+3}^h - \mu_{n+2}^h}{\mu_{n+1}^h - \mu_n^h} + \cdots. \tag{6.3.1}$$

Using the assumption $\{\mu_n^h\}$ is a Cauchy sequence and following the steps of the proof of

Theorem 1 in [133], we have

$$\frac{v_{n+2}^h + v_{n+3}^h + v_{n+4}^h + \cdots}{v_{n+1}^h} \leq \frac{\dfrac{1}{(n+2)!}}{\dfrac{1}{(n+1)!}} + \frac{\dfrac{1}{(n+3)!}}{\dfrac{1}{(n+1)!}} + \cdots . \tag{6.3.2}$$

Then $\dfrac{v_{n+2}^h + v_{n+3}^h + v_{n+4}^h + \cdots}{v_{n+1}^h} \approx \mathscr{O}(\frac{1}{n+1})$, which implies that

$$\log\left|\frac{\mu_n^h - \mu}{\mu_{n+1}^h}\right| = \log\left|1 + \mathscr{O}(\frac{1}{n+1})\right|.$$

Since $\mathscr{O}(\frac{1}{n+1}) \ll 1$, the right-hand side of the above relation tends to 0 as n increases. □

Remark 6.3.1. *The above theorem demonstrates that for the constant convergence control value h, by augmenting the number of iterations n, we can obtain the optimal iteration of the IIM. This theorem enables us to employ $\mu_n^h - \mu_{n+1}^h$ for the cessation of the series solution rather than $\mu_n^h - \mu$ in the algorithm. Furthermore, this theorem reveals that the number of common significant digits between two consecutive approximations μ_n^h and μ_{n+1}^h is nearly identical to the number of common significant digits between μ_n^h and μ.*

Theorem 6.3.3. *Considering the components $v_1, v_2, \cdots, v_n$ expressed in Remark 6.3.1, the proposed iterative solution is convergent if $\exists 0 < \lambda < 1$ such that $\|v_{i+1}\| \leq \lambda \|v_i\|$, $\forall i \geq i_0$ for some $i_0 \in \mathbb{N}$, where*

$$\|v_i(x,t)\| = \max |v_i(x,t)|,$$

defined on the space

$$\mathscr{W} := \{(x,t) : \alpha < x < \beta, 0 < t < \mathscr{T}\},$$

for a fixed $\mathscr{T}$ and $\alpha, \beta \in \mathbb{R}$.

Proof. Let us consider the sequence of partial sum $(\psi_n)_{n=0}^{\infty}$ as

$$\begin{cases} \psi_0 = & v_0, \\ \psi_1 = & v_0 + v_1, \\ \psi_2 = & v_0 + v_1 + v_2, \\ \vdots & \\ \psi_n = & v_0 + v_1 + v_2 + \cdots + v_n. \end{cases}$$

Now, we will prove that the sequence $(\psi_n)_{n=0}^{\infty}$ is a Cauchy sequence in Hilbert space $\mathbb{R}$. Consider

$$\|\psi_n - \psi_m\| = \|v_{n+1}\| \leq \lambda \|v_n\| \leq \lambda^2 \|v_{n-1}\| \leq \cdots \leq \lambda^{n-i_0+1} \|v_{i_0}\|.$$

For every $n \geq m \geq i_0$ where n and m are natural numbers, one can observe that

$$\begin{aligned} \|\psi_{n+1} - \psi_n\| =& \|(\psi_n - \psi_{n-1}) + (\psi_{n-1} - \psi_{n-2}) + \cdots + +(\psi_{m+1} - \psi_m)\| \\ \leq& \lambda^{n-i_0} \|v_{i_0}\| + \lambda^{n-i_0-1} \|v_{i_0}\| + \cdots + \lambda^{m-i_0+1} \|v_{i_0}\| \\ =& \frac{1-\lambda^{n-m}}{1-\lambda} \lambda^{m-i_0+1} \|v_{i_0}\| \leq \frac{1}{1-\lambda} \lambda^{m-i_0+1} \|v_{i_0}\|, \end{aligned}$$

since $0 < \lambda < 1$, we get

$$\lim_{n,m \to \infty} \|\psi_n - \psi_m\| = 0. \tag{6.3.3}$$

Therefore, $(\psi_n)_{n=0}^{\infty}$ is a Cauchy sequence in $\mathbb{R}$, implying that the iterative solution (6.2.5) is convergent. □

Theorem 6.3.4. *Considering the iterative solution of the equation* (6.2.1) *converging to the exact solution* $\mu(x,t)$ *and the finite m term truncated solution governed by* $\psi_m(x,t) :=$

$\sum_{j=0}^{m} v_j(x,t)$, *the maximum error is given by*

$$\|\mu(x,t) - \psi_m(x,t)\| \leq \frac{1}{1-\lambda}\lambda^{m+1}\|v_0\|.$$

Proof. From the above theorem, we have

$$\|\psi_n(x,t) - \psi_m(x,t)\| \leq \frac{1-\lambda^{n-m}}{1-\lambda}\lambda^{m+1}\|v_0\|, \quad \forall n \geq m.$$

Further, if $n \to \infty$, $\psi_n(x,t) \to \mu(x,t)$. Therefore, for a fixed m,

$$\|\mu(x,t) - \psi_m(x,t)\| \leq \frac{1}{1-\lambda}\lambda^{m+1}\|v_0\|.$$

Here, $0 < \lambda < 1$, $\lambda^{n-m} \to 0$ as $n \to \infty$ and hence, complete the proof. □

Remark 6.3.2. *If we define the parameters $\beta_i's$ [125] for each $i \in \mathbb{N} \cup \{0\}$ as*

$$\beta_i = \begin{cases} \frac{\|v_{i+1}\|}{\|v_i\|}, & \|v_i\| \neq 0, \\ 0, & \|v_i\| = 0. \end{cases} \tag{6.3.4}$$

Then, Theorem 6.3.4 concludes that the truncated solution for IIM converges to the exact solution $\mu(x,t)$, if $0 \leq \beta_i < 1$, $\forall i \in \mathbb{N} \cup \{0\}$ and $\lambda = \max\{\beta_i's\}$. Furthermore, by following Theorem 2, the maximum absolute error is calculated to be $\|\mu(x,t) - v_n\| \leq \frac{1}{1-\beta}\beta^{n+1}\|v_0\|$.

6.4 Numerical validation

This section presents four examples that demonstrate the effectiveness and performance of the suggested method over exiting iterative solutions derived by the HAM, HPM, ADM, and ODM. Specifically, two ODEs, one PDE and one stiff ODE are examined.

Example 6.4.1. *Consider the non-linear Ricatti equation*

$$\frac{d\mu(t)}{dt} = 1 - \mu^2(t), \quad t > 0$$

under the initial condition $\mu(0) = \mu_0 \in \mathbb{R}$. *The exact solution for the problem is given as [25]*

$$\mu(t) = \frac{\mu_0 + \tanh(t)}{1 + \mu_0 \tanh(t)}. \tag{6.4.1}$$

As per the IIM described in Section 6.2, the linear and nonlinear operators are selected as $\mathscr{L}[\mu] = \dfrac{d\mu}{dt}$ and $\mathscr{N}[\mu] := 1 - \mu^2$, respectively. Therefore, iterations to obtain the approximated solutions are provided as follows

$$\mathscr{L}[v_0(t)] = 0, \text{ with initial condition } v_0(0) = \mu_0,$$

and the higher order iterations are computed via

$$\mathscr{L}[v_{i+1}(t)] + v_{i+1}(t)\mathscr{C}(t) = -\mathscr{N}[v_i(t)] + v_i(t)\mathscr{C}(t) - g(t), \quad i \geq 1.$$

The above iterations give the approximated solutions as

$$v_0(t) = \mu_0, \quad v_1(t) = \frac{1}{2\mu_0} e^{-2\mu_0 t}\left(-h\mu_0^2 + h\mu_0^2 e^{2\mu_0 t} + he^{2\mu_0 t} - h + 2\mu_0^2\right).$$

Following the similar trend, one can find the higher order iterative solutions using MATHEMATICA©. For numerical simulations, a five term truncated series solution is considered. The convergence control parameter is assessed for iterative solutions involving three, four, and five terms, yielding values of 0.995, 0.998, and 0.999, respectively. These values exhibit close similarity, thus confirming the validity of Theorem 6.3.2 and one can consider the value of $h = 0.99$.

The iterative solutions derived from HPM, HAM, ADM, ODM, and the new proposed methods IIM and IIM-h are compared in Figure 6.1(a). All the methods show good accuracy for a short duration, but the HPM errors increase rapidly as time progresses, and the ODM solution eventually becomes unstable after some time. On the other hand, IIM and IIM-h keep their accuracy for a longer duration. Figure 6.1(b) indicates a remarkable

increase in the error of iterative solutions derived via HPM, HAM, ADM, and ODM, while IIM and IIM-*h* have a tolerable error. The importance of using the convergence control parameter is demonstrated in Figure 6.1(c). The accuracy is slightly affected by the convergence control parameter at the beginning, but it enhances the accuracy for a longer duration. Table 6.1 outlines the error trends across multiple iterations for distinct

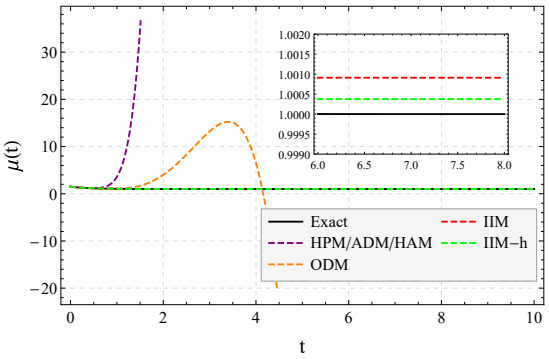

(a) Exact and approximate solutions

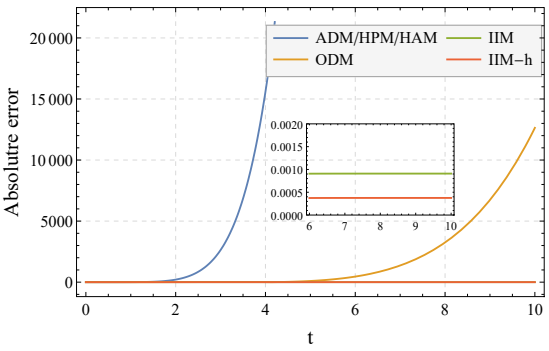

(b) Error of approximate solutions

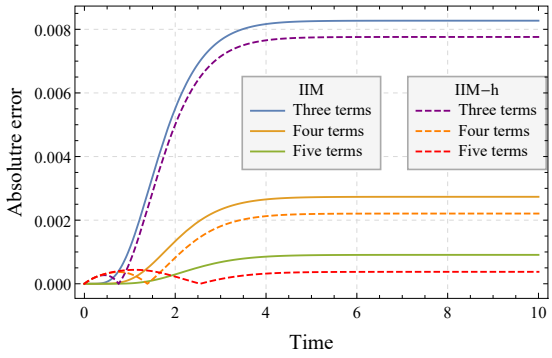

(c) Comparison between IIM and IIM-*h*

Figure 6.1: Solution and errors for Example 6.4.1

time intervals. The error increases with the progression of time for both IIM and IIM-*h* methods, albeit opting for a higher-order iterative solution can enhance accuracy. Notably, integrating the convergence control parameter somewhat enhances accuracy but comes with a heightened computational burden. Additionally, Table 6.2 compares the error with other iterative solutions. It can be seen that the HPM, HAM, and ADM solutions exhibit extreme behavior for a longer duration, and ODM solutions are better than the other solutions, but errors are still unacceptable. On the other hand, IIM and IIM-*h* perform well

Time Level (t)	Number of Iterations					
	IIM			IIM-h		
	$n=3$	$n=4$	$n=5$	$n=3$	$n=4$	$n=5$
2	5.51E-3	1.33E-3	2.93E-4	5.00E-3	8.22E-4	2.25E-4
4	8.16E-3	2.65E-3	8.52E-4	7.65E-3	2.12E-3	3.19E-4
6	8.26E-3	2.735E-3	9.07E-4	7.75E-3	2.20E-3	3.73E-4
8	8.27E-3	2.736E-3	9.08E-4	7.75E-3	2.20E-3	3.75E-4
10	8.28E-3	2.73E-3	9.09E-4	7.76E-3	2.207E-3	3.75E-4

Table 6.1: Error comparison of IIM and IIM-h methods

and demonstrate high accuracy for the higher time. Table 6.3 presents the experimental

	Values of t				
	1	2	3	4	5
HAM	2.535	208.826	2630.16	15602.8	61582.5
ODM	2.43E-2	2.992	12.2178	5.499	95.593
IIM	1.31E-5	2.938E-4	6.808E-4	8.527E-4	8.98E-4
IIM-h	4.34E-4	2.254E-4	1.49E-4	3.19E-4	3.64E-4

Table 6.2: Error distribution for different schemes considering $n=5$ with parameters $v_0=1.5$ for Example 6.4.1

order of convergence for diverse methods, uniformly indicating a convergence of first order across all methodologies. It is noteworthy that the IIM and IIM-h methods demonstrate a relatively enhanced convergence rate compared to alternative schemes.

Example 6.4.2. *Consider the nonlinear differential equation*

$$\frac{d\mu(t)}{dt} = -\alpha\mu(t) - \beta\mu^3(t), \tag{6.4.2}$$

with the initial condition $\mu(0)=\mu_0$ *and* $\alpha,\beta,\mu_0 \in \mathbb{R}$. *The exact solution of the problem is given by [25]*

$$\mu(t) = \frac{\mu_0 e^{\alpha t}}{\sqrt{1+\frac{\beta}{\alpha}\mu_0^2(1-exp^{-2at})}}.$$

Grid	HAM	ODM	IIM	IIM-h
0.5				
	0.930	0.929	0.982	0.988
0.25				
	0.964	0.964	0.991	0994
0.25/2				
	0.982	0.981	0.995	0.997
0.25/4				
	0.991	0.990	0.997	0.998
0.25/8				

Table 6.3: Order of convergence using ADM, ODM, IIM and IIM-h with parameters $v_0 = 1.5$ in Example 6.4.1

Comparing the equation (6.4.2) with equation (6.2.1), one can deduce that $\mathscr{L}[\mu(t)] = \frac{d\mu(t)}{dt}$ and $\mathscr{N}[\mu(t)] = \alpha\mu(t) + \beta\mu^3(t)$. Hence iterations to obtained the approximated solutions are provided as follows

$$\begin{cases} v_0(t) & = \mu_0, \\ v'_{i+1}(t) + v_{i+1}(t)\mathscr{C}(x) & = -\alpha\mu(t) - \beta\mu^3(t) + v_i(t)\mathscr{C}(x), \quad i \geq 0. \end{cases}$$

Simplifying the above iterations, first few approximated solutions are obtained as

$$\begin{aligned} v_0(t) =& \mu_0, \\ v_1(t) =& \frac{1}{1.69\beta + 0.75}\left(0.75e^{-1.69\beta t - 0.75t}\left(1.69\beta - 1.13\beta h + 1.13\beta h e^{(1.69\beta+0.75)t} + 0.75\right)\right). \end{aligned}$$

Following the same approach, one can obtain higher-order iterative solutions to enhance the accuracy. A four-term truncated series solution is considered, and exact and approximate solutions are contrasted in Figure 6.2(a). The graph shows that ADM/HPM and HAM are consistent with the exact solution for a shorter time, while ODM performs better for a longer time than ADM, HPM, and HAM but still exhibits a sharp increase for the further extended time domain. On the other hand, IIM and IIM-h demonstrate a remarkable agreement for a considerably longer time. In Figure 6.2(b), error plots are displayed

and illustrate the same findings for the error. Figure 6.2(c) emphasizes the effect of the convergence control parameter. As the previous example shows, the convergence control parameter substantially lowers the error with a slight perturbation at the initial time.

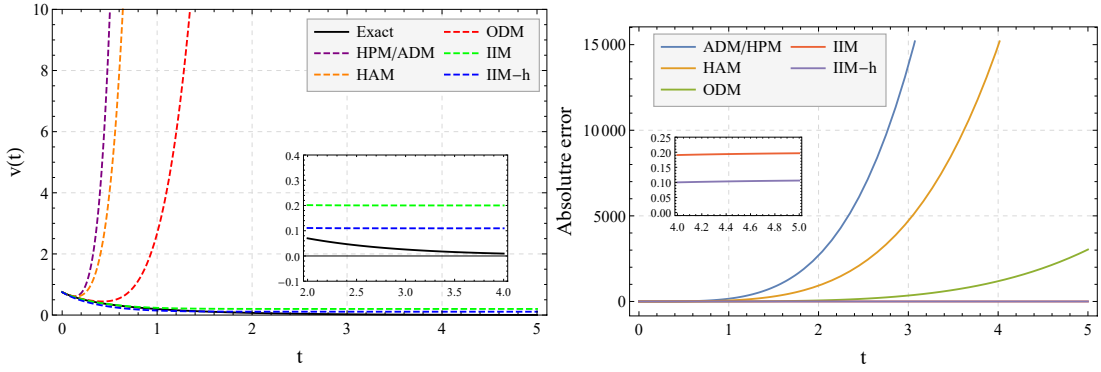

(a) Exact and approximate solutions

(b) Error of approximate solutions

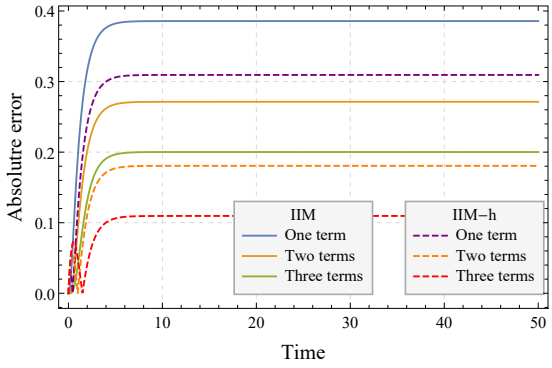

(c) Comparison between IIM and IIM-*h*

Figure 6.2: Solution and errors for Example 6.4.2

Example 6.4.3. *Consider the inviscid Burgers' equation*

$$\frac{\partial \mu}{\partial t}(x,t)+\mu(x,t)\frac{\partial \mu}{\partial x}=0, \tag{6.4.3}$$

with the initial guess $\mu(x,0)=\alpha x+\beta$ *and the exact solution of the problem is provided as [125]*

$$\mu(x,t)=\frac{\alpha x+b}{1+\alpha t}.$$

By following the iterative procedure defined in equation (6.2.5), first few approximated solutions are obtained as

$$\mu_0(x,t_) = \beta + \alpha x, \quad \mu_1(x,t) = e^{\alpha(-t)}(\beta + \alpha x), \quad \mu_2(x,t) = e^{-2\alpha t}\left(\alpha t e^{\alpha t} + 1\right)(\beta + \alpha x),$$
$$\mu_3(x,t) = \frac{1}{6}e^{-4\alpha t}\left(e^{\alpha t}\left(e^{2\alpha t}\left(3\alpha^2 t^2 - 5\right) + 6e^{\alpha t}(\alpha t + 1)^2 + 6\alpha t + 3\right) + 2\right)(\beta + \alpha x).$$

Following the same pattern, higher-order iterative solutions can be derived. A four-term iterative solution is used for numerical computation. In Figure 6.3(a), the exact solution and the solutions obtained by ADM, HPM, HAM, and ODM are compared for $\alpha = \beta = 1$. As seen in the previous example, the solutions by ADM, HPM, and HAM agree well with the exact solution, but they diverge after a short time. On the other hand, the ODM solution remains stable for a longer time. However, the IIM solution is superior to all the other methods. This observation is consistent across both Figure 6.3(b) and 6.4.

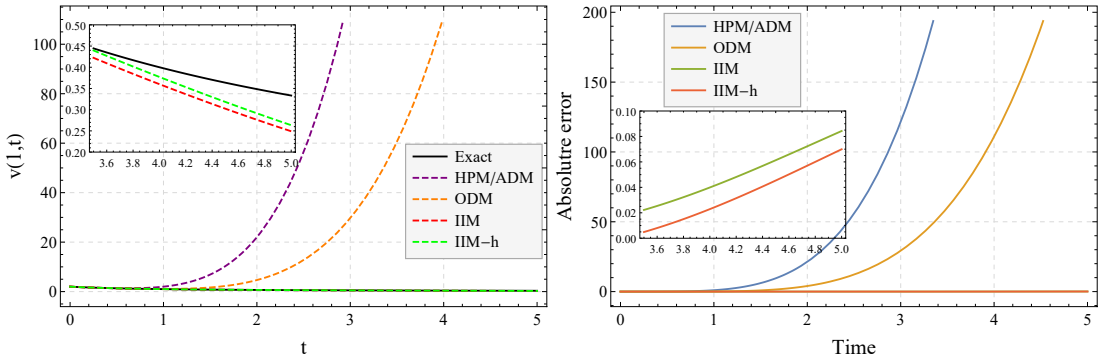

(a) Exact and approximate solutions (b) Error of approximate solutions

Figure 6.3: Solution and errors for Example 6.4.3

In Figure 6.5(a), it is evident that the IIM solution exhibits a disturbance as time progresses, leading to an increase in error. Conversely, Figure 6.5(b) illustrates that the solution can be enhanced over time by augmenting the number of iterations. Hence, the choice of the number of iterations can be tailored to achieve the desired level of accuracy for the solution. It is worth mentioning here that for PDEs, the experimental order of convergence is observed one. Therefore, we have chosen to omit the table illustrating the experimental

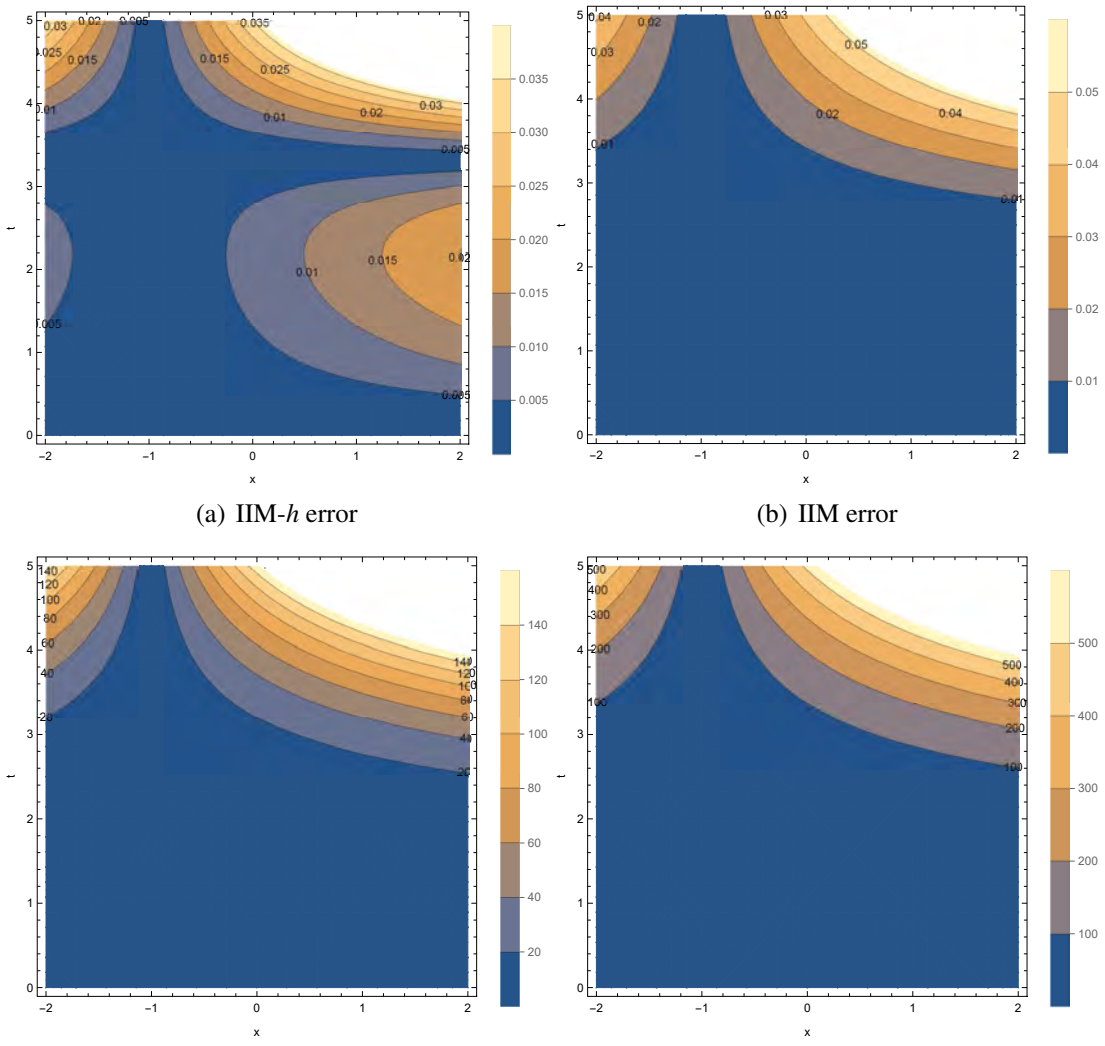

(a) IIM-h error

(b) IIM error

(c) ODM error

(d) ADM error

Figure 6.4: Absolute errors for Example 6.4.3

order of convergence in this context.

6.4.1 Stiff Ordinary Differential Equation

This section consider an stiff ordinary differential equation and to validate the efficiency and accuracy of the proposed scheme, IIM approximated solutions are compared with the FDM solution.

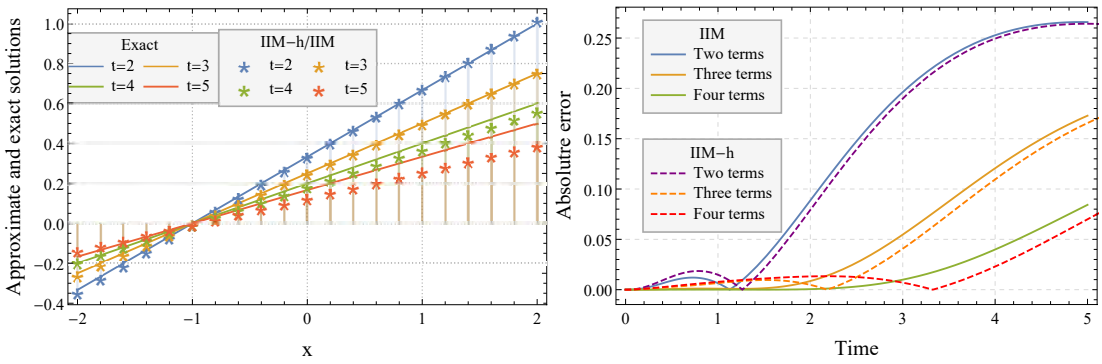

(a) Exact and approximate solutions (b) Error of approximate solutions

Figure 6.5: Solution and errors for Example 6.4.3

Example 6.4.4. *Consider the non-linear oscillator equation*

$$\frac{d\mu(t)}{dt} = \sigma(\mu(t) - \mu^3(t)), \tag{6.4.4}$$

with the initial condition $\mu(0) = a$.

Again, by following the iterative procedure defined in equation (6.2.5), first few approximated solutions are obtained as

$$\begin{aligned}
\mu_0(t) =& a, \quad \mu_1(t) = \frac{ae^{\sigma t - 3a^2\sigma t}\left(2a^2 e^{(3a^2-1)\sigma t} + a^2 - 1\right)}{3a^2 - 1}, \\
\mu_2(t) =& \frac{a}{2\left(3a^2-1\right)^4}\Big(92a^8 - 72a^6 + 12a^4 - 23a^2 e^{t(\sigma-3a^2\sigma)} - a^2 e^{3t(\sigma-3a^2\sigma)} + 6a^2\sigma t e^{t(\sigma-3a^2\sigma)} \\
&+ 2e^{t(\sigma-3a^2\sigma)} + 90a^{10}\sigma t e^{t(\sigma-3a^2\sigma)} + 57a^8 e^{t(\sigma-3a^2\sigma)} + 12a^8 e^{2t(\sigma-3a^2\sigma)} + a^8 e^{3t(\sigma-3a^2\sigma)} \\
&- 228a^8\sigma t e^{t(\sigma-3a^2\sigma)} - 117a^6 e^{t(\sigma-3a^2\sigma)} - 24a^6 e^{2t(\sigma-3a^2\sigma)} - 3a^6 e^{3t(\sigma-3a^2\sigma)} \\
&+ 192a^6\sigma t e^{t(\sigma-3a^2\sigma)} + 81a^4 e^{t(\sigma-3a^2\sigma)} + 12a^4 e^{2t(\sigma-3a^2\sigma)} + 3a^4 e^{3t(\sigma-3a^2\sigma)} \\
&- 60a^4\sigma t e^{t(\sigma-3a^2\sigma)}\Big).
\end{aligned} \tag{6.4.5}$$

Due to the complexity involve in the iterations two and three term truncated series solution is considered and plotted against the FDM solution, as presented in Figure 6.6. For a fixed value of a and σ, Figure 6.6(a) illustrates that the two-term truncated series solution

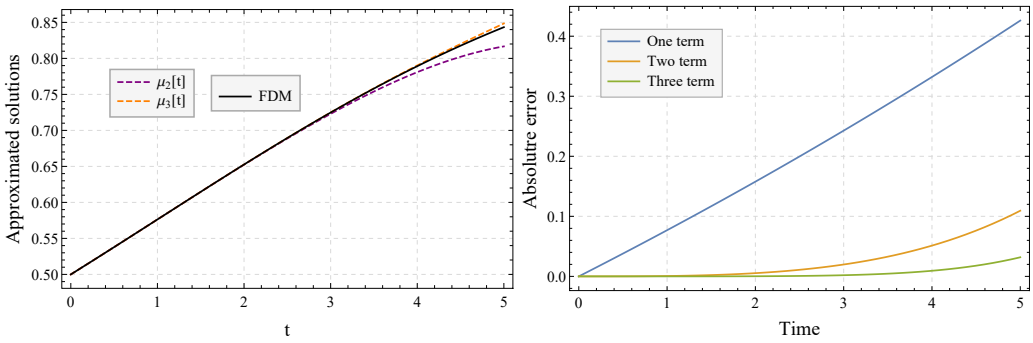

(a) IIM and FDM Solution (b) Error of approximate solutions

Figure 6.6: Solution and errors with $a = 0.5$ and $\sigma = 0.2$ for Example 6.4.4

closely aligns with the FDM solution for smaller values of t. This alignment can be further enhanced by considering more terms, as evidenced by the three-term truncated solution matching well with the FDM solution. Furthermore, Figure 6.6(b) presents the absolute difference between consecutive approximated solutions, indicating that higher-order truncated series solutions have a reduced impact on the solution for the specified time. This observation prompted us to truncate the solution for three terms. Additional higher-order terms can be obtained to achieve the desired accuracy. It is important to note that the IIM-h can also be implemented to obtain a more accurate solution. However, due to the time complexity involved, we have omitted the discussion of IIM-h for this particular case.

6.5 Conclusions

The work introduced a novel semi-analytical approach, IIM, to address ODEs and PDEs. It examined two instances of ODEs and one instance of a PDE, contrasting their outcomes with approximated solutions like HPM, ADM, HAM, and ODM. The proposed methodology yielded more accurate results compared to other semi-analytical methods. Moreover, it integrated a convergence control parameter to refine the semi-analytical solution further. However, it is noted that the proposed approach could be more computationally intensive despite providing results with a minimal number of terms. The proposed technique is a powerful and versatile tool for solving ODEs and PDEs and can be extended to other

differential equations. Future work may include improving the computational efficiency of the technique and applying it to fractional, stochastic, integral, and integral-partial differential equations.

Chapter 7

Conclusions and future scopes

This comprehensive study delved into applying various mathematical methods to solve complex equations related to aggregation and fragmentation processes.

Initially study introduced the VIM for aggregation and coupled aggregation breakage equations. Compared to ADM, VIM provided better estimates for the number density and moments. For the pure growth process, both ADM and VIM formulations were precisely the same for the particle density and finite term series solutions were shown in excellent agreement with the analytical ones. ADM and VIM gave closed-form solutions with a constant growth rate for the pure growth equation. To accelerate the accuracy of the solution, OVIM was implemented to solve the growth model and aggregation equation with a constant kernel. However, the computational cost restricted us from applying the technique to other considered problems. Despite its advantages, the VIM was noted to have limitations, including complex terms and high computational costs for finding higher-order components of the series solutions.

The AHPETM was employed in the next part of the study. This method was used to solve fragmentation, multi-dimensional coagulation, and coupled aggregation-fragmentation equations. It was observed that AHPETM significantly outperformed the results of ADM, HAM, HPM, and ODM for non-linear aggregation equation, demonstrating its reliabil-

ity and applicability. AHPETM was also designed to solve non-linear 2-D aggregation and combined aggregation-fragmentation equations due to the accuracy and efficiency observed in the pure aggregation equation, and remarkable results were obtained in each case.

Further, IOHAM was employed to solve aggregation and coupled aggregation-growth equations. The convergence analysis of the truncated series solution for this method was examined for the aggregation equation. The numerical results were compared with the existing HAM, HPM, ADM, and ODM solutions. It was observed that HAM, HPM, and ADM provided the same results, while ODM improved the solution to some extent. However, the proposed IOHAM scheme improved all the solutions obtained via predefined semi-analytical methods. Moreover, for the first time, an analytical approximate method was implemented for solving the coupled aggregation-growth equation. In the last part of the study, a novel semi-analytical approach, the IIM, was introduced to address ODEs and PDEs. The proposed methodology yielded more accurate results compared to other semi-analytical methods. Moreover, it integrated a convergence control parameter to refine the semi-analytical solution further. However, it was noted that the proposed approach could be more computationally intensive despite providing results with a minimal number of terms.

The study further focused on the ADM and HPM to solve CCM and LSE. ADM and HPM provided a recursive relation for obtaining exact solutions in terms of the sum of an infinite series and approximate solutions. Interestingly, it was observed that the solutions obtained through HPM were identical to those obtained via ADM. A closed-form solution is obtained for the product and constant kernels. The errors between truncated series solutions were reported for the sum and Ruckenstein kernels to justify the convergence of the scheme in the absence of exact solutions. Similar results were also obtained for the LSE, further validating the effectiveness of these methods.

In conclusion, each method has its strengths and limitations, and the choice of method depends on the specific requirements of the problem. This study contributes to understanding these methods and their applications in solving complex aggregation and fragmentation

equations. Future work could explore the use of considered methods for tackling other engineering non-linear problems, potentially enhancing the approach with a convergence control parameter and Pade approximation. This would offer a more refined and practical scheme for solving complex mathematical problems.

Future Scope

Based on the work done in the thesis, the possible scopes are as follows:

1. To study the semi-analytical technique, namely modified veriational iteration method for collision-induced breakage equation and study its convergence analysis.

2. To implement the implicit iterative method on aggregation and breakage models to obtain the accurate solutions for longer time domain.

3. Implementation of finite volume scheme for cancer coagulation model and validate the results with experimental data.

4. The explore the numerical and semi-analytical methods to solve the Rennet-coagulation model.

Bibliography

[1] M. V. Smoluchowski. “Versuch einer mathematischen Theorie der Koagulationskinetik kolloider Lösungen”. *Zeitschrift für Physikalische Chemie* 92.1 (1918), pp. 129–168.

[2] Y. Bie, X. Cui, and Z. Li. “A coupling approach of state-based peridynamics with node-based smoothed finite element method”. *Computer Methods in Applied Mechanics and Engineering* 331 (2018), pp. 675–700.

[3] M. Singh, T. Matsoukas, A. B. Albadarin, and G. Walker. “New volume consistent approximation for binary breakage population balance equation and its convergence analysis”. *ESAIM: Mathematical Modelling and Numerical Analysis* 53.5 (2019), pp. 1695–1713.

[4] M. Singh and G. Walker. “Finite volume approach for fragmentation equation and its mathematical analysis”. *Numerical Algorithms* 89.2 (2022), pp. 465–486.

[5] A. K. Giri and E. Hausenblas. “Convergence analysis of sectional methods for solving aggregation population balance equations: The fixed pivot technique”. *Nonlinear Analysis: Real World Applications* 14.6 (2013), pp. 2068–2090.

[6] M. Singh. “Accurate and efficient approximations for generalized population balances incorporating coagulation and fragmentation”. *Journal of Computational Physics* 435 (2021), p. 110215.

[7] M. Singh, V. Ranade, O. Shardt, and T. Matsoukas. “Challenges and opportunities concerning numerical solutions for population balances: a critical review”. *Journal of Physics A: Mathematical and Theoretical* 55.38 (2022), p. 383002.

[8] G. Kaur, R. Singh, and H. Briesen. “Approximate solutions of aggregation and breakage population balance equations”. *Journal of Mathematical Analysis and Applications* 512.2 (2022), p. 126166.

[9] G. Kaur, R. Singh, M. Singh, J. Kumar, and T. Matsoukas. “Analytical approach for solving population balances: A homotopy perturbation method”. *Journal of Physics A: Mathematical and Theoretical* 52.38 (2019), p. 385201.

[10] S. Kaushik, S. Hussain, and R. Kumar. “Laplace transform-based approximation methods for solving pure aggregation and breakage equations”. *Mathematical Methods in the Applied Sciences* 46.16 (2023), pp. 17402–17421.

[11] G. Arora, R. Kumar, and Y. Mammeri. “Homotopy perturbation and adomian decomposition methods for condensing coagulation and Lifshitz-Slyzov models”. *GEM-International Journal on Geomathematics* 14.1 (2023), p. 4.

[12] S. Hussain and R. Kumar. “Elzaki projected differential transform method for multi-dimensional aggregation and combined aggregation-breakage equations”. *Journal of Computational Science* 75 (2024), p. 102211.

[13] J. Su, Z. Gu, Y. Li, S. Feng, and X. Y. Xu. “Solution of population balance equation using quadrature method of moments with an adjustable factor”. *Chemical Engineering Science* 62.21 (2007), pp. 5897–5911.

[14] R. Ahrens and S. Le Borne. “FFT-based evaluation of multivariate aggregation integrals in population balance equations on uniform tensor grids”. *Journal of Computational and Applied Mathematics* 338 (2018), pp. 280–297.

[15] Z. Hammouch and T. Mekkaoui. “A Laplace-variational iteration method for solving the homogeneous Smoluchowski coagulation equation” (2010).

[16] R. Singh, J. Saha, and J. Kumar. “Adomian decomposition method for solving fragmentation and aggregation population balance equations”. *Journal of Applied Mathematics and Computing* 48.1 (2015), pp. 265–292.

[17] A. Dutta, Z. Pınar, D. Constales, and T. Öziş. “Population balances involving aggregation and breakage through homotopy approaches”. *International Journal of Chemical Reactor Engineering* 16.6 (2018).

[18] G. Arora, S. Hussain, and R. Kumar. “Comparison of variational iteration and Adomian decomposition methods to solve growth, aggregation and aggregation-breakage equations”. *Journal of Computational Science* 67 (2023), p. 101973.

[19] S. Kaushik and R. Kumar. “A novel optimized decomposition method for Smoluchowski’s aggregation equation”. *Journal of Computational and Applied Mathematics* 419 (2023), p. 114710.

[20] S. Kaushik, S. Hussain, and R. Kumar. “Laplace transform-based approximation methods for solving pure aggregation and breakage equations”. *Mathematical Methods in the Applied Sciences* 46.16 (2023), pp. 17402–17421.

[21] N. Yadav, M. Singh, S. Singh, R. Singh, and J. Kumar. “A note on homotopy perturbation approach for nonlinear coagulation equation to improve series solutions for longer times”. *Chaos, Solitons & Fractals* 173 (2023), p. 113628.

[22] D. Ganji and A Sadighi. “Application of He’s homotopy-perturbation method to nonlinear coupled systems of reaction-diffusion equations”. *International Journal of Nonlinear Sciences and Numerical Simulation* 7.4 (2006), pp. 411–418.

[23] M. Dehghan, Y. Rahmani, D. D. Ganji, S. Saedodin, M. S. Valipour, and S. Rashidi. “Convection–radiation heat transfer in solar heat exchangers filled with a porous medium: homotopy perturbation method versus numerical analysis”. *Renewable Energy* 74 (2015), pp. 448–455.

[24] J.-H. He. “Application of homotopy perturbation method to nonlinear wave equations”. *Chaos, Solitons & Fractals* 26.3 (2005), pp. 695–700.

[25] Z. Odibat. “An optimized decomposition method for nonlinear ordinary and partial differential equations”. *Physica A: Statistical Mechanics and its Applications* 541 (2020), p. 123323.

[26] J. Fernandez-Diaz and G. Gomez-Garcia. “Exact solution of Smoluchowski’s continuous multi-component equation with an additive kernel”. *EPL (Europhysics Letters)* 78.5 (2007), p. 56002.

[27] Y. P. Kim and J. H. Seinfeld. “Simulation of multicomponent aerosol condensation by the moving sectional method”. *Journal of Colloid and Interface Science* 135.1 (1990), pp. 185–199.

[28] N. V. Mantzaris, P. Daoutidis, and F. Srienc. “Numerical solution of multi-variable cell population balance models: I. Finite difference methods”. *Computers & Chemical Engineering* 25.11-12 (2001), pp. 1411–1440.

[29] T Matsoukas, T Kim, and K Lee. “Bicomponent aggregation with composition-dependent rates and the approach to well-mixed state”. *Chemical Engineering Science* 64.4 (2009), pp. 787–799.

[30] M. Attarakih, M. Jaradat, C Drumm, H Bart, S Tiwari, V Sharma, J Kuhnert, and A. Klar. “A multivariate sectional quadrature method of moments for the solution of the population balance equation”. *Computer Aided Chemical Engineering* 28 (2010), pp. 1551–1556.

[31] J. Favero and P. Lage. “The dual-quadrature method of generalized moments using automatic integration packages”. *Computers & Chemical Engineering* 38 (2012), pp. 1–10.

[32] M. Singh, J. Kumar, A. Bück, and E. Tsotsas. “An improved and efficient finite volume scheme for bivariate aggregation population balance equation”. *Journal of Computational and Applied Mathematics* 308 (2016), pp. 83–97.

[33] M. Singh. “New finite volume approach for multidimensional Smoluchowski equation on nonuniform grids”. *Studies in Applied Mathematics* 147.3 (2021), pp. 955–977.

[34] D. Patil and J. Andrews. “An analytical solution to continuous population balance model describing floc coalescence and breakage—a special case”. *Chemical Engineering Science* 53.3 (1998), pp. 599–601.

[35] R. Kumar, J. Kumar, and G. Warnecke. “Moment preserving finite volume schemes for solving population balance equations incorporating aggregation, breakage, growth and source terms”. *Mathematical Models and Methods in Applied Sciences* 23.07 (2013), pp. 1235–1273.

[36] J. Saha, J. Kumar, A. Bück, and E. Tsotsas. “Finite volume approximations of breakage population balance equation”. *Chemical Engineering Research and Design* 110 (2016), pp. 114–122.

[37] M. Singh, H. Y. Ismail, T. Matsoukas, A. B. Albadarin, and G. Walker. “Mass-based finite volume scheme for aggregation, growth and nucleation population balance equation”. *Proceedings of the Royal Society A* 475.2231 (2019), p. 20190552.

[38] M. M. Attarakih, C. Drumm, and H.-J. Bart. “Solution of the population balance equation using the sectional quadrature method of moments (SQMOM)”. *Chemical Engineering Science* 64.4 (2009), pp. 742–752.

[39] D. L. Marchisio and R. O. Fox. “Solution of population balance equations using the direct quadrature method of moments”. *Journal of Aerosol Science* 36.1 (2005), pp. 43–73.

[40] M. Pigou, J. Morchain, P. Fede, M.-I. Penet, and G. Laronze. “New developments of the extended quadrature method of moments to solve population balance equations”. *Journal of Computational Physics* 365 (2018), pp. 243–268.

[41] N. Ahmed, G. Matthies, and L. Tobiska. “Stabilized finite element discretization applied to an operator-splitting method of population balance equations”. *Applied Numerical Mathematics* 70 (2013), pp. 58–79.

[42] C. Dorao and H. Jakobsen. “hp-Adaptive least squares spectral element method for population balance equations”. *Applied Numerical Mathematics* 58.5 (2008), pp. 563–576.

[43] F. Guiaş. “A stochastic approach for simulating spatially inhomogeneous coagulation dynamics in the gelation regime”. *Communications in Nonlinear Science and Numerical Simulation* 14.1 (2009), pp. 204–222.

[44] Y. Lin, K. Lee, and T. Matsoukas. “Solution of the population balance equation using constant-number Monte Carlo”. *Chemical Engineering Science* 57.12 (2002), pp. 2241–2252.

[45] R. I. Patterson, W. Wagner, and M. Kraft. “Stochastic weighted particle methods for population balance equations”. *Journal of Computational Physics* 230.19 (2011), pp. 7456–7472.

[46] S. Le Borne and L. Shahmuradyan. “Algorithms for the Haar wavelet based fast evaluation of aggregation integrals in population balance equations”. *Applied Numerical Mathematics* 108 (2016), pp. 1–20.

[47] M. Singh, J. Chakraborty, J. Kumar, and R. Ramakanth. “Accurate and efficient solution of bivariate population balance equations using unstructured grids”. *Chemical Engineering Science* 93 (2013), pp. 1–10.

[48] M. Singh, D. Ghosh, and J. Kumar. “A comparative study of different discretizations for solving bivariate aggregation population balance equation”. *Applied Mathematics and Computation* 234 (2014), pp. 434–451.

[49] M. Kostoglou and A. Karabelas. “On sectional techniques for the solution of the breakage equation”. *Computers & Chemical Engineering* 33.1 (2009), pp. 112–121.

[50] Y Liao, R Oertel, S Kriebitzsch, F Schlegel, and D Lucas. “A discrete population balance equation for binary breakage”. *International Journal for Numerical Methods in Fluids* 87.4 (2018), pp. 202–215.

[51] K. Lee and T. Matsoukas. “Simultaneous coagulation and break-up using constant-N Monte Carlo”. *Powder Technology* 110.1-2 (2000), pp. 82–89.

[52] A. W. Mahoney and D. Ramkrishna. “Efficient solution of population balance equations with discontinuities by finite elements”. *Chemical Engineering Science* 57.7 (2002), pp. 1107–1119.

[53] G. Madras and B. J. McCoy. “Reversible crystal growth–dissolution and aggregation–breakage: numerical and moment solutions for population balance equations”. *Powder Technology* 143 (2004), pp. 297–307.

[54] W. H. Hundsdorfer, J. G. Verwer, and W. Hundsdorfer. *Numerical solution of time-dependent advection-diffusion-reaction equations*. Vol. 33. Springer, 2003.

[55] Y. I. Lim, J.-M. Le Lann, X. M. Meyer, X. Joulia, G. Lee, and E. S. Yoon. “On the solution of population balance equations (PBE) with accurate front tracking methods in practical crystallization processes”. *Chemical Engineering Science* 57.17 (2002), pp. 3715–3732.

[56] R. Gunawan, I. Fusman, and R. D. Braatz. “High resolution algorithms for multidimensional population balance equations”. *AIChE Journal* 50.11 (2004), pp. 2738–2749.

[57] S. Kumar and D Ramkrishna. “On the solution of population balance equations by discretization—III. Nucleation, growth and aggregation of particles”. *Chemical Engineering Science* 52.24 (1997), pp. 4659–4679.

[58] J. Kumar. “Numerical approximations of population balance equations in particulate systems”. PhD thesis. Citeseer, 2006.

[59] S. Qamar and G. Warnecke. “Numerical solution of population balance equations for nucleation, growth and aggregation processes”. *Computers & Chemical Engineering* 31.12 (2007), pp. 1576–1589.

[60] V. S. Safronov. “Evolution of the Protoplanetary Cloud and Formation of the Earth and the Planets”. *Israel Program for Scientific Translations* (1972).

[61] P. Dubovski. “A triangle’of interconnected coagulation models”. *Journal of Physics A: Mathematical and General* 32.5 (1999), p. 781.

[62] M. Lachowicz, P. Laurençot, and D. Wrzosek. “On the Oort–Hulst–Safronov Coagulation Equation and Its Relation to the Smoluchowski Equation”. *SIAM J. Mathematical Analysis* 34.6 (2003), pp. 1399–1421.

[63] J. Davidson. “Mathematical Theory of Condensing Coagulation”. PhD thesis. Stevens Institute of Technology, 2016.

[64] J.-H. He. “Variational iteration method for autonomous ordinary differential systems”. *Applied Mathematics and Computation* 114.2-3 (2000), pp. 115–123.

[65] J.-H. He and X.-H. Wu. “Construction of solitary solution and compacton-like solution by variational iteration method”. *Chaos, Solitons & Fractals* 29.1 (2006), pp. 108–113.

[66] S. Guo and L. Mei. “The fractional variational iteration method using He’s polynomials”. *Physics Letters A* 375.3 (2011), pp. 309–313.

[67] D. Ganji, M Nourollahi, and E Mohseni. “Application of He’s methods to nonlinear chemistry problems”. *Computers & Mathematics with Applications* 54.7-8 (2007), pp. 1122–1132.

[68] A. Yıldırım. “Variational iteration method for modified Camassa–Holm and Degasperis–Procesi equations”. *International Journal for Numerical Methods in Biomedical Engineering* 26.2 (2010), pp. 266–272.

[69] R. W. Samsel and A. S. Perelson. “Kinetics of rouleau formation. I. A mass action approach with geometric features”. *Biophysical Journal* 37.2 (1982), pp. 493–514.

[70] L. Zheng and X. Zhang. *Modeling and analysis of modern fluid problems*. Academic Press, 2017.

[71] B. A. Finlayson. *The method of weighted residuals and variational principles*. SIAM, 2013.

[72] M. Turkyilmazoglu. "An optimal variational iteration method". *Applied Mathematics Letters* 24.5 (2011), pp. 762–765.

[73] M. Turkyilmazoglu. "Accelerating the convergence of Adomian decomposition method (ADM)". *Journal of Computational Science* 31 (2019), pp. 54–59.

[74] M. Turkyilmazoglu. "Equivalence of ratio and residual approaches in the homotopy analysis method and some applications in nonlinear science and engineering". *CMES-Computer Modeling In Engineering & Sciences* 120.1 (2019).

[75] M. Turkyilmazoglu. "An efficient computational method for differential equations of fractional type". *CMES-Computer Modeling In Engineering & Sciences* 133.1 (2022).

[76] M. Turkyilmazoglu. "Nonlinear problems via a convergence accelerated decomposition method of Adomian". *Computer Modeling in Engineering & Sciences* 127.1 (2021), pp. 1–22.

[77] G. H. Ibraheem, M. Turkyilmazoglu, and M. Al-Jawary. "Novel approximate solution for fractional differential equations by the optimal variational iteration method". *Journal of Computational Science* 64 (2022), p. 101841.

[78] G. Adomian. "A review of the decomposition method in applied mathematics". *Journal of Mathematical Analysis and Applications* 135.2 (1988), pp. 501–544.

[79] J. Biazar, Z. Ayati, and M. R. Yaghouti. "Homotopy perturbation method for homogeneous Smoluchowski's equation". *Numerical Methods for Partial Differential Equations* 26.5 (2010), pp. 1146–1153.

[80] P. Singh, U. Buragohain, and N. Senroy. “Time Domain Simulation of DFIG-Based Wind Power System using Differential Transform Method”. *arXiv preprint arXiv:2202.07208* (2022).

[81] J. Li and A. Wu. “Influence of non-ideal factors on the boundary control of buck converters with curved switching surfaces”. *IEEE Access* 7 (2019), pp. 52790–52803.

[82] G Adomian and R Rach. “Inversion of nonlinear stochastic operators”. *Journal of Mathematical Analysis and Applications* 91.1 (1983), pp. 39–46.

[83] J. Kumar, M. Peglow, G. Warnecke, and S. Heinrich. “An efficient numerical technique for solving population balance equation involving aggregation, breakage, growth and nucleation”. *Powder Technology* 182.1 (2008), pp. 81–104.

[84] T. M. Elzaki. “The new integral transform Elzaki transform”. *Global Journal of Pure and Applied Mathematics* 7.1 (2011), pp. 57–64.

[85] T. M. Elzaki. “Application of new transform “Elzaki transform” to partial differential equations”. *Global Journal of Pure and Applied Mathematics* 7.1 (2011), pp. 65–70.

[86] T. M. Elzaki et al. “On The New Integral Transform”Elzaki Transform”Fundamental Properties Investigations and Applications”. *Global Journal of Mathematical Sciences: Theory and Practical* 4.1 (2012), pp. 1–13.

[87] S. Jasrotia and P. Singh. “Accelerated Homotopy Perturbation Elzaki Transformation Method for Solving Nonlinear Partial Differential Equations”. In: *Journal of Physics: Conference Series*. Vol. 2267. 1. IOP Publishing. 2022, p. 012106.

[88] W. T. Scott. “Analytic studies of cloud droplet coalescence I”. *Journal of Atmospheric Sciences* 25.1 (1968), pp. 54–65.

[89] M. Ranjbar, H. Adibi, and M. Lakestani. “Numerical solution of homogeneous Smoluchowski’s coagulation equation”. *International Journal of Computer Mathematics* 87.9 (2010), pp. 2113–2122.

[90] P. Lage. “Comments on the”An analytical solution to the population balance equation with coalescence and breakage-the special case with constant number of particles”by DP Patil and JRG Andrews [Chemical Engineering Science 53 (3) 599-601]”. *Chemical Engineering Science* 19.57 (2002), pp. 4253–4254.

[91] M. Singh, R. Singh, S. Singh, G. Walker, and T. Matsoukas. “Discrete finite volume approach for multidimensional agglomeration population balance equation on unstructured grid”. *Powder Technology* 376 (2020), pp. 229–240.

[92] H. Temimi, A. R. Ansari, and A. M. Siddiqui. “An approximate solution for the static beam problem and nonlinear integro-differential equations”. *Computers & Mathematics with Applications* 62.8 (2011), pp. 3132–3139.

[93] M. Ben-Romdhane and H. Temimi. “An Iterative Numerical Method for Solving the Lane–Emden Initial and Boundary Value Problems”. *International Journal of Computational Methods* 15.04 (2018), p. 1850020.

[94] H. Temimi, M. Ben-Romdhane, S. El-Borgi, and Y.-J. Cha. “Time-delay effects on controlled seismically excited linear and nonlinear structures”. *International Journal of Structural Stability and Dynamics* 16.07 (2016), p. 1550031.

[95] S. Qamar, G. Warnecke, and M. P. Elsner. “On the solution of population balances for nucleation, growth, aggregation and breakage processes”. *Chemical Engineering Science* 64.9 (2009), pp. 2088–2095.

[96] S. Liao. *Beyond perturbation: introduction to the homotopy analysis method*. Chapman and Hall/CRC, 2003.

[97] R. C. Rach. “A new definition of the Adomian polynomials”. *Kybernetes* (2008).

[98] J.-H. He. “Homotopy perturbation method for solving boundary value problems”. *Physics Letters A* 350.1-2 (2006), pp. 87–88.

[99] J.-H. He. “Homotopy perturbation technique”. *Computer Methods in Applied Mechanics and Engineering* 178.3-4 (1999), pp. 257–262.

[100] J.-H. He. “A coupling method of a homotopy technique and a perturbation technique for non-linear problems”. *Int. Journal of Non-linear Mechanics* 35.1 (2000), pp. 37–43.

[101] M. El-Shahed. “Application of He’s homotopy perturbation method to Volterra’s integro-differential equation”. *Int. Journal of Nonlinear Sciences and Numerical Simulation* 6.2 (2005), pp. 163–168.

[102] A Nazari-Golshan, S. Nourazar, H Ghafoori-Fard, A. Yildirim, and A Campo. “A modified homotopy perturbation method coupled with the Fourier transform for nonlinear and singular Lane–Emden equations”. *Applied Mathematics Letters* 26.10 (2013), pp. 1018–1025.

[103] M. Singh, K. Vuik, G. Kaur, and H.-J. Bart. “Effect of different discretizations on the numerical solution of 2D aggregation population balance equation”. *Powder Technology* 342 (2019), pp. 972–984.

[104] J Kumar, G Warnecke, M Peglow, and S Heinrich. “Comparison of numerical methods for solving population balance equations incorporating aggregation and breakage”. *Powder Technology* 189.2 (2009), pp. 218–229.

[105] E Ruckenstein and B Pulvermacher. “Growth kinetics and the size distributions of supported metal crystallites”. *Journal of Catalysis* 29.2 (1973), pp. 224–245.

[106] I. M. Lifshitz and V. V. Slyozov. “The kinetics of precipitation from supersaturated solid solutions”. *Journal of Physics and Chemistry of Solids* 19.1-2 (1961), pp. 35–50.

[107] T. Goudon and L. Monasse. “Fokker–Planck Approach of Ostwald Ripening: Simulation of a Modified Lifshitz– Slyozov–Wagner System with a Diffusive Correction”. *SIAM Journal on Scientific Computing* 42.1 (2020), B157–B184.

[108] L. F. B. Moyano, C. A. P. Padilla, and D. A. Tacle. “AN INVESTIGATION OF THE USE OF ORDINARY DIFFERENTIAL EQUATIONS APPLIED TO ME-

CHANICAL ENGINEERING PROBLEMS." *Ann. For. Res* 66.1 (2023), pp. 4394–4402.

[109] A. H. Ganie, L. H. Sadek, M. Tharwat, M. A. Iqbal, M. M. Miah, M. M. Rasid, N. S. Elazab, and M. Osman. "New investigation of the analytical behaviors for some nonlinear PDEs in mathematical physics and modern engineering". *Partial Differential Equations in Applied Mathematics* 9 (2024), p. 100608.

[110] R. G. Rice, D. D. Do, and J. E. Maneval. *Applied mathematics and modeling for chemical engineers*. John Wiley & Sons, 2023.

[111] I. Ali and S. U. Khan. "A Dynamic Competition Analysis of Stochastic Fractional Differential Equation Arising in Finance via Pseudospectral Method". *Mathematics* 11.6 (2023), p. 1328.

[112] A. J. Linot, J. W. Burby, Q. Tang, P. Balaprakash, M. D. Graham, and R. Maulik. "Stabilized neural ordinary differential equations for long-time forecasting of dynamical systems". *Journal of Computational Physics* 474 (2023), p. 111838.

[113] S. David Müzel, E. P. Bonhin, N. M. Guimarães, and E. S. Guidi. "Application of the finite element method in the analysis of composite materials: A review". *Polymers* 12.4 (2020), p. 818.

[114] Ş. Toprakseven and P. Zhu. "Error analysis of a weak Galerkin finite element method for two-parameter singularly perturbed differential equations in the energy and balanced norms". *Applied Mathematics and Computation* 441 (2023), p. 127683.

[115] M. Baccouch and H. Temimi. "Analysis of optimal error estimates and superconvergence of the discontinuous Galerkin method for convection-diffusion problems in one space dimension". *International Journal of Numerical Analysis and Modeling* 13.3 (2016), p. 403.

[116] Z.-Z. Sun, Q. Zhang, and G.-h. Gao. *Finite difference methods for nonlinear evolution equations*. Vol. 8. Walter de Gruyter GmbH & Co KG, 2023.

[117] H. Temimi, M. Ben-Romdhane, A. R. Ansari, and G. I. Shishkin. “Finite difference numerical solution of Troesch’s problem on a piecewise uniform Shishkin mesh”. *Calcolo* 54.1 (2017), pp. 225–242.

[118] J.-S. Duan, R. Rach, D. Baleanu, and A.-M. Wazwaz. “A review of the Adomian decomposition method and its applications to fractional differential equations”. *Communications in Fractional Calculus* 3.2 (2012), pp. 73–99.

[119] S. Liao. “On the homotopy analysis method for nonlinear problems”. *Applied Mathematics and Computation* 147.2 (2004), pp. 499–513.

[120] J.-H. He. “Homotopy perturbation method: a new nonlinear analytical technique”. *Applied Mathematics and Computation* 135.1 (2003), pp. 73–79.

[121] S. Liao. “Comparison between the homotopy analysis method and homotopy perturbation method”. *Applied Mathematics and Computation* 169.2 (2005), pp. 1186–1194.

[122] M. B. M. Ben-Romdhane H. Temimi. “An Iterative Finite Difference Method for Approximating the Two-Branched Solution of Bratu’s Problem.” *Applied Numerumerical Mathematics* 139 (2019), pp. 62–76.

[123] M. M. M. H. Temimi M. Ben-Romdhane. “A two-branched numerical solution of the two-dimensional Bratu’s problem.” *Applied Numerumerical Mathematics* 153 (2020), pp. 202–216.

[124] H. Temimi and M. Ben-Romdhane. “Numerical solution of falkner-skan equation by iterative transformation method”. *Mathematical Modelling and Analysis* 23.1 (2018), pp. 139–151.

[125] S. Hussain, G. Arora, and R. Kumar. “An efficient semi-analytical technique to solve multi-dimensional Burgers’ equation”. *Computational and Applied Mathematics* 43.1 (2024), p. 11.

[126] S. E.-B. Y. C. H. Temimi M. Ben-Romdhane. “Time-delay effects on controlled seismically excited nonlinear structures.” *International Journal of Structural Stability and Dynamics* 16 (2016), pp. 1–22.

[127] G Adomian. “A new approach to nonlinear partial differential equations”. *Journal of Mathematical Analysis and Applications* 102.2 (1984), pp. 420–434.

[128] G Adomian and R Rach. “On the solution of algebraic equations by the decomposition method”. *Journal of Mathematical Analysis and Applications* 105.1 (1985), pp. 141–166.

[129] L. Bougoffa, A. Mennouni, and R. C. Rach. “Solving Cauchy integral equations of the first kind by the Adomian decomposition method”. *Applied Mathematics and Computation* 219.9 (2013), pp. 4423–4433.

[130] R. Novin, M. A. F. Araghi, and Y. Mahmoudi. “A novel fast modification of the Adomian decomposition method to solve integral equations of the first kind with hypersingular kernels”. *Journal of Computational and Applied Mathematics* 343 (2018), pp. 619–634.

[131] Y. Khan and Q. Wu. “Homotopy perturbation transform method for nonlinear equations using He’s polynomials”. *Computers & Mathematics with Applications* 61.8 (2011), pp. 1963–1967.

[132] S. Hussain, G. Arora, and R. Kumar. “Semi-analytical methods for solving nonlinear differential equations: a review”. *Journal of Mathematical Analysis and Applications* (2023), p. 127821.

[133] S. Noeiaghdam, M. A. Fariborzi Araghi, and S. Abbasbandy. “Finding optimal convergence control parameter in the homotopy analysis method to solve integral equations based on the stochastic arithmetic”. *Numerical Algorithms* 81 (2019), pp. 237–267.

[134] J.-M. Chesneaux and F. Jézéquel. “Dynamical control of computations using the Trapezoidal and Simpson’s rules”. *Journal of Universal Computer Science* 4.1 (1998), pp. 2–10.

List of Research Publications

Journal Publication

- Arora, G., Kumar, R., & Temimi, H.(2024). An implicit semi-analytical technique: development, analysis and applications. Mathematics and Computers in Simulations. (Accepted)

- Arora, G., Kumar, R., & Mammeri, Y. (2024). Elzaki Transform Based Accelerated Homotopy Perturbation Method for Multi-dimensional Smoluchowski's Coagulation and Coupled Coagulation-fragmentation Equations. Journal of Applied Analysis and Computation, 14(5), 1-32. https://doi.org/10.11948/20240004

- Hussain, S., Arora, G., & Kumar, R. (2024). An efficient semi-analytical technique to solve multi-dimensional Burgers' equation. Computational and Applied Mathematics, 43(1), 11. https://link.springer.com/article/10.1007/s40314-023-02512-6

- Arora, G., Hussain, S., & Kumar, R. (2023). Comparison of variational iteration and Adomian decomposition methods to solve growth, aggregation and aggregation-breakage equations. Journal of Computational Science, 67, 101973. https://doi.org/10.1016/j.jocs.2023.101973

- Arora, G., Kumar, R., & Mammeri, Y. (2023). Homotopy perturbation and adomian decomposition methods for condensing coagulation and Lifshitz-Slyzov models. GEM-International Journal on Geomathematics, 14(1), 4. https://link.springer.com/article/10.1007/s13137-023-00215-y

- **Arora, G.**, Kumar, R., & Temimi, H. (2024). An implicit semi-analytical technique: Development, analysis and applications. Mathematics and Computers in Simulation, 226, 500-510. https://doi.org/10.1016/j.matcom.2024.07.020

- Hussain, S., **Arora, G.**, & Kumar, R. (2024). An analytic approach for nonlinear collisional fragmentation model arising in bubble column. Physics of Fluids, 36(10). https://doi.org/10.1063/5.0231347

- Shweta, **Arora, G.**, & Kumar, R. (2024). Large time solution for collisional breakage model: Laplace transformation based accelerated homotopy perturbation method. Mathematics and Computers in Simulation. https://doi.org/10.1016/j.matcom.2024.11.001

Communicated Work

- Arora, G., Hussain, S., & Kumar, R., "New approximate solutions for Smoluchowski's aggregation and coupled aggregation-growth equations", (Under Review).

- Arora, G., Hussain, S., Kumar, R., Mammeri, Y., & Temimi, H., "An Improved Solution Based on Temimi-Ansari Method for Coagulation and Coupled Coagulation Fragmentation Equations," (Under Review).

- Shweta, Arora, G., & Kumar, R.,"A Comprehensive Study of Korteweg-de Vries Burgers' Equation with an Improved Optimal Homotopy Analysis Method", (Under Review).

- Arora, G., Kumar, R., & Mammeri, Y., "Mathematical Study of BLUES Function Method for KdV Burgers' and BBM-Burgers' Equations", (Under Review).

Conference Proceedings/Book Chapters

- **Arora, G.**, Hussain, S., Kumar, R., & Mammeri, Y. (2024, February). Semi-Analytical Solution for Condensing Coagulation and Lifshitz-Slyozov Models: Variational Iteration Method. In International Conference on Nonlinear Dynamics and Applications (pp. 587-598). link.springer.com/chapter/10.1007/978-3-031-66874-6_48

- Hussain, S., **Arora, G.**, & Kumar, R. (2024, February). Solving Population Balance Models via a Novel Semi-analytical Method. In International Conference on Nonlinear Dynamics and Applications (pp. 3-16).
  link.springer.com/chapter/10.1007/978-3-031-69134-8_1

- Kumar Bariwal, S., **Arora, G.**, & Kumar, R. (2024, February). Semi-analytical Solutions for Breakage and Aggregation-Breakage Equations via Daftardar-Jafari Method. In International Conference on Nonlinear Dynamics and Applications (pp. 599-614).
  link.springer.com/chapter/10.1007/978-3-031-66874-6_49

List of Attended Conferences/Workshops/Schools

1. Presented a paper titled **"Semi-Analytical Solution for Condensing Coagulation and Lifshitz-Slyozov Models: Variational Iteration Method"**, International Conference on Nonlinear Dynamics and Applications (ICNDA24), SMIT, INDIA on 21-23 February, 2024.

2. Presented a paper titled **"Semi Analytical Approach Based on Tamimi-Ansari Method for Solving Fragmentation and Coagulation Equations"**, International Conference on Differential Equations and Control Problems (ICDECP23), IIT Mandi, INDIA on 15-17 June, 2023.

3. Presented a paper titled **"Mathematical Study for Condensing Coagulation and Lifshitz-Slyozov Models using Variational Iteration Method"**, International Conference on Dynamical Systems, Control and their Applications (ICDSCA-2022), IIT Rookee, INDIA on 1-3 July, 2022.

4. Presented a paper with title "**Finite Volume and Semi-analytical Techniques for Solvig Oort-Hulst Safronov Model**", Advances in Mechanics, Modelling, Computing, and Statistics (ICAMMCS-2022)", BITS PILANI, Pilani campus on 19-21 March, 2022.

5. Attended the AESIM School "**Mathematics for Health and Sciences**", BITS Pilani, India from 28 December 2023 to 6 January, 2024.

6. Attended a workshop on "**Numerical Method for Differential Equations and Applications" (WNMDEA-2023)**, BITS Pilani, India on 27-28 March, 2023.

7. Attended a workshop on "Mathematics of Computer Vision", Maharishi Markandeshwar University , India on 28 April, 2022.

Biography of the Candidate

Gourav Arora, a scholar from Rohtak, Haryana, has an impressive academic record, with outstanding scores in his 10th and 12th grades. He pursued his B.Sc. in Mathematics (Hons.) from Pandit Neki Ram Sharma Government College, Maharishi Dayanand University, graduating in 2017. He furthered his education with an M.Sc. in Mathematics (Hons.) from the same university in July 2019.

After clearing the Net (Mathematics) examination in December 2019, Gourav embarked on his journey towards higher education. He was admitted to the Ph.D. program in the Department of Mathematics at BITS PILANI, Pilani Campus, Rajasthan. Here, he worked under Prof. Rajesh Kumar's supervision and Prof. Youcef Mammeri's co-supervision. His research interests span across population balance equations, finite volume method, and semi-analytical methods. During his Ph.D., Gourav had the opportunity to visit the University of Jean Monnet, Saint Etienne, France, for three months. He was also awarded funding for attending the CIMPA School 2024, held at Silpakorn University, Nakhon Pathom, Thailand. Gourav has served as a teaching assistant for courses such as calculus, probability, and statistics. His research journey has been fruitful, with five articles published in peer-reviewed journals and three conference proceedings. He has presented his work at four international conferences and attended three workshops, showcasing his dedication to his field. For a deeper exploration of his research contributions, his profile on ResearchGate offers valuable insights: https://www.researchgate.net/profile/Gourav_Arora2. To connect with him directly, contact at p20190421@pilani.bits-pilani.ac.in.

Biography of the Supervisor

Rajesh Kumar is an accomplished Associate Professor in the Department of Mathematics at Birla Institute of Technology and Science Pilani, Pilani Campus, India. His academic journey includes a Bachelor's degree in Mathematics from Delhi University, an M.Sc. in Applied Mathematics from IIT Roorkee, and an Erasmus Mundus Fellowship, leading to a dual-degree M.Sc. in Industrial Maths and Scientific Computing from universities in Germany and Austria. He earned his Ph.D. from Otto-von-Guericke University Magdeburg, Germany. Throughout his career, he has held various academic and research positions, including a Postdoctoral Fellow at MOX, Politecnico di Milano, Italy; a scientific collaborator at EPFL, Switzerland and a research scientist at RICAM, Austria. His research contributions span differential and partial-integro differential equations, nonlinear analysis, population dynamics, hyperbolic conservation laws, numerical linear algebra, and more. Prof. Kumar has supervised numerous students, published research papers extensively in reputable journals, and actively participated in academic and research committees at BITS Pilani. He has organized several international workshops including GIAN, IFCAM workshop and AESIM School.

Biography of the Co-supervisor

Youcef Mammeri is a distinguished figure in the field of mathematics, particularly known for his expertise in applied mathematics and its applications in life sciences. Holding the esteemed position of Full Professor at the Institut Camille Jordan CNRS UMR 5208, Université Jean Monnet in Saint-Etienne, France, Mammeri has made significant contributions to the academic and research community. His academic journey is marked by a strong foundation in mathematics, having earned his PhD under the supervision of Professor N. Tzvetkov at Université Lille, Laboratoire Paul Painlevé. He has delved into a broad spectrum of topics ranging from population dynamics, identification, and sensitivity analysis to asymptotic behavior and stochastic instability. His work extends to the study of nonlinear partial differential equations, including Korteweg-de Vries, KdV-Burgers with memory, and the Cauchy problem. In addition to his research, Mammeri has held several prestigious positions, including Director of the research federative structure MODMAD and joint in-charge of VaLSEM (Valorisation Lyon Saint-Etienne en Mathématiques). He also serves as a Professor Convidado at Universidade Aberta in Lisbon, reflecting his international influence and collaboration. Mammeri's interdisciplinary approach has led him to intersect with fields such as ecology, medicine, and biochemistry, where his mathematical expertise has provided valuable insights. His dedication to scientific computing, employing methods like spectral method and finite volumes, further underscores his role in advancing computational techniques in research. Throughout his career, Mammeri has been recognized for his academic excellence, receiving grants and accolades that highlight his top-tier research supervising capabilities. His involvement in the educational community is extensive, serving as a reviewer for international journals, editor for EMS Magazine, and guest editor for Computational and Mathematical Biophysics.